

SEISMIC PERFORMANCE OF DUAL STEEL FRAMES OF CFRHS AND WELDED BEAM-TO-COLUMN JOINTS

Teză destinată obținerii
titlului științific de doctor inginer
la
Universitatea "Politehnica" din Timișoara
în domeniul INGINERIE CIVILĂ
de către

Ing. Mihai Cristian VULCU

Conducător științific: Prof.dr.ing. Dr.H.C. Dan Dubină
M.C. al Academiei Române
Referenți științifici: prof.univ.dr.ing. Darko Beg
prof.univ.dr.ing. Bozidar Stojadinovic
conf.univ.dr.ing. Aurel Stratan

Ziua susținerii tezei: 22 Februarie 2013

Seriile Teze de doctorat ale UPT sunt:

- | | |
|------------------------|---|
| 1. Automatică | 7. Inginerie Electronică și Telecomunicații |
| 2. Chimie | 8. Inginerie Industrială |
| 3. Energetică | 9. Inginerie Mecanică |
| 4. Ingineria Chimică | 10. Știința Calculatoarelor |
| 5. Inginerie Civilă | 11. Știința și Ingineria Materialelor |
| 6. Inginerie Electrică | |

Universitatea „Politehnica” din Timișoara a inițiat seriile de mai sus în scopul diseminării expertizei, cunoștințelor și rezultatelor cercetărilor întreprinse în cadrul școlii doctorale a universității. Seriile conțin, potrivit H.B.Ex.S Nr. 14 / 14.07.2006, tezele de doctorat susținute în universitate începând cu 1 octombrie 2006.

Copyright © Editura Politehnica – Timișoara, 2006

Această publicație este supusă prevederilor legii dreptului de autor. Multiplicarea acestei publicații, în mod integral sau în parte, traducerea, tipărirea, reutilizarea ilustrațiilor, expunerea, radiodifuzarea, reproducerea pe microfilme sau în orice altă formă este permisă numai cu respectarea prevederilor Legii române a dreptului de autor în vigoare și permisiunea pentru utilizare obținută în scris din partea Universității „Politehnica” din Timișoara. Toate încălcările acestor drepturi vor fi penalizate potrivit Legii române a drepturilor de autor.

România, 300159 Timișoara, Bd. Republicii 9,
tel. 0256 403823, fax. 0256 403221
e-mail: editura@edipol.upt.ro

Acknowledgements

The thesis was developed during my activity (2009 - 2013) within the Department of Steel Structures and Structural Mechanics (CMMC) and the Centre of Excellence in the Mechanics of Materials and Safety of Structures (CEMSIG), from the "Politehnica" University of Timișoara.

I would like to express my gratitude towards my advisor, Prof.dr.ing. Dr. H.C. Dan Dubină, for sharing his knowledge and experience, and for his support and guidance throughout my research activity. I would also like to thank him for involving me in "HSS-SERF" research project – which represented the research framework of the thesis, and during which I have met remarkable personalities in the field and was able to work with research teams from all over Europe.

My sincere thanks to Assoc.Prof.dr.ing. Aurel Stratan for his support, assistance and for sharing his knowledge and experience throughout my research activity. Thanks also to Assoc.Prof.dr.ing. Adrian Ciutina for his support and advices, to Assoc.Prof.dr.ing. Raul Zaharia for his support and collaboration, and to my colleagues Ing. Ionel Mărginean and Ing. Ovidiu Abrudan for their help with the laboratory work and assistance to the experimental investigations.

I would like to thank to Hermann Beck, Romeo Jakubik, Cosmin Gafton and Ioan Pinteau-Ungureanu – from Hilti Corporation, for their coloboration, for providing the powder actuated fasteners and additional accessories, for the installation instructions of nails and for their support.

Thanks to Dr.ing. Ramona Gabor, Dr.ing. Sorin Bordea, Dr.ing. Călin Neagu, Dr.ing. Filip-Văcărescu Norin, Dr.ing. Ioan Both, Dr.ing. Andrei Crișan, William Prentice, George Gilia, Ung Miloico, Dan Scarlat, for their help related to the administrative aspects and/or laboratory work.

The most important, I am grateful to my parents for their support and help throughout my PhD stage.

Timișoara, Februarie 2013

Mihai Cristian VULCU

Mihai Cristian VULCU

Seismic performance of dual steel frames of CFRHS and welded beam-to-column joints

(Performanța seismică a structurilor în cadre „dual-steel” cu stâlpi din țevi rectangulare umplute cu beton și îmbinări riglă-stâlp sudate)

Teze de doctorat ale UPT, Seria 5, Nr. 102, Editura Politehnica, 2013, 234 pagini, 251 figuri, 66 tabele.

ISSN: 1842-581X

ISBN: 978-606-554-631-8

Key words:

dual steel, concrete filled tubes, rectangular hollow sections, welded beam-to-column joints, reduced beam section, cover plates, high strength steel, composite columns, steel-concrete connection, shot fired nails, finite element method (FEM), component method;

Abstract:

The aim of the thesis was to observe the behaviour and to characterise in terms of stiffness, capacity and ductility, the seismic performance of welded beam-to-column joints for multi-storey building frames of CFT high strength steel columns and mild carbon steel beams. For this purpose, two connection solutions (with reduced beam section and with cover-plates) have been proposed for the beam-to-column joints. A set of frames were analysed using static and dynamic nonlinear analyses in order to assess the seismic performance and to determine the seismic demand for beam-column joints. Results from the experimental investigations are shown related to material samples (concrete and steel), steel-concrete connection (friction, friction+connectors), and beam-to-column joints. The behaviour and response of the joints were investigated also through advanced finite element modeling. Consequently, pre-test numerical simulations were performed with the aim to have an accurate prediction of the response for each joint configuration. The numerical models of the joints were further calibrated based on tests performed under monotonic and cyclic loading. In addition, numerical simulation of complementary cases were performed in order to assess the influence of different parameters (i.e. concrete core, beams welded on two sides, axial force in the column) on the behaviour of the beam-to-column joints. A component method approach was developed for the design of dual steel IPE beam-to-CFRHS column welded joints with reduced beam section, and respectively cover-plate connections. The relations for the design capacity of the joint components were validated by experimental and numerical means. Conclusions of the PhD study, the main contributions of the author and dissemination of results are finally presented.

Table of contents

Table of contents	5
List of figures	8
List of tables	13
Notations, abbreviations & acronyms.....	15
Rezumat.....	21
Summary.....	25
1. Introduction	28
1.1. Scope.....	28
1.2. Objectives	28
1.3. Research framework (RFSR-CT-00024 HSS-SERF)	28
2. High performance steels in construction.....	32
2.1. Introduction: steel as a construction material.....	32
2.2. Carbon steel grades for construction industry	32
2.3. High performance steels for construction industry	33
2.3.1. High strength steels	34
2.3.2. Low yield steels	39
2.3.3. Corrosion resistant steels	40
2.3.4. Shape memory alloy.....	41
2.3.5. Higher temperature resistant steels.....	41
2.3.6. Lower temperature resistant steels.....	41
2.4. Steels for seismic resistant structures	41
2.5. Design criteria for choice of steels for seismic resistant structures	42
2.5.1. Code provisions	42
2.5.2. Choice of steel for seismic resistant structures.....	43
2.6. Examples of application	44
2.7. Concluding remarks	46
3. Tubular structures for buildings.....	48
3.1. Introduction	48
3.2. Tubular steel sections for construction industry	48
3.3. Joining steel tubes in framed structures: connecting technology & detailing	50
3.4. Code provisions	53
3.5. Summary review of research on welded beam-to-CFT column joints	57
3.5.1. C.T. Cheng and L.L. Chung [59]	58
3.5.2. C.C. Chen and N.J. Lin [60]	59
3.5.3. K.J. Shin, I.J. Kim, Y.S. Oh, and T.S. Moon [61].....	60
3.5.4. T. Fukumoto and K. Morita [62]	61
3.5.5. J.W. Park, S.M. Kang, and S.C. Yang [63]	62
3.5.6. C.C. Chou, C.C. Wu, C.K. Jao, and Y.Y. Wang [64]	63
3.5.7. C.T. Cheng, C.F. Chan, and L.L. Chung [65]	64
3.5.8. M.S. Ghobadi, A. Mazroi, and M. Ghassemieh [66]	64
3.5.9. O.S. Bursi et al. [67] [68]	65
3.5.10. W. Wang, Y. Chen, W. Li, and R.T. Leon [69].....	66
3.6. Steel-concrete connection in CFT through the use of shot fired nails.....	67
3.6.1. H. Beck [73].....	67
3.6.2. G. Hanswille, H. Beck and T. Neubauer [75]	67
3.7. Examples of application	68

6 Table of contents

3.7.1. Commerzbank Tower in Frankfurt (1997)	68
3.7.2. Millenium Tower in Vienna (1999)	69
3.7.3. Post Tower in Bonn (2002)	69
3.7.4. HighLight Towers in Munich (2004)	70
3.8. Concluding remarks	70
4. Performance based seismic design of reference dual steel frames	73
4.1. Introduction	73
4.2. Dual frame typology: MRF; MRF+CBF; MRF+EBF	73
4.3. Code based design	74
4.3.1. Pre-design of frames	74
4.4. Joint detailing	76
4.4.1. Reduced beam section joint	76
4.4.2. Cover plate joint	77
4.5. Performance based evaluation and final design	78
4.5.1. Final design of frames	78
4.5.2. Performance based evaluation	79
4.5.3. Seismic performance demand for beam to-column joints	85
4.7. Concluding remarks	86
5. Experimental evaluation of seismic performance of dual steel IPE beam-to CFRHS column welded joints	88
5.1. Introduction	88
5.2. Design of experimental program	88
5.2.1. Material samples	90
5.2.2. Load introduction tests	91
5.2.3. Beam-to-column joint tests	94
5.3. Material sample tests	99
5.3.1. Concrete samples	99
5.3.2. Steel samples	100
5.4. Load introduction tests	104
5.4.1. S700-F-M / S700-F-C	104
5.4.2. S700-F-H-M / S700-F-H-C	105
5.4.3. S460-F-H-M / S460-F-H-C	106
5.4.4. Graphical comparison of results	107
5.4.5. Investigation of the failure mode	108
5.5. Numerical simulation of testing	110
5.5.1. Calibration of the material model	110
5.5.2. Pre-test numerical investigation of the beam-to-column joints	112
5.6. Beam-to-column joint tests	114
5.6.1. S460-RBS-M / S460-RBS-C	114
5.6.2. S700-RBS-M / S700-RBS-C	116
5.6.3. S460-CP-M / S460-CP-C	118
5.6.4. S700-CP-M / S700-CP-C	120
5.6.5. S460-RBS-R-M / S460-RBS-R-C	122
5.6.6. S700-RBS-R-M / S700-RBS-R-C	124
5.6.7. S460-CP-R-M / S460-CP-R-C	126
5.6.8. S700-CP-R-M / S700-CP-R-C	128
5.6.9. Interpretation of results	130
5.7. NDT quality control of specimens	136
5.7.1. Liquid penetrant testing	136
5.7.2. Magnetic particle testing	137
5.7.3. Ultrasonic testing	137

5.8. Calibration of FE models and simulation of complementary cases.....	138
5.8.1. Calibration of the numerical models.....	138
5.8.2. Influence of concrete core	148
5.8.3. Behaviour of joints with beams welded on two sides.....	149
5.8.4. Influence of axial force.....	151
5.9. Concluding remarks	152
6. Component method approach for design of dual steel IPE beam-to CFRHS column welded joints.....	157
6.1. Introduction	157
6.2. RBS welded joints.....	157
6.2.1. Plastic hinge (dissipative zone)	158
6.2.2. Welded on-site connection.....	159
6.2.3. External diaphragm	159
6.2.6. Column panel zone	160
6.3. Cover plate welded joints.....	162
6.3.1. Plastic hinge (dissipative zone)	163
6.3.2. Welded connection	163
6.3.3. Cover plates and on-site connection	164
6.3.4. External diaphragm	165
6.4. Experimental and numerical validation	169
6.4.1. Dissipative zone (plastic hinge).....	174
6.4.2. External diaphragm (S460 steel grade).....	175
6.4.3. External diaphragm (S690 steel grade).....	177
6.4.4. Column panel	179
6.5. Design flow chart.....	184
6.6. Concluding remarks	186
7. Conclusions of PhD study. Contributions of Author	188
7.1. Conclusions of PhD study.....	188
7.2. Contributions of the author	195
7.3. Dissemination of results	196
7.4. Acknowledgements	197
References.....	198
Annex A.....	206
Annex B.....	208
Annex C.....	217
Annex D	224
Annex E.....	227

List of figures

Fig. 1-1. Structural typologies and cross sections for columns [1]	29
Fig. 1-2. Weld details and T-stub typologies (Univ. Stuttgart) [2]	29
Fig. 1-3. Bolted beam-to-column joint configurations (Univ. Liege) [3]	30
Fig. 1-4. Welded beam-to-column joint configurations: (a) stiffened and cover plate joints with fully-encased wide-flange columns (Univ. Ljubljana) [4], (b) reduced beam section and cover plate joints with CFT RHS columns (Univ. Timisoara) [4]	30
Fig. 2-1. Historical development of production processes for rolled steel products [7].....	35
Fig. 2-2. Relative costs in % for S355 and DILLIMAX 550, 690, 890, 965, and 1100 regarding base material, weld, welding, and plate thickness [10]	36
Fig. 2-3. Weight and material cost comparison for a column made of S235, S355 and S460 dimensioned at compression 4400 kN (left) and 25000 kN (right) [11].....	36
Fig. 2-4. Manufacturing technology of normalized steel profiles [12]	37
Fig. 2-5. Comparison between the rolling processes [13]	38
Fig. 2-6. QST process applied on beams in the rolling heat [13]	38
Fig. 2-7. Examples of application in Europe	44
Fig. 2-8. Example of applications – other parts of the world	45
Fig. 3-1. Roll-forming method [47]	49
Fig. 3-2. Press-forming method [47]	49
Fig. 3-3. Parts of a beam-to-column joint configuration [49]	53
Fig. 3-4. Welded joint connecting an H section to a RHS member [49]	54
Fig. 3-5. Welded connection between a transverse plate and a RHS [49]	54
Fig. 3-6. Composite column: (a) partially encased wide flange section, and (b) concrete filled rectangular hollow section [1]	55
Fig. 3-7. Beam-to-column connection with through diaphragm for field welding [51].....	56
Fig. 3-8. Examples of through diaphragm connections: (a) with horizontal haunches, (b) with U-shaped welded joints, and (c) reduced beam section (RBS) connections [51]	56
Fig. 3-9. Beam-to-column connections with internal diaphragms [51].....	56
Fig. 3-10. Beam-to-column connections with external diaphragms [51]	56
Fig. 3-11. Connections with external diaphragms to concrete-filled hollow sections [51] [52]	57
Fig. 3-12. Concrete-filled steel tube column system in Japan: connections with (a) through diaphragm, (b) inner diaphragm, (c) outer diaphragm, and (d) ring stiffener [58].....	58
Fig. 3-13. Experimental test set-up [59]	59
Fig. 3-14. Connection typology [59]	59
Fig. 3-15. Experimental test set-up [60]	60
Fig. 3-16. Configuration of beam-to-column joints [60]	60
Fig. 3-17. Experimental test set-up and joint response [61]	61
Fig. 3-18. Experimental test set-up and joint configurations [62].....	62
Fig. 3-19. Experimental test set-up (a), elevation of joint (b), connection typologies (c) [63]	62
Fig. 3-20. Experimental test set-up (a), joint configurations (b) and (c) [64]	63
Fig. 3-21. Specimen configuration [65].....	64
Fig. 3-22. Connection details [65]	64
Fig. 3-23. Experimental test set-up (a), joint configuration (b) and (c) [66].....	65
Fig. 3-24. Experimental test set-up (a) and connection details of the joint (b) [67].....	65
Fig. 3-25. Experimental test set-up (a) and joint configurations (b) [69]	66
Fig. 3-26. Push-out test setup: (a) Pipe 508/8.8, and (b) Pipe 323.9/6.3 [73].....	67
Fig. 3-27. Test set-up for long term tests [75].....	68
Fig. 3-28. Commerzbank Tower in Frankfurt (a), cross section of column (b)	68
Fig. 3-29. Millennium Tower in Vienna (a); Cross section of column (b)	69
Fig. 3-30. Composite column cross-section (a) and component model for joint (b) - [78].....	69
Fig. 3-31. Post Tower in Bonn (a), and cross section of column (b)	70
Fig. 3-32. HighLight Towers in Munich (a), and cross section of columns (b)	70
Fig. 4-1. Frames (MRF, D-CBF, and D-EBF) realized in the dual-steel concept.....	73
Fig. 4-2. Pre-designed frames with CFT columns: (a) D-CBF, and (b) D-EBF [86]	75
Fig. 4-3. Welded beam to column joint with reduced beam section.....	76

Fig. 4-4. Preparation details for full penetration welds between external diaphragm and top flange (a), and bottom flange (b).....	77
Fig. 4-5. Welded beam to column joint with cover plates	77
Fig. 4-6. Preparation details for full penetration welds between external diaphragm and top cover plate (a), and bottom cover plate (b).....	77
Fig. 4-7. Configuration of frames considered for the performance based evaluation.....	78
Fig. 4-8. Determination of the target displacement for the equivalent SDOF, capacity curves, and the state of the MRF with CP joints at $\lambda=0.5$, 1.0, and 1.5	80
Fig. 4-9. Determination of the target displacement for the equivalent SDOF, capacity curves, and the state of the D-CBF with CP joints at $\lambda=0.5$, 1.0, and 1.5	81
Fig. 4-10. Determination of the target displacement for the equivalent SDOF, capacity curves, and the state of the D-EBF with CP joints at $\lambda=0.5$, 1.0, and 1.5	81
Fig. 4-11. Inter-storey drift and plastic hinges for MRF with CP joints at $\lambda=0.5$, 1.0, and 1.5	82
Fig. 4-12. Inter-storey drift and plastic hinges for MRF with RBS joints at $\lambda=0.5$, 1.0, and 1.5	82
Fig. 4-13. Inter-storey drift and plastic hinges for D-CBF with CP joints at $\lambda=0.5$ and 1.0	83
Fig. 4-14. Inter-storey drift and plastic hinges for D-CBF with RBS joints at $\lambda=0.5$ and 1.0	83
Fig. 4-15. Inter-storey drift and plastic hinges for D-EBF with CP joints at $\lambda=0.5$, 1.0, and 1.5	83
Fig. 4-16. Inter-storey drift and plastic hinges for D-EBF with RBS joints at $\lambda=0.5$, 1.0, and 1.5	84
Fig. 5-1. Joint components for tests on steel samples.....	90
Fig. 5-2. Specimen configuration for the load introduction tests.....	91
Fig. 5-3. Specimen configuration (front and lateral view)	92
Fig. 5-4. Conceptual scheme (front and lateral view), and illustration of the test set-up.....	92
Fig. 5-5. Conceptual scheme and illustration of instrumentation arrangement	93
Fig. 5-6. Detail of instrumentation (top and bottom)	93
Fig. 5-7. Determination of yield displacement, and ECCS loading procedure [93].....	94
Fig. 5-8. Designed joints (a), and corresponding joints with reinforced beam (b)	95
Fig. 5-9. Conceptual scheme and illustration of the test assembly	96
Fig. 5-10. Global instrumentation and local joint instrumentation.....	96
Fig. 5-11. Instrumentation of beam, welded connection, external diaphragm, and connection zone prepared by whitewashing	97
Fig. 5-12. Definition of parameters for tests on beam to column joints	97
Fig. 5-13. ANSI/AISC 341-10 (2010) cyclic loading procedure [94]	98
Fig. 5-14. Testing device and concrete cubes (before and after compression test).....	99
Fig. 5-15. Stress-strain curves and tested steel samples.....	100
Fig. 5-16. Stress-strain curves and tested steel samples.....	101
Fig. 5-17. Stress-strain curves and tested steel samples.....	102
Fig. 5-18. Stress-strain curves and tested steel samples.....	103
Fig. 5-19. Conceptual scheme of specimen (front and lateral view), and the test assembly .	104
Fig. 5-20. Monotonic response of steel-concrete adhesion.....	104
Fig. 5-21. Cyclic response of steel-concrete adhesion	104
Fig. 5-22. Conceptual scheme of specimen (front and lateral view), and the test assembly .	105
Fig. 5-23. Monotonic response of steel-concrete bonding combined with connectors.....	105
Fig. 5-24. Cyclic response of steel-concrete bonding combined with connectors.....	105
Fig. 5-25. Conceptual scheme of specimen (front and lateral view), and the test assembly .	106
Fig. 5-26. Monotonic response of steel-concrete bonding combined with connectors.....	106
Fig. 5-27. Cyclic response of steel-concrete bonding combined with connectors.....	106
Fig. 5-28. Contribution of the connectors under monotonic loading	107
Fig. 5-29. Contribution of the connectors under cyclic loading	107
Fig. 5-30. Cyclic response of the stubs with steel-concrete bonding and connectors	108
Fig. 5-31. Flame cutting of the concrete filled tubes	108
Fig. 5-32. Specimens (S460-F-H-C / S460-F-H-M) with removed tube faces.....	108
Fig. 5-33. Response of concrete and connectors to monotonic loading	109
Fig. 5-34. Detail of concrete and connector after monotonic loading	109
Fig. 5-35. Response of concrete and connectors to cyclic loading	109
Fig. 5-36. Detail of concrete and connector after cyclic loading	110

10 List of figures

Fig. 5-37. Stress-strain relationship for concrete.....	110
Fig. 5-38. Calibration of IPE 400 flange (S355) material model: comparison between test and simulation (a); Mises stress (b) and plastic strain (c) at fracture.....	111
Fig. 5-39. Calibration of IPE 400 web (S355) material model: comparison between test and simulation (a); Mises stress (b) and plastic strain (c) at fracture.....	111
Fig. 5-40. Calibration of Tube RHS 300x12.5 (S460) material model: comparison between test and simulation (a); Mises stress (b) and plastic strain (c) at fracture.....	111
Fig. 5-41. Calibration of Tube RHS 250x10 (S700) material model: comparison between test and simulation (a); Mises stress (b) and plastic strain (c) at fracture.....	112
Fig. 5-42. S460-RBS: Mises stress, plastic strain; Moment-rotation curves for RBS joints..	113
Fig. 5-43. S460-CP: Mises stress, plastic strain; Moment-rotation curves for CP joints	113
Fig. 5-44. S460-RBS-R: Mises stress, plastic strain; Moment-rotation curves for RBS-R joints	113
Fig. 5-45. S460-CP-R: Mises stress, plastic strain; Moment-rotation curves for CP-R joints	113
Fig. 5-46. S460-RBS test assembly and connection zone – before test	114
Fig. 5-47. S460-RBS-M joint: monotonic response and illustration of the failure mode.....	115
Fig. 5-48. Out of plane deformation of beam web (Vic 3D)	115
Fig. 5-49. S460-RBS-C joint: cyclic response and illustration of the failure mode	115
Fig. 5-50. Strain " ϵ_{yy} " in beam web (Vic 3D).....	115
Fig. 5-51. S700-RBS test assembly and connection zone – before test	116
Fig. 5-52. S700-RBS-M joint: monotonic response and illustration of the failure mode.....	117
Fig. 5-53. Out of plane deformation of beam web (Vic 3D)	117
Fig. 5-54. S700-RBS-C joint: cyclic response and illustration of the failure mode	117
Fig. 5-55. Strain " ϵ_{yy} " in beam web (Vic 3D).....	117
Fig. 5-56. S460-CP test assembly and connection zone – before test.....	118
Fig. 5-57. S460-CP-M joint: monotonic response and illustration of the failure mode.....	119
Fig. 5-58. Out of plane deformation of beam web (Vic 3D).....	119
Fig. 5-59. S460-CP-C joint: cyclic response and illustration of the failure mode	119
Fig. 5-60. Strain " ϵ_{yy} " in beam web (Vic 3D).....	119
Fig. 5-61. S700-CP test assembly and connection zone – before test.....	120
Fig. 5-62. S700-CP-M joint: monotonic response and illustration of the failure mode.....	121
Fig. 5-63. Out of plane deformation of beam web (Vic 3D).....	121
Fig. 5-64. S700-CP-C joint: cyclic response and illustration of the failure mode	121
Fig. 5-65. Strain " ϵ_{yy} " in beam web (Vic 3D).....	121
Fig. 5-66. S460-RBS-R test assembly and connection zone – before test	122
Fig. 5-67. S460-RBS-R-M joint: monotonic response and illustration of the failure mode	123
Fig. 5-68. Strain " ϵ_{xy} " in external diaphragm and HAZ of beam flange (Vic 3D).....	123
Fig. 5-69. S460-RBS-R-C joint: cyclic response and illustration of the failure mode.....	123
Fig. 5-70. Strain " ϵ_{yy} " in external diaphragm and HAZ of beam flange (Vic 3D).....	123
Fig. 5-71. S700-RBS-R test assembly and connection zone – before test	124
Fig. 5-72. S700-RBS-R-M joint: monotonic response and illustration of the failure mode	125
Fig. 5-73. Strain " ϵ_{yy} " in external diaphragm and HAZ of beam flange (Vic 3D).....	125
Fig. 5-74. S700-RBS-R-C joint: cyclic response and illustration of the failure mode.....	125
Fig. 5-75. Strain " ϵ_{yy} " in external diaphragm and HAZ of beam flange (Vic 3D).....	125
Fig. 5-76. S460-CP-R test assembly and connection zone – before test	126
Fig. 5-77. S460-CP-R-M joint: monotonic response and illustration of the failure mode.....	127
Fig. 5-78. Strain " ϵ_{xy} " in the column panel zone (Vic 3D)	127
Fig. 5-79. S460-CP-R-C joint: cyclic response and illustration of the failure mode.....	127
Fig. 5-80. Strain " ϵ_{xy} " in the column panel zone (Vic 3D)	127
Fig. 5-81. S700-CP-R test assembly and connection zone – before test	128
Fig. 5-82. S700-CP-R-M joint: monotonic response and illustration of the failure mode.....	129
Fig. 5-83. Strain " ϵ_{xy} " in the column panel zone (Vic 3D)	129
Fig. 5-84. S700-CP-R-C joint: cyclic response and illustration of the failure mode.....	129
Fig. 5-85. Strain " ϵ_{xy} " in the column panel zone (Vic 3D)	129
Fig. 5-86. Contribution of components to joint rotation (S460-RBS-M / C)	130
Fig. 5-87. Contribution of components to joint rotation (S700-RBS-M / C)	130
Fig. 5-88. Contribution of components to joint rotation (S460-CP-M / C)	131
Fig. 5-89. Contribution of components to joint rotation (S700-CP-M / C)	131

Fig. 5-90. Contribution of components to joint rotation (S460-RBS-R-M / C)	131
Fig. 5-91. Contribution of components to joint rotation (S700-RBS-R-M / C)	132
Fig. 5-92. Contribution of components to joint rotation (S460-CP-R-M / C)	132
Fig. 5-93. Contribution of components to joint rotation (S700-CP-R-M / C)	132
Fig. 5-94. Overstrength of connection zone for RBS joints.....	133
Fig. 5-95. Overstrength of connection zone for CP joints.....	133
Fig. 5-96. S460-RBS joint: cyclic response and the corresponding dissipated energy	134
Fig. 5-97. S700-RBS joint: cyclic response and the corresponding dissipated energy	134
Fig. 5-98. S460-CP joint: cyclic response and the corresponding dissipated energy	134
Fig. 5-99. S700-CP joint: cyclic response and the corresponding dissipated energy	134
Fig. 5-100. S460-RBS-R joint: cyclic response and the corresponding dissipated energy	135
Fig. 5-101. S700-RBS-R joint: cyclic response and the corresponding dissipated energy	135
Fig. 5-102. S460-CP-R joint: cyclic response and the corresponding dissipated energy	135
Fig. 5-103. S700-CP-R joint: cyclic response and the corresponding dissipated energy	135
Fig. 5-104. Weld failure within S700-CP-R-M joint.....	136
Fig. 5-105. Reinforced beam-to-column joint configurations.....	136
Fig. 5-106. Liquid penetrant testing	136
Fig. 5-107. Magnetic particle testing (S460-RBS-R-C, and S700-CP-R-C).....	137
Fig. 5-108. Ultrasonic testing	137
Fig. 5-109. Joint with full length discontinuity of weld between plates of the external diaphragm (un-penetrated weld root).....	137
Fig. 5-110. Beam-to-column joint with lateral contact (a), and cyclic loading procedure (b)	139
Fig. 5-111. Comparison between test and simulation for RBS joints	140
Fig. 5-112. Mises stress, plastic strain, and illustration of failure mode: (a) S460-RBS joint, and (b) S700-RBS joint	140
Fig. 5-113. Comparison between test and simulation for CP joints	141
Fig. 5-114. Mises stress, plastic strain, and illustration of failure mode: (a) S460-CP joint, and (b) S700-CP joint.....	141
Fig. 5-115. Comparison between test and simulation for reinforced RBS joints	142
Fig. 5-116. Mises stress, plastic strain, and illustration of failure mode: (a) S460-RBS-R joint, and (b) S700-RBS-R joint	142
Fig. 5-117. Comparison between test and simulation for reinforced CP joints	143
Fig. 5-118. Mises stress, plastic strain, and illustration of failure mode: (a) S460-CP-R joint, and (b) S700-CP-R joint	143
Fig. 5-119. Cyclic response (test and simulation) of S460-RBS joint.....	144
Fig. 5-120. Cyclic response (test and simulation) of S700-RBS joint.....	144
Fig. 5-121. Cyclic response (test and simulation) of S460-CP joint.....	145
Fig. 5-122. Cyclic response (test and simulation) of S700-CP joint.....	145
Fig. 5-123. Cyclic response (test and simulation) of S460-RBS-R joint.....	146
Fig. 5-124. Cyclic response (test and simulation) of S700-RBS-R joint.....	146
Fig. 5-125. Cyclic response (test and simulation) of S460-CP-R joint.....	147
Fig. 5-126. Cyclic response (test and simulation) of S700-CP-R joint.....	147
Fig. 5-127. Influence of concrete core – RBS joints	148
Fig. 5-128. Influence of concrete core – CP joints	148
Fig. 5-129. Influence of concrete core – reinforced CP joint.....	148
Fig. 5-130. Behaviour of joint with beams welded on two sides (CFT).....	149
Fig. 5-131. Behaviour of joint with beams welded on two sides (column without concrete core)	149
Fig. 5-132. Response of CP joints with beams welded on two sides	149
Fig. 5-133. Behaviour of joint with beams welded on two sides (CFT).....	150
Fig. 5-134. Behaviour of joint with beams welded on two sides (column without concrete core)	150
Fig. 5-135. Response of RBS joints with beams welded on two sides	150
Fig. 5-136. Mises stress - influence of axial force ($0.5 \cdot N_{pl,Rd,composite}$) on S460-CP joints.....	151
Fig. 5-137. Moment-rotation curves: influence of axial force ($0.5 \cdot N_{pl,Rd,composite}$) on S460-CP joint	151
Fig. 5-138. Influence of axial force ($0.5 \cdot N_{pl,Rd,steel}$) on S460-CP joint.....	152
Fig. 6-1. Beam to column joint with reduced beam section.....	157

12 List of figures

Fig. 6-2. Shear failure of the external diaphragm	160
Fig. 6-3. Evaluation of the shear force within the column web panel.....	160
Fig. 6-4. Beam to column joint with cover plates	162
Fig. 6-5. Capable forces of the fillet welds between beam flange and cover plate	164
Fig. 6-6. Considered failure mode of the external diaphragm.....	166
Fig. 6-7. Evaluation of the shear force within the column web panel.....	166
Fig. 6-8. Component model for RBS joint (a), and for CP joint (b).....	173
Fig. 6-9. Beam-to-column joint: loading and reactions.....	179
Fig. 6-10. Beam-to-column joint: shear force (a) and bending moment (b).....	179
Fig. 6-11. Evaluation of shear force within the column web panel.....	179
Fig. 6-12. Design flow-chart for reduced beam section joints.....	184
Fig. 6-13. Design flow-chart for cover plate joints	185
Fig. A-1. Frame typologies	206
Fig. B-1. Designed beam-to-column joints (a), and corresponding reinforced joints (b)	208
Fig. B-2. Geometry of S460-RBS joint	209
Fig. B-3. Geometry of S700-RBS joint	210
Fig. B-4. Geometry of S460-CP joint	211
Fig. B-5. Geometry of S700-CP joint	212
Fig. B-6. Geometry of S460-RBS-R joint.....	213
Fig. B-7. Geometry of S700-RBS-R joint.....	214
Fig. B-8. Geometry of S460-CP-R joint	215
Fig. B-9. Geometry of S700-CP-R joint	216
Fig. C-1. Tensile test on steel sample – universal testing machine	217
Fig. C-2. Tensile test on steel sample – video extensometer and tested sample.....	217
Fig. C-3. Stress-strain curves and tested steel samples	218
Fig. C-4. Stress-strain curves and tested steel samples	219
Fig. C-5. Stress-strain curves and tested steel samples	220
Fig. C-6. Stress-strain curves and tested steel samples	221
Fig. C-7. Stress-strain curves and tested steel samples	222
Fig. C-8. Stress-strain curves and tested steel samples	223
Fig. D-1. Calibration of cover plate (S355) material model: comparison between test and simulation (a); Mises stress (b) and plastic strain (c) at fracture.....	224
Fig. D-2. Calibration of splice plate (S355) material model: comparison between test and simulation (a); Mises stress (b) and plastic strain (c) at fracture.....	224
Fig. D-3. Calibration of external diaphragm (S460) material model: comparison between test and simulation (a); Mises stress (b) and plastic strain (c) at fracture.....	225
Fig. D-4. Calibration of external diaphragm (S690) material model: comparison between test and simulation (a); Mises stress (b) and plastic strain (c) at fracture.....	225
Fig. D-5. Calibration of vertical column stiffener (S460) material model: comparison between test and simulation (a); Mises stress (b) and plastic strain (c) at fracture	225
Fig. D-6. Calibration of vertical column stiffener (S690) material model: comparison between test and simulation (a); Mises stress (b) and plastic strain (c) at fracture	226
Fig. E-1. Yielding sequence: S460-RBS-M	227
Fig. E-2. Yielding sequence: S460-RBS-C.....	227
Fig. E-3. Yielding sequence: S700-RBS-M	228
Fig. E-4. Yielding sequence: S700-RBS-C.....	228
Fig. E-5. Yielding sequence: S460-CP-M	228
Fig. E-6. Yielding sequence: S460-CP-C.....	229
Fig. E-7. Yielding sequence: S700-CP-M	229
Fig. E-8. Yielding sequence: S700-CP-C.....	229
Fig. E-9. Yielding sequence: S460-RBS-R-M	230
Fig. E-10. Yielding sequence: S460-RBS-R-C.....	230
Fig. E-11. Yielding sequence: S700-RBS-R-M	230
Fig. E-12. Yielding sequence: S700-RBS-R-C.....	231
Fig. E-13. Yielding sequence: S460-CP-R-M	231
Fig. E-14. Yielding sequence: S460-CP-R-C.....	231
Fig. E-15. Yielding sequence: S700-CP-R-M	232
Fig. E-16. Yielding sequence: S700-CP-R-C.....	232

List of tables

Table 2-1 – Structural steels for construction	33
Table 2-2 – Strength requirements for high strength steel	35
Table 2-3 – Minimal material properties of some high strength steels [15]	39
Table 2-4 – High performance steel with earthquake resistance for building structures [16] ..	40
Table 3-1 – Special shapes [45]	48
Table 3-2 – Column splice connections [48]	50
Table 3-3 – Common examples of simple connections [48]	51
Table 3-4 – Common examples of moment connections [48]	52
Table 4-1 – Frame configurations for preliminary design [86]	74
Table 4-2 – Cross sections for the dual concentrically braced frames [86]	75
Table 4-3 – Cross sections for the dual eccentrically braced frames [86]	75
Table 4-4 – Cross sections for links [86]	75
Table 4-5 – MRF – cross sections of members [86]	78
Table 4-6 – D-CBF - cross sections of members	78
Table 4-7 – D-EBF - cross sections of members	79
Table 4-8 – Target displacements	79
Table 4-9 – Maximum top displacements	84
Table 4-10 – Inter-storey drift demand MRF	85
Table 4-11 – Inter-storey drift demand D-CBF and D-EBF	85
Table 5-1 – Summary of testing program	89
Table 5-2 – List of joint components for the tensile and Charpy V-notch tests	90
Table 5-3 – Experimental program on column stubs	91
Table 5-4 – Experimental program on beam-to-column joints	94
Table 5-5 – Beam-to-column joint configurations	95
Table 5-6 – Test results on concrete	99
Table 5-7 – Stress and elongation results for IPE 400 flange – S355 JR (J2+N)	100
Table 5-8 – Impact test results for IPE 400 flange – S355 JR (J2+N)	100
Table 5-9 – Stress and elongation results for IPE 400 web – S355 JR (J2+N)	101
Table 5-10 – Impact test results for IPE 400 web – S355 JR (J2+N)	101
Table 5-11 – Stress and elongation results for Tube RHS 300x12.5 – S460 M	102
Table 5-12 – Impact test results for Tube RHS 300x12.5 – S460 M	102
Table 5-13 – Stress and elongation results for Tube RHS 250x10 (S700 QL)	103
Table 5-14 – Impact test results for Tube RHS 250x10 (S700 QL)	103
Table 5-15 – Input for plastic behaviour of beam (flange and web), S460 tube and S700 tube	112
Table 6-1 – Dissipative zone (plastic hinge)	169
Table 6-2 – Welded connections	170
Table 6-3 – Design capacity of components	170
Table 6-4 – Stiffness coefficients for joint components	172
Table 6-5 – Dissipative zone (RBS joint)	174
Table 6-6 – Dissipative zone (CP joint)	174
Table 6-7 – External diaphragm (S460-RBS-R joint)	175
Table 6-8 – External diaphragm (S460-CP-R joint)	176
Table 6-9 – External diaphragm (S690-RBS-R joint)	177
Table 6-10 – External diaphragm (S690-CP-R joint)	178
Table 6-11 – Column panel (CF-RHS S460) – validation of steel component	180
Table 6-12 – Column panel (CF-RHS S460) – validation of composite section	181
Table 6-13 – Column panel (CF-RHS S700) – validation of steel section	182
Table 6-14 – Column panel (CF-RHS S700)	183
Table A-1 – MRF (S460) – cross section of members [1]	206
Table A-2 – D-CBF (S460) - cross section of members [1]	206
Table A-3 – D-CBF (S690) - cross section of members [1]	206
Table A-4 – D-EBF (S460) - cross section of members [1]	207

14 List of tables

Table A-5 – D-EBF (S690) - cross sections of members [1].....	207
Table C-1 – Stress and elongation results for cover plates – S355 J0.....	218
Table C-2 – Impact test results for cover plates – S355 J0.....	218
Table C-3 – Stress and elongation results for splice plate – S355 J2.....	219
Table C-4 – Impact test results for splice plate – S355 J2.....	219
Table C-5 – Stress and elongation results for external diaphragm – S460 NL.....	220
Table C-6 – Impact test results for external diaphragm – S460 NL.....	220
Table C-7 – Stress and elongation results for external diaphragm – S690 QL.....	221
Table C-8 – Impact test results for external diaphragm – S690 QL.....	221
Table C-9 – Stress and elongation results for vertical stiffener – S460 NL.....	222
Table C-10 – Impact test results for vertical stiffener – S460 NL.....	222
Table C-11 – Stress and elongation results for vertical stiffener – S690 QL.....	223
Table C-12 – Impact test results for vertical stiffener – S690 QL.....	223
Table D-1 – Input for plastic behaviour.....	226

Notations, abbreviations & acronyms

Notations

Chapter 1

q	Behaviour factor;
Ω	Overstrength factor;

Chapter 2

f_y	Yield strength;
f_u	Ultimate strength;
$f_{y,act}$	Actual yield strength;
$f_{y,max}$	Maximum yield strength;
ϵ_y	Strain corresponding to yield;
ϵ_u	Strain corresponding to ultimate strength;
E	Modulus of elasticity;
T_{k100}	Temperature (also T_0) related to a toughness of $KV=100 \text{ MPa}\cdot\text{m}^{1/2}$;
T_{US}	Lowest temperature on the upper-shelf;

Chapter 3

$M_{pl,Rd}$	Design resistance of the plastic bending moment;
$V_{Ed,G}$	Design shear force from gravity loads in the seismic design situation;
$V_{Md,G}$	Design shear force corresponding to the application of the plastic moments;
θ_p	Rotation capacity of the plastic hinge region;
$V_{wp,Ed}$	Design shear force in column web panel;
$V_{wp,Rd}$	Shear strength of the column web panel;
q	Behaviour factor;
$M_{ip,1,Rd}$	Capable bending moment for welded I or H section to RHS member;
$N_{1,Rd}$	Capable axial force of welded flange to RHS member;
h_1	Beam depth;
t_1	Flange thickness;
N_1	Capable axial force of equivalent transverse plate welded to RHS member;
b_i	Width of transverse plate;
t_i	Thickness of transverse plate;
b_0	Width of RHS member;
h_0	Depth of RHS member;

16 Notations, abbreviations & acronyms

t_0	Thickness of RHS member;
b_1	Width of transverse plate;
f_{y1}	Yield strength of transverse plate;
f_{y0}	Yield strength of RHS member;
b_{eff}	Effective width for a brace member to chord connection;
$b_{e,p}$	Effective width for punching shear
Y_{M5}	Partial safety factor for resistance of joints in hollow section lattice girder;
$V_{wp,c,Rd}$	Shear strength of the concrete section from the column web panel;
b_c	Width of the column section;
h_c	Depth of the column section;
t_w	Web thickness of the steel section;
t_f	Flange thickness of the steel section;
v	Reduction factor;
A_c	Cross-sectional area of concrete;
f_{cd}	Design value of the cylinder compressive strength of concrete
N_{Ed}	Design compressive normal force in the column;
$N_{pl,Rd}$	Design plastic resistance of the column's cross-section;
$V_{wp,Rd}$	Shear strength of the column web panel considering a composite section;

Chapter 4

Y_I	Importance factor;
a_g	Design ground acceleration on type A ground;
$\psi_{2,i}$	Combination coefficient for the quasi-permanent value of a variable action i ;
$\psi_{E,i}$	Combination coefficient for a variable action i , to be used when determining the effects of the design seismic action;
D_t	Target displacement;
λ	Intensity factor;

Chapter 5

K_{ini}	Initial stiffness;
d_y	Yield displacement;
θ	Inter-storey drift of the test assembly;
M	Bending moment at the column centreline;
δ	Deformation of the beam to column joint assembly, defined as the lateral displacement at the tip of the beam, "cleared" of any support displacements;
L	Beam length to column centreline;
F	Force applied at the tip of the beam;

A_c	Cross-sectional area of concrete;
F_{\max}	Maximum compressive force from tests on concrete cubes;
f_c	Compressive strength of concrete;
R_m	Ultimate strength to product standards;
R_{eH}	Yield strength to product standards;
R_{p02}	Yield strength;
A	Elongation at fracture;
A_g	Elongation at maximum force;
$N_{pl,Rd,composite}$	Design plastic resistance of the composite section;
$N_{pl,Rd,steel}$	Design plastic resistance of the steel section;
τ_{Rd}	Design shear strength;
P_{Rd}	Design value of the shear resistance of a single connector;
f_u	Ultimate strength;
d	Diameter of the connector;
γ_v	Partial factor for design shear resistance of a headed stud;
b	A material constant (determines the changing rate of the yield surface size with the equivalent plastic strain);
Q_∞	A material constant (representative of the maximum change in size of the yield surface);
C_1	Initial kinematic hardening modulus;
γ_1	Dynamic recovery term associated with non-linear kinematic hardening;

Chapter 6

L	Beam span to column face;
L_0	Distance between column centrelines;
L'	Distance between plastic hinges;
e	Distance between column face and the centre of RBS;
a, b, c	Geometry of the reduced beam section;
b_b	Beam flange width;
h_b	Beam height;
$M_{pl,RBS}$	Design resistance of the plastic bending moment in the reduced beam section;
$V_{Ed,RBS}$	Design shear force in the reduced beam section;
$V_{Ed,G}$	Design shear force from gravity loads in the seismic design situation;
$V_{Ed,M}$	Design shear force corresponding to the application of the plastic moments;
p	Permanent load;
q	Live load;

18 Notations, abbreviations & acronyms

f_y	Yield strength;
Y_{sh}	Strain hardening;
Y_{ov}	Overstrength factor;
Y_{M0}	Partial factor for resistance of cross-sections;
$W_{pl,RBS}$	Plastic section modulus at the centre of the reduced beam section;
$W_{pl,beam}$	Plastic section modulus of beams cross section;
t_f	Thickness of beam flanges;
t_w	Thickness of beam web;
$M_{Ed,sc}$	Design bending moment at the on-site connection;
$V_{Ed,sc}$	Design shear force at the on-site connection;
e'	Distance from the centre of plastic hinge to the on site connection;
$M_{Rd,sc}$	Design resistance of the plastic bending moment at the on-site connection;
$V_{Rd,sc}$	Design shear force at the on-site connection;
$W_{pl,sc}$	Plastic section modulus at the on-site connection;
$M_{Ed,cf}$	Design bending moment at column face;
$V_{Ed,cf}$	Design shear force at column face;
z	Lever arm;
$F_{v,Ed}$	Design force developed in the external diaphragm;
$F_{v,Rd}$	Design resistance of the external diaphragm;
A_v	Shear area of external diaphragm;
A_w	Shear area of weld;
β_w	Appropriate correlation factor;
β	Transformation factor;
$F_{w,Rd}$	Design resistance of the weld connection;
$V_{wp,Ed}$	Design shear force in column web panel;
V_c	Shear force in the column;
$\sum M_{b,cf}$	Sum of bending moments in the beam at the column face;
$M_{Ed,cf,red}$	Reduced bending moment at column face (the overstrength factor and the strain hardening were not taken into account for the computation of the plastic bending moment in the beam);
$M_{Ed,cl,red}$	Reduced bending moment at column centerline (the overstrength factor and the strain hardening were not taken into account for the computation of the plastic bending moment in the beam);
H	Length of column, storey height;
$M_{pl,RBS,red}$	Design resistance of the reduced plastic bending moment in the RBS (the overstrength factor and the strain hardening were not taken into account for the computation of the plastic bending moment in the beam);
$V_{Ed,RBS,red}$	Design shear force in the RBS;
$V_{wp,s,Rd}$	Design shear strength of the steel section from the column web panel;

b_c	Width of the column section;
h_c	Depth of the column section;
t_t	Thickness of the tube (rectangular hollow section);
A	Area of the steel cross section;
$V_{wp,c,Rd}$	Design shear strength of the concrete section from column web panel;
v	Reduction factor;
A_c	Area of the concrete cross section;
f_{cd}	Design value of the cylinder compressive strength of concrete;
N_{Ed}	Design compressive normal force in the column;
$N_{pl,Rd}$	Design plastic resistance of the column's cross-section;
$V_{wp,Rd}$	Design shear strength of the column web panel considering a composite section;
$M_{pl,hinge}$	Design resistance of the plastic bending moment in the plastic hinge;
$V_{Ed,hinge}$	Design shear force in the plastic hinge;
$F_{w,Ed}$	Design force transmitted by the welded connection;
$F_{w,Rd,1}$	Design force transmitted by the weld parallel to the force direction;
$F_{w,Rd,2}$	Design force transmitted by the weld perpendicular to the force direction;
a_1, a_2	Throat thickness;
l_1, l_2	Length of weld;
f_u	Ultimate strength;
γ_{M2}	Partial safety factor for resistance of welds;
$W_{pl,cp}$	Plastic section modulus computed for cover plates;
b_{cp}	Width of cover plate;
t_{cp}	Thickness of cover plate;
b_d	Width of external diaphragm;
t_d	Thickness of external diaphragm;
σ_{\perp}	Normal stress;
τ_{\parallel}	Tangential stress;
σ_{equiv}	Equivalent stress;

Abbreviations

HPS	High performance steel
HSS	High strength steel
MCS	Mild carbon steel
CFT	Concrete filled tube
TM	Thermo-mechanical steels
QST	Quenching and self tempering

20 Notations, abbreviations & acronyms

AHSS	Advanced High Strength Steels
SMA	Shape memory alloy
CFRHS	Concrete filled rectangular hollow section
RHS	Rectangular hollow section
CHS	Circular hollow section
SHS	Square hollow section
RBS	Reduced beam section
CP	Cover plate
MRF	Moment resisting frame
CBF	Centrally braced frame
EBF	Eccentrically braced frame
FE	Finite element
FEM	Finite element method
IDA	Incremental Dynamic Analysis
PGA	Peak ground acceleration
ULS	Ultimate limit state
SLS	Serviceability limit state
CPLS	Collapse prevention limit state
IO	Immediate occupancy
LS	Life safety
CP	Collapse prevention
DCH	High Ductility Class
DCM	Medium Ductility Class

Acronyms

HSS-SERF	“High Strength Steel in Seismic Resistant Building Frames” – research project;
AISC	American Institute of Steel Construction (http://www.aisc.org/);
CEMSIG	Research centre for Mechanics of Materials and Structural Safety – CEMSIG is a RTD (Research and Technical Development) unit of the „Politehnica” University of Timisoara, at the faculty of Civil Engineering, Department of Steel Structures and Structural Mechanics
FEMA	Federal Emergency Management Agency is an agency of the United States Department of Homeland Security (http://www.fema.gov/);
ECCS	European Convention for Constructional Steelwork;

REZUMAT

Utilizarea oțelurilor de înaltă rezistență în industria construcțiilor reprezintă una din direcțiile principale de dezvoltare în domeniu. Sistemul de cadre cu stâlpi din țevi de oțel umplute cu beton și îmbinări grindă-stâlp sudate a fost studiat și aplicat pe o scară largă în Asia, Australia și America. Spre deosebire, în Europa, această soluție a fost utilizată la o scară mai mică. Așadar, cu scopul de a evalua performanța seismică a cadrelor multietajate realizate în mod particular considerând: soluția "dual-steel", stâlpi din țevi rectangulare de oțel umplute cu beton și îmbinări grindă-stâlp sudate, a fost realizat un amplu program de cercetări experimentale și investigații numerice avansate la Centrul de Cercetare CEMSIG din cadrul Universității "Politehnica" din Timișoara. Teza prezintă rezultatele încercărilor experimentale și a analizelor numerice, precum și concluziile principale ale cercetării și contribuțiile autorului.

Capitolul 1: Introducere

În primul capitol se face o introducere temei de cercetare abordată. Sunt prezentate scopul și obiectivele tezei de doctorat, precum și cadrul în care s-a realizat cercetarea, acesta fiind reprezentat de un proiect de cercetare european al Fondului de Cercetare pentru Cărbune și Oțel RFSR-CT-2009-00024 "High Strength Steel in Seismic Resistant Building Frames".

Capitolul 2: Oțeluri de înaltă performanță utilizate în construcții

Capitolul al doilea este dedicat oțelurilor de înaltă performanță destinate industriei construcțiilor. O scurtă introducere este realizată privind oțelul ca material de construcție, și modificările semnificative pe care acest material le-a suferite de-a lungul timpului, modificări care au dus la un grup de materiale (oțeluri de înaltă performanță HPS) caracterizate de performanță bună la tracțiune, tenacitate, sudabilitate, formarea la rece și coroziune. Cu toate acestea, în Europa, majoritatea elementelor din oțel structural sunt realizate din oțel marca S275 și S355. Pe lângă oțelurile obișnuite, în industria construcțiilor sunt disponibile și oțeluri de înaltă performanță și oțeluri speciale. În Europa, profile laminate la cald (IPE, HEA, HEB, HEM) sunt produse și din oțel marca S460. Utilizarea oțelului de înaltă rezistență în industria construcțiilor reprezintă una din direcțiile principale de dezvoltare în domeniu. Prin folosirea oțelurilor caracterizate de un raport rezistență/greutate ridicat, se pot obține economii de material mai ales în cazul construcțiilor cu greutate ridicată. Utilizarea oțelurilor de înaltă rezistență, în cadrul structurilor amplasate în zone seismice, ar putea fi realizată considerând două moduri de abordare: (a) structuri realizate în conceptul "dual-steel", cu elemente disipative din oțeluri carbon (MCS), și cu elemente nedisipative din oțeluri de înaltă rezistență (HSS); (b) structuri realizate doar cu oțeluri de înaltă rezistență, spre exemplu oțel marca S460 care este caracterizat de o anumită ductilitate ce ar permite utilizarea acestuia în structuri din clasa de ductilitate medie.

În capitol sunt prezentate și aspecte privind criteriile de alegere a oțelurilor pentru structuri antiseismice, și anume cerințe din normele de proiectare actuale, și

recomandări privind alegerea oțelurilor pentru structuri antiseismice [30]. În cele din urmă sunt prezentate exemple de aplicare cu privire la utilizarea oțelurilor de înaltă rezistență în clădiri multietajate din Japonia, China, Australia, SUA, și din Europa.

Capitolul 3: Structuri din elemente tubulare pentru clădiri

Capitolul trei tratează particularități ale structurilor din elemente tubulare pentru clădiri. În introducere sunt prezentate aspecte generale privind proprietățile geometrice și mecanice, precum și procesul de fabricație a elementelor tubulare. În consecință, acest tip de elemente sunt caracterizate de proprietăți excelente cu privire la solicitările de compresiune, torsiune și încovoiere după toate direcțiile. Elementele tubulare sunt realizate din oțeluri similare cu cele utilizate pentru alte secțiuni de oțel, dar pot fi produse și din oțeluri de înaltă rezistență. Ca parte dintr-o structură în cadre pentru clădiri multietajate, elementele cu secțiune tubulară pot fi utilizate pentru contravântuiri și respectiv pentru stâlpi. Stâlpii realizați din secțiuni tubulare de oțel pot fi umpluți cu beton, cu scopul de a combina proprietățile celor două materiale, elementul final fiind caracterizat de o rigiditate, capacitate și ductilitate mai mare precum și de o rezistență la foc sporită. În ciuda avantajelor oferite de secțiunile tubulare, o atenție deosebită trebuie acordată zonelor de îmbinare dintre grinzi și stâlpi. Sistemul de cadre cu stâlpi din țevi de oțel umplute cu beton și îmbinări grindă-stâlp sudate a fost studiat și aplicat pe o scară largă în Asia, Australia și America. În schimb, această soluție a fost utilizată la o scară mai mică în Europa.

În cadrul temei de cercetare, se dorește investigarea nodurilor sudate grindă-stâlp realizate cu grinzi din profile dublu T și stâlpi din țevi de oțel umplute cu beton caracterizate de o rezistență totală, în vederea utilizării la cadre necontravântuite (MRF), și respectiv la cadrele necontravântuite ce fac parte din structurile duale (MRF+CBF, și MRF+EBF), pentru care îmbinările nu constituie elementul disipativ, iar articulațiile plastice sunt dezvoltate în grinzi. În privința stâlpului, scopul este de a conta pe ambele materiale (oțel și beton) și de a asigura efectul compozit al secțiunii prin intermediul conectorilor de tipul bolțurilor împușcate.

Sunt descrise prescripțiile din normele curente privind proiectarea nodurile sudate grindă-stâlp cu stâlpi din țevi umplute cu beton, și respectiv privind evaluarea capacității la forfecare a panoului de inimă al stâlpului. Întrucât această soluție a fost utilizată la o scară redusă în Europa, au fost observate un set de limitări ale normelor. Se arată necesitatea utilizării unor rigidizări transversale în zona nodului pentru a asigura o îmbinare cu rezistență totală. Sunt prezentate exemple tipice de noduri sudate grindă-stâlp utilizate în mod frecvent în Japonia, precum și cercetări recente asupra nodurilor sudate grindă-stâlp și asupra conexiunii oțel-beton realizată prin intermediul bolțurilor împușcate. În final, sunt prezentate un set de exemple de aplicații în ceea ce privește utilizarea stâlpilor din țevi de oțel umplute cu beton la realizarea clădirilor multietajate.

Capitolul 4: Proiectarea seismică bazată pe performanță a cadrelor de referință realizate în soluție dual-steel

Capitolul patru face o descriere a cadrelor realizate prin conceptul "dual-steel" cu elemente din mărci de oțel diferite, și anume oțeluri carbon (MCS) pentru elemente disipative, și oțeluri de înaltă rezistență (HSS) pentru elemente nedisipative. Trei tipologii de cadre au fost luate în considerare și anume cadre necontravântuite (MRF), cadre duale contravântuite centric (MRF+CBF), și cadre

duale contravântuite excentric (MRF+EBF). Este prezentată configurația cadrelor proiectate în cadrul proiectului de cercetare HSS-SERF care au stat la baza definirii programului experimental. Astfel, secțiunile elementelor pentru nodurile grindă-stâlp au fost alese din acest set de cadre. Pentru nodurile grindă-stâlp, au fost propuse două tipologii de îmbinare considerând soluția sudată și anume îmbinare cu secțiunea redusă a grinzii, și îmbinare cu plăci pe talpă. Configurația și detalierea celor două tipologii de noduri sunt așadar prezentate. În final, cu scopul de a evalua cerința seismică pentru nodurile grindă-stâlp, au fost analizate un set de cadre utilizând analize statice și dinamice neliniare. Rezultatele și observațiile investigațiilor sunt prezentate la finalul capitolului.

Capitolul 5: Evaluarea experimentală a performanțelor nodurilor sudate, realizate din grinzi IPE și stâlpi CFRHS

În capitolul cinci se prezintă evaluarea experimentală a performanțelor seismice a nodurilor realizate în soluție "dual-steel" cu îmbinarea sudată a grinzilor dublu T și a stâlpilor din țevi rectangulare de oțel umplute cu beton. Așadar, este prezentat programul experimental în cadrul căruia au fost realizate investigații experimentale asupra probelor de material (beton și oțel), asupra conexiunii oțel-beton pentru asigurarea efectului compozit al stâlpilor din țevi de oțel umplute cu beton, precum și asupra ansamblor de noduri grindă-stâlp fabricate la scară reală.

O descriere se face în raport cu standul experimental, configurația de instrumentare, și protocoalele de încărcare – atât pentru încercările pe conexiune oțel-beton cât și pentru încercările pe noduri. Sunt prezentate rezultatele ale investigațiilor experimentale efectuate asupra probelor de material și respectiv performanțele conexiunii oțel-beton realizată prin intermediul bolțurilor împușcate. Rezultatele obținute în urma încercărilor la tracțiune a probelor de oțel au permis calibrarea modelului de material care a fost utilizat în cadrul modelelor numerice ale nodurilor grindă-stâlp pentru simularea pre-test. Datorită configurației inovative a nodurilor, a fost necesară anticiparea cu o acuratețe ridicată a comportării nodurilor, pentru a evita o cedare nedorită din timpul încercărilor experimentale. Sunt prezentate așadar rezultatele și modul de comportare al nodurilor obținute în urma simulărilor numerice pre-test. Apoi sunt prezentate rezultatele investigațiilor experimentale asupra nodurilor grindă-stâlp pentru fiecare configurație în parte având în vedere următoarele: aranjamentul experimental, observații din timpul încercării, comportamentul și performanțele nodurilor solicitate în regim monoton și ciclic. Se face o interpretare și comparare a rezultatelor, precum și calibrarea modelelor numerice pe baza încercărilor în regim monoton și ciclic. Simularea numerică a unor cazuri de testare adiționale a permis evaluarea influenței unui set de parametrii (miezul de beton, grinzi sudate pe două laturi, forța axială în stâlp) asupra modului de comportare al nodurilor grindă-stâlp.

Capitolul 6: Proiectarea prin procedeul metodei componentelor a nodurilor sudate grindă-stâlp cu grinzi IPE și stâlpi din țevi rectangulare umplute cu beton

Capitolul șase tratează modul de proiectare a nodurilor sudate grindă-stâlp cu grinzi IPE și stâlpi din țevi rectangulare umplute cu beton, considerând două tipologii de îmbinare: cu secțiunea redusă a grinzii, și cu plăci pe talpă. Se prezintă procedura detaliată de proiectare utilizată pentru fiecare din cele două configurații de nod grindă-stâlp. Astfel, proiectarea nodurilor a fost efectuată luând în considerare formarea articulațiilor plastice în grindă. Mai departe, cu momentul încovoietor și forța tăietoare dezvoltate în articulația plastică, au fost dimensionate

celălalte componente ale nodurilor pentru a avea un anumit grad de suprarezistență comparativ cu zona disipativă a grinzii.

Capitolul prezintă de asemenea o imagine de ansamblu cu privire la: relațiile de proiectare ale îmbinărilor sudate, relațiile de evaluare a capacității componentelor, coeficienții de rigiditate ai componentelor. În plus, se face validarea experimentală și numerică a relațiilor de proiectare a capacității componentelor. Etapele de proiectare pentru fiecare dintre cele două tipologii de noduri grindă-stâlp sunt ilustrate prin intermediul schemelor logice.

Capitolul 7: Concluziile tezei de doctorat. Contribuții ale autorului

Ultimul capitol prezintă concluziile tezei de doctorat, principalele contribuții ale autorului și diseminarea rezultatelor.

Anexe

În anexe, sunt prezentate informații suplimentare cu privire la configurația cadrelor, geometria ansamblelor de noduri sudate grindă-stâlp, rezultate ale încercărilor asupra probelor de oțel, calibrarea modelului de material pentru componentele din oțel, și respectiv succesiunea apariției deformațiilor plastice pentru fiecare configurație de nod grindă-stâlp conform observațiilor din cadrul încercărilor experimentale.

SUMMARY

The use of high strength steels for building industry represents one of the main development directions in the field. The framing system with concrete filled columns and welded joints has been studied and applied on a large scale in Asia, Australia and America. In contrast, this solution was used at a lower scale in Europe. Therefore, with the aim to evaluate the seismic performance of multi-storey frames of: dual-steel solution, concrete filled rectangular hollow section columns and welded beam-to-column joints, extensive experimental research and advanced numerical investigations were carried out at the CEMSIG Research Centre from the University "Politehnica" of Timisoara. The thesis summarises the experimental and numerical investigations and presents the main conclusions of the research.

Chapter 1: Introduction

In the first chapter, an introduction is made in relation to the research topic. The scope and the objectives of the thesis are shown as well as the research framework which was represented by a European research project of the Research Fund for Coal and Steel RFSR-CT-2009-00024 "High Strength Steel in Seismic Resistant Building Frames".

Chapter 2: High performance steels in construction

The second chapter is dedicated to high performance steels for construction industry. A brief introduction is made with regard to steel as a construction material and the significant changes it suffered throughout time – which lead to a group of materials defined by good performance in tensile stress, toughness, weldability, cold forming and corrosion – High Performance Steels (HPS). However, in Europe, almost all structural steel is realised from S275 and S355 steel grades. In addition to the common steels, high performance and special steels are available for construction industry as well. In Europe, hot rolled profiles (IPE, HEA, HEB, and HEM) are produced from S460 steel grade. The use of High Strength Steels (HSS) for building industry represents one of the main development directions in the field. By using steels with higher resistance/weight ratio material savings can be obtained especially in the case of heavy constructions. The use of high strength steel within seismic resistant structures could be done considering two approaches: (I) dual steel structures in which mild carbon steel (MCS) is used for dissipative members and high strength steel is used in nondissipative members (HSS); (II) structures realised with HSS, i.e. S460 which is characterised by a certain amount of ductility and therefore could be used in structures of medium ductility class (DCM). Requirements from current code provisions and recommendations on choice of steel for seismic resistant structures [30] are shown as well. Finally some examples of application are shown related to the use of high strength in high rise buildings from Japan, China, Australia, US, and from Europe.

Chapter 3: Tubular structures for buildings

The third chapter is related to structures of tubular elements for buildings. In introduction general aspects are shown with regard to the geometrical and

mechanical properties as well as the manufacturing process of tubular elements. Accordingly, this type of elements are characterised by excellent properties with regard to loading in compression, torsion and bending in all directions. Hollow sections are made of similar steel as used for other steel sections, and can be produced from high strength steel as well. As part of a multi-storey frame, tubular elements can be used as braces or as columns. Columns realised from steel hollow sections can be filled with concrete with the aim to combine the properties of the two materials, the final element being characterised by higher stiffness, capacity and ductility, as well as enhanced fire resistance in comparison with bare steel configurations. In spite of the advantages of the tubular sections, a special attention needs to be paid to the connections between beams and columns. The framing system with concrete filled columns and welded joints has been studied and applied on a large scale in Asia, Australia and America. In contrast, this solution was used at a lower scale in Europe.

The interest within the current research is related to full strength welded I beam-to-CFRHS column joints for moment resisting frames (MRF) and moment resisting bays of dual frames (MRF+CBF, and MRF+EBF), for which the connections do not suffer plastic deformations while the plastic hinges develop in the beams. In relation to the column, the goal is to count on both materials steel tube and concrete core, and to have a composite action ensured by the use of shot fired nails, a relatively new method for assuring shear connection.

A description is made concerning the current code provisions in relation to the design of welded beam to CFT column joints, and evaluation of the shear capacity of the column web panel. Since this solution was used at a lower scale in Europe, a set of limitations were observed. It is shown that with the aim to develop full moment capacity, transverse column stiffeners are usually. Examples of typical joints used in Japan are shown, and a summary review of research on welded beam-to-CFT column joints and on shear connection realised with shot fired nails, is made. Finally, a set of application examples are shown in relation to the use of concrete filled tubes for columns within multi-storey buildings.

Chapter 4: Performance based seismic design of reference dual steel frames

Chapter four makes a description of frames realised in the dual-steel concept with elements from different steel grades, i.e. mild carbon steel (MCS) for dissipative members and high strength steel (HSS) for non-dissipative members. Three frame typologies were considered i.e. moment resisting frames (MRF), dual concentrically braced frames (MRF+CBF), and dual eccentrically braced frames (MRF+EBF). A brief description is made in relation to the frames that were designed within HSS-SERF research project and that were used as basis for the definition of the experimental program. Consequently, the cross-section of the members for the beam-to-column joint specimens was chosen from these frames. For the connection of beams and columns, two joint typologies were proposed considering the welded solution and two joint typologies: with reduced beam section and with cover plates.

The configuration and detailing of the two joint typologies, i.e. reduced beam section joints (RBS) and cover plate joints (CP) is shown. Finally, with the aim to assess the seismic demand for the beam-to-column joints, a set of frames were analysed using static and dynamic nonlinear analyses. The results and observations from the investigations are therefore shown.

Chapter 5: Experimental evaluation of seismic performance of dual steel IPE beam-to CFRHS column welded joints

Chapter five is related to the experimental evaluation of the seismic performance of dual steel IPE beam to concrete filled rectangular hollow section column welded joints. Consequently, a description is made in relation to the experimental program that covered extensive experimental investigations on material samples (concrete and steel), on steel-concrete connection needed for the composite action of CFT columns, as well as on full scale beam-to-column joints.

A description is made in relation to the experimental test set-up, instrumentation arrangement and loading protocols for both tests on steel-concrete connection and tests on joints. Results from the experimental investigations are shown related to material samples (concrete and steel) and to the performance of the steel-concrete connection realised through shot fired nails. The results from tensile tests performed on steel samples allowed the calibration of the material model which was used further within the pre-test numerical simulations. Due to the innovative joint configurations, an accurate prediction was needed in order to avoid unacceptable failure during the tests. Predictions from the numerical investigations are therefore shown. Finally, results from the experimental investigations on the beam-to-column joints are presented for each configuration considering the following: test assembly, observations from test, and joint response under monotonic and cyclic loading. Interpretation and comparison of results are shown as well as the calibration of numerical models based monotonic and cyclic tests. Numerical simulation of complementary testing cases allowed assessing the influence of different parameters (i.e. concrete core, beams welded on two sides, axial force in the column) on the behaviour of the beam to column joints.

Chapter 6: Component method approach for design of dual steel IPE beam-to-CFRHS column welded joints

Chapter six is related to the design of IPE beam-to-CFRHS column joints i.e. welded reduced beam section and welded cover plate beam-to-column joints with concrete filled rectangular hollow sections. The detailed design procedure used for the design of each of the two joint typologies is presented. Consequently, the design of the joints was performed considering plastic hinge formation in the beam. Further with the bending moment and shear force from the plastic hinge, the components of the joint were designed for the required degree of overstrength.

A summary is made with regard to: design relations of the welded connections, design relations for the capacity of the components, and the stiffness coefficients of the components. In addition, several cases are considered for experimental and numerical validation of the relations for the design capacity of the components. Design flow charts, prepared for each of the two joint typologies, show an overview of the design procedures.

Chapter 7: Conclusions of PhD study. Contributions of author

The last chapter presents the conclusions of the PhD study, as well as the main contributions of the author and dissemination of results.

Annexes

In the annexes, additional information is shown in relation to frame configurations, geometry of the beam-to-column joints, tests on steel samples, calibration of the material model for steel components, and the yielding sequence observed during the tests on beam-to-column joints.

1. INTRODUCTION

1.1. Scope

The aim of the thesis is to observe the behaviour and to characterise in terms of stiffness, capacity and ductility, the seismic performance of welded beam-to-column joints for multi-storey building frames of CFT high strength steel columns and mild carbon steel beams.

1.2. Objectives

The main objectives of the thesis are:

- To propose two connection solutions for beam-to-column joints taking into consideration the welding of members (wide-flange hot rolled beams, and concrete filled rectangular hollow section columns) from different steel grades;
- To evaluate, through experimental and numerical investigations, the seismic performance of beam-to-column joints (including the detailing), particularly considering:
 - Evaluation of the efficiency provided by shot fired nails for the connection between the steel tube and the concrete core;
 - Evaluation of structural performance (resistance, rigidity, ductility) of beam-to-column joints according to the proposed solutions;
 - Identification of the base components of the joints and connections
 - Calibration, based on the experimental tests on joints, of a model for advanced investigation with FE;
 - Extension of the experimental program through numerical simulations;
- Elaboration of a component method approach for design of dual steel IPE beam-to-CFRHS column welded joints.

1.3. Research framework (RFSR-CT-00024 HSS-SERF)

The research framework of the thesis is represented by a European research project of the Research Fund for Coal and Steel RFSR-CT-2009-00024 "High Strength Steel in Seismic Resistant Building Frames". The partnership is composed of two steel producers – RIVA (Italy) and RUUKKI (Finland), two research centres – VTT (Finland) and CPR (Italy), as well as five universities – Univ. Federico II Napoli (Italy), Univ. of Stuttgart (Germany), Univ. of Ljubljana (Slovenia), Univ. of Liege (Belgium) and Univ. „Politehnica“ of Timișoara (Romania).

The main objectives of the research project are:

- To find reliable structural typologies (e.g. moment-resisting frames, concentrically braced frames, eccentrically braced frames) and connection detailing for dual-steel building frames, and to validate them by tests and advanced numerical simulations;

- To develop design criteria and performance based design methodology for dual-steel structures using high strength steel;
- To recommend relevant design parameters (i.e. behaviour factor q , overstrength factor Ω) to be implemented in further versions of the seismic design code (EN 1998-1) in order to apply capacity design approach for dual steel framing typologies;
- To evaluate technical and economical benefit of dual-steel approach involving high strength steel;

The research activities of the research project are divided into several work packages as follows:

WP1 - Selection of structural typologies and design of optimised dual-steel multi-storey frames

The tasks covered by WP1 are related to: selection of structural typologies and pre-design of frames, performance based evaluation and final design of selected frames based on pushover analysis, and design of test specimens for joints.

WP2 - Evaluation of seismic performance of typical dual-steel frame typologies

The tasks covered by WP2 are related to: selection and pre-design of frames for parametrical study (see Fig. 1-1), nonlinear time-history analyses of frames, performance based evaluation of ductility and over-strength demands, and evaluation of q -factors associated with different performance levels.

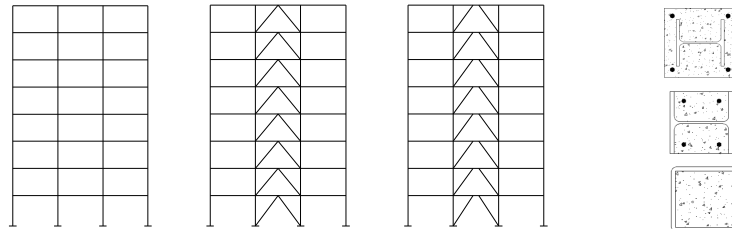


Fig. 1-1. Structural typologies and cross sections for columns [1]

WP3 - Qualification of welding for ductility and strength demands

The tasks covered by WP3 are related to: experimental analysis of weld details and T-stubs (see Fig. 1-2), interpretation and evaluation of results, and specifications for welding procedures to apply in fabrication of joint specimens.

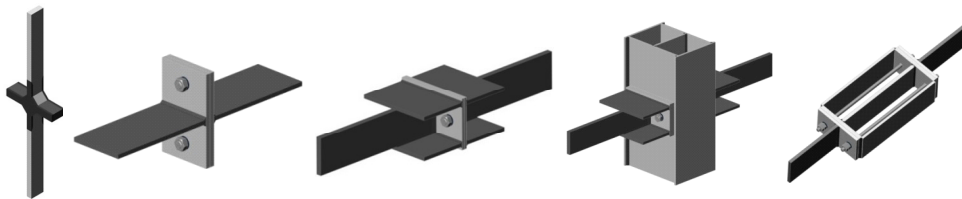


Fig. 1-2. Weld details and T-stub typologies (Univ. Stuttgart) [2]

WP4 - Prequalification tests on bolted beam-to-column joints in moment-resisting dual-steel frames

The tasks covered by WP4 are related to: tests on bolted beam-to-column joints with partially-encased wide-flange columns (Fig. 1-3a), tests on bolted beam-to-column joints with concrete-filled RHS columns (Fig. 1-3bc), and interpretation and evaluation of results.

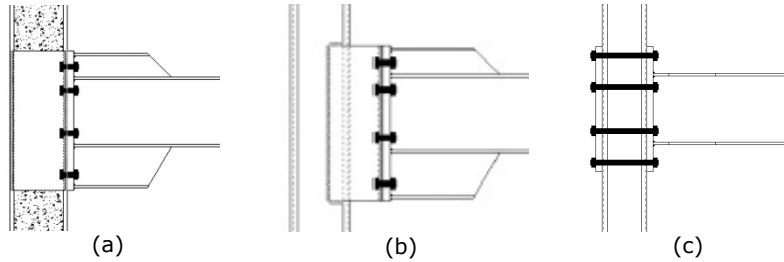


Fig. 1-3. Bolted beam-to-column joint configurations (Univ. Liege) [3]

WP5 - Prequalification tests on welded beam-to-column joints in moment-resisting dual-steel frames

The tasks covered by WP5 are related to: tests on welded stiffened and welded cover plate beam-to-column joints with fully-encased wide-flange columns (see Fig. 1-4a), tests on welded reduced beam section and welded cover plate beam-to-column joints with CFT RHS columns (see Fig. 1-4b), and interpretation and evaluation of results.

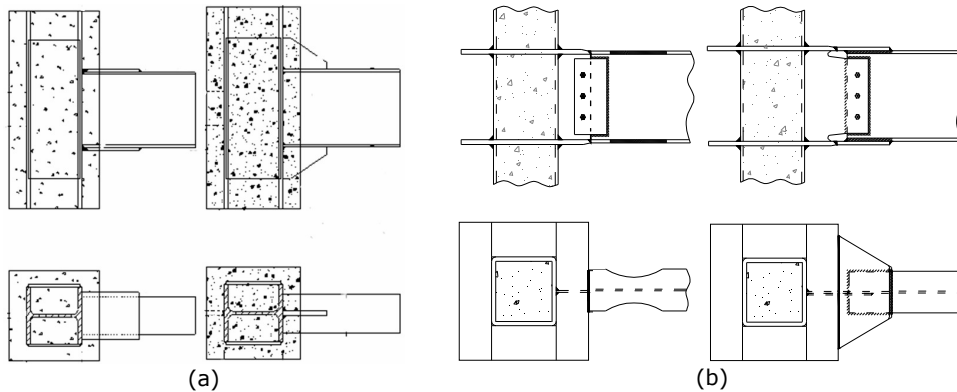


Fig. 1-4. Welded beam-to-column joint configurations: (a) stiffened and cover plate joints with fully-encased wide-flange columns (Univ. Ljubljana) [4], (b) reduced beam section and cover plate joints with CFT RHS columns (Univ. Timisoara) [4]

WP6 - Guidelines for conceptual design and PBD of dual-steel building frames under seismic actions

The tasks covered by WP6 are related to: design and detailing rules for connections and joints, design methodology and criteria for moment-resisting frames, design methodology and criteria for concentrically braced frames, and design methodology and criteria for eccentrically braced frames.

WP7 - Evaluation of technical and economic efficiency of dual-steel structures vs. conventional ones

The tasks covered by WP7 are related to: technical and economic efficiency of moment-resisting frames (study cases), technical and economic efficiency of concentrically braced frames (study cases), and technical and economic efficiency of eccentrically braced frames (study cases).

2. HIGH PERFORMANCE STEELS IN CONSTRUCTION

2.1. Introduction: steel as a construction material

Structural steel has been used in constructions for more than 100 years. The material and its many products have undergone significant changes since through time some of these prompted by demand for higher strength and improved economies of construction, and many caused by developments in joining techniques and fabrication.

The primary characteristics of structural steel include mechanical and chemical properties, metallurgical structures and weldability. In the past, structural engineers have tended to focus only on tensile properties. Since the modulus of elasticity E is constant for all grades of steel, it has rarely been a consideration other than for serviceability issues. Weldability, deformability and ductility were assumed to be adequate for all steels because the design specifications have offered limited specific requirements. In addition, the performance of the material in recent earthquakes raised a number of questions related to the design and fabrication of steel structures. Historically accepted criteria especially connection geometries were questioned. The suitability of the properties as determined by the common uni-axial tension specimen was called into question since several failure modes seemed to demand higher and better defined orthogonal strength characteristics [5].

On this background, significant research activities were undertaken to determine the necessary properties of the steels that would satisfy the requirements for acceptable service under all conditions. These materials, defined by good performance in tensile stress, toughness, weldability, cold forming and corrosion were identified as High Performance Steels (HPS).

The efficiency of steel structural members and connections can in many cases be enhanced by using steels with high values of yield stress and/or tensile strength. These steels named High Strength Steels (HSS) are already used on machine, automotive and aeronautical industries and their use for building industry represents one of the main development directions in the field, and represents a challenge for metallurgic industry, steel fabricators, researchers and designers. Their need in building industry it is motivated by strong casualties (earthquakes, low temperatures, fire and blast actions) inducing high strain rates.

2.2. Carbon steel grades for construction industry

The most common used steels in construction industry are carbon steels or low alloyed steels delivered in the form of hot rolled profiles. The steel grade is defined by the yield limit and ultimate strength. The mechanical characteristics especially the yield limit are differentiated depending on the thickness of the elements.

Steels up to S235 are carbon steels, and are characterised by remarkable plastic characteristics. Steels of type S275 and S355 are low alloyed steels, and

contain, besides carbon, other alloy elements such as manganese, silica, aluminium, and sometimes elements such as vanadium, niobium or titanium in small percentages. Low alloyed steels are characterised by good plastic properties as well.

Chemical composition is rigorously dosed and controlled with the means of avoiding fragile structures in different situation of mounting and exploitation. The maximum carbon concentration varies between 0.17 and 0.25%. The maximum manganese concentration varies between 0.85 and 1.55%, silica is found in insignificant percentages in rimmed steels and in percentages between 0.40 and 0.50% in dead-melted steels or low alloyed steels. Aluminium is found in higher percentages in low alloyed steels of superior quality. Sulphur and phosphorus are found in reduced quantities. Vanadium and titanium have the role of creating a structure with a fine granulation and are found in reduced quantities imposed by weldability conditions.

The differentiation of steels in different quality grades is made by chemical composition and toughness. Toughness, the ability of a material to absorb energy and to develop plastic deformations without fracturing, depends on the chemical composition and on the manufacturing process of the steel.

The most frequently used steels throughout Europe are specified to comply with the European standard EN 10025 [6]. Typical grades are described as 'S275J2' or 'S355K2W'. In these examples, 'S' denotes structural rather than engineering steel; 275 or 355 denotes the yield strength in N/mm²; J2 or K2 denotes the materials toughness by reference to Charpy impact test values; and the 'W' denotes weathering steel. Further letters can be used to designate fine grain steel ('N' or 'NL'); quenched and tempered steel ('Q' or 'QL'); and thermo-mechanically rolled steel ('M' or 'ML').

The normal yield strength grades available are 195, 235, 275, 355, 420, and 460, although some grades are more commonly used than others e.g. in Europe, almost all structural steel is grades S275 and S355.

2.3. High performance steels for construction industry

An overview of structural steels for construction industry is made in Table 2-1. In addition to common steels, high performance and special steels are also available for construction industry. The higher steel grades are available in quenched and tempered material (500, 550, 620, 690, 890 and 960).

Table 2-1 – Structural steels for construction

Common steels for construction industry	High performance steels	Special steels
Carbon steel or low alloyed steels delivered as rolled profiles	Low alloyed steels Thermal treatments	Steels characterised by good resistance, ductility and weldability
S235; S275; S355	HISTAR 460, 690 DILLIMAX 550, 690, 890, 965, 1100	S235, S275, S355 (M, ML) S235, S275, S355 (W)

As shown by Bjorhovde [5], a major element in the development of HPS was the fact that the acceptable response of a building structure is almost always governed by serviceability considerations such as member deflections or building drift (sway). For bridges, this is not the case, since fatigue and fracture criteria

govern many of the design requirements. The building responses are largely controlled by stiffness, as dictated by the modulus of elasticity, end support conditions (for beams), structural systems, and loading conditions. Increasing the uni-axial strength of the material for such structures would neither be sufficient nor effective, and clearly not economical. It was, therefore, decided to focus the attention on materials with better defined strength and welding properties, and to have substantial ductility and toughness to resist the formation and propagation of cracks. Finally, corrosion is a major problem in many geographical areas, especially for structures that will be directly exposed to a range of environmental conditions.

Based on the specific application, high performance steels (HPS) can be classified as follows:

- High strength steels
- Low yield steels
- Tempering and corrosion resistant steels
- Shape memory alloys
- Higher temperature resistant steels
- Lower temperature resistant steels

2.3.1. High strength steels

The development of new high strength steels has been driven by the following reasons [7]:

- Economy: by increasing the strength of steel, the structural section can be reduced; this may reduce the weight of the structure, and subsequently the volume of weld metal → and hence fabrication and erection costs;
- Architecture: the size of structural elements can be reduced enabling special aesthetic and elegant structures, which embed in the environment in an outstanding manner;
- Environment: construction with less steel means also a reduced consumption of resources;
- Safety: modern high strength steel grades do not only show high strength values, special grades combine this strength with excellent toughness properties so that a high safety both in fabrication and application of the structures is applied.

The quenching and tempering process for structural steel grades began in the 1960's. Beside the special heat treatment, the good balance between strength and toughness is based on the fact that these steels are alloyed by adding micro alloying elements (niobium, vanadium, titanium) precipitating as finely distributed carbon nitrides. Today this process enables steel grades with yield strength up to 1100 N/mm², although only grades up to 960 N/mm² yield strength are standardized (EN 10025-6 [8]). These "ultra-high" strength steels are used in the mobile crane industry due to the extraordinary role of light weight for performance. For European classical steel construction (buildings, bridges), the strength is mostly limited to steel grades up to S690.

In the 1970's the thermo mechanical (TM) rolling process was developed and first applied for pipeline plates, but then fast found the way into the fields of ship building and construction of offshore platforms both for plates and rolled sections. Thermo mechanical rolling is a process, in which final deformation is carried out in a certain temperature range leading to material properties, which cannot be achieved by heat treatment alone. The resulting steel grade has high strength as well as high toughness and at the same time a minimum alloying

content resulting in best weldability. Plates with guaranteed minimum yield strength up to 500 N/mm² are available in thickness up to 80 mm used in shipbuilding and offshore construction. For construction steel work even plates of 120 mm have been produced particularly for bridges [9].

Fig. 2-1 shows the historical development of production processes for rolled steel products in Europe.

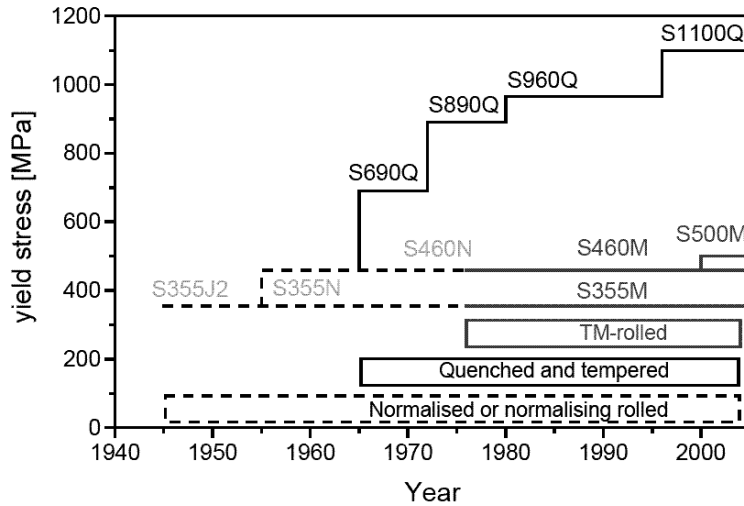


Fig. 2-1. Historical development of production processes for rolled steel products [7]

Table 2-2 presents the strength requirements for high strength steel (HSS) from Europe, United States and Japan.

Table 2-2 – Strength requirements for high strength steel

Region	Steel grade	Minimum yield strength [N/mm ²]	Ultimate tensile strength [N/mm ²]
Europe	S420M	370 - 420	470 - 680
	S460M, Q	400 - 460	500 - 720
	S550Q	490 - 550	590 - 820
	S690Q	630 - 690	710 - 940
	S890Q	830 - 890	880 - 1100
United States	HPS50W	345	485
	HPS70W	485	586 - 760
	HPS100W	690	760 - 895
Japan	SM570, 570W	420 - 460	570 - 720
	HPS485W	485	585 - 760
	BHS500, 500W	500	570
	BHS700W	700	780

The efficiency of structures for buildings designed as steel frames can be improved in certain situations by using steels with higher values of the yield strength and/or ultimate strength. By using steels with higher resistance/weight ratio material savings can be obtained especially in the case of heavy constructions.

Compared to common steels, characterised by yield limit lower or equal than 355 N/mm², high strength steels present higher levels in general between 420 N/mm² and 690 N/mm². It was shown that increasing the strength of steel, the dimension of the cross section can be reduced [10], which leads to a reduction in relation to the weight of the structure, welding volume, and implicitly lower manufacturing and assembling costs (see Fig. 2.5).

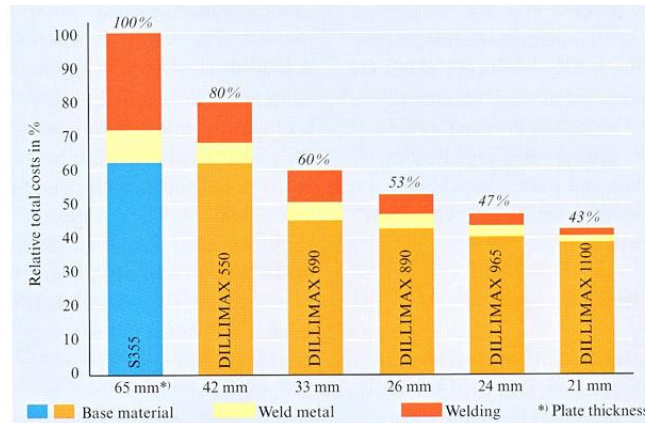


Fig. 2-2. Relative costs in % for S355 and DILLIMAX 550, 690, 890, 965, and 1100 regarding base material, weld, welding, and plate thickness [10]

A comparison between weight and material cost is shown in Fig. 2-3 for a section made of S235, S355 and S460 steel grade, and dimensioned on compression at 4400 kN (left) and 25000 kN (right). Using sections of higher steel grades can lead to reductions in both weight and material costs [11].

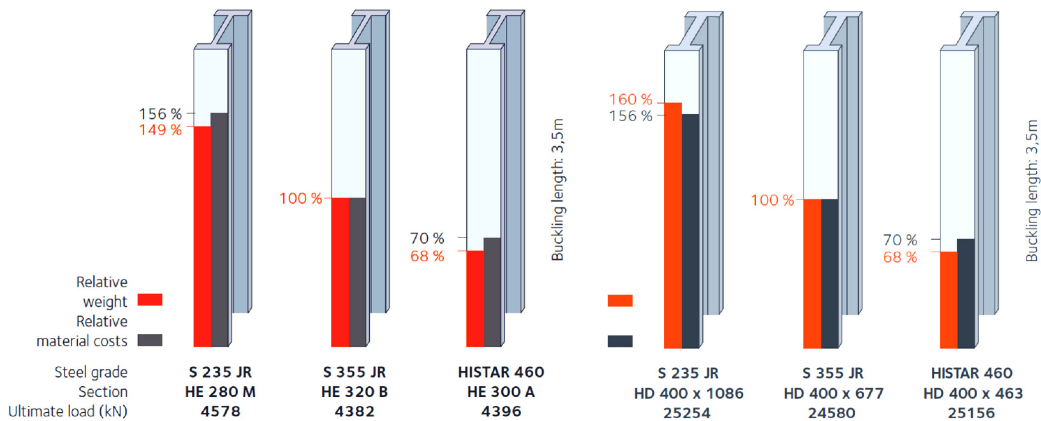


Fig. 2-3. Weight and material cost comparison for a column made of S235, S355 and S460 dimensioned at compression 4400 kN (left) and 25000 kN (right) [11]

High strength steel production

The mechanical properties of steel, such as resistance and ductility, depend on its chemical composition and its microstructure, meaning the displaying pattern

and the chemical composition of the micro crystals that compose the steel. This micro structure depends mainly on:

- chemical composition
- thermal treatment

By increasing the content of alloy elements, an increase in the resistance of steel is obtained, but also a reduction of weldability and ductility. Therefore, if weldable steel is required, the content of alloy elements must be situated between relatively restricted boundaries.

Another solution, to increase the resistance without affecting the ductility and weldability, is to apply thermal treatment and the temperature control during rolling. As a result, a few procedures are used currently for improving the resistance of the steel elements, among which the last two on a larger scale:

- Steel normalizing (N): the strength of normalized steel is mainly given by the alloy elements and not by the microstructure; if an adequate control of the temperature is ensured during rolling, further normalization is not necessary; in the classic manufacturing procedure, the steel is normalized (heated up to 920-930°C and then slowly cooled) in order to improve its mechanical characteristics, especially.

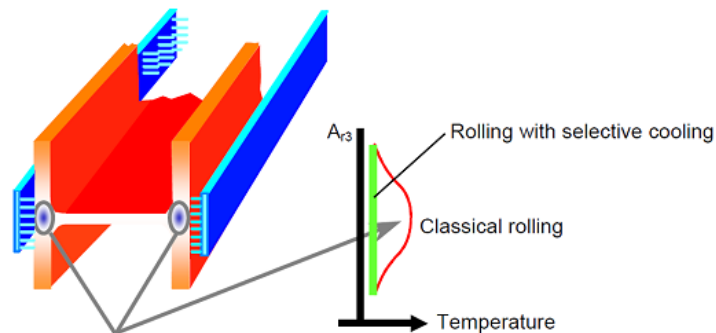


Fig. 2-4. Manufacturing technology of normalized steel profiles [12]

- Thermo-mechanical steels (TM): the resistance of thermo-mechanical steels is mainly given by the microstructure; the alloy content is lower in comparison to normalized steels.
- Hardening thermal treatment followed by regression to high temperature (QST): this is a thermal process in which the steel, after being heated, is rapidly cooled in water (quenching) in order to achieve an increase in strength, then it is heated in order to obtain a finer granulation and a better ductility and weldability; the improvement treatment is applied in most cases to steels with the yield limit between 420 N/mm² and 690 N/mm².

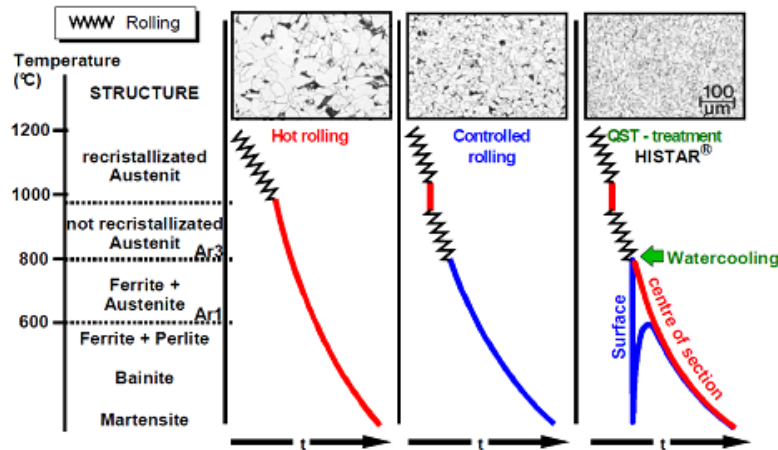


Fig. 2-5. Comparison between the rolling processes [13]

- Quenching and the reheating to high temperature of high strength steels: the improvement consists of two opposite thermal treatments, i.e. quenching and the return to high temperature;

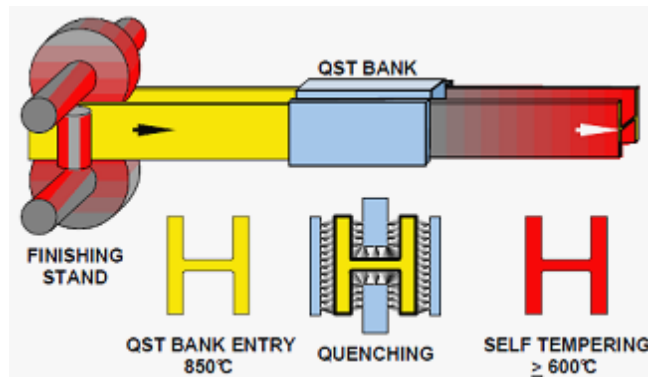


Fig. 2-6. QST process applied on beams in the rolling heat [13]

In the case of steels that have a carbon content of at least 0.3%, quenching consist of heating the metal above curve A. After this, a quick cooling in water (in the case of carbon steels) or oil (in the case of alloy steels) is done, obtaining a fragile martensite structure with very high hardness.

Due to the lack of plastic properties, quenched steel can not be used in steel structures. For this reason it is subjected to a supplementary thermal treatment called reheating, which consist in the heating of the metal at a temperature under the A_1 curve that follows a quick cooling in water or oil.

By reheating, a finer granulation is obtained and also a more uniform distribution of the mechanical properties. The carbon from the martensite diffuses in the ferrite mass and forms iron carbides; by reheating the quenched steel has a lower toughness and tensile strength but the elongation increases.

The mechanical properties of quenched and reheated steel are superior to the steel that is not terminally treated, i.e. the lower the reheating temperature the higher the mechanical resistances, and the elongation smaller.

In steels that have been subjected to quenching and reheating, the value of the yield limit and of the tensile strength is closer together; if for the steels that have not been thermally treated the ratio has values between 0.65 and 0.7, for improved steels this ratio rises to values between 0.8 and 0.9 (sometimes even higher); the ratio is even closer to unit value as the reheating temperature is lower and decreases as these increases.

Due to the fine crystalline and uniform structure obtained by improvement, low alloy improved steels present superior toughness properties compared to low alloy normalized steels, especially in the domain of low temperatures; the elements of low alloy improved steels can be welded considering some special conditions.

Recent developments in the USA lead to the so called Advanced High Strength Steels (AHSS) and Ultra High Strength High Toughness Steels, characterised by tensile strengths of $f_u > 1000 \text{ N/mm}^2$, designed for the automobile industry, having the form of thin sheets. From here to the cold formed thin wall profiles for construction industry is not a long way. Furthermore, the G550 steel ($f_y = 550 \text{ N/mm}^2$) is currently used in Australia to produce profiles (C and U shapes) with 0.4-0.9 mm thickness, that are used for houses with steel structure.

In Europe, hot rolled profiles (IPE, HEA, HEB, and HEM) are produced also from S460 steel grade. HISTAR 460 manufactured by ArcelorMittal is characterized, besides the properties shown in Table 2-3, by a very good resilience at low temperatures (45J at 0°C and 40J at -20°C).

Table 2-3 – Minimal material properties of some high strength steels [15]

Steel grade		Source	Yield limit, f_y , [N/mm ²]	Tensile strength, f_u , [N/mm ²]	Elongation
Bisplate	60	Australia	500	590-730	20%
	70		600	690-830	20%
	80		690	790-930	18%
HT690	70	Japan	590	690	----
HT780	80		685	780	----
ROT	601	UK	620	690-850	----
	701	(CORUS)	690	790-930	----
HPS	485W	USA	485	-	----
A514		USA	620-690	690-895	16-18%
S460		Europe	430-460	530-720	17%
HISTAR 460		(Arcelor)	450-460	550-720	17%

2.3.2. Low yield steels

High performance steels can be also characterised by a reduced yield limit and a high plastic deformation capacity. In Japan there are ongoing studies regarding the combination in the same structure of high strength steels (structural members that are mainly designed to work in the elastic domain), and steels with reduced yield limit (dissipative structural members) [14]. Table 2-4 summarises the high performance steels of booth categories, produced by JFE Steel Corporation in Japan (<http://www.jfe-steel.co.jp/en/>).

Table 2-4 – High performance steel with earthquake resistance for building structures [16]

Grade	Characteristics	Product description
HBL 325 HBL 355 HBL 385	High yield limit and reduced yield ratio (ratio between the yield limit and the tensile strength) made by TMCP	HBL325, 355 has a higher yield limit than JIS Standard for thicknesses between 40 and 100 mm, is authorized by the Land, Infrastructure and Transport Ministry, a high plastic deformation capacity due to a low yielding ratio. JFE Steel has developed a steel grade with an even higher yield limit: HBL385.
SA440 SA440U	High resistance, with a tensile strength of min. 590 N/mm ² , a reduced yield ratio, high toughness and weldability	SA440U is the steel with the yield limit of 590 N/mm ² that allows for drastic reduction of pre-heating before welding in comparison to the conventional SA440.
HBL 325FR HBL 355FR	Steel with improved fire resistance; guaranteed resistance to high temperatures.	In accordance to JIS G3106 and G3136 with regards to ambient temperature and it guarantees a yielding limit at 600°C higher by 2/3 from the characteristic one
JFE-LY 100 JFE-LY 160 JFE-LY 225	Reduced yield limit with an excellent deformation capacity for applications in dissipative elements.	Possesses an extremely low yield limit, for the use in dissipative elements with a high capacity of energy dissipation. Three levels of the yielding limit can be selected.

A particular application of steel grades with reduced yield limit is related to steel dampers. The steel dampers are composed of steel as the damping material to absorb the seismic energy using its plastic deformation. For the usage as damping material, the steel has to be furnished with narrow dispersion of yield strength and large elongation capacity. For this reason, special steels for the steel damper, named low yield-point steels (LY100 and LY225) with improved mechanical properties have been developed in Japan [17][18], and have recently become the main steel products for this application [19].

2.3.3. Corrosion resistant steels

Corrosion resistant steel, also named weathering steel, is a low alloy steel containing small amounts of corrosion resistant elements such as Cu, Cr and Ni. These types of steel alloys were developed to eliminate the need for painting and thus reducing the costs related to maintenance and assuring a long service life [20].

Due to its chemical compositions, unprotected weathering steel [21], exhibits increased resistance to atmospheric corrosion compared to unalloyed steels. A protective layer forms on its surface under the influence of the weather. The corrosion retarding effect of the protective layer is produced by the nature of its structure components and the particular distribution and concentration of alloying elements in it. The protective layer of the surface develops and regenerates continuously when subjected to the influence of the weather. Formation, duration of development and protective effect of the covering layer on weathering steels depend largely upon the corrosive character of the atmosphere. Its influence varies and depends mainly upon general weather condition (e.g. continental) macroclimate (e.g. industrial, urban, maritime or countryside climate) and the orientation of the structure components (e.g. exposed to or shaded from the weather, vertical or horizontal position). The amount of aggressive agents in the air has to be taken into account. In general the covering layer offers protection against atmospheric corrosion in industrial, urban and countryside climate. When utilising this steel in unprotected condition it is up to the designer to take into account the expected loss

of thickness due to corrosion and as far as necessary, compensate for it by increasing the thickness of the material. In case of particular air pollution by aggressive agents conventional surface protection is recommended.

2.3.4. Shape memory alloy

A shape-memory alloy (SMA) is an alloy that has the ability to recover its pre-deformed shape when exposed to heat. Due to their properties SMA's have found increasing applications in many areas. Recently, research efforts have been extended to using SMA for control of civil structures. Application examples of SMA were shown in [22]:

- SMA's for passive structural control:
 - SMA isolation devices;
 - SMA energy dissipation devices (SMA braces and damping elements for bridges, Structural reinforcement for earthquake retrofit;
- Shape restoration using super-elastic SMA's;
- SMA's for active structural frequency tuning;
- SMA's for structural self-rehabilitation.

2.3.5. Higher temperature resistant steels

In the construction of fire-resistant buildings, it is required that the columns, beams and other main structural members conform to certain fire proving specifications, or that the corresponding fire resistance be confirmed through calculations. As the temperature rises the strength of steel decreases. Therefore, an approach that is used to satisfy certain fire proving specifications is to provide fire protection that will keep the temperature of the steel below 350°C. Another solution is to use fire-resistant steel, which is able to keep a high value of the yield strength when subjected to elevated temperatures up to 600°C [23]. This property of fire-resistant steel is due to appropriate additions of alloying elements such as Mo, Nb and Cr and because of strict control of the heat-treatment processing conditions. The performance and elevated-temperature properties of fire-resistant steel were confirmed by experimental tests conducted at elevated temperatures on columns, beams and other structural members [24].

2.3.6. Lower temperature resistant steels

Carbon and alloy grades for low-temperature service are required to provide the high strength, ductility, and toughness in vehicles, vessels, and structures that must serve at -45°C and lower. Other alloy steels are suitable for service in the low-temperature range. The steels A201 and T-1 can suffice to -45°C, nickel steels with 2.25% Ni can suffice to -59°C, and nickel steels with 3.5% Ni to -101°C.

2.4. Steels for seismic resistant structures

In the construction industry, high strength steels are required for structures with high dimensions and loads, multi-storey buildings, bridges, marine platforms, and structures subjected to: severe loads, high intensity earthquakes, powerful winds, explosions, great live loads, and impact forces. The hybrid beams, used for bridge building, that are manufactured with flanges of high strength steel and with web of steel with lower resistance, have already proven their efficiency in both technical and economical performance [25]. These types of beams can be used with

success not only for bridges, but also for other type of structures with large spans. Another application is related to the pipe lattice beams or profiles with flanges from HSS and diagonals and posts from regular carbon steel.

As shown in previous paragraphs, "thermo-mechanical steels" possess high mechanical resistances, a good toughness, strength to fatigue, resistance to corrosion and weldability. Concerning the required properties for applications in multi-storey buildings and bridges, these can be synthesized as follows [26]:

- High resistances and a reduced ratio between the yield limit and tensile strength associated with big elongations at failure (>15%), in order to allow post elastic deformations in case of structures subjected to seismic action;
- The reduced variation of the yield limit in order to ensure the consecutive appearance of the plastic hinges foreseen in the analysis, respectively a relatively constant level of the yield limit in structural elements;
- A higher elasticity modulus than for normal steels (experimentally proven) with the aim to increase the rigidity, reduce of deformations, increase the stability and limit the IInd order effects.

The use of high strength steel for seismic resistant structures could be done considering two approaches:

- One solution is related to dual-steel structures in which the dissipative members are realised from mild carbon steel (ductile steel), while the nondissipative members are realised from high strength steel; examples of application depending on the height of the building are:
 - For big heights (>P+10E), dual frames that combine un-braced spans with braced spans (dissipative braces, or panels from steel with low yield limit); there are incipient applications in Japan [14];
 - For medium heights (<P+10E), un-braced frames, with columns with mixed section – steel (HSS) and concrete, partially embedded in concrete, with controlled dissipation through reduced beam section (RBS) and/or web panels of columns;
- The other solution is to use high strength steel for both: dissipative and nondissipative members; for example, the S460 steel grade is characterised by a certain amount of ductility which makes it possible to be used for structures of medium ductility class (DCM).

2.5. Design criteria for choice of steels for seismic resistant structures

2.5.1. Code provisions

According to the current seismic design code EN 1998-1 [27], the structural steel aimed for buildings in seismic regions shall conform to standards referred to in the design code of steel structures EN 1993-1-1 [28], which is limited to steel grades S235 up to S460. According to the design code of steel structures [28], the steel grades should satisfy some requirements related to the minimum ductility expressed in terms of limits:

- $f_u/f_y \geq 1.10$;
- elongation at failure not less than 15%;
- $\epsilon_u \geq 15\epsilon_y$, where ϵ_y is the yield strain ($\epsilon_y = f_y/E$).

According to the seismic design code EN 1998-1 [27], the distribution of material properties in the structure, such as yield strength and toughness shall be

such that the development of dissipative zones occur as intended in the design. This requirement may be satisfied if the yield strength of the steel from dissipative zones and the design of the structure conform to one of the following conditions:

- the actual maximum yield strength $f_{y,max}$ of the steel from the dissipative zones satisfies the following expression $f_{y,max} \leq 1,1\gamma_{ov}f_y$;
- the design of the structure is made on the basis of a single grade and nominal yield strength f_y for the steels both in dissipative and non dissipative zones; an upper value $f_{y,max}$ is specified for the steel of dissipative zones; the nominal value f_y of the steels specified for non dissipative zones and connections exceeds the upper value of the yield strength $f_{y,max}$ of dissipative zones;
- the actual yield strength $f_{y,act}$ of the steel of each dissipative zone is determined from measurements and the overstrength factor is computed for each dissipative zone as $\gamma_{ov,act}=f_{y,act}/f_y$, where f_y is the nominal yield strength of the steel from the dissipative zones.

2.5.2. Choice of steel for seismic resistant structures

The design rules for steel structures in EN 1993-1-1 [28] are based on evaluation of experimental tests carried out at room temperature – conditions under which the steel is in general characterised by a ductile failure mode. The brittle failure mode that may occur at low temperatures is excluded from these rules by an appropriate choice of material according to its toughness properties specified in EN 1993-1-10 [29]. These specifications are based on fracture tests carried out on representative test specimens at low temperatures.

For the identification of the upper-shelf toughness and the temperature to which the upper shelf toughness is extended, an international research project, "Plastotough" [30], was launched with the aim to develop tools for deriving toughness demands for plastic design according to EN 1993-1-1 [28] and design of seismic resistant structures according to EN 1998-1 [27].

Tools for choice of material to avoid brittle fracture for monotonic loading and for seismic loading were evaluated, considering materials such as S355J2 and S460M steel grades as part of two different hot rolled profiles i.e. IPE 500 and HEA 300. It was observed that a correlation is available i.e. the EricksonKirk correlation [31] which is related to the T_{k100} -value and the T_{US} -value, and which is limited to homogenous pressure vessel steels and naval ship building steels with high upper-self toughness values.

The EricksonKirk correlation was checked for the mentioned hot rolled sections, and it was observed that the steels comply with the correlation. In addition, from the investigation of plates (S355J2, S460N, S690QL) for built up sections, it was revealed that correlations were not homogenous (some plates comply, i.e. S690QL, others not, i.e. S355J2 and S460N).

The main conclusions of the project in relation to the choice of steel for seismic resistant structures showed that:

- Steels from rolled sections fulfilled the EricksonKirk correlation and that it is sufficient to apply full plastic design;
- Considering the plates for built up sections, the EricksonKirk correlation is not automatically fulfilled; additional quality specifications are necessary;
- Ordering of steel should refer to the quality level of the steels needed to comply with the EricksonKirk correlation;
- Material properties for seismic design:

- Both by fracture mechanics and by damage mechanics it was proven in the project that for steel qualities, i.e. S355J2 and S460M as part of IPE500 and HEA300 profiles, the values of upper shelf Charpy-impact energy and the maximum strain resistance are sufficient to allow full plastic design with local notch effect and global plastic rotations;
- For studied steel qualities, i.e. S355J2 and S460M as part of IPE500 and HEA300, ultra-low-cycle fatigue is not a problem that could limit the use of behaviour factor q , provided that a useful limitation of the inter-storey drift (3.5%) has been used to define the q -factor;
- The key to a safe application of plastic design for monotonic or seismic loading is the toughness quality of the steels, that should be by far higher than the minimum requirements from EN 10025 [6];
- To guarantee the properties of steels (complying with the EricksonKirk correlation) the steel producers should market these steels with a specific name (e.g. seismic resistant steels) or an option should be included in the EN 10025 standards [6] [8] that specifies the minimum properties complying with the EricksonKirk correlation.

2.6. Examples of application

AFPC/OTUA (1997) [32] presented a remarkable number of applications in Europe for bridges and marine platforms, which were realised using members of S420, S450 and S460 steel grades. The applications in buildings are more reduced:

- MAPFRE tower from Barcelona (see Fig. 2-7a), having 42 floors and 150 m, H columns were made of S460M steel grade, resulting a 24% weight reduction compared to the solution with S355;
- Europe Tower in Madrid (see Fig. 2-7b), having 26 floors and an inclination of 15° - has all its structural elements made of S460M steel grade;
- Pleiade Towers in Brussels (see Fig. 2-7c), with columns of S460N, which lead to a 20% economy compared to the solution with S355J0 steel grade;
- Conference centres "Espace Leopold" (see Fig. 2-7d) at the European Parliament in Brussels, with columns of S420M and beams of S355.

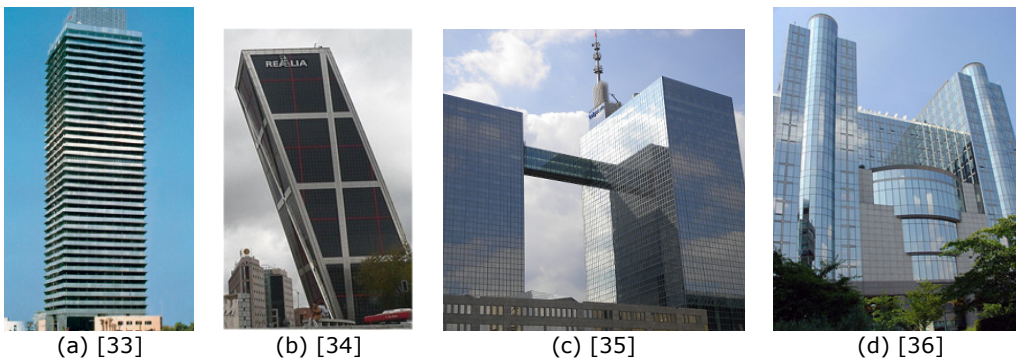


Fig. 2-7. Examples of application in Europe

Example of application from other parts of the world (i.e. Japan, China, Australia, US) include the following:

- Grosvenor Place in Sydney (Australia) see Fig. 2-8a, with a number of 50 storeys, completed in 1988, was realised with columns of S690 steel grade;
- Central Park in Perth (Australia) see Fig. 2-8b, with a number of 50 storeys, completed in 1989, was realised with columns of S690 steel sections encased in concrete;
- Latitude Tower in Sydney (Australia) see Fig. 2-8c, with a number of 55 storeys, completed in 2005, was realised with columns of S690 steel hollow sections filled with concrete;
- World Financial Centre in Shanghai (China) see Fig. 2-8d, with a number of 101 storeys, completed in 2008, was realised with structural elements of S460M steel grade;
- Yokohama Landmark Tower in Yokohama (Japan) see Fig. 2-8e, with a number of 70 storeys, completed in 1993, was realised with columns of SA440 steel grade;
- JR East Head Office Building in Tokyo (Japan) see Fig. 2-8f, with a number of 28 storeys, completed in 1997, was realised with columns and girders of SA440 steel grade;
- Roppongi Hills Mori Tower in Tokyo (Japan) see Fig. 2-8g, with 54 storeys, completed in 2003, was realised with SA440 steel grade columns;
- Freedom Tower in New York (US) see Fig. 2-8h, with a number of 104 storeys, completion date 2013, is realised with columns of ASTM A572 Gr. 65 TM (characterised by a minimum yield point of 450 N/mm²).

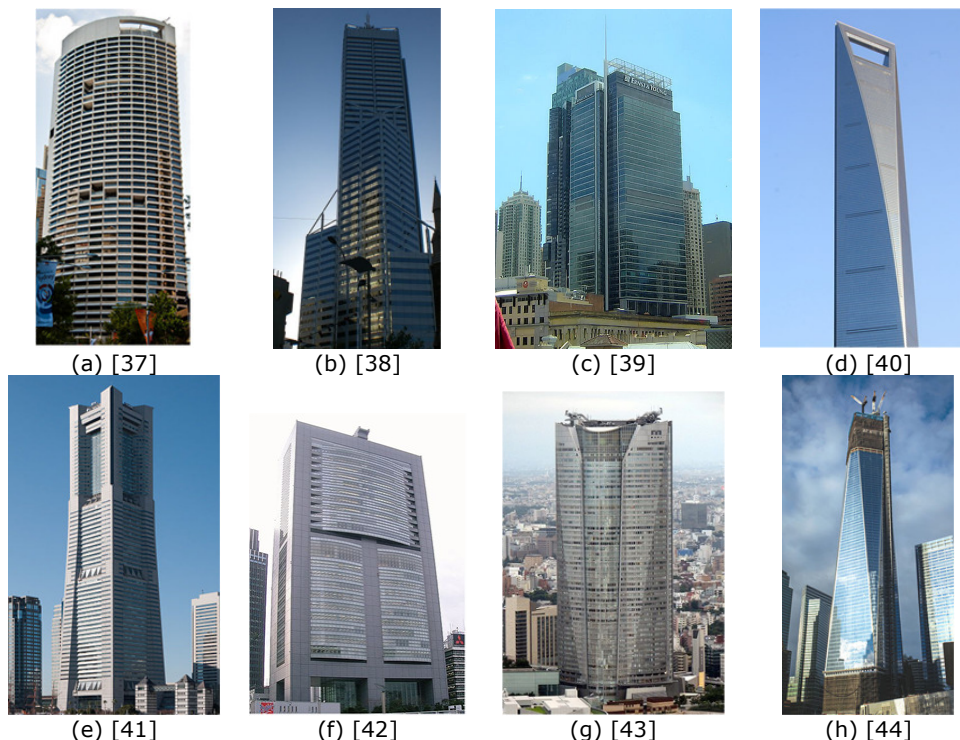


Fig. 2-8. Example of applications – other parts of the world

2.7. Concluding remarks

In the current chapter, a brief introduction was made with regard to steel as a construction material. Used in constructions for more than 100 years, steel has undergone significant changes throughout time - some of these were prompted by demand for higher strength and improved economies of construction, and many caused by developments in joining techniques and fabrication.

On this background, significant research activities were undertaken to determine the necessary properties of the steels that would satisfy the requirements for acceptable service under all conditions. These materials, defined by good performance in tensile stress, toughness, weldability, cold forming and corrosion were identified as High Performance Steels (HPS) and cover the following:

- High strength steels;
- Low yield steels;
- Corrosion resistant steels;
- Shape memory alloy;
- Higher temperature resistant steels;
- Lower temperature resistant steels;

The most common used steels in construction industry are carbon steels or low alloyed steels delivered as hot rolled profiles. In Europe, almost all structural steel is realised from S275 and S355 steel grades. In addition to common steels, high performance and special steels are available for construction industry as well. The higher steel grades are available in quenched and tempered material (500, 550, 620, 690, 890 and 960). In Europe, hot rolled profiles (IPE, HEA, HEB, and HEM) are produced also from S460 steel grade. HISTAR 460 manufactured by ArcelorMittal is characterized also by a very good resilience at low temperatures (45J at 0°C and 40J at -20°C).

By using steels with higher resistance/weight ratio material savings can be obtained especially in the case of heavy constructions. Compared to common steels, characterised by yield limit lower or equal than 355 N/mm², high strength steels present higher levels in general between 420 N/mm² and 690 N/mm². By increasing the strength of steel, the dimension of the cross section can be reduced, which leads to a reduction in relation to the weight of the structure, welding volume, and implicitly lower manufacturing and assembling costs.

The use of High Strength Steels (HSS) for building industry is one of the main development directions in the field, and represents a challenge for metallurgic industry, steel fabricators, researchers and designers. Their need in building industry it is motivated by strong actions (earthquakes, low temperatures, fire and blast actions) inducing high strain rates.

The use of high strength steel within seismic resistant structures could be performed considering two approaches, namely:

- Structures realised according to the dual-steel concept - in which the dissipative members are realised from mild carbon steel (ductile steel), and the nondissipative members are realised from high strength steel;
- Structures realised from high strength steel; for example, the S460 steel grade is characterised by a certain amount of ductility which makes it possible to be used for structures of medium ductility class.

Some aspects were presented in relation to the design criteria for choice of steels for seismic resistant structures, i.e. requirements from current code provisions, and recommendations on choice of steel for seismic resistant structures.

According to the current seismic design code EN 1998-1 [27], the structural steel aimed for buildings in seismic regions shall conform to standards referred to in the design code of steel structures EN 1993-1-1 [28], which is however limited to steel grades S235 up to S460. The distribution of material properties in the structure according to the seismic design code EN 1998-1 [27], such as yield strength and toughness shall be such that the development of dissipative zones occur as intended in the design.

In relation to the recommendations on choice of steel for seismic resistant structures, as part of "Plastotough" research project [30], it was shown that the key to a safe application of plastic design for monotonic or seismic loading is the toughness quality of the steels, that according to usual practice should be by far higher than the minimum requirements specified in EN 10025 [6]. Both by fracture mechanics and by damage mechanics it was proven in the project that for steel qualities, i.e. S355J2 and S460M as part of IPE500 and HEA300, the values of upper shelf Charpy-impact energy and the maximum strain resistance were sufficient to allow full plastic design with local notch effect and global plastic rotations. To guarantee the properties of steels (complying with the EricksonKirk correlation [31]) the steel producers should market these steels with a specific name (e.g. seismic resistant steels) or an option should be included in EN 10025 [6] [8] that specifies the minimum properties complying with the EricksonKirk correlation. Ordering of steel should refer to the quality level of the steels needed to comply with the EricksonKirk correlation.

Finally, some application examples were shown related to the use of high strength steels in construction industry, particularly to high rise buildings from Japan, China, Australia, US, and from Europe.

3. TUBULAR STRUCTURES FOR BUILDINGS

3.1. Introduction

Many examples in nature show the excellent properties of the tubular shape with regard to loading in compression, torsion and bending in all directions. These excellent properties are combined with an attractive shape for architectural applications. Furthermore, the closed shape without sharp corners reduces the area to be protected and extends the corrosion protection life [45].

Another aspect which is favourable especially for circular hollow sections is the lower drag coefficients if exposed to wind or water forces. The internal void can be used in various ways, e.g. to increase the bearing resistance by filling with concrete or to provide fire protection. Although the manufacturing costs of hollow sections are higher than for other sections, leading to higher unit material cost, economical applications are achieved in many fields. The application field covers all areas, e.g. architectural, civil, offshore, mechanical, chemical, aeronautical, transport, agriculture and other special fields.

As part of a multi-storey frame, i.e. MRF, CBF or EBF, tubular section elements can be used as conventional braces (circular, square), to the manufacturing of buckling restrained braces, but also as columns (circular, square) without infill or with concrete inside (concrete filled tubes – CFT). In spite of the advantages of the tubular sections, a special attention needs to be paid to the connections between beams and columns. The framing system with concrete filled columns and welded joints has been studied and applied on a large scale in Asia, Australia and America. In contrast, this solution was used at a lower scale in Europe.


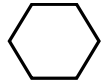
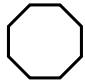



3.2. Tubular steel sections for construction industry

Geometry vs. fabrication technology

The tubular steel sections can be produced as hot finished or cold formed hollow sections with a wide variety of cross sections as can be seen in Table 3-1. However, the most frequently used tubular steel sections in the construction industry are:

- circular hollow sections (CHS)
- rectangular hollow sections (RHS)

Table 3-1 – Special shapes [45]

triangular	hexagonal	octagonal	flat-oval	elliptical	half-elliptical
					

The manufacturing process of tubular hollow sections is illustrated in Fig. 3-1 and Fig. 3-2. Consequently, two methods are shown [46], i.e. roll forming, and press forming.

The manufacturing processes of hot finished and cold formed hollow sections are very different [47]. Hot finished hollow sections are formed at normalising temperature (approx 900°C). Cold formed hollow sections are formed at ambient temperature. This results in several key differences. The main difference is that hot finished hollow sections pass through a furnace and have a much tighter corner profile as a result of the metal flow during the forming process. Cold formed, on the other hand, exhibit a high degree of cold working in the corner regions during the forming process. This means that they could be susceptible to corner cracking if manufactured with tight radius corners. Therefore, the cold formed sections are characterised by a larger radius.

After the tubular hollow section is roll or press-formed, a longitudinal weld is performed by electrical resistance welding processes or with an induction welding process. The edges are heated, e.g. by electrical resistance, and then the rollers push the edges together, resulting in a pressure weld. The outer part of the weld is trimmed immediately after welding [45].

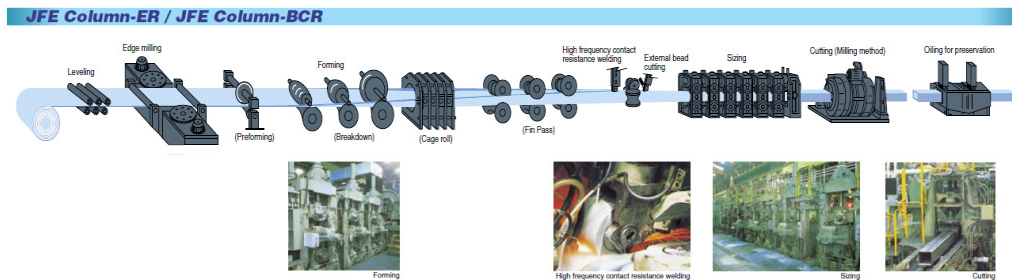


Fig. 3-1. Roll-forming method [47]

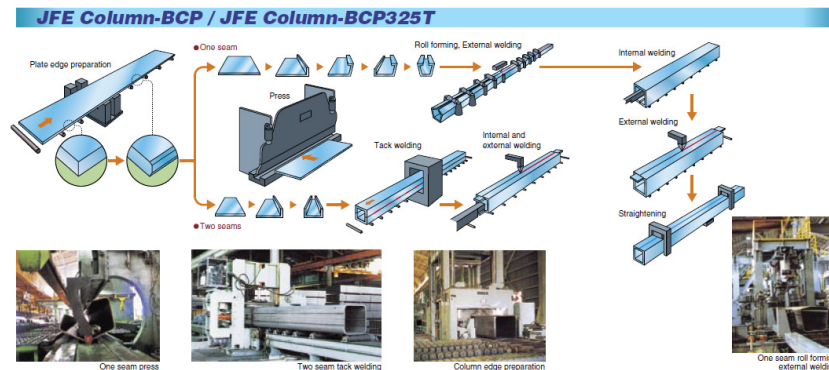


Fig. 3-2. Press-forming method [47]

Mechanical properties

Hollow sections are made of similar steel as used for other steel sections, thus in principle there is no difference. Hollow sections can also be produced in special steels, e.g. high strength steel with yield strengths up to 690 N/mm² or higher, but also as weathering steels and steel with improved or special chemical compositions [45]. In the case of thick walled sections, the strength and ductility in the thickness direction should be sufficient to avoid cracking, also named lamellar tearing. In most of the structural steel specifications, the yield strength, ultimate

tensile strength, elongation, and in some situations also the Charpy V-notch values, are specified. Another aspect is the effect of cold forming on the mechanical properties of the parent steel. In the case of cold forming of hollow sections, the yield strength and the ultimate tensile strength are increased, especially in the corners.

3.3. Joining steel tubes in framed structures: connecting technology & detailing

Framed structures for buildings, consist of a three dimensional assemblage of horizontal beams and vertical columns on a rectangular grid. The beams support floor slabs, which span in one direction only, from beam to beam.

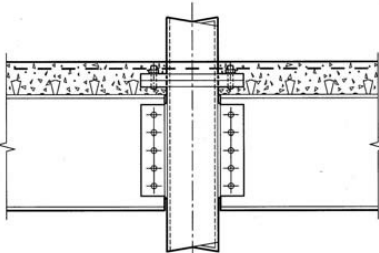
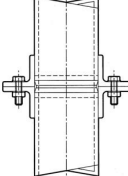
At each intersection between beams and columns, the columns are usually continuous and the beams are attached to their external faces by connections. The connections can be realised as pinned, semi-rigid or rigid joints.

Columns realised from steel hollow sections can be filled with concrete with the aim to combine the properties of the two materials. Therefore, this type of member combines aesthetic appearance with favourable structural properties including stiffness, capacity and ductility, as well as enhanced fire resistance in comparison with bare steel configurations and are becoming increasingly used in multi-storey and tall buildings. A particular advantage of using a composite column is the reduction in column cross-sectional area, and by using steel tubes as permanent formwork, construction speed is increased. Because of the inherently high fire resistance of concrete filled columns, fire protection of steel is in many cases not necessary and the steel can be exposed to achieve attractive appearance.

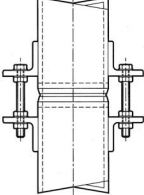
Column Splices and Flange plate connections

Column splices are generally made either by butt-welding lengths together, or by providing bolted flange connections at the ends of column lengths [48]. Some common examples of these connections are shown in Table 3-2.

Table 3-2 – Column splice connections [48]

	<p>Flange plate connection</p> <p>Section through floor with flange plates on RHS or CHS columns cast into concrete slab. The bottom plate has projecting studs welded to it; for flange plates connected above the slab, in a raised floor space, a normal bolting arrangement may be used. In general, the flange plate connection provides transfer of axial forces but only limited moment transfer.</p>
	<p>Welded splice connection</p> <p>Elevation on RHS column with weld backing strip and angle brackets for erection; brackets are removed after some welding completed; backing strip also used as alignment spigot. For CHS Columns, vertical plates are used instead of brackets.</p>

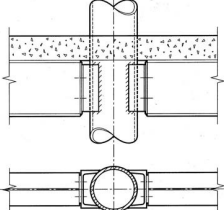
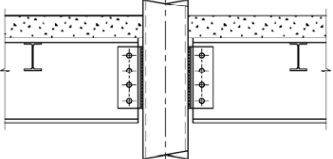
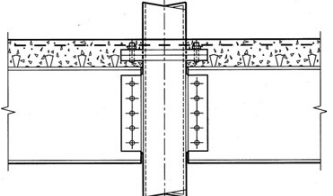
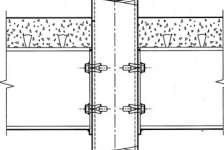
3.3. Joining steel tubes in framed structures: connecting technology & detailing 51

	<p>Welded splice connection with long bolts</p> <p>The use of long bolts with double nuts permits accurate alignment of the SHS and backing material before site welding.</p>
---	---

Beam-to-column connections

Simple connections are normally assumed to give vertical support but to provide only limited restraint against rotation: these connections are assumed to be able to rotate without damage. A selection of some common examples is shown in Table 3-3.

Table 3-3 – Common examples of simple connections [48]

	<p>Reverse channel connection</p> <p>Steel beams are connected to CHS columns by a channel fixing; a standard flexible end plate is normal at the beam end, which then develops only nominal moments. A similar detail is used for RHS columns.</p>
	<p>Web cleat connection</p> <p>Beams are connected to RHS columns by a T-section web cleat; this connection can have greater stiffness and robustness than the equivalent fin plate connection.</p>
	<p>Fin plate/shear tab connection</p> <p>Beams connected to RHS or CHS column by a fin-plate; a very economic joint; a seating cleat may be used to help erection, with removal afterwards if required.</p>
	<p>Hollbolt or Flowdrill connection</p> <p>Beams are connected to face of RHS column by hollbolts or fully threaded bolts in flow-drill holes; only nominal moments develop with flush or partial depth flexible end plates.</p>

The most common arrangements for beam-to-column joints make use of bolted connections via attachments welded to the faces of the hollow section column. By far the most common connection of this type is the fin plate connection, using a flat plate welded to each column face. For RHS columns, an alternative is the web cleat connection, using single angle sections, or T-sections, welded to the column face. The use of double angles is a further option and provides greater

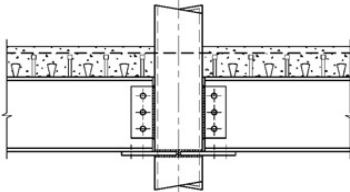
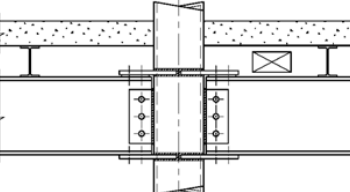
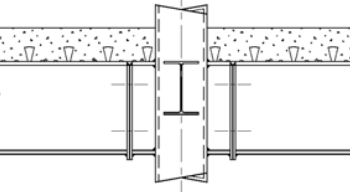
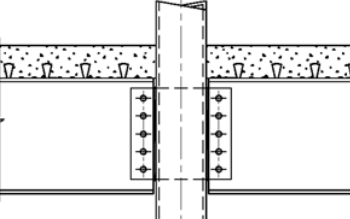
capacity than a single angle would. An increasingly popular option for CHS or RHS columns is the use of the reverse channel connection. Of these, the most economic is the fin plate connection or the web cleat connection using a single angle.

Simple steel connections using flexible end plates or double angle cleats, which are bolted direct to the column, are also possible with RHS columns. These joints use either expanding bolt types, such as Hollobolt, or fully threaded bolts in tapped holes produced by the Flowdrill system.

Moment connections are those that are assumed to give vertical support, to provide a degree of restraint against rotation and to develop some moment capacity. A selection of some common examples is shown in Table 3-4.

Rigid or semi-rigid moment connections are feasible with all types of hollow section columns. These may use flange plates or beam stubs, which are usually of the same section as the beam being connected. Through-plated connections are another popular type of moment connection; this is similar in appearance to the fin plate connection but has slots in the column to allow a single plate to be taken through it. In almost all cases, moment connections are more expensive than simple connections, but the extra cost of the connection can be more than offset by savings in beam sizes, or by provision of more usable floor space.

Table 3-4 – Common examples of moment connections [48]

	<p>Composite beam moment connection</p> <p>Composite beams are connected to RHS or CHS columns by fin plates and bottom flange plate to provide continuous or semi-continuous joints; the top reinforcement in the concrete slab is designed to provide the other arm of the moment couple.</p>
	<p>Steel beam moment connection</p> <p>Beams are connected to RHS or CHS columns by fin plates and flange plates to provide continuous or semi-continuous joints.</p>
	<p>Stub connection</p> <p>Beam sections welded to face of RHS columns; moment capacity usually limited by yielding of column face; large moments require internal diaphragms or external flange plates.</p>
	<p>Through-plate connection</p> <p>Through-plate passed through slots and welded to each face of RHS or CHS column; the through plate connection allows significant axial forces and bending moments to be transferred from the beam, if this is required.</p>

3.4. Code provisions

Different methods for joining steel tubes in framed structures are available. Based on EN 1993-1-8 [49], joints can be characterised by stiffness and by strength. Therefore, considering the stiffness criteria, joints can be pinned, semi-rigid and rigid, and considering the strength criteria, joints can be pinned, partial-strength and full-strength. Depending on the connecting technology, joints can be realised in bolted solution or in welded solution. Considering the typology of the members that are connected together, the connections can be realised between circular hollow sections (CHS), between rectangular hollow sections (RHS), and between hollow sections and open sections.

According to EN 1998-1 [27], moment resisting frames shall be designed so that plastic hinges form in the beams or in the connections of the beams to the columns, but not in the columns. This requirement is waived at the base of the frame, at the top level of multi-storey buildings and for single storey buildings.

The interest within the current research is related to full strength welded I beam-to-CFRHS column joints for moment resisting frames (MRF) and moment resisting bays of dual frames (MRF+CBF, and MRF+EBF), for which the connections are not intended to suffer plastic deformations.

With the above considerations, according to the seismic design code EN 1998-1 [27], the following specifications should be fulfilled:

- The connections of the beams to the columns should be designed for the required degree of overstrength taking into account the moment of resistance $M_{pl,Rd}$ and the shear force $(V_{Ed,G} + V_{Ed,M})$;
- The connection design should be such that the rotation capacity of the plastic hinge region θ_p is not less than 35 mrad for structures of ductility class DCH, and 25 mrad for structures of ductility class DCM with $q > 2$;
- The rotation capacity of the plastic hinge region θ_p should be ensured under cyclic loading without degradation of strength and stiffness upper than 20%;
- In experiments made to assess θ_p the column web panel shear resistance should conform to eq. (3.1) and the column web panel shear deformation should not contribute more than 30% of the plastic rotation capability θ_p ;

$$\frac{V_{wp,Ed}}{V_{wp,Rd}} \leq 1.0 \quad (3.1)$$

The code for the design of joints EN 1993-1-8 [49] defines the *joint* as the zone where two or more members are interconnected, i.e. it is the assembly of all the basic components required to represent the behaviour during the transfer of the relevant internal forces and moments between the connected members. A beam-to-column joint consists of a web panel and either one connection (single sided joint, see Fig. 3-3a) or two connections (double sided joint, see Fig. 3-3b).

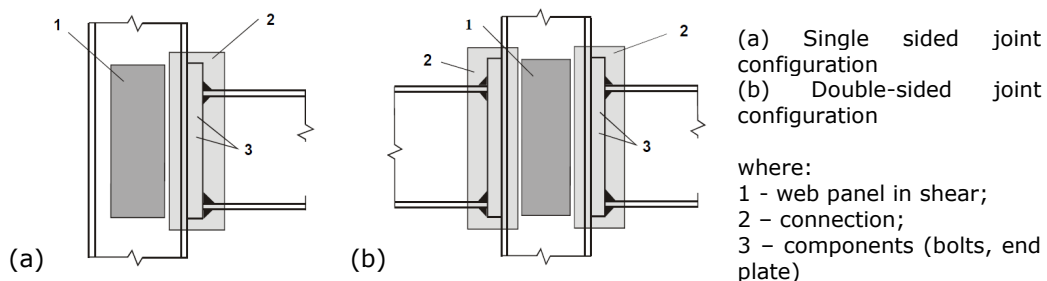


Fig. 3-3. Parts of a beam-to-column joint configuration [49]

According to EN 1993-1-8 [49], the design moment-rotation characteristic of a joint should depend on the properties of its basic components. A list of basic joint components are provided (in section 6.1.3(2) of [49]) which are of general application and can also be applied to similar components in other joint configurations.

Design resistances of welded joints connecting I or H sections to RHS members

According to EN 1993-1-8 [49] the design moment resistances of welded joints connecting I or H sections to RHS members (see Fig. 3-4) can be computed as:

$$M_{ip,1,Rd} = N_{1,Rd} \cdot (h_1 - t_1) \quad (3.2)$$

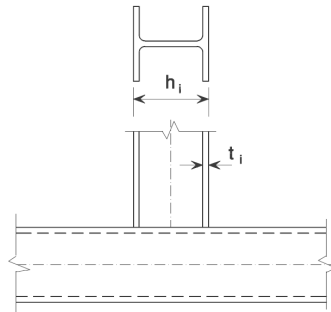


Fig. 3-4. Welded joint connecting an H section to a RHS member [49]

As a conservative approximation, $N_{1,Rd}$ for an I or H section may be assumed to be equal to the design resistance of two transverse plates of similar dimensions to the flanges of the I or H section (see Fig. 3-5) which can be computed as shown below, considering the minimum capacity of the three failure modes expressed by equations (3.3), (3.4), and (3.5).

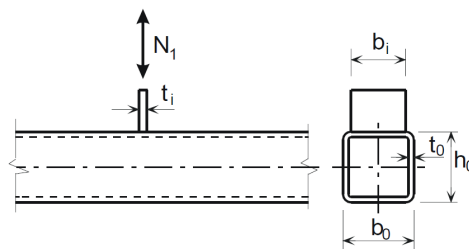


Fig. 3-5. Welded connection between a transverse plate and a RHS [49]

(brace failure)
$$N_{1,Rd} = f_{y1} \cdot t_1 \cdot b_{eff} / \gamma_{M5} \quad (3.3)$$

(chord side wall crushing)
when $b_1 \geq b_0 - 2 \cdot t_0$
$$N_{1,Rd} = f_{y0} \cdot t_0 \cdot (2 \cdot t_1 + 10 \cdot t_0) / \gamma_{M5} \quad (3.4)$$

(punching shear)
when $b_1 \leq b_0 - 2 \cdot t_0$
$$N_{1,Rd} = \frac{f_{y0} \cdot t_0}{\sqrt{3}} \cdot (2 \cdot t_1 + 2 \cdot b_{e,p}) / \gamma_{M5} \quad (3.5)$$

$$b_{eff} = \frac{10}{b_0/t_0} \cdot \frac{f_{y0} \cdot t_0}{f_{y1} \cdot t_1} \cdot b_1 \quad \text{but} \quad b_{eff} \leq b_i \quad (3.6)$$

$$b_{e,p} = \frac{10}{b_0/t_0} \cdot b_1 \quad \text{but} \quad b_{e,p} \leq b_i \quad (3.7)$$

As can be observed in equation (3.3), the design resistance of a transverse plate welded to a RHS member, depends on an effective width (see equation (3.6)) which is due to the flexibility of the front wall of the RHS in tension or compression. Therefore, this effective width might not be enough to assure the required degree of overstrength in case of a welded beam-to-RHS connection, as required by EN 1998-1 [27] for full strength connections.

A limitation of the current design codes is related to the evaluation of the shear capacity of the column web panel corresponding to a rectangular hollow section filled with concrete. According to the design code for composite structures EN 1994-1-1 [50], in case of a single-sided joint, or a double-sided joint in which the beam depths are similar, the design shear resistance of concrete encasement to the column web panel $V_{wp,c,Rd}$ should be determined using:

$$V_{wp,c,Rd} = 0,85 \cdot v \cdot A_c \cdot f_{cd} \cdot \sin \theta \quad (3.8)$$

where:

$$A_c = 0,8 \cdot (b_c - t_w) \cdot (h_c - 2 \cdot t_f) \cdot \cos \theta \quad (3.9)$$

$$\theta = \arctg \left(\frac{h_c - 2 \cdot t_f}{z} \right) \quad (3.10)$$

$$v = 0,55 \cdot \left(1 + 2 \cdot \left(\frac{N_{Ed}}{N_{pl,Rd}} \right) \right) \leq 1,1 \quad (3.11)$$

The design method shown above is however related to a partially encased wide flange section (see Fig. 3-6a) and not to a concrete filled rectangular hollow section (see Fig. 3-6b).



Fig. 3-6. Composite column: (a) partially encased wide flange section, and (b) concrete filled rectangular hollow section [1]

Beside the provisions from EN 1993-1-1 [28], EN 1993-1-8 [49], EN1994-1-1 [50], and EN 1998-1 [27], design guides were developed for structural hollow section connections (see [45], [48], [51]).

The connection typologies covered in "Hollow sections in Structural applications" [45] are mainly related to hollow section trusses, i.e. welded connections between circular hollow sections, welded connections between rectangular hollow sections, and welded connections between hollow sections and open sections. The design of welded I-beam to CHS or RHS column moment

connections is also shown but as un-stiffened configuration (partial strength) and with plain hollow sections for columns.

The connections between beams and columns covered in "Design guide for structural hollow section column connections" [51] are simple shear connections, semi-rigid connections, as well as moment connections (rigid and full-strength connections). In order to develop full moment capacity, transverse column stiffeners are usually required to transfer axial loads in the beam flanges. The stiffener can be either a through diaphragm (see Fig. 3-7 and Fig. 3-8), internal diaphragm (see Fig. 3-9) or external diaphragm (see Fig. 3-10).

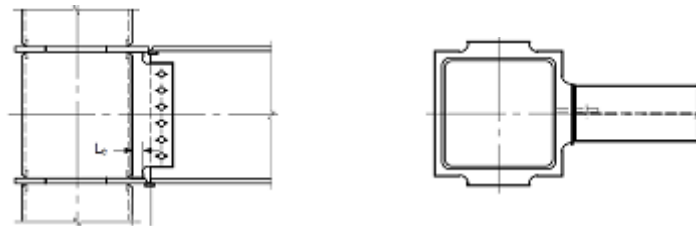


Fig. 3-7. Beam-to-column connection with through diaphragm for field welding [51]

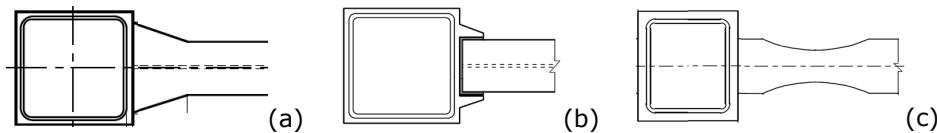


Fig. 3-8. Examples of through diaphragm connections: (a) with horizontal haunches, (b) with U-shaped welded joints, and (c) reduced beam section (RBS) connections [51]

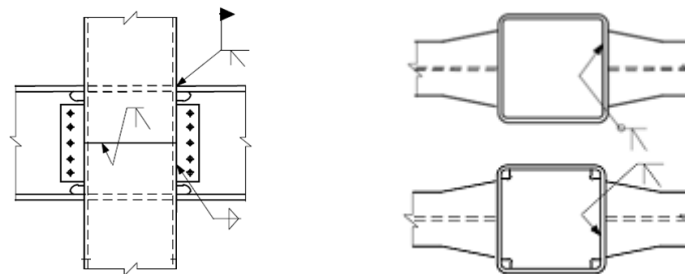


Fig. 3-9. Beam-to-column connections with internal diaphragms [51]

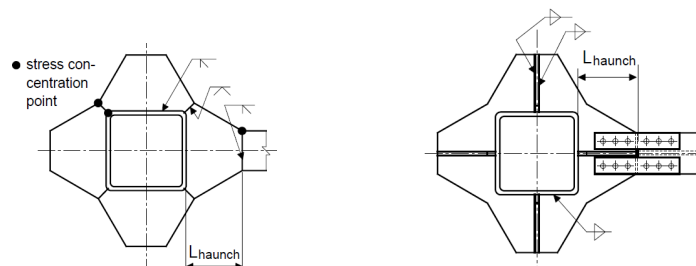


Fig. 3-10. Beam-to-column connections with external diaphragms [51]

The concrete-filled hollow section column is frequently a preferred option to the bare steel column for seismic design, because of the increased strength of the column due to confinement of concrete as well as continuous bracing of the steel tube to delay local buckling and enhanced ductility of the column in cyclic loading. Fig. 3-11 shows typical connections with external diaphragms to concrete-filled hollow sections. Design provisions for these connections are given in [51], and are based on the AIJ standard for steel reinforced concrete structures [52].

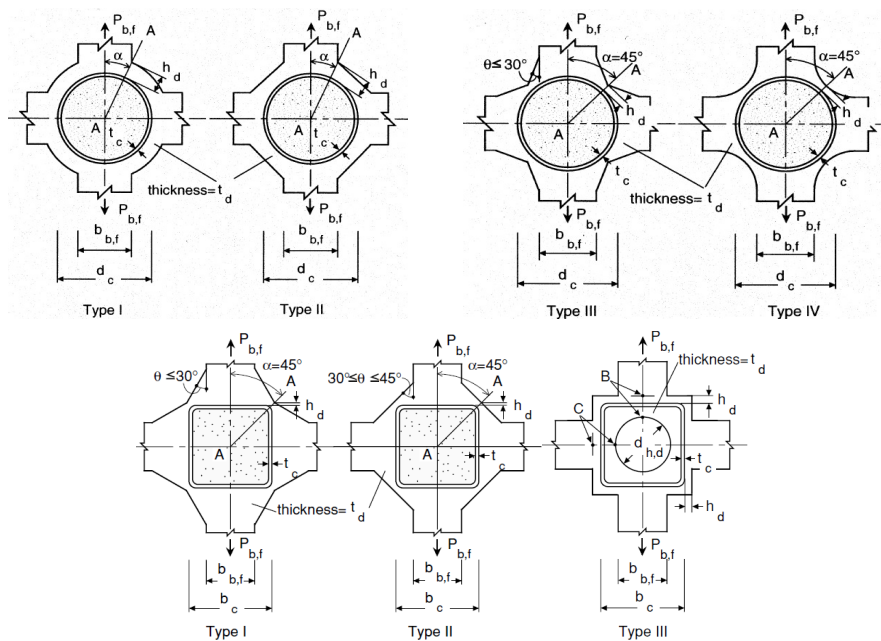


Fig. 3-11. Connections with external diaphragms to concrete-filled hollow sections [51] [52]

3.5. Summary review of research on welded beam-to-CFT column joints

Initial investigations on I-beam-to-RHS connections have been carried out by Kanatani et al. (1980) [53] and further flange plate to RHS connections have been investigated by Wardenier (1982) [54] and Davies and Packer (1982) [55]. For I-beam-to-RHS column connections, Lu (1997) [56] has carried out similar investigations as de Winkel (1998) [57] did for I-beam to-CHS column connections.

In order to develop full moment capacity, transverse column stiffeners are usually required to transfer the forces from the beam flanges to the column. As shown by Morino and Tsuda (2003) [58], the typical connections between a concrete filled tube (CFT) and I-beams often used in Japan are based on the use of stiffeners which can be either a through diaphragm, internal diaphragm or external diaphragm (see Fig. 3-12). The connection is fabricated by shop welding, and the beams are bolted to the brackets on-site. In the case of connections using inner and through-type diaphragms, the diaphragm plates are located inside the tube, and a hole is opened for concrete casting. A cast steel ring stiffener is used for circular CFT columns. In the case of a ring stiffener and an outer diaphragm, there is no object

inside the tube to interfere with the smooth casting of the concrete. From these joining examples, the through diaphragm is the most popular option in Japan because the axial load in the beam flange is directly transferred to the column web in the simplest manner. The other factor for the frequent use of through diaphragms is that most Japanese fabricators have established production resources, particularly welding robots, most suited for the production of this type of connection.

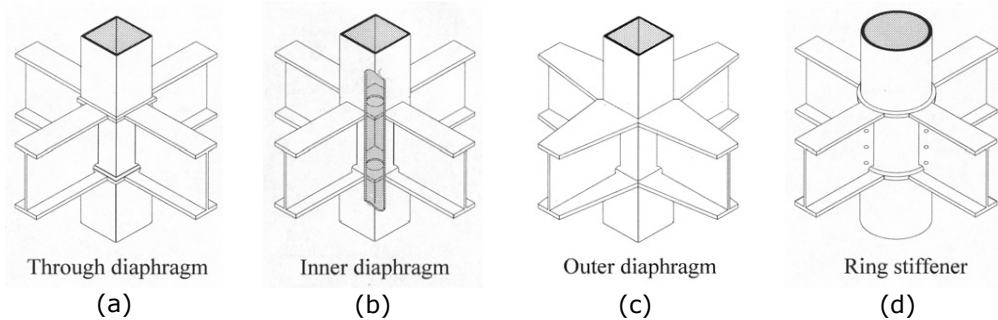


Fig. 3-12. Concrete-filled steel tube column system in Japan: connections with (a) through diaphragm, (b) inner diaphragm, (c) outer diaphragm, and (d) ring stiffener [58]

In 1985, five general contractors and a steel manufacturer won the Japan's Ministry of Construction proposal competition for the construction of urban apartment houses in the 21st century. Since then, these industries and the Building Research Institute (BRI) of the Ministry of Construction started a five-year experimental research project called New Urban Housing Project (NUHP), which accelerated the investigation of this system. Another five-year research project on composite and hybrid structures started in 1993 as the fifth phase of the U.S.-Japan Cooperative Earthquake Research Program, and the investigation of the CFT column system was included in the program. Research findings obtained from this project formed present design recommendations for the CFT column system.

In the NUHP, 86 specimens of centrally-loaded stub columns and beam-columns were tested under combined compression, bending and shear. In the U.S.-Japan Program, the experimental study conducted by the Japanese side consisted of centrally-loaded stub columns, eccentrically loaded stub columns, beam-columns, and beam-to-column connections. A total of 154 specimens were tested. A unique feature of this test program was that it covered high-strength materials, such as 800 N/mm² steel and 90 N/mm² concrete. It covered a large D/t ratio, and some of the beam-column specimens were tested under variable axial load.

In addition to these two organized programs, numerous specimens of CFT members and frames have been tested in research projects conducted in universities and industries. More recent research activities carried out on joints with welded connections between I-beams and concrete filled hollow sections are further shown.

3.5.1. C.T. Cheng and L.L. Chung [59]

The study of Cheng and Chung [59] proposed a nonlinear force-deformation model to simulate shear transfer behaviour in the panel zone of CFT beam-column connections. In this model, influence of axial load on the shear transfer behaviour was accounted for. To validate the proposed theory, five circular CFT beam-column connections were constructed and tested (see Fig. 3-13). The steel grades used for

3.5. Summary review of research on welded beam-to-CFT column joints 59

the steel tubes (with 6 and 10 mm thickness) were characterized by yield strength of 422 N/mm^2 , and respectively 304 N/mm^2 . The joints were characterized by the use of through diaphragm, and the connection was realized in two solutions, i.e. full penetration weld between flange and diaphragm (see Fig. 3-14a), and with fillet weld all around between beam flange and the diaphragm (see Fig. 3-14b).

Test results showed that all specimens failed by the welding fracture while entering nonlinear stage. It is found that the higher the axial load was applied, the better the ductility of connections was obtained. Comparison of analytical and experimental results showed that the proposed prediction for panel shear was in a reasonable range for higher axial load tests, but conservative for lower axial level.

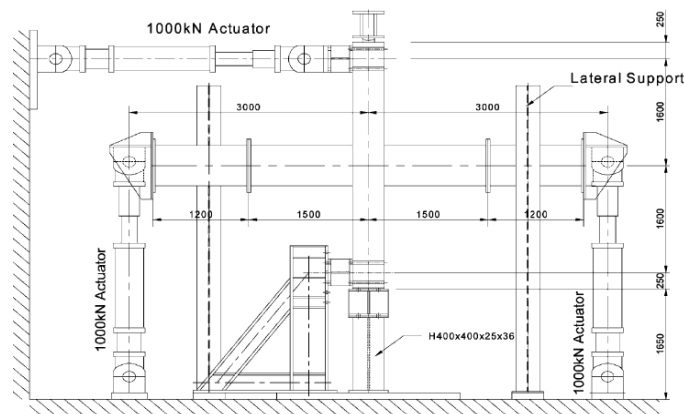


Fig. 3-13. Experimental test set-up [59]

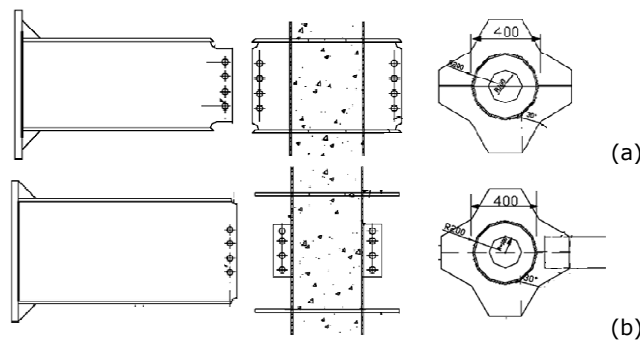


Fig. 3-14. Connection typology [59]

3.5.2. C.C. Chen and N.J. Lin [60]

The study of Chen and Lin [60] investigated the cyclic behaviour of flange plate connections between steel beam and rectangular CFT column, in which the flange plates were penetrated through the CFT column. The experimental test set-up is shown in Fig. 3-15. Specimens were designed to simulate exterior and interior beam-to-column connections (see Fig. 3-16). Square hollow sections of 350 mm width and 9 mm thickness were used for columns. The steel tube confirmed the ASTM A572 Gr. 50 steel, and the average concrete strength measured during the test of the specimens was 46 N/mm^2 .

The test results of three specimens with exterior flange plate connection showed that the tearing of the steel tube initiated at the both tips of the weld joining the flange plate to the steel tube because of the possible localized stress concentration. However, the plastic hinge formed in the beam beyond the flange plate. The specimen with the beam through the CFT column did not tear at the steel tube and formed the plastic hinge in the beam. Two interior connection specimens with weak panel zone failed due to the premature fracture of the steel tube and the shear cracking in the concrete core.

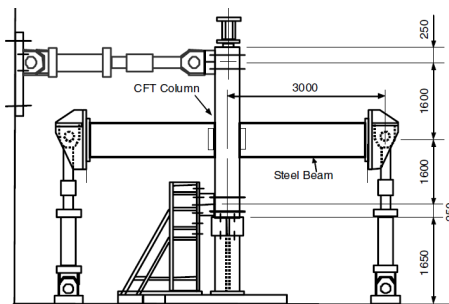


Fig. 3-15. Experimental test set-up [60]

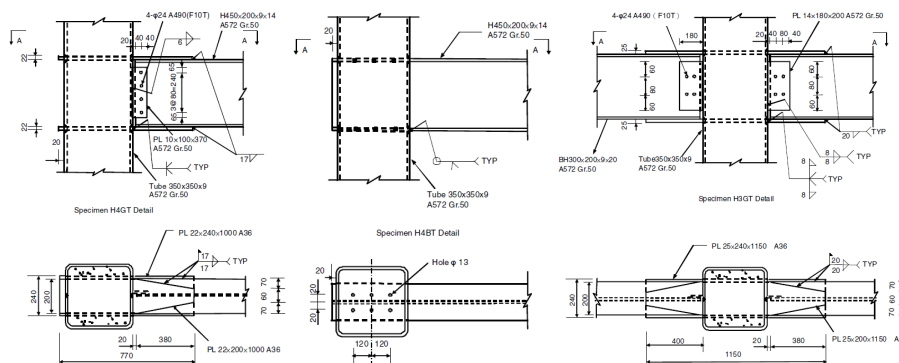


Fig. 3-16. Configuration of beam-to-column joints [60]

3.5.3. K.J. Shin, I.J. Kim, Y.S. Oh, and T.S. Moon [61]

The study of Shin et al. [61] focused on the experimental and analytical behaviour of concrete filled tubular (CFT) column to H-beam welded moment connections with external T-stiffeners. Six full-scale specimens were tested cyclically (see Fig. 3-17). All specimens were designed and manufactured using the following main test parameters: (a) the strength ratio of the horizontal stiffener to the beam flange; and (b) the strength ratio of the vertical stiffener to the beam flange. The yield strength of the build up tube (500x500x12 mm) was in amount of 271 N/mm².

Three types of failure modes, horizontal stiffener failure, vertical stiffener failure and beam failure, were obtained. The connections reinforced with T-stiffeners having 130% of strength to beam flanges showed stable hysteretic behaviour and good ductility. Finite element models were used to simulate the experimental

behaviour. The results obtained from the finite element were evaluated by comparing the load–displacement responses and the potential of failure modes.

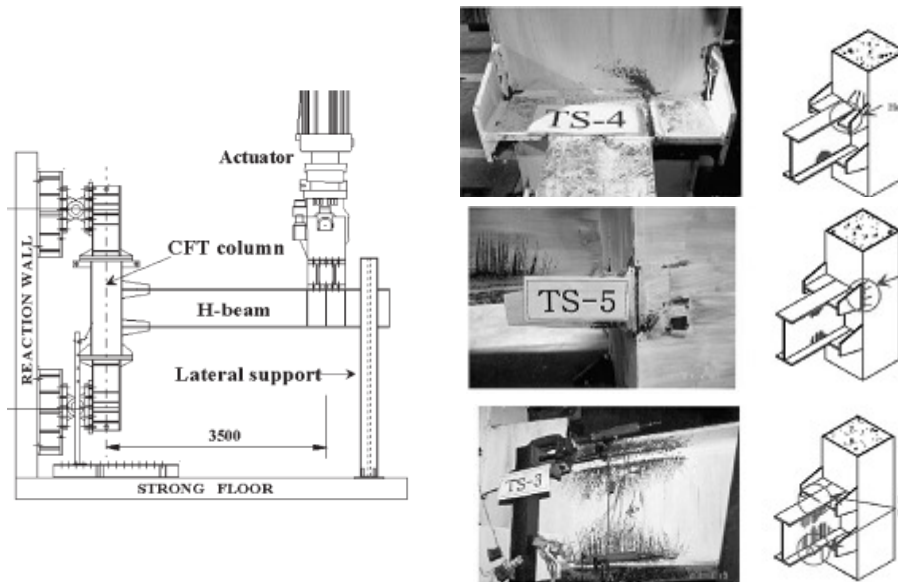


Fig. 3-17. Experimental test set-up and joint response [61]

3.5.4. T. Fukumoto and K. Morita [62]

The study of Fukumoto and Morita [62] covered sub-assembly tests conducted on the panel zone within beam-to-concrete filled steel tube (CFT) column moment connections made from high-strength material to investigate their elastoplastic behaviour. Fig. 3-18 shows the experimental test set-up and the joint configurations, i.e. RHS with internal diaphragm, and CHS with external diaphragm.

The parameters investigated in the study include CFT column cross section (square, circular steel tube), weak element (weak panel zone, weak beam configuration), width–thickness ratio for square steel tube ($d_s/t_s=22$ and 33), radius–thickness ratio for circular steel tube ($d_s/t_s=21$ and 38), steel grade (590 and 780 N/mm²) and concrete strength (60 , 120 N/mm²). The specimens with the weak panel zone configuration were designed to develop yielding primarily in the panel zone to examine their elastoplastic behaviour. The specimens with the weak beam configuration were designed to have yielding develop primarily in the beams to investigate the performance of the panel zone in the weak-beam–strong-column system. A nonlinear shear force–deformation model was proposed for the panel zone for predicting the elastoplastic behaviour. The proposed model included a superposed model based on a tri-linear shear–deformation relationship for the steel tube superposed on one for the concrete core, and a simple model provided as a tri-linear model having a yield strength point and an ultimate strength point for this panel zone, as a practical model for design. The authors also proposed a method for evaluation of the load resistance, with a new theoretical compression strut mechanism taking into account the confinement of the tube flange.

The results predicted using the superposed and the simple model were found to agree approximately with the experimental results up to a large shear deformation of 0.04 rad.

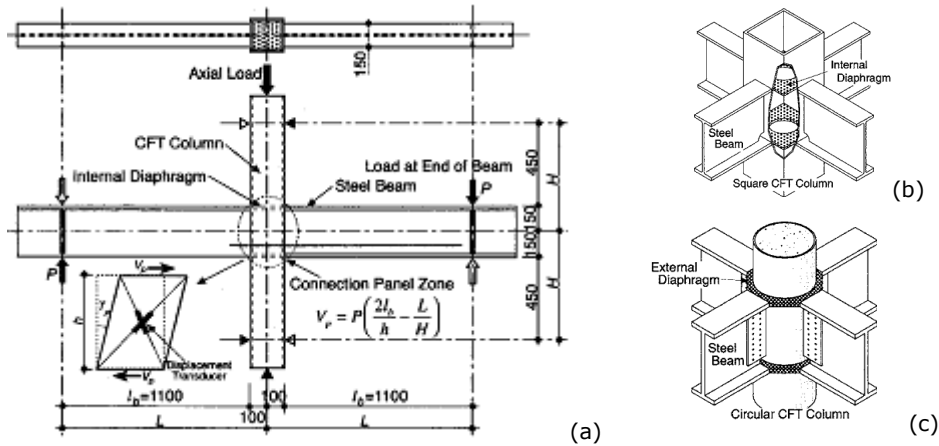


Fig. 3-18. Experimental test set-up and joint configurations [62]

3.5.5. J.W. Park, S.M. Kang, and S.C. Yang [63]

The study of Park, Kang and Yang [63] investigated the force transfer mechanism and the cyclic performance of wide flange beams to square concrete-filled tube column joints reinforced with stiffening plates around the column. It was shown that the strength and stiffness of wide flange beams to rectangular tube column joints are reduced significantly if the connections are not reinforced. However, the reinforcement for the connections can be complex and increase the fabrication costs significantly because the tube columns are closed sections.

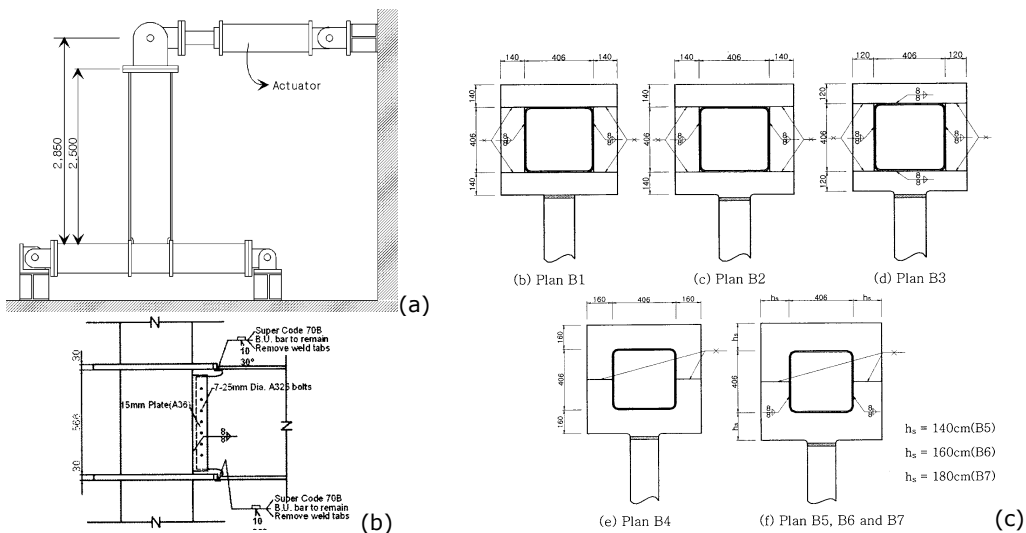


Fig. 3-19. Experimental test set-up (a), elevation of joint (b), connection typologies (c) [63]

The first phase of the research program was to assess the force transfer mechanism at the joint using an analytical yield line method. An experimental program was conducted to verify the proposed model. The test results showed that the derived nominal strength equation provided a reasonable prediction. As the second phase of the research program, full-scale joint sub-assembly tests were conducted to assess the cyclic performance of the joints (see Fig. 3-19). A total of seven specimens were tested under cyclic loading. As can be seen in Fig. 3-19c, the connection solution was based on the use of stiffening plates welded in several configurations around the steel tube.

Test results showed that total rotation of 0.04 rad which is required for special moment resisting frames could be obtained.

3.5.6. C.C. Chou, C.C. Wu, C.K. Jao, and Y.Y. Wang [64]

The study of Chou et al. [39] investigated through cyclic testing of six full-scale specimens (see Fig. 3-20a) the effectiveness of using reduced flange plates (RFP) or rib plates for seismic response of steel moment connections. The first scheme utilized RFP to connect the beam flanges to the column, without any direct connection of the beam flange to the column (Fig. 3-20b). Plastic hinges were forced to form in the RFP instead of the steel beam due to strong-beam-weak-RFP, so the weakened moment connection eliminated buckling of the beam and reduced cost of repairing after earthquakes. The second scheme was to strengthen a connection by welding rib plates between the column face and inner side of the beam flanges (see Fig. 3-20c).

Test results of the weakened connections showed that (1) the connections developed beam plastic moment and reach more than an interstory drift of 4% without strength degradation, (2) the RFP was effective in dissipating energy before buckling, and (3) no buckling of the beam was observed. Test results of the strengthened connection showed that the rib plates significantly reduced the beam flange strain by 75% compared to a non-retrofitted steel moment connection.

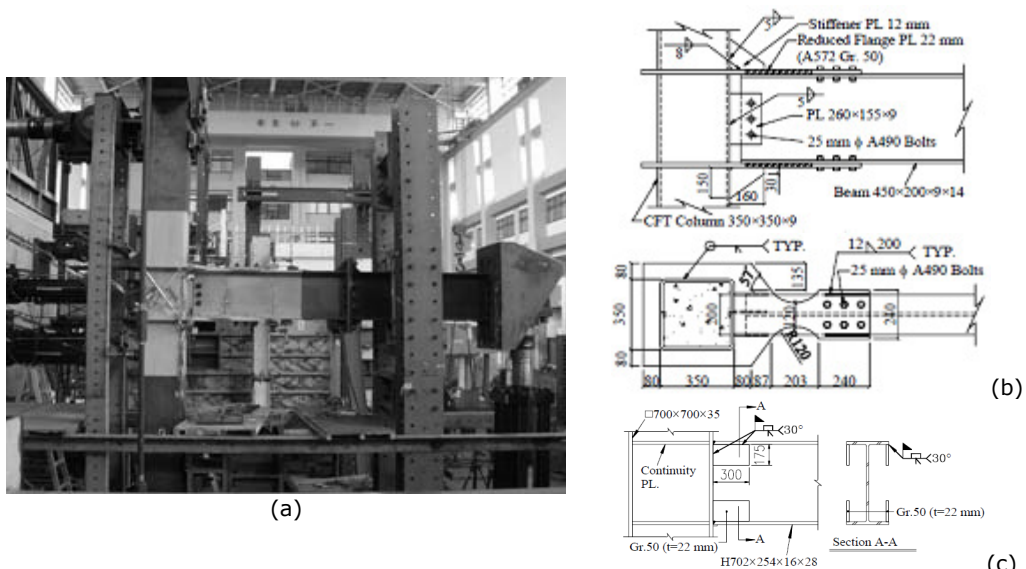


Fig. 3-20. Experimental test set-up (a), joint configurations (b) and (c) [64]

3.5.7. C.T. Cheng, C.F. Chan, and L.L. Chung [65]

The study of Cheng, Chan and Chung [65] investigated the seismic performance of four steel beams to concrete filled steel tube (CFT) column connections with floor slabs, including two interior and two exterior joints (see Fig. 3-21). The objective of the research was to evaluate the composite effect of the steel beam and floor slab commonly used in Taiwan in practice. Another objective was to investigate the seismic behaviour of new connection details such as the taper flange or larger shear tab in the beam-end (see Fig. 3-22) so as to prevent complete joint penetration welds of the girder flanges from the unexpected brittle failure found in the latter after the Northridge earthquake. The transfer of forces to the side walls of the RHS column was assured by the use of interior diaphragms.

The test results show that the tapered beam flanges and lengthened shear tabs stiffened at the beam-ends and effectively moved the plastic hinges away from the column face to prevent premature brittle failure of the CJP welds in the beam flange, resulting in the ductile performance of the connections.

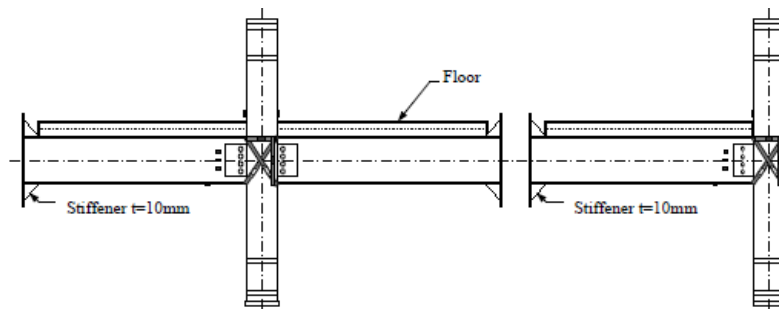


Fig. 3-21. Specimen configuration [65]

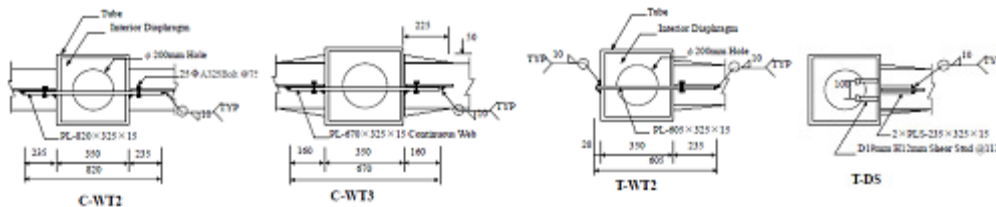


Fig. 3-22. Connection details [65]

3.5.8. M.S. Ghobadi, A. Mazroi, and M. Ghassemieh [66]

The study of Ghobadi, Mazroi and Ghassemieh [66] was related to experimental investigations conducted with the aim to assess the behaviour of the weld in steel moment resisting connections. A total of forty seven reduced-scale subassembly model specimens were tested that represent welded moment resisting connections of the beam to box column. These specimens were used to study the following aspects in fabrication and retrofitting of moment resisting connections: complete joint penetration groove (CJP) weld behaviour, transversely loaded fillet weld behaviour, grinding and re-welding influence on weld behaviour, reinforcing of connection with T-stiffener and rib plates, strain rate effect on weld and material characteristics and electrode toughness effect on weld behaviour.

Following test result interpretations, five full-scale moment resisting connections of beam to box column were fabricated and tested (see Fig. 3-23a). These models included one specimen fabricated with details of an outdated connection, two specimens with an improved CJP groove weld detail (see Fig. 3-23b), and two specimens retrofitted by T-stiffeners (Fig. 3-23c). As can be seen internal diaphragms were used for the joint reinforcement.

Overall, the improved and retrofitted specimens performed well, achieving total (elastic plus plastic) story drift ratios of at least 4% radians in magnitude before experiencing 20% strength degradation.

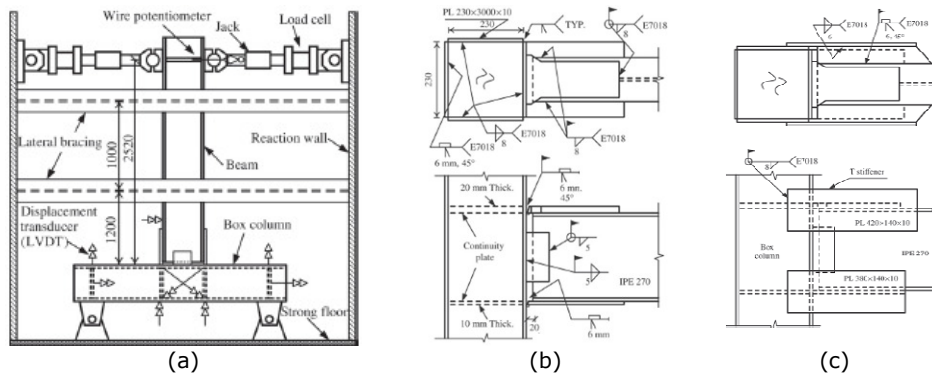


Fig. 3-23. Experimental test set-up (a), joint configuration (b) and (c) [66]

3.5.9. O.S. Bursi et al. [67] [68]

The study of Bursi et al. [67] [68] was focused on the design of the beam-to-column joints under seismic-induced fire loading together with the definition of adequate structural details for composite columns. Experimental investigations were carried out on four full-scale substructures representing interior full-strength bolted beam to column joints (see Fig. 3-24). The columns were concrete-filled circular tubes of 457 mm diameter and 12 mm thickness realised from S355 steel grade. External diaphragms were used for the bolted connection of the beam and a vertical stiffener passed through the circular tube. The presence of the composite slab on the top of the beams was considered as well.

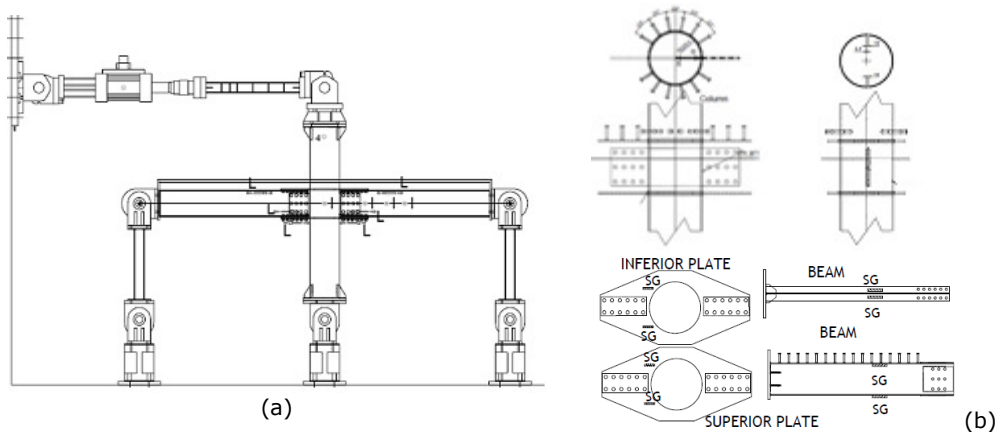


Fig. 3-24. Experimental test set-up (a) and connection details of the joint (b) [67]

Experimental and numerical results showed how the joint details influence the beam-column sub-assembly response. All sub-assemblies exhibited rigid behaviour for the designed composite joints and good performance in terms of resistance, stiffness, energy dissipation and local ductility. Plastic hinges developed in beams and confirmed the capacity based design. Numerical simulations showed a satisfactory performance of joints under seismic-induced fire loading.

3.5.10. W. Wang, Y. Chen, W. Li, and R.T. Leon [69]

The study of Wang et al. [69] investigated the seismic behaviour of H-beam to circular tubular column connections stiffened by an outer ring diaphragm. An innovative three-dimensional (3D) connection subassembly testing system was used (see Fig. 3-25a). Specimens representative of two-dimensional (2D) interior columns, 3D interior and exterior columns in a steel building frame (see Fig. 3-25b), were tested to failure under unidirectional or bidirectional cyclic loading.

Test results indicate significantly different failure modes for 2D and 3D weak panel connections, with panel shear buckling and local distortion of outer diaphragm occurring only for 3D connections. The weak beam connections unexceptionally exhibited final fracture at the junction between diaphragm and beam flange. In contrast with weak beam connections, weak panel connections demonstrated better seismic performance and ductility. As a result, a seismic design philosophy considering panel zone yielding before beam flexural yielding was proposed.

Based on experiment observations, small diaphragm width and simplified fillet welding were found to be feasible especially for weak beam connections, improving architectural appearance and facilitating construction. Strength evaluations showed that current AIJ [52] design provisions may be appropriate when applied to panel zones in 3D connections.

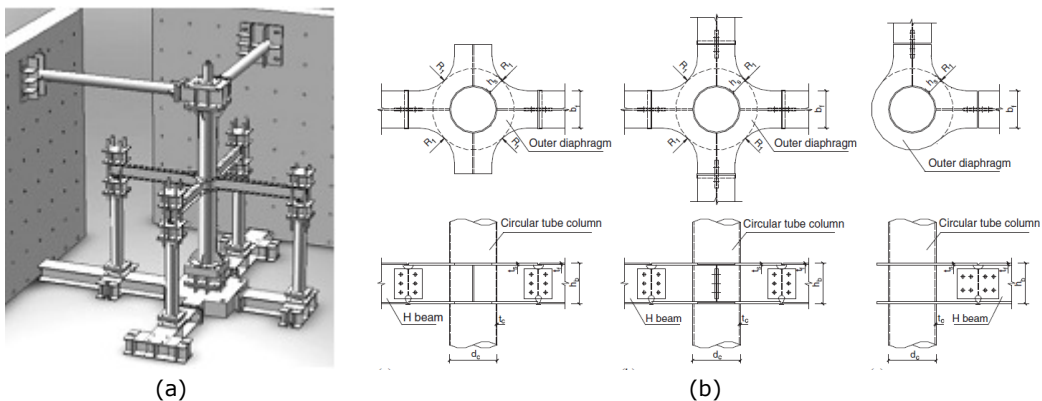


Fig. 3-25. Experimental test set-up (a) and joint configurations (b) [69]

3.6. Steel-concrete connection in CFT through the use of shot fired nails

The use of Hilti powder-actuated fasteners is a relatively new method for assuring shear connection in areas where loads are induced to composite tubular columns [70]. The powder actuated fasteners are driven through the tube walls from the outside and then protrude inside the tube. The connection between the surrounding tubular section and the concrete inside is then provided by direct pressure of the concrete against the shanks of the nails. The main advantage of this solution is that it is quick and easy to apply, especially for columns which are continuous over several storeys. The nailed shear connection was developed in a research project conducted at the Technical University of Innsbruck [71] [72].

3.6.1. H. Beck [73]

The study of Beck [73] investigated an alternative method for providing shear connection in composite tube columns, i.e. the use of shot fired nails that provide a mechanical shear connection with their protruding tips.

Experimental investigations were performed covering 30 push-out tests with pipe specimens (Fig. 3-26). Influences of pipe geometry, concrete strength and type of fastener on the load-deflection characteristics were investigated. The load-deflection behaviour exhibited excellent ductility combined with high load-bearing capacity per fastener. Based on these findings the nailed shear connection was introduced into practice with the Millennium-Tower in Vienna [74] (see Fig. 3-29), a fifty storey high rise building completed in 1999, where it has proven to be a reliable and cost effective connection method as no welding work was required.

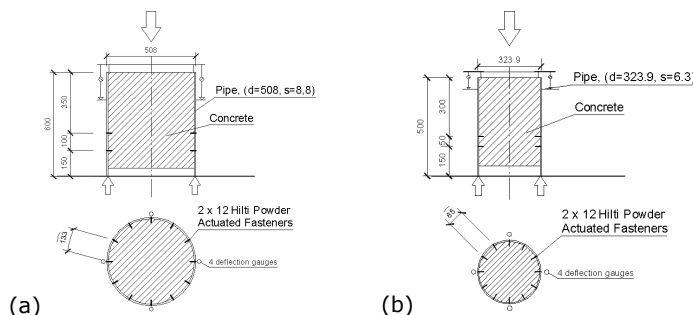


Fig. 3-26. Push-out test setup: (a) Pipe 508/8.8, and (b) Pipe 323.9/6.3 [73]

3.6.2. G. Hanswille, H. Beck and T. Neubauer [75]

Based on the behaviour derived experimentally from push-out tests, Hanswille, Beck and Neubauer [75], proposed a design resistance of nails for ultimate and serviceability limit states, providing requirements in relation to the minimum steel thickness, concrete grade and nail spacing. It was shown that a more realistic knowledge of the deformation behaviour in serviceability limit states, the combined shear resistance of the nails and the shear strength due to bond and friction and including long-term effects has to be considered. Consequently, experimental investigations were performed with the aim to investigate the behaviour of the shear connection subjected to a serviceability limit state loading sequence.

Tests were performed also with the aim to investigate the long-term behaviour and influence of creep of concrete of the nailed shear connections. Tests were performed at both Hilti Corporation (see Fig. 3-27) and at the University of Innsbruck. Only four nails were used per specimen, and the inner pipe surface was lubricated. The load was applied at a concrete age of eight days.

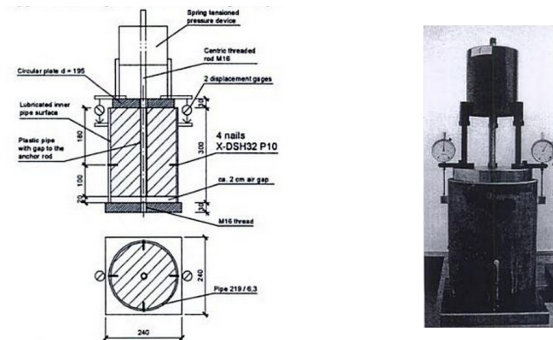


Fig. 3-27. Test set-up for long term tests [75]

The observations at Hilti Corporation were that up to 10 days the load-deformation curve exhibited a parabolic shape, beyond which the curve flattened significantly. The creep deformations after 10 days represented 75% of the deformations measured after one year of loading. In contrast, the tests at the University of Innsbruck lead to complete different results. It was speculated that bond, adhesion and friction were not adequately prevented by the lubrication of the inner tube. Therefore, the tests were stopped after 90 days with the aim to perform push-out tests on the specimens.

3.7. Examples of application

3.7.1. Commerzbank Tower in Frankfurt (1997)

Commerzbank Tower has a total height of 259 m and was completed in 1999. Fig. 3-28 shows the completed building and a column cross-section. The columns were realised in composite solution with steel tubes and additional steel cores. The cross section of the columns was realised in triangular shape.

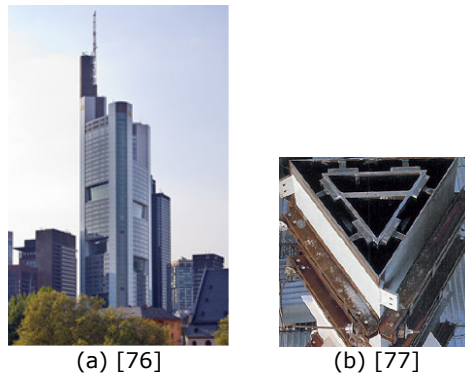


Fig. 3-28. Commerzbank Tower in Frankfurt (a), cross section of column (b)

3.7.2. Millenium Tower in Vienna (1999)

Millenium Tower has a total height of 202 m, is the tallest building in Austria, and was completed in April 1999. Fig. 3-29 shows a view of the tower under construction and a column cross-section with implanted shot fired nails for the shear connection between steel tube and concrete core.

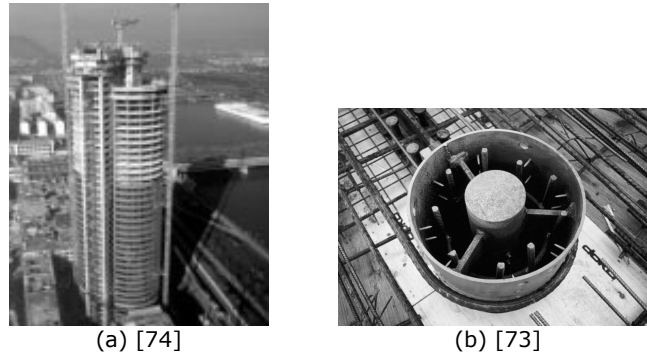


Fig. 3-29. Millennium Tower in Vienna (a); Cross section of column (b)

The columns were realised in composite solution with steel tubes and additional steel cores, both S355 [74]. The diameter of the tube, the size of the core and the concrete grade has been adjusted to the actual stresses depending on the floor number (see Fig. 3-30a). Composite slim floor beams were built of welded T-shaped steel sections and a concrete slab. The beam-to-column joints were realised as semi-continuous moment connections for which a component model (see Fig. 3-30b) was developed by Huber [78].

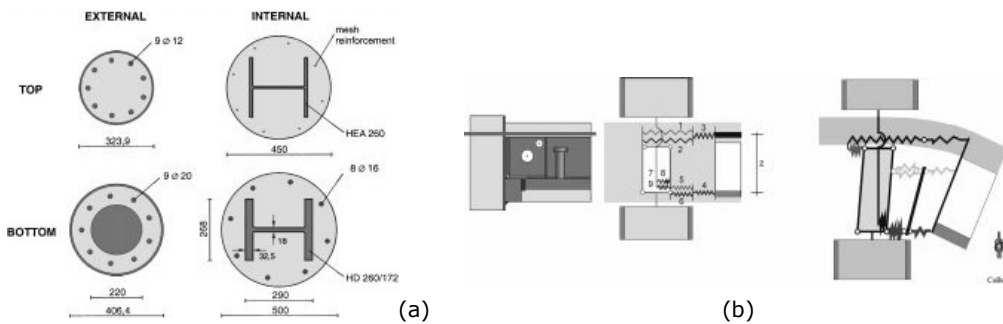


Fig. 3-30. Composite column cross-section (a) and component model for joint (b) - [78]

3.7.3. Post Tower in Bonn (2002)

Post Tower has a total height of 162 m and was completed in December 2002. Fig. 3-31 shows the completed building and a column cross-section. The columns were realised in composite solution with steel tubes and additional steel cores, both of S355 steel grade [79].

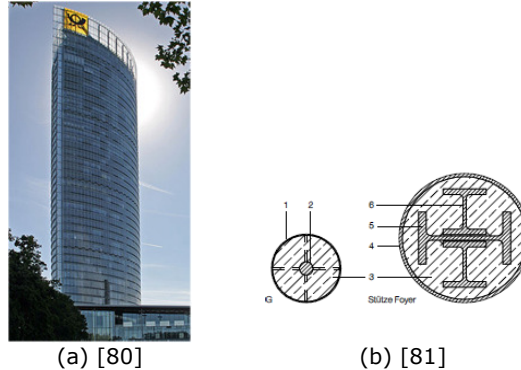


Fig. 3-31. Post Tower in Bonn (a), and cross section of column (b)

3.7.4. HighLight Towers in Munich (2004)

HighLight Towers have a total height of 126 m and were completed in 2004. Fig. 3-32 shows the completed building and an illustration of the column cross-section. The columns were realised in composite solution with steel tubes and additional steel cores. Generally, S355 steel grade was used. High-strength steel grades S460 and S690 were used in the connections, taking account of weldability and low residual stress [82].

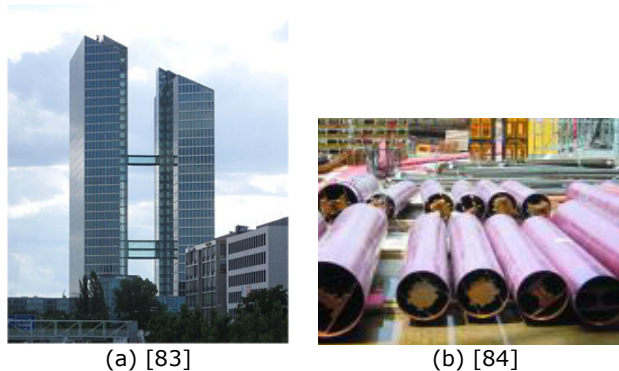


Fig. 3-32. HighLight Towers in Munich (a), and cross section of columns (b)

3.8. Concluding remarks

In the current chapter a brief description was made in relation to the tubular elements characterised by excellent properties with regard to the loading in compression, torsion and bending in all directions. The tubular steel sections can be produced as hot finished or cold formed hollow sections with a wide variety of cross sections, however the most frequently used tubular steel sections in the construction industry are circular hollow sections (CHS) and rectangular hollow sections (RHS). In relation to the mechanical properties, the hollow sections are made of similar steel as used for other steel sections, but can also be produced from high strength steel.

In the construction industry, as part of a multi-storey frame, i.e. MRF, CBF or EBF, tubular section elements can be used as conventional braces (circular, square), or as columns (circular, square) without infill or with concrete inside (concrete filled tubes – CFT). A particular attention should be given to the joining aspect of steel tubes in framed structures – from the point of view of the connection technology and detailing. At each intersection between beams and columns, the columns are usually continuous and the beams are attached to their external faces by connections. The connections can be realised as pinned, semi-rigid or rigid joints.

Columns realised from steel hollow sections can be filled with concrete with the aim to combine the properties of the two materials, the final element being characterised by higher stiffness, capacity and ductility, as well as enhanced fire resistance in comparison with bare steel configurations. A particular advantage of using a composite column is the reduction in column cross-sectional area, and by using steel tubes as permanent formwork, construction speed is increased. Because of the inherently high fire resistance of concrete filled columns, fire protection of steel is in many cases not necessary.

In spite of the advantages of the tubular sections, a special attention needs to be paid to the connections between beams and columns. The framing system with concrete filled columns and welded joints has been studied and applied on a large scale in Asia, Australia and America. In contrast, this solution was used at a lower scale in Europe

The interest within the current research is related to full strength welded I beam-to-CFRHS column joints for moment resisting frames (MRF) and moment resisting bays of dual frames (MRF+CBF, and MRF+EBF), for which the connections are not intended to suffer plastic deformations.

In relation to the welded connection between I or H profile to RHS members, current code provisions (EN 1993-1-8) state that the moment resistance may be assessed based on the design resistance of two transverse plates of similar dimensions to the flanges of the I or H section. A limitation of the current design codes is related to the evaluation of the shear capacity of the column web panel corresponding to a rectangular hollow section filled with concrete. The design code for composite structures EN 1994-1-1 [50], provides a method for determining the design shear resistance of concrete encasement to the column web panel, but the method is related to partially encased wide flange sections.

It was shown that with the aim to develop full moment capacity within a beam-to-column joint, transverse column stiffeners are usually required to transfer the loads from beam flanges to the column. Typical examples of welded joints used in Japan were characterised by the use of a through diaphragm, internal diaphragm or external diaphragm. Further, a summary review of research on welded beam-to-CFT column joints was made. Accordingly, several experimental investigations were undertaken for the evaluation of full strength welded beam-to-column joints. The columns were considered as circular as well as rectangular hollow sections, in most of the cases realised from MCS. As stiffening solution most of the investigations employed internal and through diaphragms. Other configurations used T-stiffeners or outer diaphragms. In some study cases the influence of the composite slab was taken into account as well as the behaviour of the joint with beams welded on two sides.

In case of composite columns, several situations are practiced with regard to the load introduction:

- The case in which the beam passes through the steel tube and transfers the load directly to the concrete core; the tube has a secondary role;

- The case in which the concrete inside the tube is inactive (connectors are not positioned); it is counted on the concrete core only in case of fire;
- The case in which the concrete is active and the efforts are introduced using connectors.

In the current research program, the goal is to count on both materials steel tube and concrete core, and to have a composite action ensured by the use of shot fired nails. These connectors are driven through the tube walls from the outside and then protrude inside the tube. The connection between the surrounding tubular section and the concrete inside is then provided by direct pressure of the concrete against the shanks of the nails. The main advantage of this solution is that it is quick and easy to apply, especially for columns which are continuous over several storeys. Experimental investigations were performed by Beck [73] i.e. push-out tests with pipe specimens. Influences of pipe geometry, concrete strength and type of fastener on the load-deflection characteristics were investigated. The load-deflection behaviour exhibited excellent ductility combined with high load-bearing capacity per fastener. Based on these findings the nailed shear connection was introduced into practice with the Millennium-Tower in Vienna [74], where it has proven to be a reliable and cost effective connection method as no welding work was required. In addition, experimental investigations were carried at Hilti Corporation and University of Innsbruck [75] with the aim to investigate the long-term behaviour and influence of creep of concrete of the nailed shear connections. The observations at Hilti Corporation were that the creep deformations after 10 days represented 75% of the deformations measured after one year of loading. In contrast, the tests at the University of Innsbruck lead to complete different results. It was speculated that bond, adhesion and friction was not adequately prevented by the lubrication of inner tube. Therefore, the tests were stopped after 90 days with the aim to perform push-out tests on the specimens.

Finally, a set of application examples were shown in relation to the use of concrete filled tubes for columns within high rise multi-storey buildings.

4. PERFORMANCE BASED SEISMIC DESIGN OF REFERENCE DUAL STEEL FRAMES

4.1. Introduction

Within the current chapter a description is made in relation to the dual steel frames realised with elements from different steel grades, i.e. mild carbon steel (MCS) for dissipative members and high strength steel (HSS) for non-dissipative members. Three frame typologies were considered i.e. moment resisting frames (MRF), dual concentrically braced frames (MRF+CBF), and dual eccentrically braced frames (MRF+EBF). A brief description is made in relation to the frames that were used as basis for the definition of the experimental program, i.e. cross-section of members for the beam-to-column joint specimens. Further, a description is made in relation to the configuration and detailing used for two joint typologies, i.e. reduced beam section joints (RBS) and cover plate joints (CP). The detailed design procedures of the two joints are shown in Chapter 6. Finally, with the aim to assess the seismic demand for the beam-to-column joints, a set of frames were analysed using static and dynamic nonlinear analyses.

4.2. Dual frame typology: MRF; MRF+CBF; MRF+EBF

Multi-storey steel buildings are assigned to one of the following structural types, depending to the behaviour of their lateral force resisting systems [27]:

- moment resisting frames (MRF), in which the horizontal forces are mainly resisted by members acting essentially in flexural mode; for such structures the performance of MR joints is crucial;
- frames with concentric bracings (CBF), in which the horizontal forces are mainly resisted by members subjected to axial forces;
- frames with eccentric bracings (EBF), in which the horizontal forces are mainly resisted by axially loaded members, but where the eccentricity of the layout is such that energy can be dissipated in seismic links by means of either cyclic bending or cyclic shear;

Combining a MRF with one of the lateral resisting systems, i.e. MRF+CBF, MRF+EBF, leads to a building frame called dual-frame. In addition, the frames that are realised from two steel grades, i.e. mild carbon steel for dissipative members and high strength steel for non-dissipative members (see Fig. 4-1), are called dual-steel frames.

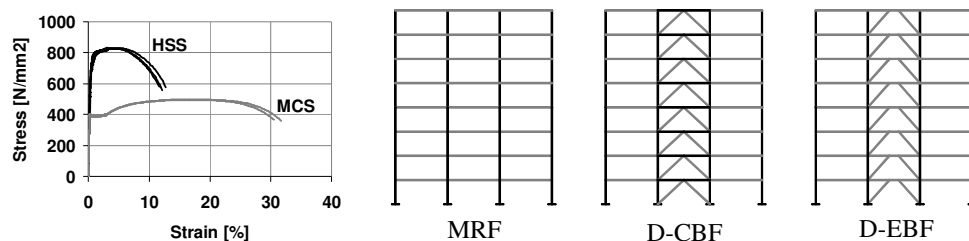


Fig. 4-1. Frames (MRF, D-CBF, and D-EBF) realized in the dual-steel concept

4.3. Code based design

The current seismic design code, EN 1998-1 [27], applies to the design and construction of buildings and civil engineering works in seismic regions. Its purpose is to ensure that in the event of earthquakes – the human lives are protected, the damage is limited, and that the important structures for civil protection remain operational. The seismic design code contains only those provisions that, in addition to the provisions of the other relevant Eurocodes, must be observed for the design of structures in seismic regions. Consequently, it complements the design code for concrete structures EN 1992-1 [85], the design code of steel structures EN 1993-1 [28] and respectively the design code for composite structures EN 1994-1 [50].

The seismic resistant structures can be designed according to one of the following concepts:

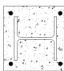
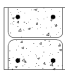
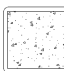
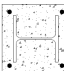
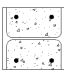
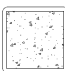
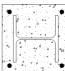
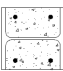
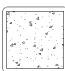
- Concept (a) - Low-dissipative structural behaviour – for which the action effects may be calculated on the basis of an elastic global analysis without taking into account a significant non-linear material behaviour;
- Concept (b) - Dissipative structural behaviour – the capability of parts of the structure (dissipative zones) to resist earthquake actions through inelastic behaviour is taken into account.

The structures designed in accordance with the dissipative structural behaviour concept, shall belong to structural ductility classes DCM (medium ductility) or DCH (high ductility). These classes correspond to increased ability of the structure to dissipate energy in plastic mechanisms. The structures have to be designed so that the dissipative zones develop in those parts of the structure where the plastic deformations, local buckling, do not affect the global structural stability.

4.3.1. Pre-design of frames

The design of three structural systems – moment resisting frames (MRF), dual concentrically braced frames (D-CBF) and dual eccentrically braced frames (D-EBF) – was performed within HSS-SERF research project by one of the partners, i.e. GIPAC [86]. Table 4-1 makes an overview of the frame configurations considered for the preliminary design. Beside the three frame typologies, two other parameters were taken into account, i.e. the column cross section (full encased wide flange FE-WF, partially encased wide flange PE-WF, concrete filled tube CFT) and steel grade for column (S355, S460, S690 → hot rolled sections and plates / S700 → rectangular hollow sections).

Table 4-1 – Frame configurations for preliminary design [86]

Frame type		MRF – 8 storeys			D-CBF – 8 storeys			D-EBF – 8 storeys		
Column type										
Column Steel grade	S355	frame 1.1.1	frame 1.2.1	-	-	-	-	-	-	-
	S460	frame 1.1.2	frame 1.2.2	-	frame 2.1.2	frame 2.2.2	frame 2.3.2	frame 3.1.2	frame 3.2.2	frame 3.3.2
	S690 S700	frame 1.1.3	frame 1.2.3	-	frame 2.1.3	frame 2.2.3	frame 2.3.3	frame 3.1.3	frame 3.2.3	frame 3.3.3

For the design it was considered that the buildings have 28 m height with 8 floors of 3.5 m height and 7.5 m span. The steel beams and composite columns

were connected together with rigid joints. The beams and braces were realised from mild carbon steel (S355), and the columns from high strength steel (S460, S700) and C30/37 concrete class. A permanent load in amount of 4 kN/m² and a live load of 3 kN/m² were considered in the design. The seismic load was defined by seismic spectrum according to EN 1998-1 [27] (spectrum type 1, $\gamma_I=1.0$, $a_g=0.32g$, $\psi_{2,i}=0.3$, $\phi=0.8$, $\psi_{E,i}=0.24$). The seismic masses were corresponding to 1 bay for MRF and 2 bays for D-CBF and D-EBF. The cross-sections of the members obtained from the design, corresponding to the D-CBF and D-EBF realised with CFT columns, are summarised in Table 4-2, Table 4-3, and Table 4-4.

The cross sections of the members, i.e. beams and columns that were used for the design of the beam-to-column joint specimens, were chosen from the upper floors of the D-CBF's (see Fig. 4-2a).

Table 4-2 – Cross sections for the dual concentrically braced frames [86]

Frames	Columns		Beams		Braces		
	Ground to 4 th floor	5 th to 8 th floor	External	Internal	Ground to 5 th floor	5 th to 7 th floor	7 th to 8 th floor
Frame 2.3.2	SHS 400x20	SHS 300x12.5	IPE 400	IPE 750x147	HEB 200	HEB 180	HEB 140
Frame 2.3.3	SHS 350x16	SHS 250x10	IPE 400	IPE 750x147	HEB 200	HEB 180	HEB 140

Table 4-3 – Cross sections for the dual eccentrically braced frames [86]

Frames	Columns		External beams	Braces				
	Ground to 4 th floor	5 th to 8 th floor		ground - 3 rd floor	3 rd - 5 th floor	5 th -6 th floor	6 th - 7 th floor	7 th - 8 th floor
Frame 3.3.2	SHS 350x12.5	SHS 250x10	IPE 400	HEB 260	HEB 240	HEB 220	HEB 200	HEB 180
Frame 3.3.3	SHS 300x10	SHS 220x8	IPE 400	HEB 260	HEB 240	HEB 220	HEB 200	HEB 180

Table 4-4 – Cross sections for links [86]

Frames	Internal beams (links)		
	1 st and 2 nd floor	3 rd and 4 th floor	5 th to 8 th floor
Frame 3.3.2	IPE 360	IPE 330	IPE 300
Frame 3.3.3	IPE 360	IPE 330	IPE 300

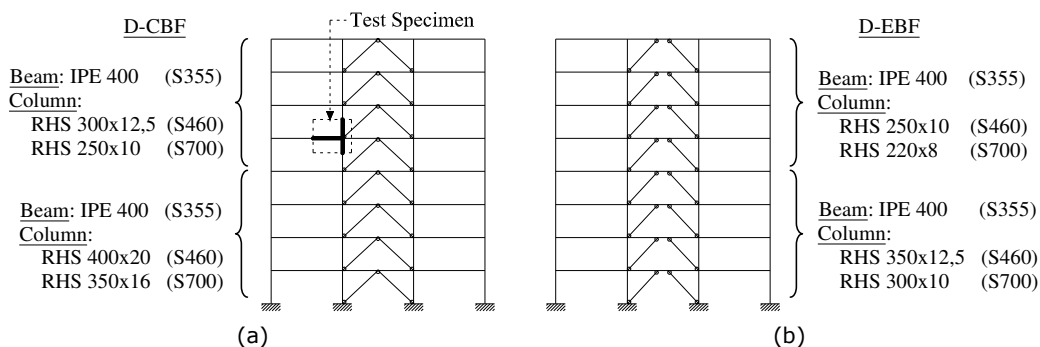


Fig. 4-2. Pre-designed frames with CFT columns: (a) D-CBF, and (b) D-EBF [86]

4.4. Joint detailing

As basis for definition of the experimental program on beam-column joints, cross-sections from the D-CBF frame were used (see Fig. 4-2), considering two combinations of HSS/MCS:

- RHS 300x12,5 S460 column and IPE 400 S355 beam;
- RHS 250x10 S700 column and IPE 400 S355 beam;

The beams are welded to the columns considering two types of connections: with reduced beam section (RBS), and with cover plates (CP). Due to the flexibility of the tube walls under transverse forces, the connection solution of the beams and columns within the current research was based on the use of external diaphragms.

The detailed procedure used for the design of the two joint typologies is shown in Chapter 6. The design was performed considering the development of the plastic hinge in the beams. Further with the bending moment and shear force from the plastic hinge, the joint components were designed so as to comprise a higher capacity in comparison to the fully yielded and strain hardened plastic hinge.

4.4.1. Reduced beam section joint

The joint connects a wide-flange hot rolled beam with a concrete filled tube (CFT) column using field welding (see Fig. 4-3.). A reduced beam section is used in order to alleviate stresses in the beam-column connection and control the location of the plastic hinge. An external diaphragm is shop-welded to the column in order to transfer the forces from beam to the side walls of the column.

Beam flanges are welded to the external diaphragm using full-penetration butt welds (see Fig. 4-3.). The preparation details for full penetration welds between external diaphragm and beam flanges are shown in Fig. 4-4. As can be seen, the thickness of the external diaphragm obtained from design was higher than the flange thickness. Therefore, in order to avoid the concentration of the stresses due to thickness variation, the preparation details shown in Fig. 4-4 were proposed. The solution does not require weld access holes, and the advantage is that no preparations are necessary for beam flanges.

A shear tab bolted connection between the beam web and vertical column stiffener was considered for erection only. The final connection of the beam web is realised using full-penetration weld, using the shear tab as backing plate. The design of the reduced beam section was done based on provisions from AISC 358-05 [87]. The design procedure was adapted to the particular joint configuration employing CFT column reinforced with external diaphragm.

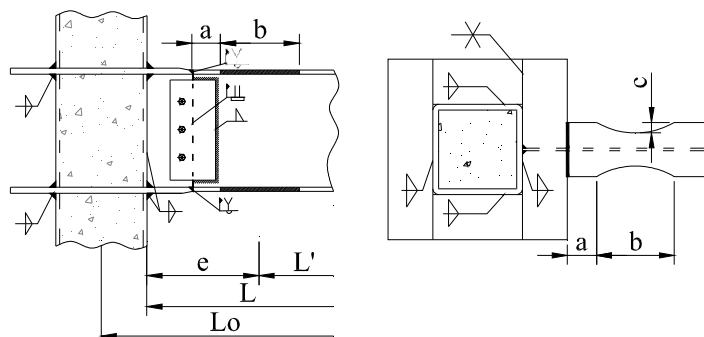


Fig. 4-3. Welded beam to column joint with reduced beam section

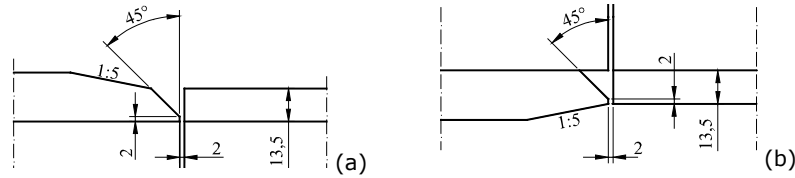


Fig. 4-4. Preparation details for full penetration welds between external diaphragm and top flange (a), and bottom flange (b)

4.4.2. Cover plate joint

The joint connects a wide-flange hot rolled beam with a concrete filled tube (CFT) column using field welding (see Fig. 4-5). An external diaphragm is shop-welded to the column in order to reduce the out-of plane bending of the column walls. Cover plates are used in order to reinforce the beam-column connection, forcing the plastic hinge to form in the beam.

The cover plates are welded to the external diaphragm using full-penetration butt welds. The preparation details shown in Fig. 4-6 are based on the weld access hole details recommended in FEMA-350 [88]. As can be seen, the thickness of the external diaphragm obtained from design was higher compared to the thickness of the cover plates. Therefore, in order to avoid the concentration of the stresses due to thickness variation, the preparation details shown in Fig. 4-6 were proposed. The advantage is that no preparations are necessary for beam flanges.

A bolted connection between the beam web and vertical column stiffener was considered for erection only. The final connection of the beam web is realized using fillet welds.

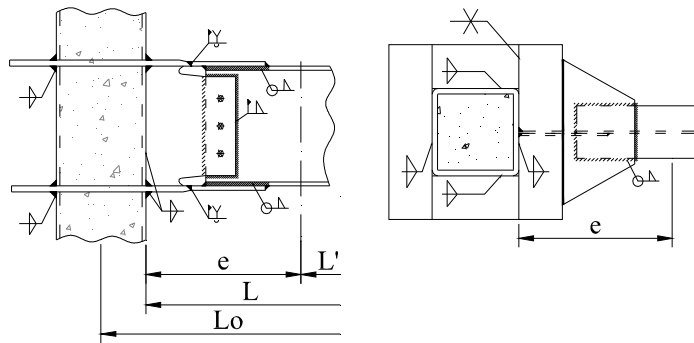


Fig. 4-5. Welded beam to column joint with cover plates

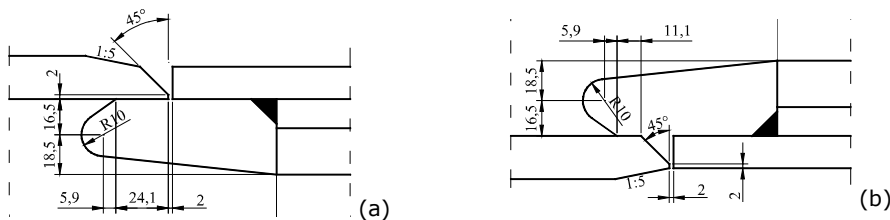


Fig. 4-6. Preparation details for full penetration welds between external diaphragm and top cover plate (a), and bottom cover plate (b)

4.5. Performance based evaluation and final design

4.5.1. Final design of frames

The final design of frames (see Fig. 4-7) was performed within HSS-SERF research project by GIPAC, UNINA and VTT [1]. The cross sections of the members obtained from design are summarised in Annex A. The columns from 5th to 8th floor were realised from S355 steel grade. This is due to the fact that if realised from S460 the cross section would be too small for the connection with the beam.

It is to be noted that the performance evaluation was performed by the author considering the frames shown in Fig. 4-7 and which are based on the designed frames from HSS-SERF project [1]. Consequently, the cross-sections of members from the MRF were kept the same as designed within the research project. In contrast, for the dual concentrically braced frame (D-CBF) and dual eccentrically braced frame (D-EBF) some changes were undertaken regarding the beams from the moment resisting bays, the dissipative links from the D-EBF and braces from both D-CBF and D-EBF. The beams from the moment resisting bays of the D-CBF and D-EBF were changed from HEA type to IPE type, particularly to IPE400 for the comparison with the experimental investigations. An overview of the members is shown in Table 4-5 for MRF, Table 4-6 and for D-CBF, and in Table 4-7 for D-EBF.

In the performance based evaluation, for each frame configuration – two joint typologies were considered, i.e. joint with reduced beam section (RBS) and joint with cover plates (CP). In addition, the actual position of the plastic hinges was taken into account in each frame configuration.

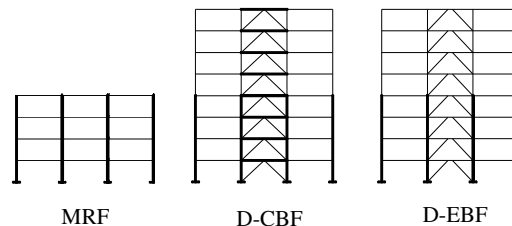


Fig. 4-7. Configuration of frames considered for the performance based evaluation

Table 4-5 – MRF – cross sections of members [86]

Columns	Beams	
Storeys: 1-4	1-2	3-4
CF-RHS 400x20 S460 / C30/37	IPE 400 S355	IPE 360 S355

Table 4-6 – D-CBF - cross sections of members

Storey	Columns	Beams		Braces
		Inner S460	Outer S355	CHS S355
1	CF-RHS 400x16 S460 / C30/37	HEB 450	IPE 400	193.7x6.3
2				193.7x6.3
3				177.8x6.3
4				177.8x6.3
5	CF-RHS 300x10 S355 / C30/37	HEA 450	IPE 400	168.3x6.3
6				139.7x6.3
7				139.7x5
8				HEA 320

Table 4-7 – D-EBF - cross sections of members

Storey	Columns	Beams		Braces
		Inner (link) S355	Outer S355	CHS S355
1	CF-RHS 400x16 S460 / C30/37	IPE 270	IPE 400	323.9X16
2		IPE 300		323.9X16
3		IPE 270		323.9X12.5
4		IPE 270		323.9X12.5
5	CF-RHS 300x8 S355 / C30/37	IPE 270	IPE 400	273X12
6		IPE 270		244.5X12
7		IPE 240		193.7X12.5
8		IPE 240		193.7X10

4.5.2. Performance based evaluation

In order to evaluate the response of the structures in the inelastic domain, static nonlinear analyses were performed using the N2 method, as well as dynamic nonlinear analyses.

Static nonlinear analysis

The N2 method was developed at the University of Ljubljana by Fajfar [89] and can be used to verify the seismic performances of buildings designed by current methods (i.e. spectral analysis). The method combines the non-linear static analysis (push-over) of a system with multiple degrees of freedom MDOF with an analysis based on the response spectrum of a system with one degree of freedom SDOF.

The static nonlinear analysis was performed using SAP2000 [90]. The lateral storey forces were assumed to be proportional to the 1st mode of vibration. The P-Delta effect of the seismic masses that were not tributary to the frame was considered employing a leaning column.

According to N2 method, the comparison between the seismic demand and the capacity is made in terms of displacements by applying the equivalent single degree of freedom (SDOF) substitution approach and by plotting the capacity spectrum. Based on the nonlinear static procedure, the structure is pushed to a certain displacement, termed "target displacement", and the forces and deformations are evaluated. The target displacement represents the maximum displacement to be experienced during the design earthquake.

The elastic acceleration response spectrum was determined according to EN 1998-1 [27] considering a peak ground acceleration of 0.24g for the MRF, and a peak ground acceleration of 0.32g for the D-CBF and D-EBF. Table 4-8 summarises the values of the computed target displacements, D_t , for the three studied frames.

Table 4-8 – Target displacements

Frame type		MRF		D-CBF		D-EBF	
Joint type		RBS	CP	RBS	CP	RBS	CP
D_t [m]	$\lambda=0.5$	0.082	0.082	0.113	0.108	0.147	0.141
	$\lambda=1.0$	0.168	0.151	0.225	0.221	0.290	0.287
	$\lambda=1.5$	0.251	0.225	0.338	0.329	0.435	0.423

Three performance levels were considered:

- serviceability limit state (SLS);
- ultimate limit state (ULS);
- collapse prevention limit state (CPLS);

The intensity of earthquake action at the ULS is equal to the design one (intensity factor $\lambda=1.0$). The seismic hazard level corresponding to serviceability limit states (SLS) and collapse prevention limit states (CPLS) are related to $\lambda=0.5$ and respectively $\lambda=1.5$. Based on FEMA 356 [91], the following acceptance criteria were considered in the study:

- link deformations at SLS, ULS and CPLS are $\gamma_u=0.005$ rad, $\gamma_u=0.11$ rad and $\gamma_u=0.14$ rad;
- for conventional braces in compression (except EBF braces), plastic deformations at SLS, ULS and CPLS are $0.25\Delta_c$, $1\Delta_c$ and $2\Delta_c$, where Δ_c is the axial deformation at expected buckling load;
- for conventional braces in tension (except EBF braces), plastic deformations at SLS, ULS and CPLS are $0.25\Delta_t$, $7\Delta_t$ and $9\Delta_t$, where Δ_t is the axial deformation at expected tensile yielding load;
- for beams in flexure, the rotation at SLS, ULS and CPLS are $0.25\theta_y$, $2\theta_y$ and $3\theta_y$, where θ_y is the yield rotation;
- for columns in flexure, the plastic rotation at SLS, ULS and CPLS are $0.25\theta_y$, $2\theta_y$ and $3\theta_y$, where θ_y is the yield rotation;

Fig. 4-8, Fig. 4-9 and Fig. 4-10 show the comparison between the seismic demand and the capacity curve of the equivalent SDOF. In addition the base-shear force vs. top displacement curve is shown for each frame typology and considering the two joint solutions (RBS and CP). The target displacements corresponding to the three seismic intensity levels are marked on the capacity curves. It can be observed that the capacity is higher for the frames with CP joints. The state of the frames (with CP joints) is shown at the three seismic intensity levels ($\lambda=0.5$, 1.0, and 1.5) leading to the following observations:

- MRF: plastic hinges developed in the beams corresponding to $\lambda=1.0$ for MRF with RBS joints, and at $\lambda=1.5$ for MRF with CP joints;
- D-CBF: at $\lambda=0.5$ no plastic hinges were developed, at $\lambda=1.0$ plastic hinges from braces reached the collapse, and at $\lambda=1.5$ plastic deformations developed also in the beams from the moment resisting bays;
- D-EBF: yielding of links occurred at $\lambda=0.5$; related to $\lambda=1.0$ link failure was observed at the 2nd floor and plastic hinges formed in the outer beams.

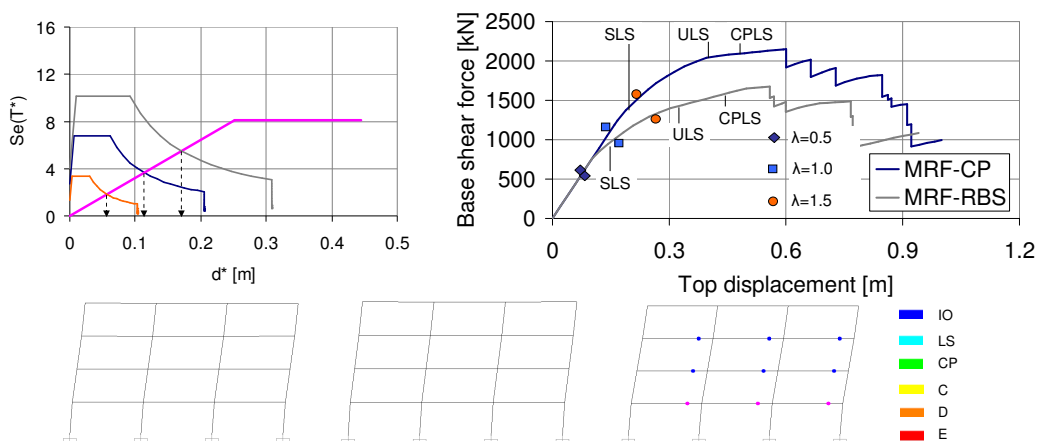


Fig. 4-8. Determination of the target displacement for the equivalent SDOF, capacity curves, and the state of the MRF with CP joints at $\lambda=0.5$, 1.0, and 1.5

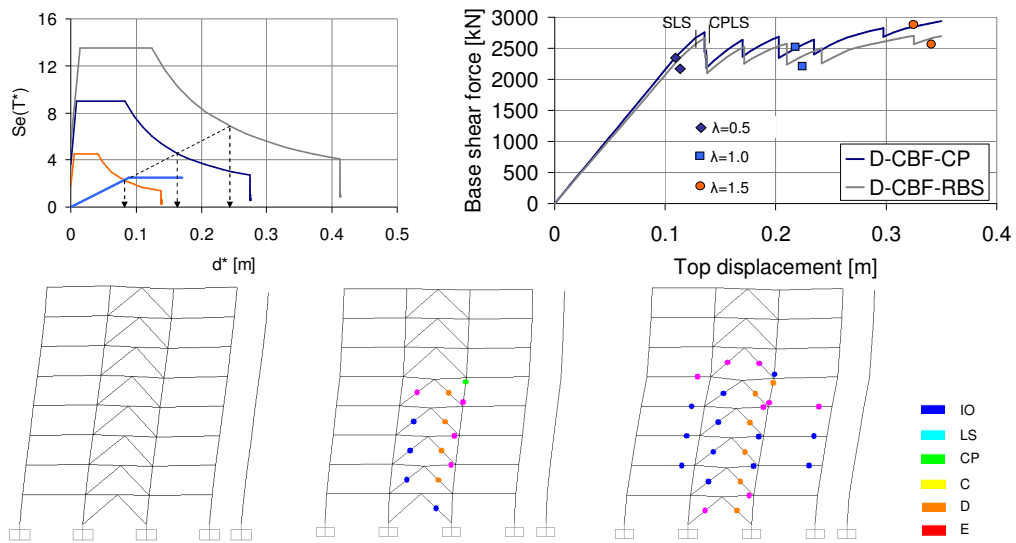


Fig. 4-9. Determination of the target displacement for the equivalent SDOF, capacity curves, and the state of the D-CBF with CP joints at $\lambda=0.5, 1.0,$ and 1.5

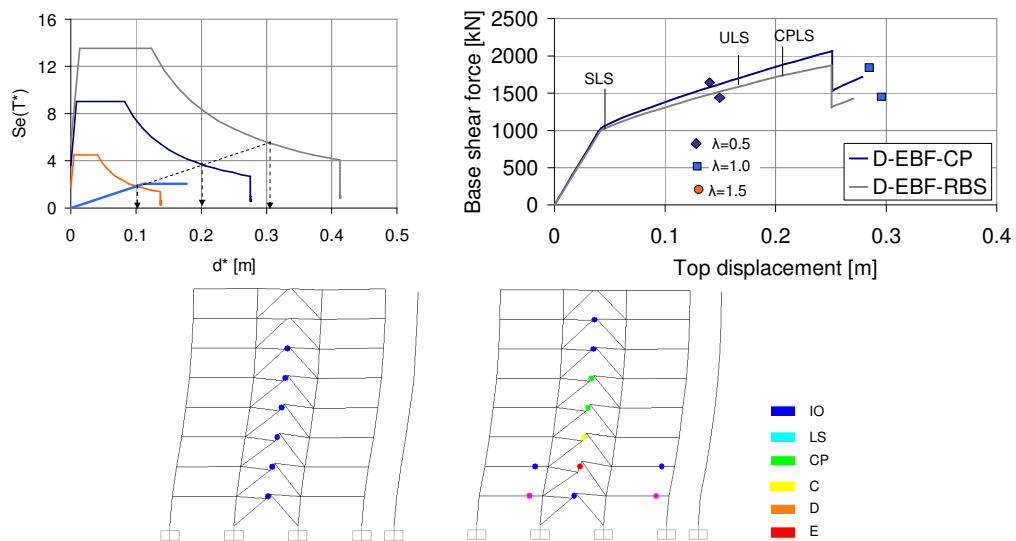


Fig. 4-10. Determination of the target displacement for the equivalent SDOF, capacity curves, and the state of the D-EBF with CP joints at $\lambda=0.5, 1.0,$ and 1.5

Based on the behaviour of the three frame typologies, it was observed that corresponding to the three intensity levels ($\lambda=0.5, 1.0,$ and 1.5) the MRF's satisfied the immediate occupancy performance levels. The D-CBF's satisfied the immediate occupancy level at $\lambda=0.5$, but at $\lambda=1.0$ and $\lambda=1.5$ the braces in compression were corresponding to collapse and therefore the performance levels were not satisfied. The D-EBF's satisfied the immediate occupancy performance level at $\lambda=0.5$, but at $\lambda=1.0$ the links were corresponding to collapse and therefore the life safety

performance level was not satisfied. In spite of these observations global collapse was not evidenced.

Dynamic nonlinear analysis

A set of dynamic nonlinear analysis were carried out with the aim to assess the structural performance under seismic loads. For this purpose, each of the three frame typologies were subjected to a set of ground motion records each scaled to multiple levels of intensity. Three accelerograms were chosen from a set of seven ground motion records and used further in the structural analyses. The results are shown as the maximum out of the three cases.

Fig. 4-11 and Fig. 4-12 show the inter-story drift and the plastic mechanism, corresponding to the three seismic intensity levels, for MRF with CP and RBS joints. Fig. 4-13 and Fig. 4-14 show the inter-story drift and plastic mechanism, corresponding to $\lambda=0.5$ and $\lambda=1.0$, for D-CBF with CP and RBS joints.

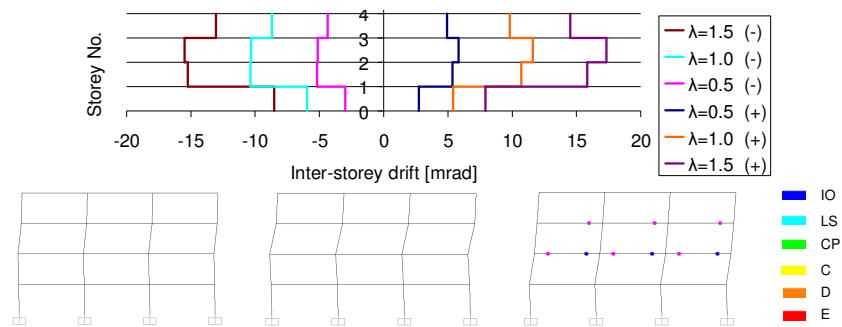


Fig. 4-11. Inter-story drift and plastic hinges for MRF with CP joints at $\lambda=0.5$, 1.0, and 1.5

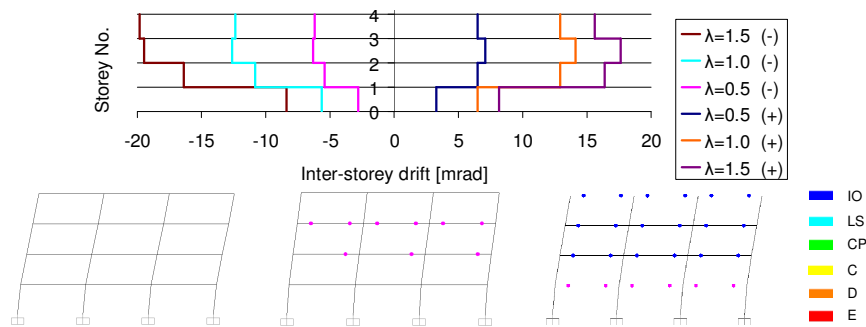
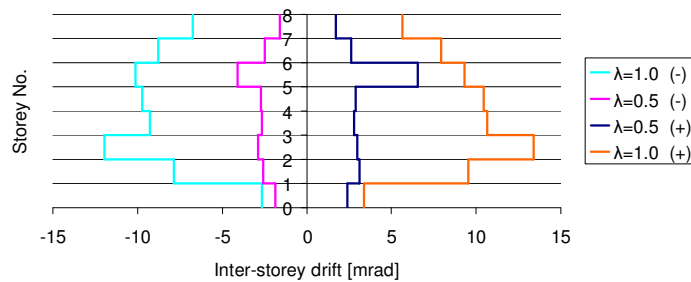


Fig. 4-12. Inter-story drift and plastic hinges for MRF with RBS joints at $\lambda=0.5$, 1.0, and 1.5



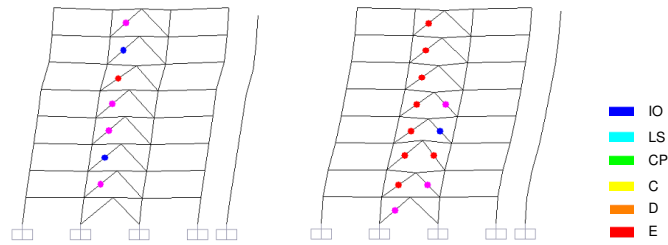


Fig. 4-13. Inter-storey drift and plastic hinges for D-CBF with CP joints at $\lambda=0.5$ and 1.0

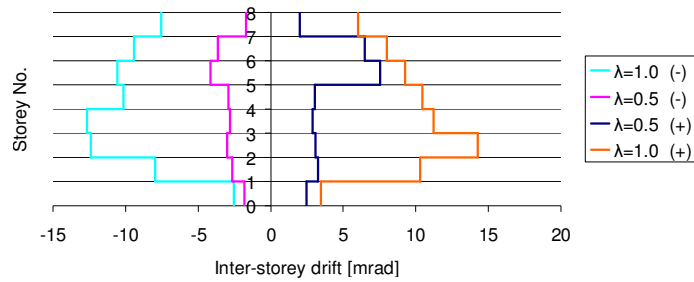


Fig. 4-14. Inter-storey drift and plastic hinges for D-CBF with RBS joints at $\lambda=0.5$ and 1.0

Fig. 4-15 and Fig. 4-16 show the inter-storey drift and plastic mechanism, corresponding to the three seismic intensity levels for D-EBF with CP and RBS joints.

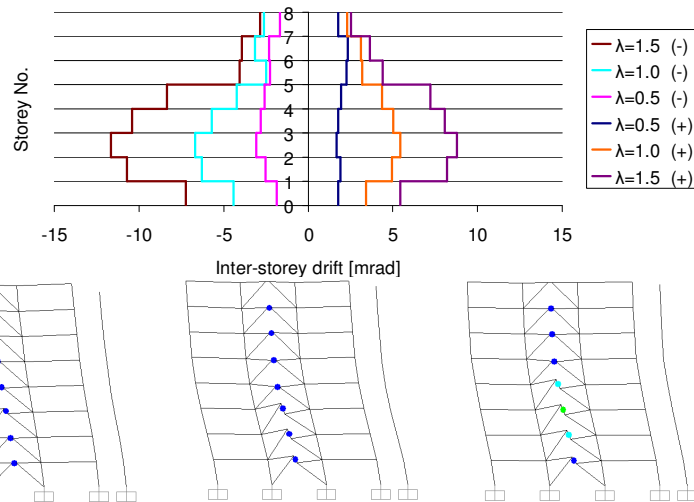


Fig. 4-15. Inter-storey drift and plastic hinges for D-EBF with CP joints at $\lambda=0.5$, 1.0, and 1.5

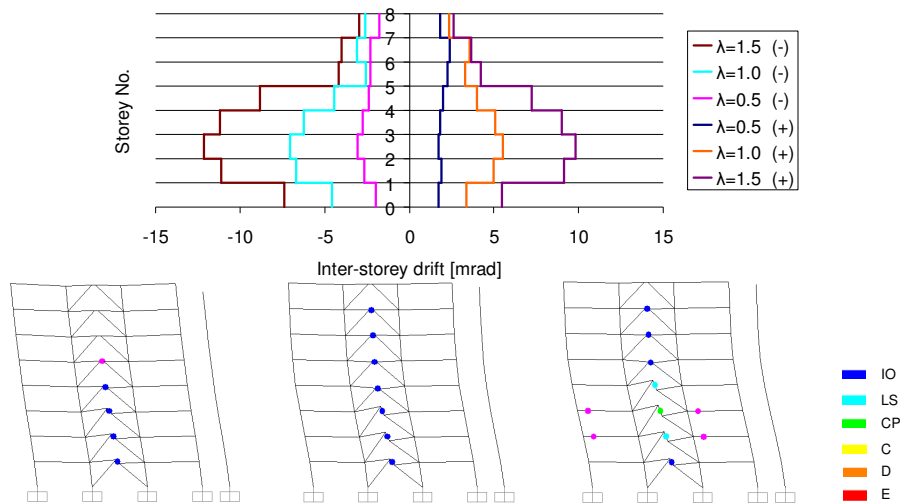


Fig. 4-16. Inter-storey drift and plastic hinges for D-EBF with RBS joints at $\lambda=0.5$, 1.0, and 1.5

Based on the behaviour of the three frame configurations, it was observed that corresponding to the three intensity levels ($\lambda=0.5$, 1.0, and 1.5) the MRF's satisfied the immediate occupancy performance level. The D-CBF's evidenced brace failure, according to the acceptance criteria provided by FEMA 356 [91] corresponding to $\lambda=0.5$ and $\lambda=1.0$; at $\lambda=1.5$ global structural collapse was observed. Therefore, the performance levels were not satisfied. The D-EBF's satisfied the immediate occupancy performance level at both $\lambda=0.5$ and $\lambda=1.0$; at $\lambda=1.5$ the maximum plastic deformations within links were corresponding to collapse prevention according to the acceptance criteria from FEMA 356, and therefore the collapse prevention performance level was satisfied.

Table 4-9 summarises the maximum displacement at the top of the building as obtained from the dynamic nonlinear analysis corresponding to the three seismic intensity levels, i.e. $\lambda=0.5$, 1.0, and 1.5. In comparison to the target displacements obtained for each frame with the N2 method (see Table 4-8), the following observations were made:

- In case of MRF with RBS joints – the maximum top displacements were very close to the target displacements, only slightly lower;
- In case of MRF with CP joints – the maximum top displacements evidenced lower values than the target displacements;
- In case of D-CBF with RBS and with CP joints – the maximum top displacements were very close to the target displacements, a bit lower corresponding to $\lambda=0.5$ and a bit higher corresponding to $\lambda=1.0$;
- In case of D-EBF with RBS and with CP joints – the maximum top displacements were significantly lower than the target displacements.

Table 4-9 – Maximum top displacements

Frame type		MRF		D-CBF		D-EBF	
Joint type		RBS	CP	RBS	CP	RBS	CP
D_t [m]	$\lambda=0.5$	0.081	0.065	0.1	0.081	0.061	0.061
	$\lambda=1.0$	0.161	0.131	0.247	0.23	0.115	0.109
	$\lambda=1.5$	0.21	0.194	-	-	0.197	0.186

4.5.3. Seismic performance demand for beam to-column joints

The results obtained from the dynamic non-linear analysis lead to the following observations:

- MRF's evidenced a good behaviour: elastic response at $\lambda=0.5$, low plastic deformation in beams at $\lambda=1.0$, and global mechanism – development of plastic hinges in all beams – corresponding to $\lambda=1.5$;
- D-CBF's evidenced for both $\lambda=0.5$ and $\lambda=1.0$ brace failure – according to the acceptance criteria provided by FEMA 356 [91] – i.e. the plastic deformations of compressed braces were higher; the structure did not suffer global collapse corresponding to $\lambda=0.5$ and $\lambda=1.0$, however at $\lambda=1.5$ global structural collapse was observed;
- D-EBF's evidenced yielding of links at $\lambda=0.5$ as observed from the push-over; all links except at the last floor were activated at $\lambda=1.0$ – however with low plastic deformations (7.6 mrad); at $\lambda=1.5$ the plastic deformations in the links increased (14.6 mrad) and plastic hinges developed also in the outer beams (MRF with RBS joint).

In case of moment resisting frames (MRF), the horizontal forces are mainly resisted by members acting essentially in flexural mode, and therefore the performance of MR joints is crucial. In contrast, the main component of the D-CBF's and D-EBF's in dissipating the seismic energy is represented by braces, and respectively by shear links, while the joints in MRF bays have secondary effect. It was observed that these frames develop plastic hinges mostly in braces (D-CBF) and links (D-EBF), and corresponding to higher intensity levels also in joints. Table 4-10 and Table 4-11 show an overview of the seismic demand in terms of maximum inter-storey drift, obtained from the dynamic nonlinear analysis, corresponding to MRS's, and respectively to D-CBF's and D-EBF's. At the three intensity levels the rotation demand for joints within MRF was in amount of 7, 14, and 17 mrad. The rotation demand for joints within D-CBF was obtained in amount of 7 and 14 mrad corresponding to $\lambda=0.5$ and $\lambda=1.0$. In contrast, for D-EBF the rotation demand was lower i.e. 3 mrad ($\lambda=0.5$), 7 mrad ($\lambda=1.0$) and 12 mrad ($\lambda=1.5$). The mentioned values correspond to frames with RBS joints. It can be observed that the demands are lower corresponding to frames with CP joints. For comparison, the acceptance criteria from FEMA 356 [91] in terms of rotation at SLS, ULS and CPLS for the RBS beam is $0.25\theta_y=2.8$ mrad, $2\theta_y=22.6$ mrad and $3\theta_y=33.9$ mrad; and respectively for the CP beam is $0.25\theta_y=2.7$ mrad, $2\theta_y=21.6$ mrad and $3\theta_y=32.4$ mrad.

Table 4-10 – Inter-storey drift demand MRF

Frame type		MRF	
Joint type		RBS	CP
$d_{r,max}/h$ [rad]	$\lambda=0.5$	0.0071	0.0058
	$\lambda=1.0$ (0.24g)	0.0141	0.0116
	$\lambda=1.5$	0.0176	0.0173

Table 4-11 – Inter-storey drift demand D-CBF and D-EBF

Frame type		D-CBF		D-EBF	
Joint type		RBS	CP	RBS	CP
$d_{r,max}/h$ [rad]	$\lambda=0.5$	0.0075	0.0065	0.0031	0.0031
	$\lambda=1.0$ (0.32g)	0.0143	0.0134	0.0071	0.0066
	$\lambda=1.5$	-	-	0.0121	0.0116

4.7. Concluding remarks

A number of three frame typologies were considered i.e. moment resisting frames (MRF), dual concentrically braced frames (MRF+CBF), and dual eccentrically braced frames (MRF+EBF). The design of the frames was performed as part of the research project HSS-SERF [86] considering the dual-steel concept. Consequently, mild carbon steel (MCS) was used for dissipative members and high strength steel (HSS) for non-dissipative members.

A description was made in relation to the frames that were used as basis for the definition of the experimental program, i.e. choice of cross-sections for beam-to-column joint specimens. Further, a description was made in relation to the configuration and detailing used for the two joint typologies, i.e. reduced beam section joints (RBS) and cover plate joints (CP). Due to the flexibility of the tube front wall under transverse forces, the connection solution was based on the use of external diaphragms for the transfer of forces to the side walls of the RHS tube.

With the aim to assess the seismic demand for the beam-to-column joints, a set of frames were analysed through static and dynamic nonlinear analyses.

For each frame, the target displacement was computed with the N2 method corresponding to three intensity levels $\lambda=0.5$, 1.0, and 1.5. It was observed that MRF's satisfied the immediate occupancy performance level for each of the three intensity levels ($\lambda=0.5$, 1.0, and 1.5). The D-CBF's satisfied the immediate occupancy level at $\lambda=0.5$, but at $\lambda=1.0$ and $\lambda=1.5$ the performance levels were not satisfied (braces in compression evidenced failure according to the acceptance criteria from FEMA 356). The D-EBF's satisfied the immediate occupancy performance level at $\lambda=0.5$, but at $\lambda=1.0$ the plastic rotation demands in links exceeded the rotation capacity and therefore the life safety performance level was not satisfied.

In addition the results obtained from the dynamic non-linear analysis lead to the following observations:

- MRF's evidenced a good behaviour: elastic response at $\lambda=0.5$, low plastic deformation in beams at $\lambda=1.0$, and global mechanism corresponding to $\lambda=1.5$; corresponding to the three intensity levels ($\lambda=0.5$, 1.0, and 1.5) MRF's satisfied the immediate occupancy performance level;
- D-CBF's evidenced for both $\lambda=0.5$ and $\lambda=1.0$ brace failure – according to the acceptance criteria provided by FEMA 356 [91]; at $\lambda=1.5$ global structural collapse was observed; therefore the performance levels were not satisfied;
- D-EBF's evidenced yielding of links at $\lambda=0.5$; all links except the last floor were activated at $\lambda=1.0$ – however with low plastic deformations (7.6 mrad); at $\lambda=1.5$ the plastic deformations in the links increased (14.6 mrad) and plastic hinges developed also in the outer beams (MRF with RBS joint); the immediate occupancy performance level was satisfied at both $\lambda=0.5$ and $\lambda=1.0$, and corresponding to $\lambda=1.5$ the collapse prevention performance level was satisfied.

From the comparison between the target displacements obtained with N2 method and the maximum displacement at the top of the building as obtained from the dynamic nonlinear analysis, the following observations were made:

- In case of MRF with RBS joints – the maximum top displacements were very close to the target displacements, only slightly lower;

- In case of MRF with CP joints – the maximum top displacements evidenced lower values than the target displacements;
- In case of D-CBF – the maximum top displacements were very close to the target displacements, a bit lower corresponding to $\lambda=0.5$ and a bit higher corresponding to $\lambda=1.0$;
- In case of D-EBF – the maximum top displacements were significantly lower than the target displacements;

In case of moment resisting frames (MRF), the horizontal forces are mainly resisted by members acting in flexural mode, and therefore the performance of MR joints is crucial. In contrast, the main component of the D-CBF's and D-EBF's in dissipating the seismic energy is represented by braces, and respectively by shear links, while the joints in MRF bays have secondary effect. It was observed that these frames develop plastic hinges mostly in braces (D-CBF) and links (D-EBF), and corresponding to higher intensity levels also in joints. At the three intensity levels the rotation demand for joints within MRF was in amount of 7, 14, and 17 mrad. The rotation demand for joints within D-CBF was obtained in amount of 7 and 14 mrad corresponding to $\lambda=0.5$ and $\lambda=1.0$. In contrast, for D-EBF the rotation demand was lower i.e. 3 mrad ($\lambda=0.5$), 7 mrad ($\lambda=1.0$) and 12 mrad ($\lambda=1.5$). The demands were lower corresponding to frames with CP joints. For comparison, the acceptance criteria from FEMA 356 [91] in terms of rotation at SLS, ULS and CPLS for the RBS beam is $0.25\theta_y=2.8$ mrad, $2\theta_y=22.6$ mrad and $3\theta_y=33.9$ mrad; and respectively for the CP beam is $0.25\theta_y=2.7$ mrad, $2\theta_y=21.6$ mrad and $3\theta_y=32.4$ mrad.

5. EXPERIMENTAL EVALUATION OF SEISMIC PERFORMANCE OF DUAL STEEL IPE BEAM-TO CFRHS COLUMN WELDED JOINTS

5.1. Introduction

The current chapter is related to the experimental evaluation of the seismic performance of dual steel IPE beam-to concrete filled rectangular hollow section column welded joints. Consequently, a description is made in relation to the experimental program that covered extensive investigations on material samples (concrete and steel), on steel-concrete connection for the composite action of CFT columns, as well as on full scale beam-to-column joints. The design of the experimental program covered activities related to the experimental test set-up, instrumentation, loading protocols, and preparation of specimens. Results from the experimental investigations are shown related to material samples and steel-concrete connection. The results from tensile tests performed on steel samples allowed the calibration of the material model which was used further within the pre-test numerical simulations. Due to the innovative joint configurations, an accurate prediction was needed in order to avoid unacceptable failure during the tests. Predictions from the numerical investigations are therefore presented. Finally, results from the experimental investigations on the beam-to-column joints are shown for each configuration considering the test assembly, observations from test, and response of the joints subjected to monotonic and cyclic loading.

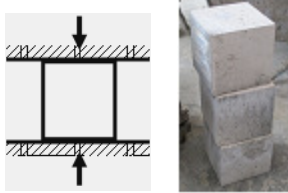

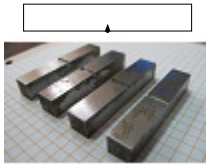
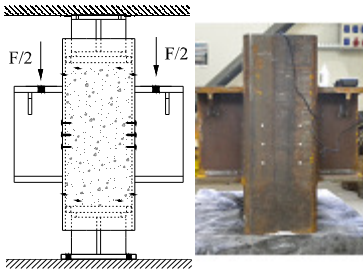
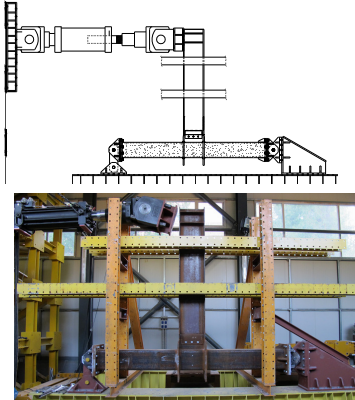
Interpretation and comparison of results are shown as well as the calibration of numerical models based monotonic and cyclic tests. Numerical simulation of complementary testing cases allowed assessing the influence of different parameters on the behaviour of the beam to column joints.

5.2. Design of experimental program

The design of the experimental program was performed with the aim to evaluate the seismic performance of dual-steel beam-to-column joints realised in welded solution and considering two joint typologies (RBS and CP).

Table 5-1 makes an overview of the entire experimental program that covered a total number of 91 test specimens. It can be observed that the experimental program enclosed three phases, i.e. investigation of material samples, investigation of steel-concrete connection, and investigation of beam-to-column joints. The tests performed on material covered compression tests on concrete cubes, as well as tensile and Charpy V-notch impact tests on steel samples (S355, S460 and S690 steel components). The parameters investigated within the steel-concrete connection tests consisted of loading (monotonic, cyclic), connection (friction, friction+connectors) and steel grade (S460, S700). The aim was to assess the efficiency of shot fired nails in providing the connection between the steel tube and the concrete core. The parameters investigated within the joint tests consisted of loading (monotonic, cyclic), joint type (RBS, CP), steel grade for column (S460, S700), and intended failure (beam, connection). The design of the experimental program covered also the design of the test set-up, instrumentation, and loading procedures. A detailed description is further shown for each aspect.

Table 5-1 – Summary of testing program

Test type	Conceptual scheme & Illustration	Test characteristics	No. of specimens
Materials		Compression test on concrete samples (C30/37) at 28 days from casting	9
		Monotonic quasi-static tensile tests S355 / S460 / S690	30
		Charpy V-notch toughness tests S355 / S460 / S690	30
Steel-concrete connection		Loading: <ul style="list-style-type: none"> • Monotonic • Cyclic Connection: <ul style="list-style-type: none"> • Friction • Friction+connectors Steel grade for column: <ul style="list-style-type: none"> • S460 • S700 	6
Joint tests		Loading procedure: <ul style="list-style-type: none"> • Monotonic • Cyclic Joint type: <ul style="list-style-type: none"> • RBS • CP Steel grade for column: <ul style="list-style-type: none"> • S460 • S700 Intended failure mode: <ul style="list-style-type: none"> • Beam • Connection 	16

5.2.1. Material samples

The tests performed on material cover compression tests on concrete cubes, as well as tensile and Charpy V-notch impact tests on steel samples.

In order to evaluate the compression strength of concrete at 28 days from casting, a number of 3 samples were collected at the concrete station, and a number of 6 samples were collected on site (at the University), from which 3 samples at the beginning and 3 samples at the ending of concrete casting.

In order to evaluate the characteristics from tensile and Charpy V-notch impact tests, samples were prepared from the additional received material (profiles and plates as summarised in Table 5-2) associated to each component of the beam-to-column joints (see Fig. 5-1).

Table 5-2 – List of joint components for the tensile and Charpy V-notch tests

Nr.	Position	Steel Grade	Nominal thickness [mm]
1	IPE 400 flange	S355 JR (J2+N)	13.5
2	IPE 400 web	S355 JR (J2+N)	8.6
3	Cover plates	S355 JR	15
4	Splice plate	S355 JR	10
5	Tube RHS 300x12.5	S460 M	12.5
6	Tube RHS 250x10	S700 QL	10
7	External diaphragm S460	S460 NL	20
8	External diaphragm S690	S690 QL	20
9	Vertical stiffeners S460	S460 NL	10
10	Vertical stiffeners S690	S690 QL	10

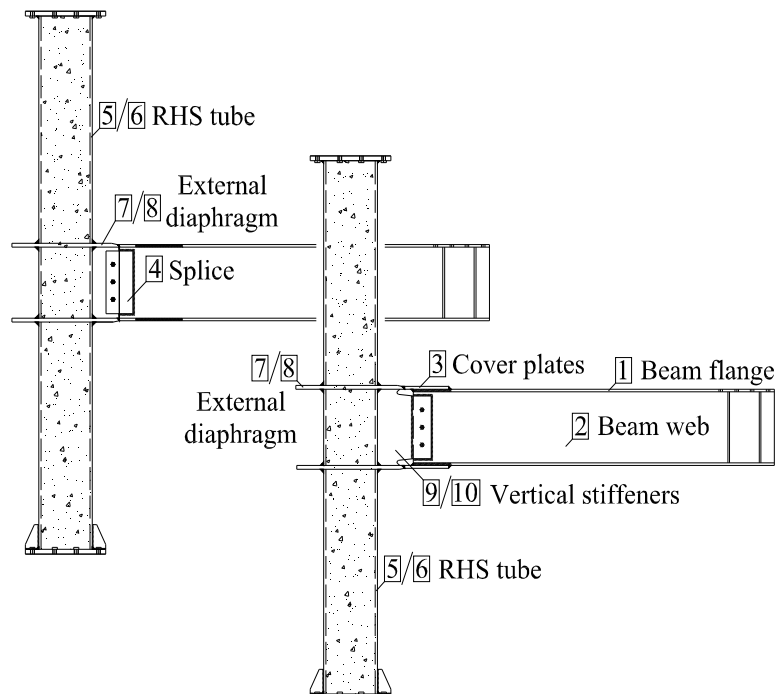


Fig. 5-1. Joint components for tests on steel samples

5.2.2. Load introduction tests

The square columns realized as concrete filled tubes (CFT) have the advantage of improved rigidity and resistance to fire, as well as similar cross-sectional properties on principal loading directions. The combination the two materials may lead to a reduced steel section. However, a particular attention should be given in order to distribute the stresses between the steel tube and the concrete core.

The aim of the experimental program was to evaluate the load introduction within composite columns realized as concrete filled tubes of high strength steel (see Fig. 5-2). For this purpose load introduction tests were considered on a number of 6 specimens varying parameters such as: loading procedure (monotonic and cyclic), connection type (steel-concrete bonding; steel-concrete bonding combined with connectors), and steel grade (S460 and S700). The objective of the research was to assess the efficiency of the shot fired nails in providing the shear connection between the steel tube and the concrete core under monotonic and cyclic loading. As connectors, a number of 24 *Hilti X-DSH32 P10* shot fired nails were considered per column stub. The connectors were applied before concreting and after a pre-drill was performed on the steel tube based on the installation instructions prepared by Hilti [92] for the particular case (steel grade, thickness) of the current specimens.



Fig. 5-2. Specimen configuration for the load introduction tests

5.2.2.1. Specimens

The experimental program on column stubs is summarised in Table 5-3. A number of 6 tests on column stubs were considered varying parameters such as: steel tube, steel-concrete connection, and loading procedure. The configuration of the specimens is illustrated in Fig. 5-3.

Table 5-3 – Experimental program on column stubs

Nr.	Specimen	Tube	Bond	Load
1	S700-F-M	RHS 250x10 S700	Friction	Monotonic
2	S700-F-C	RHS 250x10 S700	Friction	Cyclic
3	S700-F-H-M	RHS 250x10 S700	Friction & Hilti*	Monotonic
4	S700-F-H-C	RHS 250x10 S700	Friction & Hilti*	Cyclic
5	S460-F-H-M	RHS 300x12,5 S460	Friction & Hilti*	Monotonic
6	S460-F-H-C	RHS 300x12,5 S460	Friction & Hilti*	Cyclic

* 24 Hilti X-DSH32 P10 shot fired nails

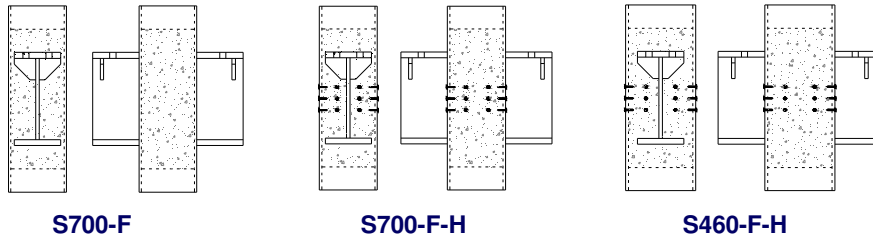


Fig. 5-3. Specimen configuration (front and lateral view)

The three configurations illustrated in Fig. 5-3, aimed for both monotonic and cyclic loading, are described as follows:

- S700-F-M / S700-F-C – adhesion (chemical bond and friction) between the steel tube and the encased concrete;
- S700-F-H-M / S700-F-H-C – adhesion combined with connectors;
- S460-F-H-M / S460-F-H-C – adhesion combined with connectors;

5.2.2.2. Test set-up

In order to assess the behaviour and the characteristics of the connection between the steel tube and the encased concrete (see Fig. 5-3), a universal testing machine was considered together with the test set-up which is illustrated in Fig. 5-4.

The experimental test set-up was designed considering:

- monotonic as well as cyclic loading conditions of the specimens;
- top and bottom supports (see Fig. 5-2) in contact with concrete core only;
- load to be applied on the steel tube;
- load path from the steel tube to the concrete core:
 - friction;
 - friction + connectors.

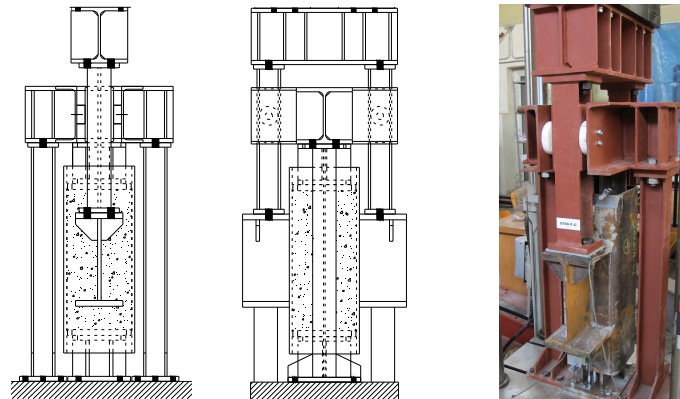


Fig. 5-4. Conceptual scheme (front and lateral view), and illustration of the test set-up

5.2.2.3. Instrumentation

The instrumentation of the specimens (see Fig. 5-5) consisted in the measurement of the force applied by the testing machine and the relative displacement between steel tube and concrete core – for which a number of 4

displacement transducers were used (two at the top side and two at the bottom side as can be seen in Fig. 5-6).

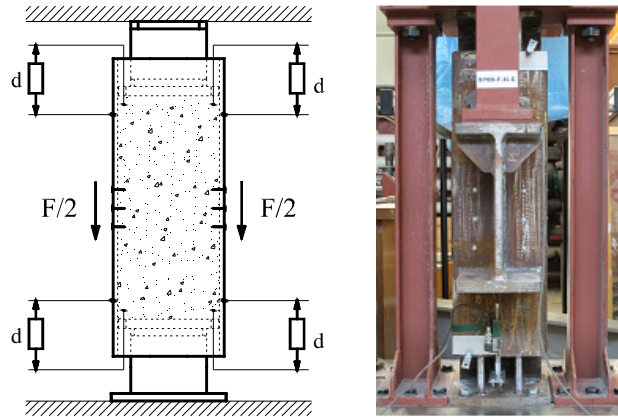


Fig. 5-5. Conceptual scheme and illustration of instrumentation arrangement



Fig. 5-6. Detail of instrumentation (top and bottom)

5.2.2.4. Loading protocols

Test control parameters

The parameters considered for the control of the load introduction tests were the relative displacement between the steel tube and the concrete core d and the force F (see Fig. 5-5). The load was applied in force control within the elastic range and in displacement control for the plastic range.

Preloading

Three alternating cycles with a peak load of up to 25% of the expected yield load were applied to the test assembly before the test itself in order to stabilize the system and check the operation of the equipment.

Monotonic loading protocol

Monotonic loading was applied by progressively increasing the displacement.

Cyclic loading protocol

The ECCS (1986) [93] procedure was considered for the cyclic loading.

The yield displacement d_y can be obtained using the method recommended by the ECCS (1986) document, as the relative displacement corresponding to intersection of the initial stiffness (K_{ini}) line and a tangent to the moment-rotation curve with a stiffness equal to $K_{ini}/10$ (see Fig. 5-7).

The cyclic loading procedure follows the steps below (ECCS), see Fig. 5-7:

- one cycle at $0.25 \cdot d_y$
- one cycle at $0.5 \cdot d_y$
- one cycle at $0.75 \cdot d_y$
- one cycle at $d = 1.0 \cdot d_y$
- three cycles at $m \cdot d_y$
- three cycles at $(m + m \cdot n) \cdot d_y$, with $n = 1, 2, 3 \dots$

The value of the m factor controls the magnitude of plastic excursions and the number of cycles performed in the plastic range. In the experimental tests a value of $m = 2$ was considered.

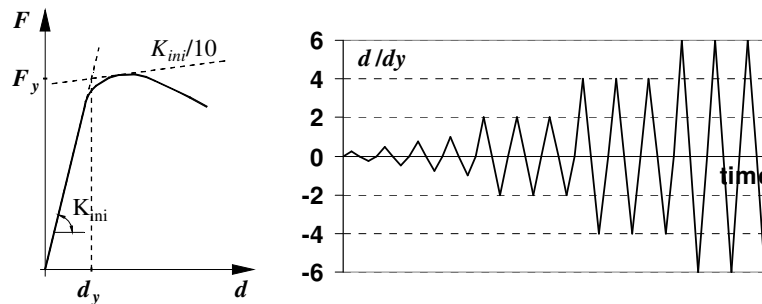


Fig. 5-7. Determination of yield displacement, and ECCS loading procedure [93]

5.2.3. Beam-to-column joint tests

The main objective of the experimental tests was to pre-qualify by tests welded connections in moment resisting frames and dual braced frames designed using the dual-steel concept. Table 5-4 summarises the experimental program on beam-to-column joints. The variations in the configuration of the joints are given by two joint typologies (reduced beam section – RBS, and cover-plate – CP), two steel grades for the concrete filled tubes (S460 and S700) and two intended failure modes (beam and connection zone). The response of each joint configuration was investigated considering a monotonic as well as a cyclic loading procedure.

Table 5-4 – Experimental program on beam-to-column joints

Parameter	Variable	No. of variations	No. of specimens
Loading procedure	Monotonic and cyclic	2	16
Joint type	Reduced Beam Section and Cover-Plate	2	
HSS grade	S460 and S700	2	
Failure mode	Weak beam / Weak connection	2	

5.2.3.1. Specimens

Considering the two joint typologies (RBS, and CP) and two steel grades for the tubes (S460 and S700), a number of four beam-to-column joint configurations were designed (see Fig. 5-8a, and Annex B). Additionally, in order to assess the overstrength of the connection zone and to observe the base components of the joint configurations, tests were planned considering the corresponding joint configurations for which the beam was strengthened (Fig. 5-8b, Annex B) with the aim to avoid the formation of the plastic hinge in the beam. For the "strengthened RBS joints", the reduced beam section was not performed and plates were welded on the top and bottom flanges considering a 30 mm distance from the welded connection to the external diaphragm to avoid overlapping of welds. The interest was to observe the behaviour of the welded connection between beam and external diaphragm for the situation in which the steel grade of the beam is much higher than ordered. For "strengthened CP joints", the cover plates were simply extended.

Table 5-5 describes for each of the 16 beam-to-column joints, the labelling, column and beam, joint typology, loading procedure and intended failure mode.

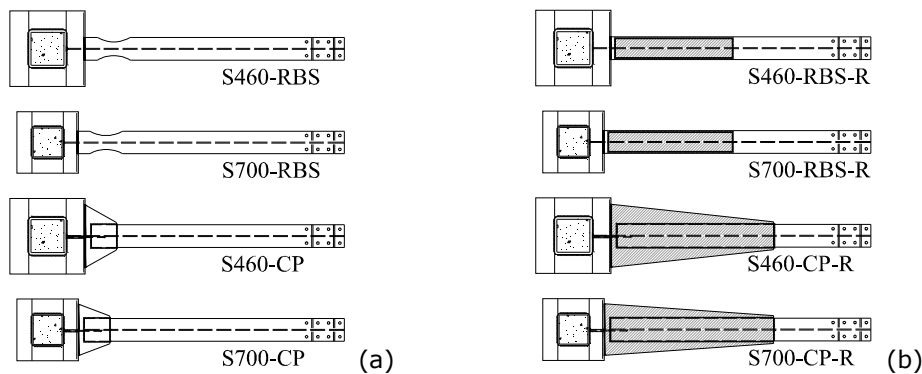


Fig. 5-8. Designed joints (a), and corresponding joints with reinforced beam (b)

Table 5-5 – Beam-to-column joint configurations

Nr.	Specimen name	Column	Beam	Joint type	Loading	Intended failure mode
1	S460-RBS-M	RHS 300x12.5 S460	IPE400 S355	RBS	Monotonic	Beam
2	S460-RBS-C				Cyclic	
3	S700-RBS-M	RHS 250x10 S700	IPE400 S355	RBS	Monotonic	Beam
4	S700-RBS-C				Cyclic	
5	S460-CP-M	RHS 300x12.5 S460	IPE400 S355	CP	Monotonic	Beam
6	S460-CP-C				Cyclic	
7	S700-CP-M	RHS 250x10 S700	IPE400 S355	CP	Monotonic	Beam
8	S700-CP-C				Cyclic	
9	S460-RBS-R-M	RHS 300x12.5 S460	IPE400 S355	RBS	Monotonic	Connection
10	S460-RBS-R-C				Cyclic	
11	S700-RBS-R-M	RHS 250x10 S700	IPE400 S355	RBS	Monotonic	Connection
12	S700-RBS-R-C				Cyclic	
13	S460-CP-R-M	RHS 300x12.5 S460	IPE400 S355	CP	Monotonic	Connection
14	S460-CP-R-C				Cyclic	
15	S700-CP-R-M	RHS 250x10 S700	IPE400 S355	CP	Monotonic	Connection
16	S700-CP-R-C				Cyclic	

5.2.3.2. Test set-up

A hydraulic actuator connected to the beam served as loading device. Besides the connection of the beam to the actuator, the column was supported at both ends considering a pinned connection (see Fig. 5-9). The support from the right side blocked the horizontal and vertical displacements, while the support from the left side blocked only the vertical displacement. A lateral support system was used with the aim to block the out of plane deformations of the beam. The conceptual scheme and illustration of test assembly are shown in Fig. 5-9.

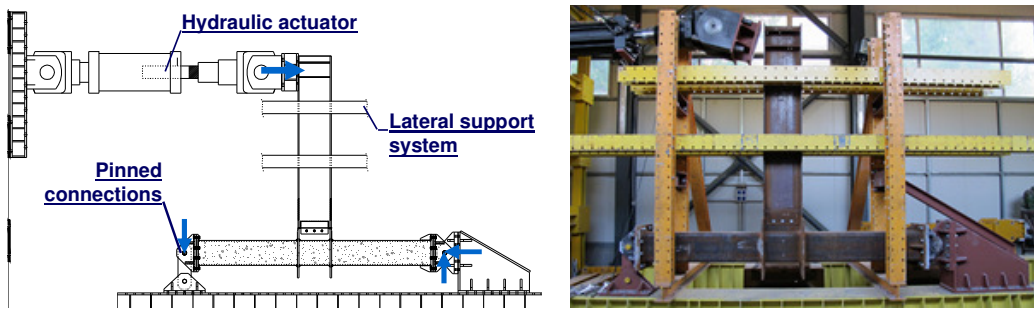


Fig. 5-9. Conceptual scheme and illustration of the test assembly

5.2.3.3. Instrumentation

In order to assess the characteristics of the joint configurations, global as well as local instrumentation of the specimens was considered using the measuring devices within the hydraulic actuator, displacement transducers, and optical measuring system (Vic 3D). In order to identify the sequence of yielding components, the connection zone was prepared by whitewashing (see Fig. 5-11). The optical measuring system Vic 3D (see Fig. 5-11) was to be used in order to observe the initiation of yielding. Depending on the joint configuration and the intended failure mode, different components were investigated, i.e. the web of the beam from the dissipative zone, the external diaphragm, and the column web panel.

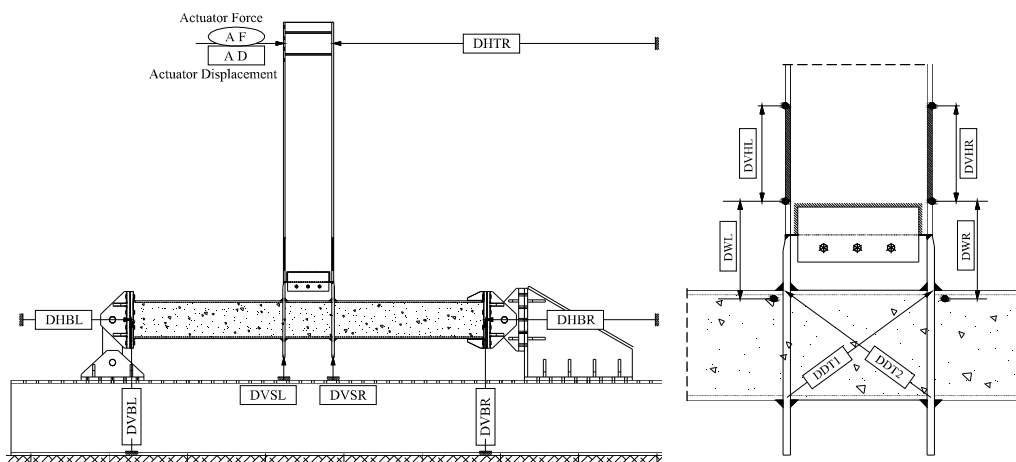


Fig. 5-10. Global instrumentation and local joint instrumentation

From the global instrumentation, information was to be obtained related to the displacement and force in the actuator, the displacement at the tip of the beam, the horizontal and vertical displacement at supports (see Fig. 5-10). The measurements at the supports were performed on both sides. Local instrumentation was aimed to measure the deformations within the dissipative and connection zone (see Fig. 5-11), as well as in the column web panel (see Fig. 5-10).

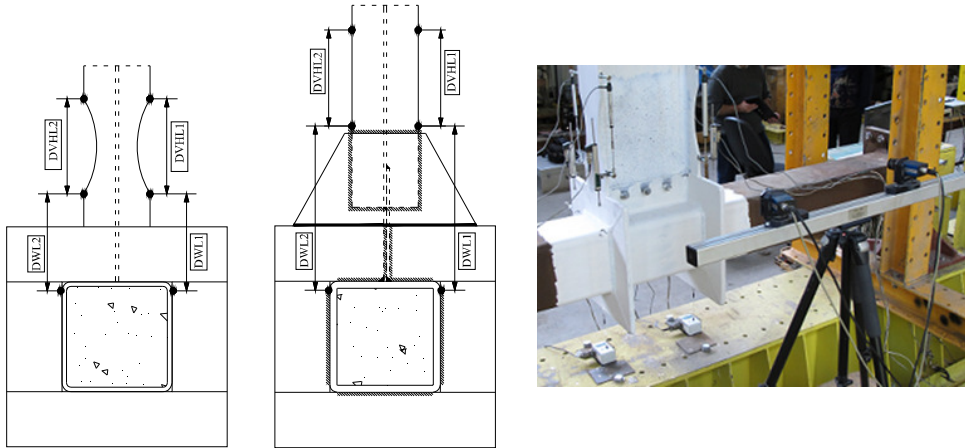


Fig. 5-11. Instrumentation of beam, welded connection, external diaphragm, and connection zone prepared by whitewashing

5.2.3.4. Loading protocols

Test control parameters

Parameters used to control the tests on beam to column joints are interstorey drift θ [rad] of test assembly and bending moment M [kNm] at the column centreline. These parameters are defined by the following expressions (Fig. 5-12):

$$\theta = \frac{\delta}{L} \quad (5.1)$$

$$M = F \cdot L \quad (5.2)$$

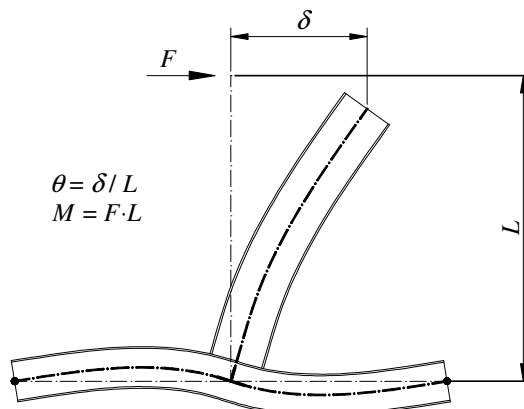


Fig. 5-12. Definition of parameters for tests on beam to column joints

where:

θ	Inter-storey drift of the test assembly;
M	Bending moment at the column centreline;
L	Beam length to column centreline;
F	Force applied at the tip of the beam;
δ	Lateral displacement at the tip of the beam "cleared" of any support displacements;

Preloading

A few pre-test load cycles were applied to the test assembly before the test in order to stabilize the system. Two alternating cycles with a peak load of up to 25% of the expected yield load were applied.

Monotonic loading protocol

Monotonic loading was applied by progressively increasing the displacement at the tip of the beam. One unloading-reloading phase was applied in order to estimate the initial stiffness.

Cyclic loading protocol

The ANSI/AISC 341-10 (2010) [94] loading procedure was considered. The procedure is prescribed in absolute values of inter-storey drift θ (see Fig. 5-13):

- 6 cycles at $\theta = 0.00375$ rad
- 6 cycles at $\theta = 0.005$ rad
- 6 cycles at $\theta = 0.0075$ rad
- 4 cycles at $\theta = 0.01$ rad
- 2 cycles at $\theta = 0.015$ rad
- 2 cycles at $\theta = 0.02$ rad
- 2 cycles at $\theta = 0.03$ rad
- 2 cycles at $\theta = 0.04$ rad

The loading is continued with increments of $\theta=0.01$ rad, with 2 cycles/step.

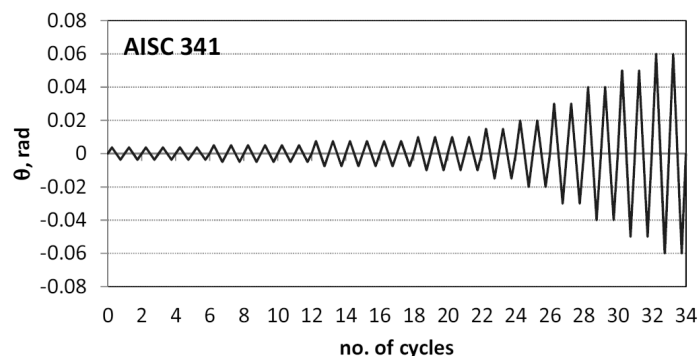


Fig. 5-13. ANSI/AISC 341-10 (2010) cyclic loading procedure [94]

5.3. Material sample tests

Further on, results from the experimental tests performed on material samples (concrete and steel) are presented. In relation to the steel samples, results are shown for beam (flange and web) and for the two rectangular hollow section tubes (RHS 300x12.5 S460, and RHS 250x10 S700). The results from tests performed on the other steel components of the joints (splice plate, cover plates, external diaphragms, vertical stiffeners), are presented in Annex C.

5.3.1. Concrete samples

At 28 days from concrete casting into the rectangular hollow sections (columns and column stubs), compression tests were performed on concrete samples. Fig. 5-14 shows the testing device, the concrete samples (before and after compression test).



Fig. 5-14. Testing device and concrete cubes (before and after compression test)

Table 5-6 summarizes the results obtained from both concrete station and University. It can be observed that the average characteristic strength was obtained in the amount of 35.88 N/mm^2 , which is slightly lower than the minimum characteristic strength (37 N/mm^2) corresponding to a C30/37 concrete class.

Table 5-6 – Test results on concrete

Test facility		Sample	A_c [mm ²]	F_{max} [kN]	f_c [N/mm ²]
Concrete station		S1	22500	804.4	35.75
		S2	22500	781.9	34.75
		S3	22500	821.3	36.50
University UPT	Samples taken at beginning	S1 - I	22500	847.7	37.68
		S2 - I	22500	747.2	33.21
		S3 - I	22500	781.9	34.75
	Samples taken at ending	S1 - II	22500	848.3	37.70
		S2 - II	22500	855.5	38.02
		S3 - II	22500	777	34.53
				Average	35.88

5.3.2. Steel samples

IPE 400 flange – S355 JR (J2+N)

The stress-strain curves and the tested samples are displayed in Fig. 5-15. An overview of the measured yield stress, ultimate strength, elongation at fracture and elongation at maximum force, is made in Table 5-7. It can be observed that the measured values satisfy the minimum requirements from EN 10025-2:2004* [6].

Table 5-7 – Stress and elongation results for IPE 400 flange – S355 JR (J2+N)

Sample	R_{eH} [N/mm ²]	R_m [N/mm ²]	A [%]	A_g [%]
S1	384.97	485.84	-	-
S2	402.57	496.07	31.50	16.33
S3	398.41	493.78	30.33	16.28
S4	389.71	492.08	-	16.16
Average	393.92	491.94	30.92	16.26
Standard*	355	470 to 630	22	

$$R_m / R_{eH} = 1.24 \tag{5.3}$$

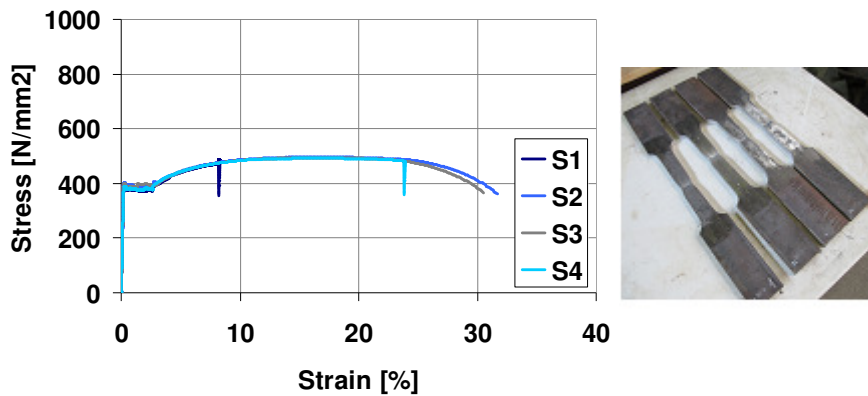


Fig. 5-15. Stress-strain curves and tested steel samples

Table 5-8 makes an overview of sample geometry, required minimum energy at 20°C temperature and measured impact energy. It can be observed that the measured values are higher, and therefore the requirements are satisfied.

Table 5-8 – Impact test results for IPE 400 flange – S355 JR (J2+N)

Sample	KV _{min} =27J at 20°C			
	10x10x55			
	S1	S2	S3	S4
KV [J]	57	59	57	-

IPE 400 web – S355 JR (J2+N)

The stress-strain curves and the tested samples are displayed in Fig. 5-16. An overview of the measured yield stress, ultimate strength, elongation at fracture and elongation at maximum force, is made in Table 5-9. It can be observed that the measured values satisfy the minimum requirements from EN 10025-2:2004* [6].

Table 5-9 – Stress and elongation results for IPE 400 web – S355 JR (J2+N)

Sample	R_{eH} [N/mm ²]	R_m [N/mm ²]	A [%]	A_g [%]
S1	443.73	512.89	29.11	15.61
S2	430.2	502.60	29.38	15.92
S3	444.68	507.10	28.89	15.74
Average	439.53	507.53	29.13	15.76
Standard*	355	470 to 630	22	

$$R_m / R_{eH} = 1.15 \tag{5.4}$$

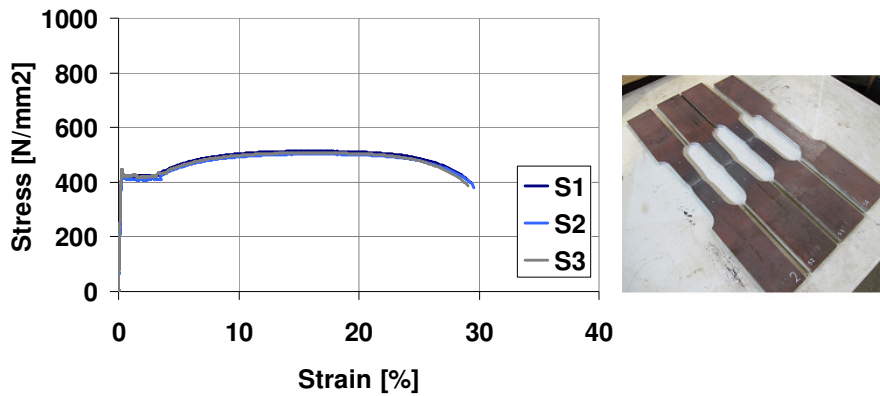


Fig. 5-16. Stress-strain curves and tested steel samples

Table 5-10 makes an overview of sample geometry, required minimum energy at 20°C temperature and measured impact energy. It can be observed that the measured values are significantly higher even though the samples were thinner (7.5 mm), and therefore the requirements are satisfied.

Table 5-10 – Impact test results for IPE 400 web – S355 JR (J2+N)

Sample	KV _{min} =27J at 20°C			7.5x10x55
	S1	S2	S3	
KV [J]	102	95	102	-

Tube RHS 300x12.5 – S460 M

The stress-strain curves and the tested samples are displayed in Fig. 5-17. An overview of the measured yield stress, ultimate strength, elongation at fracture and elongation at maximum force, is made in Table 5-11. It can be observed that the measured values satisfy the minimum requirements from EN 10025-6:2004* [8].

Table 5-11 – Stress and elongation results for Tube RHS 300x12.5 – S460 M

Sample	R_{p02} [N/mm ²]	R_m [N/mm ²]	A [%]	A_g [%]
S1	512.85	556.83	20.89	5.65
S2	483.32	551.02	24.05	9.23
S3	496.87	554.3	22.07	8.35
Average	497.68	554.05	22.39	7.74
Standard*	460	550 to 720	17	

$$R_m / R_{p02} = 1.11 \quad (5.5)$$

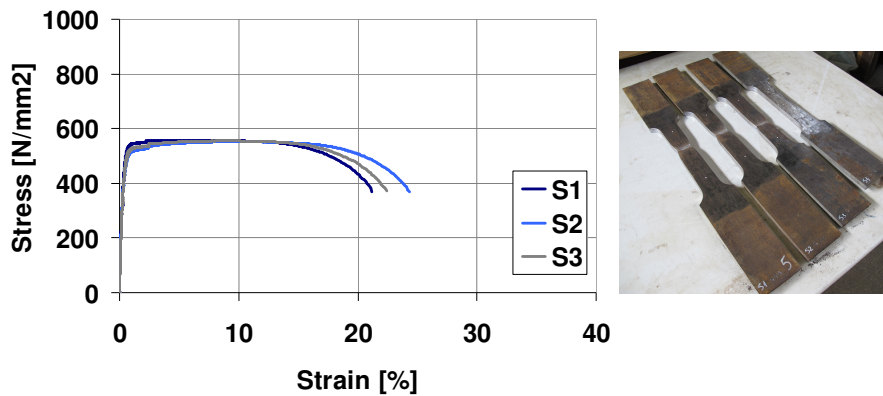
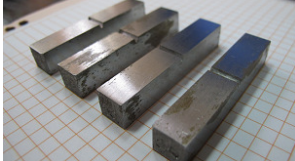



Fig. 5-17. Stress-strain curves and tested steel samples

Table 5-12 makes an overview of sample geometry, required minimum energy at -20°C temperature and measured impact energy. It can be observed that the measured values are significantly higher, and therefore the requirements are satisfied.

Table 5-12 – Impact test results for Tube RHS 300x12.5 – S460 M

Sample	kV _{min} =40J at -20°C			10x10x55
	S1	S2	S3	S4
kV [J]	286	202	254	-

Tube RHS 250x10 (S700 QL)

The stress-strain curves and the tested samples are displayed in Fig. 5-18. An overview of the measured yield stress, ultimate strength, elongation at fracture and elongation at maximum force, is made in Table 5-13. It can be observed that the measured values, excepting the elongation at fracture, satisfy the minimum requirements from EN 10025-6:2004* [8].

Table 5-13 – Stress and elongation results for Tube RHS 250x10 (S700 QL)

Sample	$R_{p0.2}$ [N/mm ²]	R_m [N/mm ²]	A [%]	A_g [%]
S1	703.84	826.76	11.24	-
S2	742.3	833.13	11.81	-
S3	730.02	830.3	12.42	-
Average	725.39	830.06	11.82	-
Standard*	690	770 to 940	14	-

$$R_m / R_{eH} = 1.14 \tag{5.6}$$

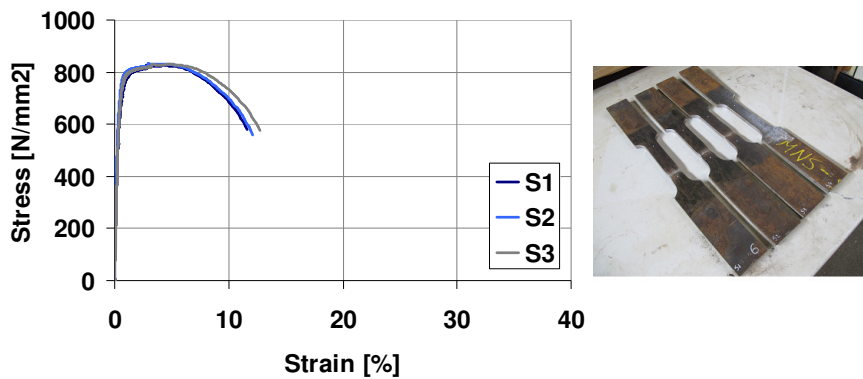

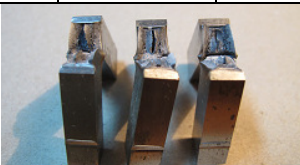


Fig. 5-18. Stress-strain curves and tested steel samples

Table 5-14 makes an overview of sample geometry, required minimum energy at -20 °C temperature and measured impact energy. It can be observed that the measured values are significantly higher even though the samples were thinner (7.5 mm), and therefore the requirements are satisfied.

Table 5-14 – Impact test results for Tube RHS 250x10 (S700 QL)

	kV _{min} =40J at -20 °C			7.5x10x55
Sample	S1	S2	S3	S4
kV [J]	101	103	103	-

5.4.2. S700-F-H-M / S700-F-H-C

The conceptual scheme of the "S700-F-H" specimens (front and lateral view) and the test assembly are shown in Fig. 5-22. From the test, information was obtained related to the response of the steel-concrete bonding combined with connectors, under monotonic loading (see Fig. 5-23) and under cyclic loading (see Fig. 5-24).

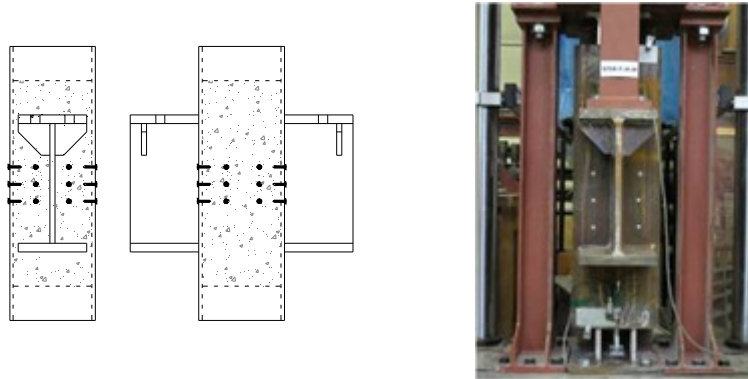


Fig. 5-22. Conceptual scheme of specimen (front and lateral view), and the test assembly

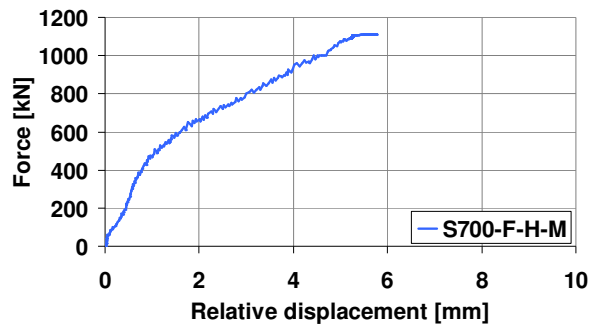


Fig. 5-23. Monotonic response of steel-concrete bonding combined with connectors

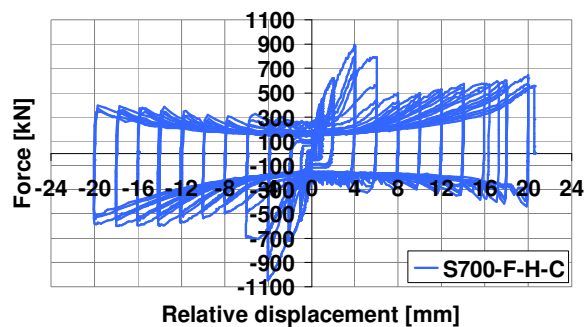


Fig. 5-24. Cyclic response of steel-concrete bonding combined with connectors

5.4.3. S460-F-H-M / S460-F-H-C

The conceptual scheme of the “S460-F-H” specimens (front and lateral view) and the test assembly are shown in Fig. 5-25. From the test, information was obtained related to the response of the steel-concrete bonding combined with connectors, under monotonic loading (see Fig. 5-26) and under cyclic loading (see Fig. 5-27).

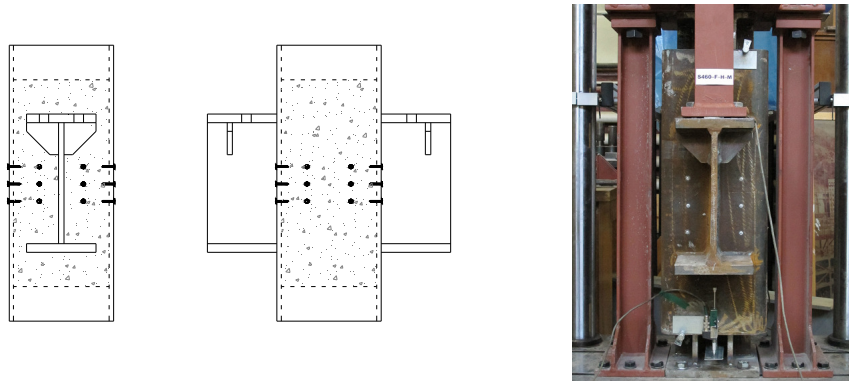


Fig. 5-25. Conceptual scheme of specimen (front and lateral view), and the test assembly

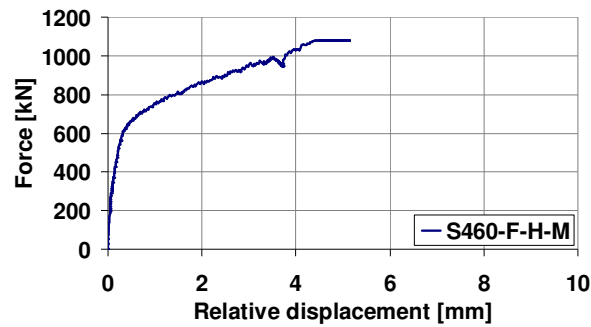


Fig. 5-26. Monotonic response of steel-concrete bonding combined with connectors

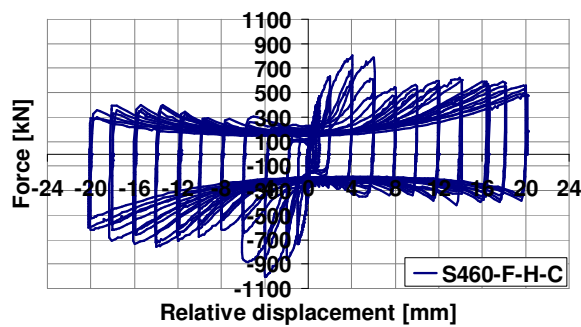


Fig. 5-27. Cyclic response of steel-concrete bonding combined with connectors

5.4.4. Graphical comparison of results

The response under monotonic loading of the column stubs without and with connectors can be seen in Fig. 5-28. It can be observed that the contribution of the 24 connectors is significant.

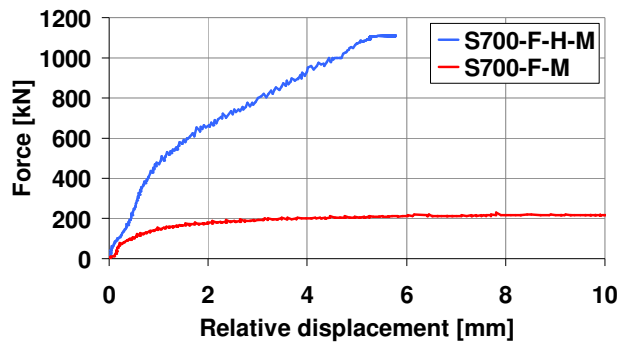


Fig. 5-28. Contribution of the connectors under monotonic loading

The response under cyclic loading of the specimens without and with connectors can be seen in Fig. 5-29. The connectors show a significant contribution also under cyclic loading conditions. It can be observed that exceeding a relative displacement of approximately 4 mm, the capacity of the steel-concrete connection decreased due to fracture of the connectors at the interface between steel tube and concrete core (see section 5.4.5.2).

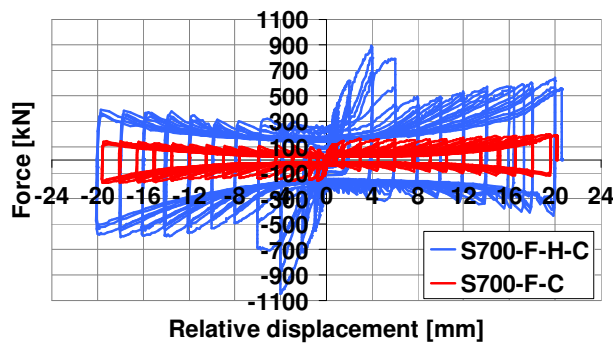


Fig. 5-29. Contribution of the connectors under cyclic loading

The response under cyclic loading of the two specimens with both connectors and steel-concrete bonding is compared in Fig. 5-30. The difference between the two configurations is given by the steel tube. The S460 tube is a square RHS 300x12.5, while the S700 tube is a square RHS 250x10. In the first case the thickness of the tube is 12.5 mm and in the other case the thickness is 10 mm. The lateral surface of the concrete core is $A_{int,RHS,S460}=660000 \text{ mm}^2$ within the S460 tube, and $A_{int,RHS,S700}=552000 \text{ mm}^2$ within the S700 tube. It is to be noted that the concrete depth in both cases was 600 mm. A slightly higher friction force was therefore developed within the column stub with larger steel tube (S460).

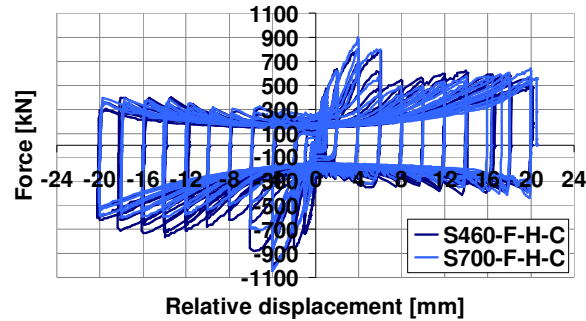


Fig. 5-30. Cyclic response of the stubs with steel-concrete bonding and connectors

5.4.5. Investigation of the failure mode

In order to observe the deformations developed within connectors and the concrete around them, two side walls of the column stubs S460-F-H-M and S460-F-H-C, were cut out with flame as can be seen in Fig. 5-31. The two specimens with the removed tube faces can be seen in Fig. 5-32.



Fig. 5-31. Flame cutting of the concrete filled tubes



Fig. 5-32. Specimens (S460-F-H-C / S460-F-H-M) with removed tube faces

5.4.5.1. Behaviour under monotonic loading

The response of concrete and connectors to monotonic loading can be observed in Fig. 5-33. A detail of concrete and connector after monotonic loading is shown in Fig. 5-34. It can be observed that the concrete was crushed in a small amount at the contact with the shot fired nails which bent.



Fig. 5-33. Response of concrete and connectors to monotonic loading



Fig. 5-34. Detail of concrete and connector after monotonic loading

5.4.5.2. Behaviour under cyclic loading

The response of the concrete core and connectors to the cyclic loading condition is shown in Fig. 5-35.



Fig. 5-35. Response of concrete and connectors to cyclic loading

A detail of concrete and connector after cyclic loading is shown in Fig. 5-36. It can be observed that under alternating cycles the connectors were broken at the interface between concrete core and steel tube. The protruding part of the steel

tube, which can be observed in Fig. 5-36, rubbed on the concrete surface and lead to marks as can be seen in Fig. 5-35.



Fig. 5-36. Detail of concrete and connector after cyclic loading

5.5. Numerical simulation of testing

Due to the innovative joint configurations, it was needed to have an accurate prediction for the behaviour of the joints in order to avoid unacceptable failure during the experimental tests. Therefore, numerical simulations have been performed with the finite element modelling software Abaqus [95]. In a first step the material model was calibrated based on results from compression tests on concrete samples and tensile tests on steel samples. Using the calibrated material model, the behaviour of each joint configuration was therefore obtained.

5.5.1. Calibration of the material model

The stress-strain relationship used for concrete (see Fig. 5-37), was computed using the results from the compression tests, and an analytical stress-strain model as reported by Ali et al. [96]. The concrete damaged plasticity model was used considering as input the stress-strain relationship shown in Fig. 5-37, and in addition the plasticity parameters, compression damage and tensile behaviour from Korotkov et al. [97].

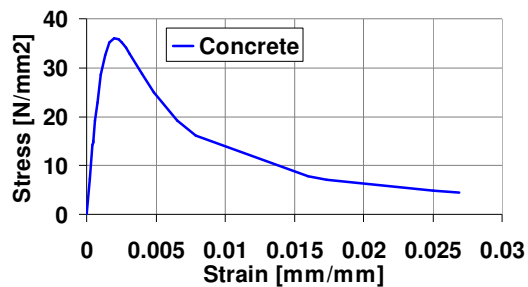


Fig. 5-37. Stress-strain relationship for concrete

The calibration of the material model for the steel grades was performed as well. Table 5-15 shows the input for the plastic behaviour of steel for beam flange, beam web, and RHS tubes (S460 and S700). Fig. 5-38, Fig. 5-39, Fig. 5-40 and Fig. 5-41 show the comparison between test and simulation in terms of force-displacement curve, the Mises stresses and the plastic strain at fracture.

Consequently, a good correlation can be observed between test and simulation. The calibration of the material model for the other steel components is shown in Annex D.

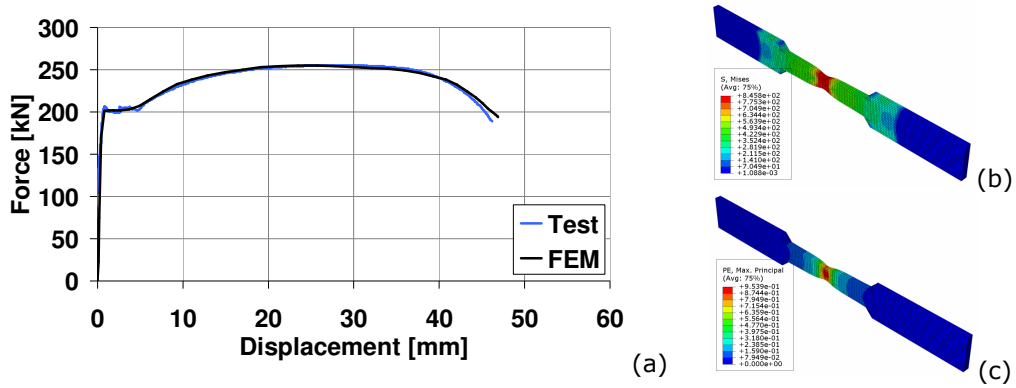


Fig. 5-38. Calibration of IPE 400 flange (S355) material model: comparison between test and simulation (a); Mises stress (b) and plastic strain (c) at fracture

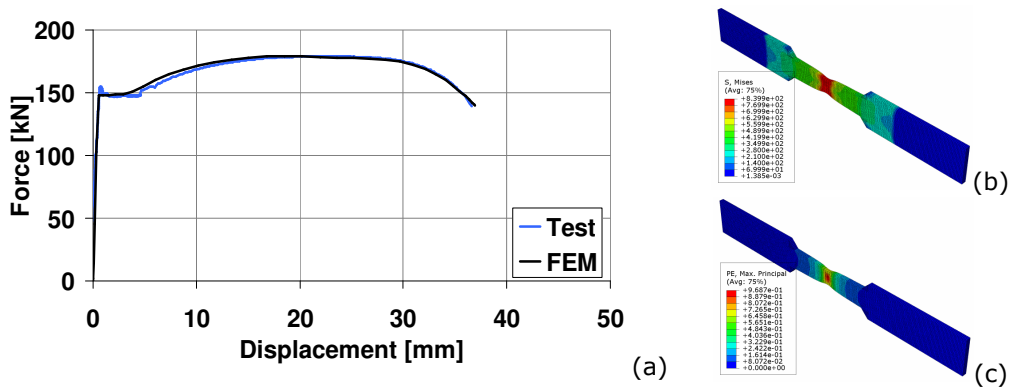


Fig. 5-39. Calibration of IPE 400 web (S355) material model: comparison between test and simulation (a); Mises stress (b) and plastic strain (c) at fracture

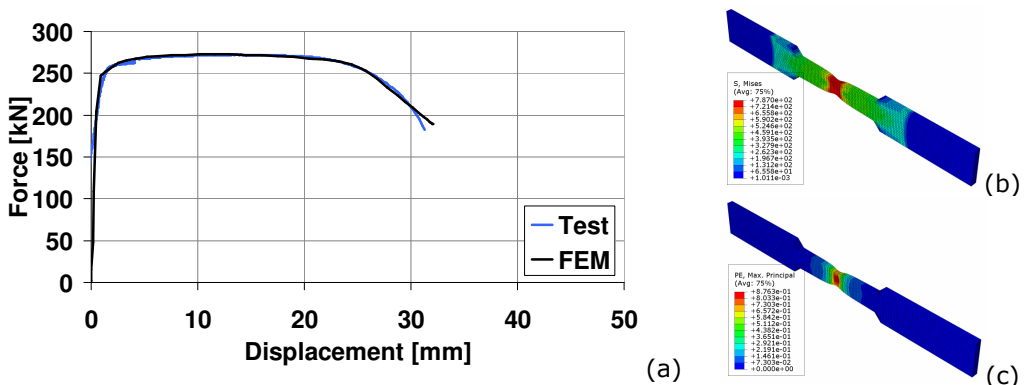


Fig. 5-40. Calibration of Tube RHS 300x12.5 (S460) material model: comparison between test and simulation (a); Mises stress (b) and plastic strain (c) at fracture

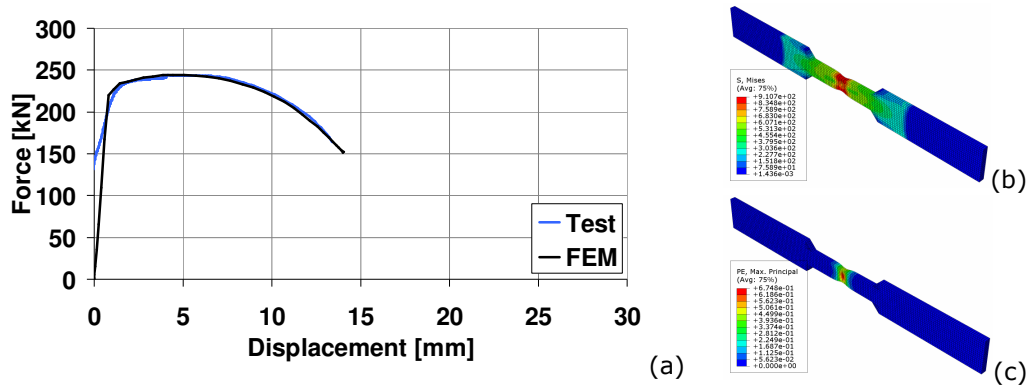


Fig. 5-41. Calibration of Tube RHS 250x10 (S700) material model: comparison between test and simulation (a); Mises stress (b) and plastic strain (c) at fracture

Table 5-15 – Input for plastic behaviour of beam (flange and web), S460 tube and S700 tube

IPE400 flange		IPE400 web		RHS 300x12.5		RHS 250x10	
True stress [N/mm ²]	True plastic strain	True stress [N/mm ²]	True plastic strain	True stress [N/mm ²]	True plastic strain	True stress [N/mm ²]	True plastic strain
390.3	0.0000	423.1	0.0000	497.8	0.0000	744.9	0.0000
402.6	0.0273	438.3	0.0294	533.9	0.0087	801.4	0.0054
465.4	0.0477	488.1	0.0480	557.5	0.0219	829.1	0.0144
503.9	0.0702	525.4	0.0697	569.7	0.0365	855.9	0.0269
532.4	0.0942	554.5	0.0942	579.2	0.0475	863.5	0.0368
551.8	0.1161	574.5	0.1164	593.8	0.0679	869.6	0.0451
567.7	0.1386	593.9	0.1443	609.8	0.0937	900.0	0.1000
578.4	0.1568	602.3	0.1599	619.8	0.1139	930.0	0.2000
590.2	0.1804	612.4	0.1821	775.0	0.4000	935.0	0.3500
710.0	0.4000	740.0	0.4000	780.0	0.6000	875.0	0.5000
825.0	0.6500	820.0	0.6500	790.0	1.0000	650.0	0.8000
850.0	0.9500	840.0	0.9500				

5.5.2. Pre-test numerical investigation of the beam-to-column joints

All the components of the beam-to-column joints were modelled using solid elements. In order to have in the end a uniform and structured mesh, some components with a complex geometry were partitioned into simple shapes. Due to the large amount of contact surfaces between the concrete core and the steel tube, the Dynamic Explicit type of analysis was used. For the interaction between the steel tube and the concrete core, a normal contact was defined that allows the two parts to separate. The load was applied through a displacement control at the tip of the beam and the column was considered as double pinned. The mesh of the elements was performed using linear hexahedral elements of type C3D8R.

The numerical simulations allowed assessing for each joint configuration, the stress distribution and plastic strain, as well as the moment-rotation curve (computed at column centreline). According to this, for the RBS and CP joints, large plastic deformations developed in the beam (Fig. 5-42 and Fig. 5-43). For these configurations, the low deformations of the concrete core confirmed that the encased concrete did not crush under the compression at the lower flange level. For the joints with strengthened beam, yielding was initiated in the adjacent area of the welded on-site connection (Fig. 5-44), and respectively in the external diaphragm and column panel zone (Fig. 5-45).

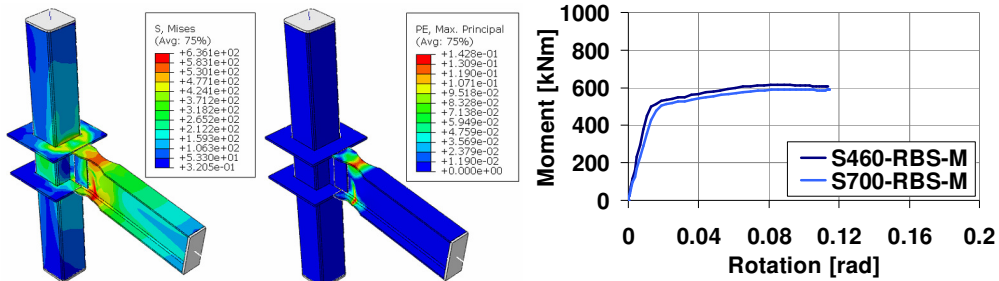


Fig. 5-42. S460-RBS: Misses stress, plastic strain; Moment-rotation curves for RBS joints

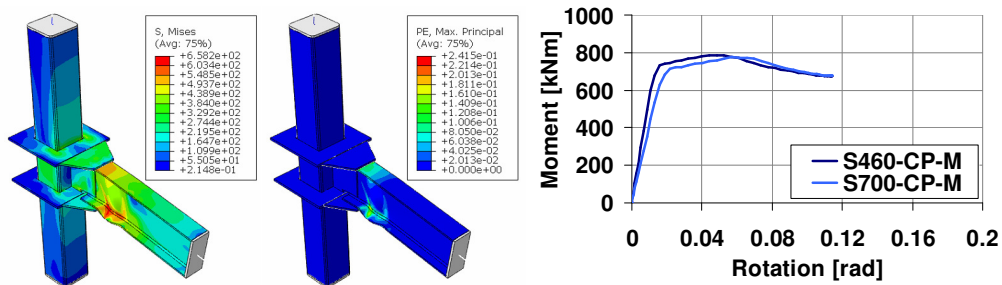


Fig. 5-43. S460-CP: Misses stress, plastic strain; Moment-rotation curves for CP joints

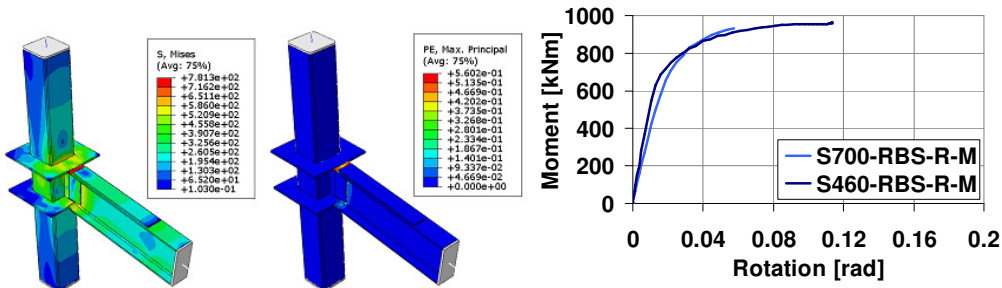


Fig. 5-44. S460-RBS-R: Misses stress, plastic strain; Moment-rotation curves for RBS-R joints

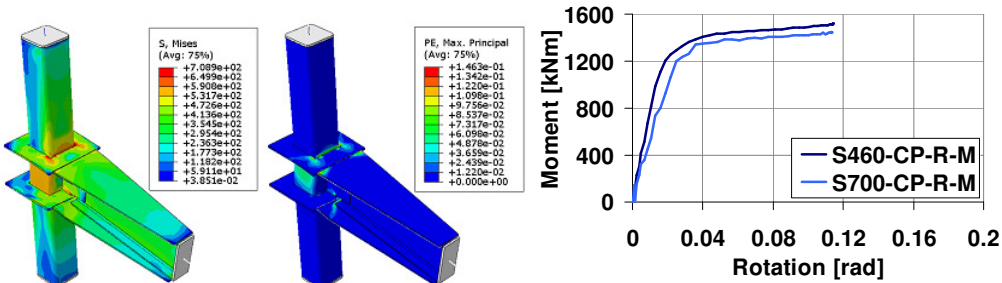


Fig. 5-45. S460-CP-R: Misses stress, plastic strain; Moment-rotation curves for CP-R joints

5.6. Beam-to-column joint tests

The results obtained within the experimental program performed on beam-to-column joints are further shown. In each case, a description is made in relation to the test assembly, yielding sequence, failure mode, and graphical results.

5.6.1. S460-RBS-M / S460-RBS-C

The test assembly and the connection zone of the S460-RBS joint configuration prior to the testing are illustrated in Fig. 5-46.



Fig. 5-46. S460-RBS test assembly and connection zone – before test

S460-RBS-M

The monotonic response, in terms of moment-rotation curve (computed at column centreline), of the S460-RBS joint is shown in Fig. 5-47. The yielding sequence of S460-RBS joint under monotonic loading is illustrated in Annex E. Consequently, the yielding was initiated in the beam flanges within the RBS zone and was followed by large plastic deformations – local buckling of the compressed flange and web. The state of the connection zone corresponding to the end of test is shown in Fig. 5-47 as well.

The measurements performed with the optical 3D system are illustrated in Fig. 5-48. Consequently, the out of plane deformations of the beam web, corresponding to the three points marked on the moment-rotation curve in Fig. 5-47, show the evolution of the plastic deformations.

S460-RBS-C

The cyclic response, in terms of moment-rotation curve (computed at column centreline), of the S460-RBS joint is shown in Fig. 5-49. The yielding sequence of S460-RBS joint under cyclic loading is illustrated in Annex E. Consequently, the yielding was initiated in the beam flanges within the RBS zone and was followed by large plastic deformations – local buckling of flanges and web under compression, and flange fracture in the RBS zone. The state of the connection zone corresponding to the end of test is shown in Fig. 5-49 as well.

The measurements performed with the optical 3D system are illustrated in Fig. 5-50. Consequently, the strain " ϵ_{yy} " in the beam web, corresponding to the points marked on the moment-rotation curve in Fig. 5-49, show the initiation zone and evolution of the plastic deformations.

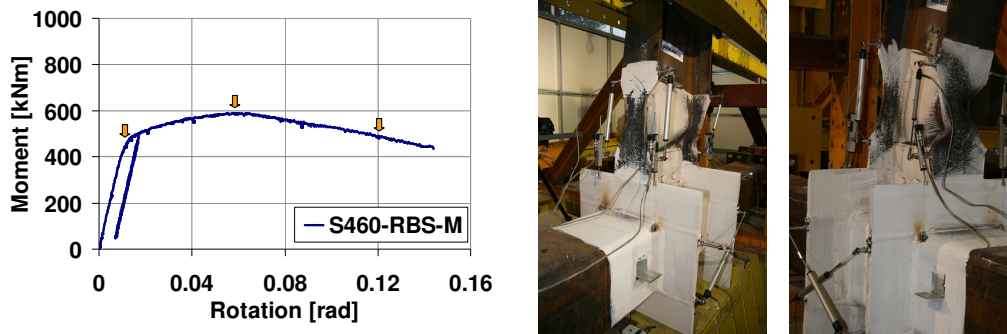


Fig. 5-47. S460-RBS-M joint: monotonic response and illustration of the failure mode

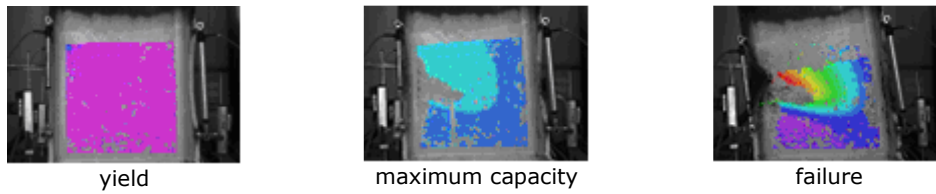


Fig. 5-48. Out of plane deformation of beam web (Vic 3D)

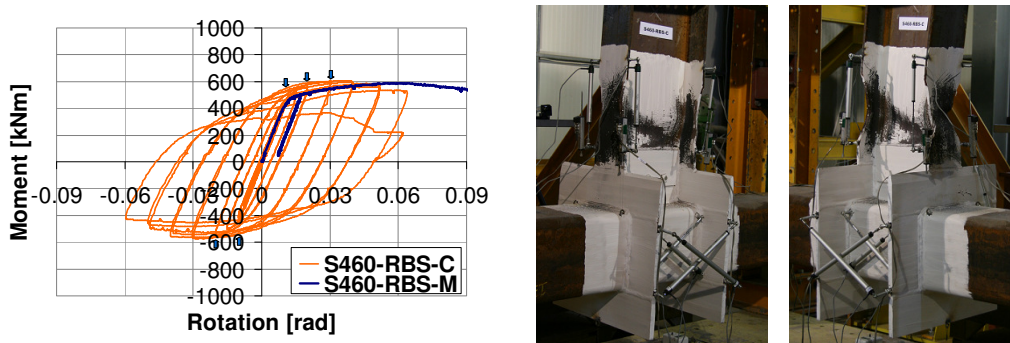


Fig. 5-49. S460-RBS-C joint: cyclic response and illustration of the failure mode

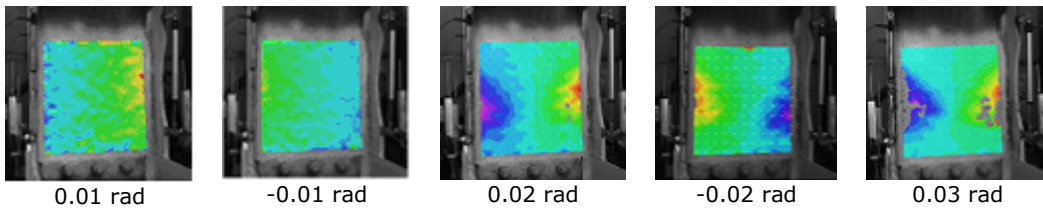


Fig. 5-50. Strain " ϵ_{yy} " in beam web (Vic 3D)

5.6.2. S700-RBS-M / S700-RBS-C

The test assembly and the connection zone of the S700-RBS joint configuration prior to the testing are illustrated in Fig. 5-51.

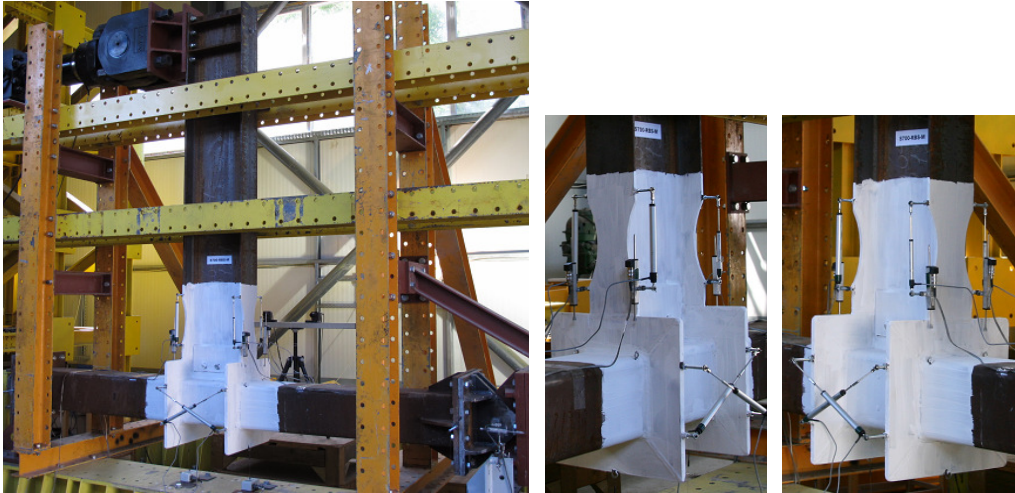


Fig. 5-51. S700-RBS test assembly and connection zone – before test

S700-RBS-M

The monotonic response, in terms of moment-rotation curve (computed at column centreline), of the S700-RBS joint is shown in Fig. 5-52. The yielding sequence of S700-RBS joint under monotonic loading is illustrated in Annex E. Consequently, the yielding was initiated in the beam flanges within the RBS zone and was followed by large plastic deformations – local buckling of the compressed flange and web. The state of the connection zone corresponding to the end of test is shown in Fig. 5-52 as well.

The measurements performed with the optical 3D system are illustrated in Fig. 5-53. Consequently, the out of plane deformations of the beam web, corresponding to the three points marked on the moment-rotation curve in Fig. 5-52, show the evolution of the plastic deformations.

S700-RBS-C

The cyclic response, in terms of moment-rotation curve (computed at column centreline), of the S700-RBS joint is shown in Fig. 5-54. The yielding sequence of S700-RBS joint under cyclic loading is illustrated in Annex E. Consequently, the yielding was initiated in the beam flanges within the RBS zone and was followed by large plastic deformations – local buckling of flanges and web under compression, and flange fracture in the RBS zone. Fig. 5-54 shows the state of the connection zone corresponding to the end of test.

The measurements performed with the optical 3D system are illustrated in Fig. 5-55. Consequently, the strain “ ϵ_{yy} ” in the beam web, corresponding to the points marked on the moment-rotation curve in Fig. 5-54, show the initiation zone and the evolution of the plastic deformations.

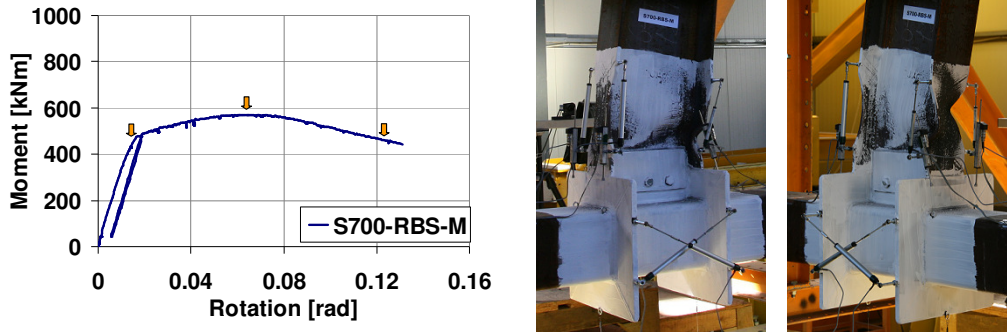


Fig. 5-52. S700-RBS-M joint: monotonic response and illustration of the failure mode

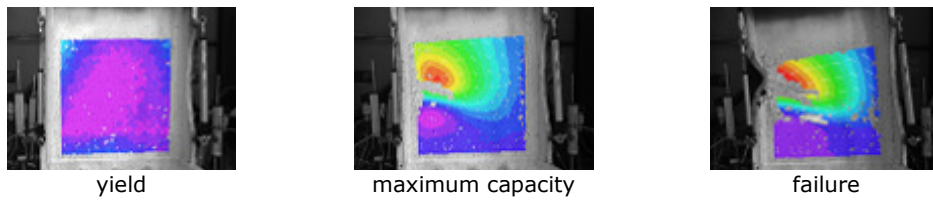


Fig. 5-53. Out of plane deformation of beam web (Vic 3D)

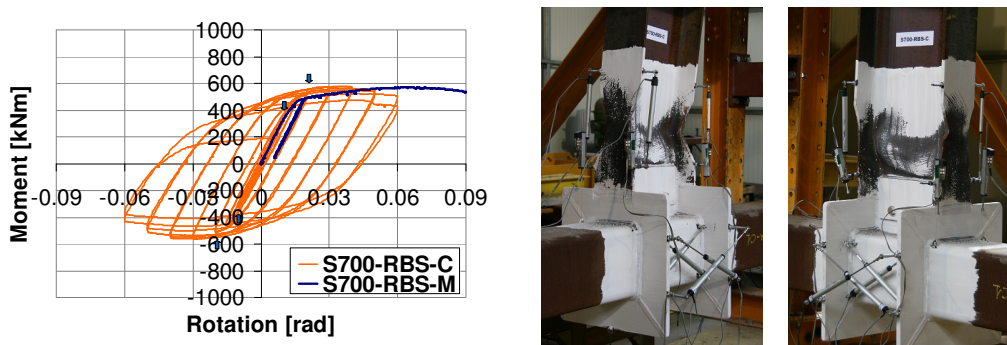


Fig. 5-54. S700-RBS-C joint: cyclic response and illustration of the failure mode

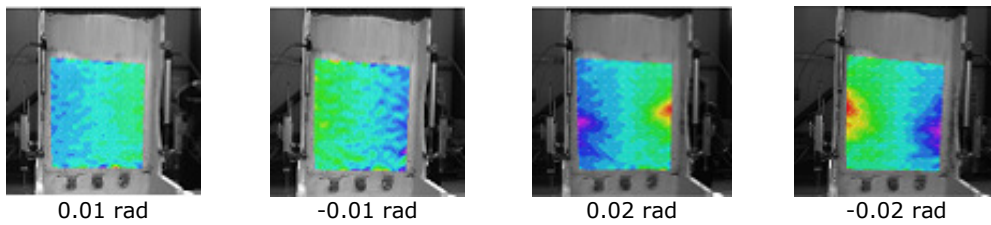


Fig. 5-55. Strain ϵ_{yy} in beam web (Vic 3D)

5.6.3. S460-CP-M / S460-CP-C

The test assembly and the connection zone of the S460-CP joint configuration prior to the testing are illustrated in Fig. 5-56.



Fig. 5-56. S460-CP test assembly and connection zone – before test

S460-CP-M

The monotonic response, in terms of moment-rotation curve (computed at column centreline), of the S460-CP joint is shown in Fig. 5-57. The yielding sequence of S460-CP joint under monotonic loading is illustrated in Annex E. Consequently, the yielding was initiated in the beam flanges near the cover plates and was followed by large plastic deformations – local buckling of flange and web under compression. No damage was observed in cover plates, ring stiffeners and column panel zone. Fig. 5-57 shows the state of the connection zone corresponding to the end of test.

The measurements performed with the optical 3D system are illustrated in Fig. 5-58. Consequently, the out of plane deformations of the beam web, corresponding to the points marked on the moment-rotation curve in Fig. 5-57, show the evolution of the plastic deformations.

S460-CP-C

The cyclic response, in terms of moment-rotation curve (computed at column centreline), of the S460-CP joint is shown in Fig. 5-59. The yielding sequence of S460-CP joint under cyclic loading is illustrated in Annex E. Consequently, the yielding was initiated in the beam flanges near the cover plates and was followed by large plastic deformations – local buckling of flanges and web under compression. No damage was observed in cover plates, ring stiffeners and column panel zone. Fig. 5-59 shows the state of the connection zone corresponding to the end of test.

The measurements performed with the optical 3D system are illustrated in Fig. 5-60. Consequently, the strain " ϵ_{yy} " in the beam web, corresponding to the

points marked on the moment-rotation curve in Fig. 5-59, show the initiation zone and the evolution of the plastic deformations.

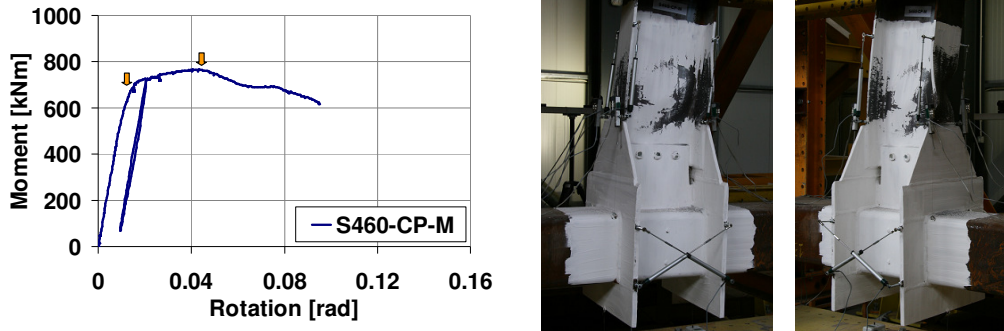


Fig. 5-57. S460-CP-M joint: monotonic response and illustration of the failure mode



Fig. 5-58. Out of plane deformation of beam web (Vic 3D)

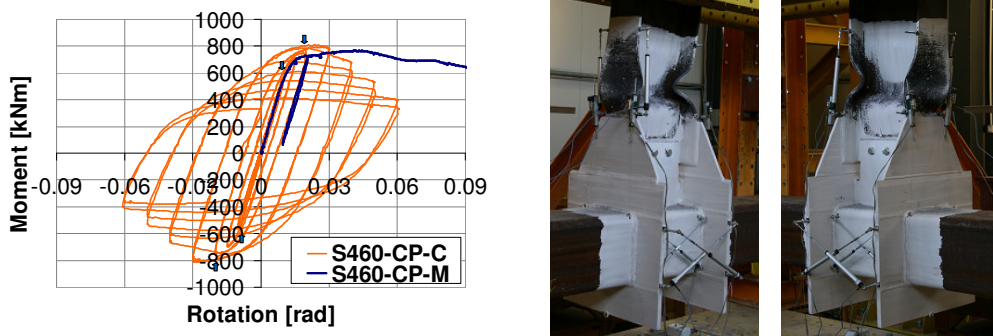


Fig. 5-59. S460-CP-C joint: cyclic response and illustration of the failure mode

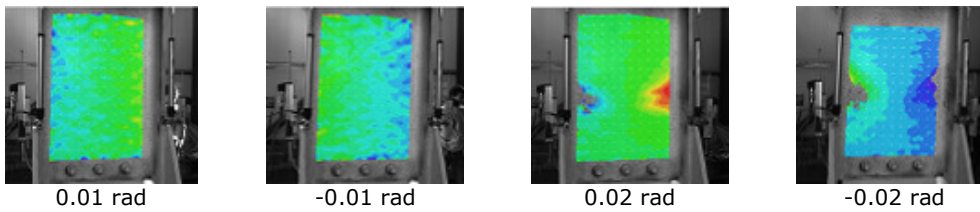


Fig. 5-60. Strain ϵ_{yy} in beam web (Vic 3D)

5.6.4. S700-CP-M / S700-CP-C

The test assembly and the connection zone of the S700-CP joint configuration prior to the testing are illustrated in Fig. 5-61.



Fig. 5-61. S700-CP test assembly and connection zone – before test

S700-CP-M

The monotonic response, in terms of moment-rotation curve (computed at column centreline), of the S700-CP joint is shown in Fig. 5-62. The yielding sequence of S700-CP joint under monotonic loading is illustrated in Annex E. Consequently, the yielding was initiated in the beam flanges near the cover plates and was followed by large plastic deformations, i.e. local buckling of flange and web under compression. No damage was observed in cover plates, ring stiffeners and column panel zone. Fig. 5-62 shows the state of the connection zone corresponding to the end of test.

The measurements performed with the optical 3D system are illustrated in Fig. 5-63. Consequently, the out of plane deformations of the beam web, corresponding to the points marked on the moment-rotation curve in Fig. 5-62, show the evolution of the plastic deformations.

S700-CP-C

The cyclic response, in terms of moment-rotation curve (computed at column centreline), of the S700-CP joint is shown in Fig. 5-64. The yielding sequence of S700-CP joint under cyclic loading is illustrated in Annex E. Consequently, the yielding was initiated in the beam flanges near the cover plates and was followed by large plastic deformations, i.e. local buckling of flanges and web under compression. No damage was observed in cover plates, ring stiffeners and column panel zone. Fig. 5-64 shows the state of the connection zone corresponding to the end of test.

The measurements performed with the optical 3D system are illustrated in Fig. 5-65. Consequently, the strain " ϵ_{yy} " in the beam web, corresponding to the

points marked on the moment-rotation curve in Fig. 5-64, show the initiation zone and evolution of the plastic deformations.

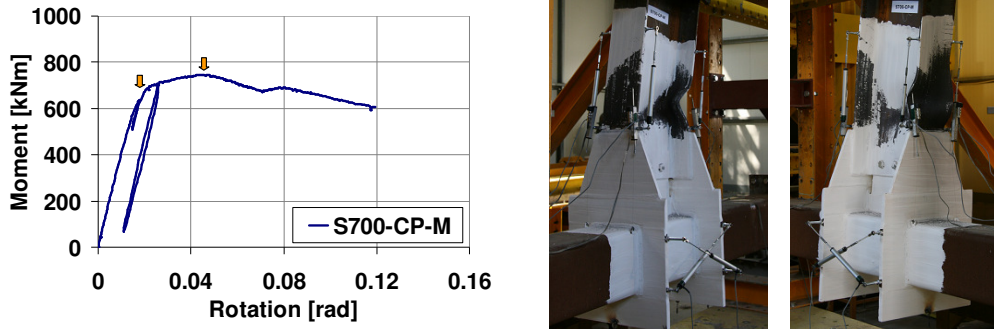


Fig. 5-62. S700-CP-M joint: monotonic response and illustration of the failure mode



Fig. 5-63. Out of plane deformation of beam web (Vic 3D)

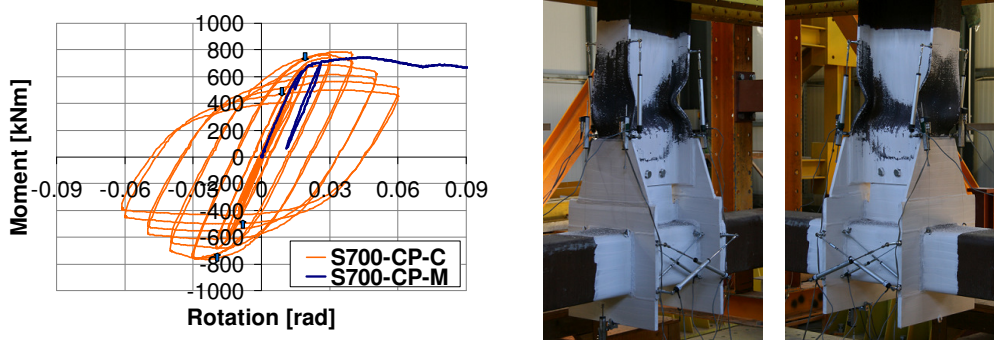


Fig. 5-64. S700-CP-C joint: cyclic response and illustration of the failure mode

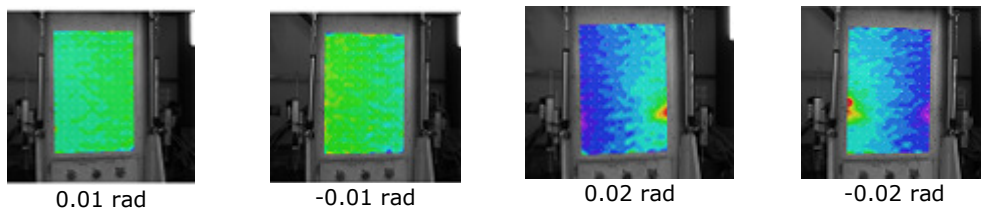


Fig. 5-65. Strain ϵ_{yy} in beam web (Vic 3D)

5.6.5. S460-RBS-R-M / S460-RBS-R-C

The test assembly and the connection zone of the reinforced S460-RBS-R joint configuration prior to the testing are illustrated in Fig. 5-66.

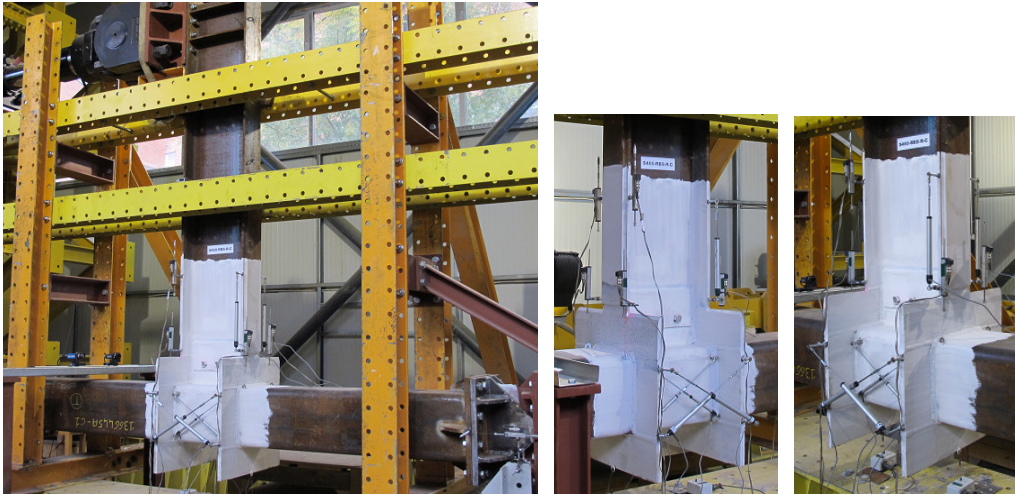


Fig. 5-66. S460-RBS-R test assembly and connection zone – before test

S460-RBS-R-M

The monotonic response, in terms of moment-rotation curve (computed at column centreline), of the S460-RBS-R joint is shown in Fig. 5-67. The yielding sequence of S460-RBS-R joint under monotonic loading is illustrated in Annex E. Consequently, the yielding was initiated in the compressed beam flange between the reinforcing plate and external diaphragm, and was followed by yielding of web, external diaphragm and tensioned beam flange which fractured in the heat affected zone (HAZ). Fig. 5-67 shows the state of the connection zone corresponding to the end of test.

The measurements performed with the optical 3D system are illustrated in Fig. 5-68. Consequently, the strain " ϵ_{yy} " in the external diaphragm and welded connection, corresponding to the points marked on the moment-rotation curve in Fig. 5-67 show the initiation and evolution of the plastic deformations.

S460-RBS-R-C

The cyclic response, in terms of moment-rotation curve (computed at column centreline), of the S460-RBS-R joint is shown in Fig. 5-69. The yielding sequence of S460-RBS-R joint under cyclic loading is illustrated in Annex E. Consequently, the yielding was initiated in the beam flanges under compression at the connection to the external diaphragm, and was followed by yielding of web and fracture of the beam flange subjected to tension. Fig. 5-69 shows the state of the connection zone corresponding to the end of test.

The measurements performed with the optical 3D system are illustrated in Fig. 5-70. Consequently, the strain " ϵ_{yy} " in the external diaphragm and welded connection, corresponding to the points marked on the moment-rotation curve in Fig. 5-69, show the initiation and evolution of the plastic deformations.

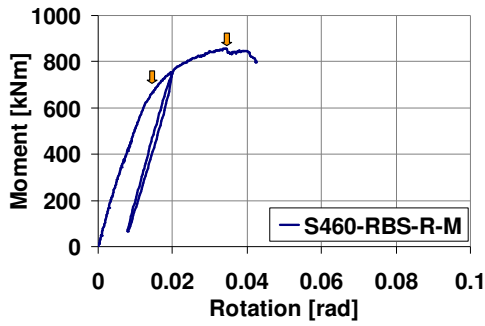
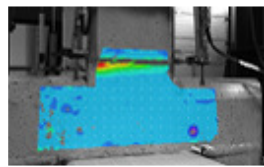
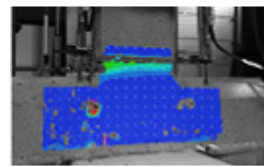


Fig. 5-67. S460-RBS-R-M joint: monotonic response and illustration of the failure mode



yield



maximum capacity

Fig. 5-68. Strain " ϵ_{yy} " in external diaphragm and HAZ of beam flange (Vic 3D)

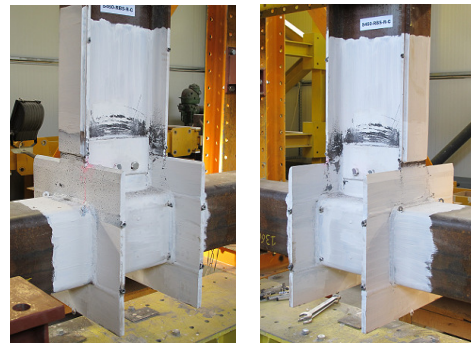
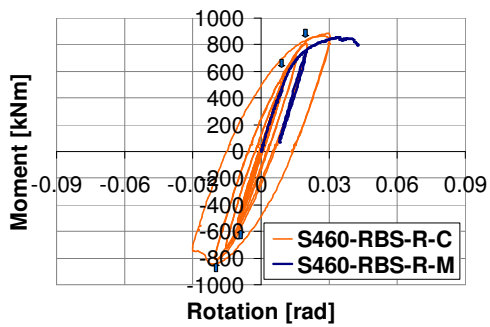
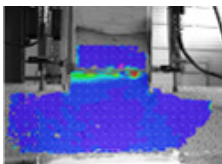
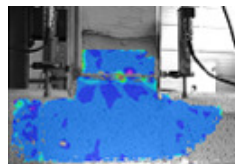


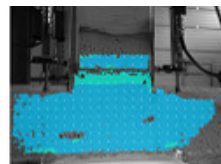
Fig. 5-69. S460-RBS-R-C joint: cyclic response and illustration of the failure mode



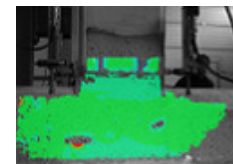
0.01 rad



-0.01 rad



0.02 rad



-0.02 rad

Fig. 5-70. Strain " ϵ_{yy} " in external diaphragm and HAZ of beam flange (Vic 3D)

5.6.6. S700-RBS-R-M / S700-RBS-R-C

The test assembly and the connection zone of the reinforced S700-RBS-R joint configuration prior to the testing are illustrated in Fig. 5-71.



Fig. 5-71. S700-RBS-R test assembly and connection zone – before test

S700-RBS-R-M

The monotonic response, in terms of moment-rotation curve (computed at column centreline), of the S700-RBS-R joint is shown in Fig. 5-72. The yielding sequence of S700-RBS-R joint under monotonic loading is illustrated in Annex E. Consequently, the yielding was initiated in the compressed beam flange between reinforcing plate and external diaphragm, and was followed by yielding of web and fracture of beam flange under tension. Fig. 5-72 shows the state of the connection zone corresponding to the end of test.

The measurements performed with the optical 3D system are illustrated in Fig. 5-73. Consequently, the strain " ε_{yy} " in the external diaphragm and welded connection, corresponding to the points marked on the moment-rotation curve in Fig. 5-72, show the initiation and evolution of the plastic deformations.

S700-RBS-R-C

The cyclic response, in terms of moment-rotation curve (computed at column centreline), of the S700-RBS-R joint is shown in Fig. 5-74. The yielding sequence of S700-RBS-R joint under cyclic loading is illustrated in Annex E. Consequently, the yielding was initiated in the beam flanges under compression at the connection to the external diaphragm, and was followed by yielding of web and fracture of the beam flange under tension. Fig. 5-74 shows the state of the connection zone corresponding to the end of test.

The measurements performed with the optical 3D system are illustrated in Fig. 5-75. Consequently, the strain " ε_{yy} " in the external diaphragm and welded connection corresponding to the points marked on the moment-rotation curve in Fig. 5-74, show the initiation and evolution of the plastic deformations.

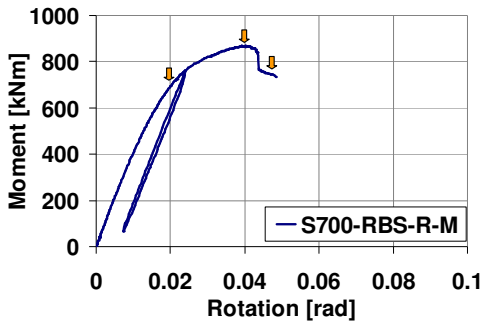


Fig. 5-72. S700-RBS-R-M joint: monotonic response and illustration of the failure mode

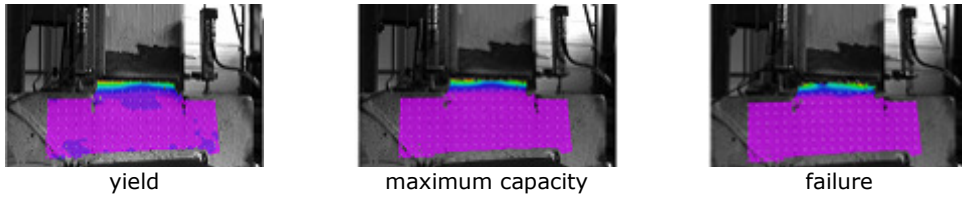


Fig. 5-73. Strain " ϵ_{yy} " in external diaphragm and HAZ of beam flange (Vic 3D)

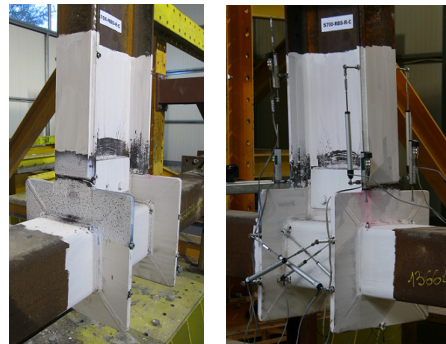
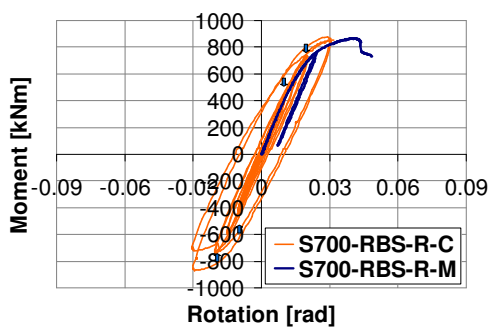


Fig. 5-74. S700-RBS-R-C joint: cyclic response and illustration of the failure mode

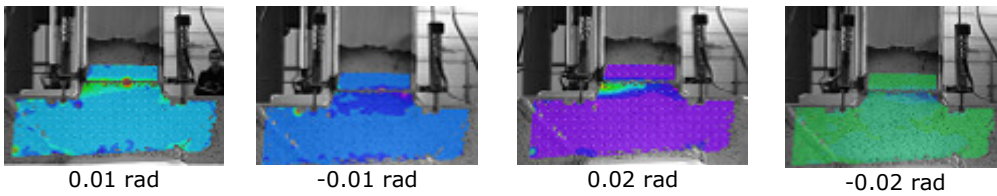


Fig. 5-75. Strain " ϵ_{yy} " in external diaphragm and HAZ of beam flange (Vic 3D)

5.6.7. S460-CP-R-M / S460-CP-R-C

The test assembly and the connection zone of the reinforced S460-CP-R joint configuration prior to the testing are illustrated in Fig. 5-76.

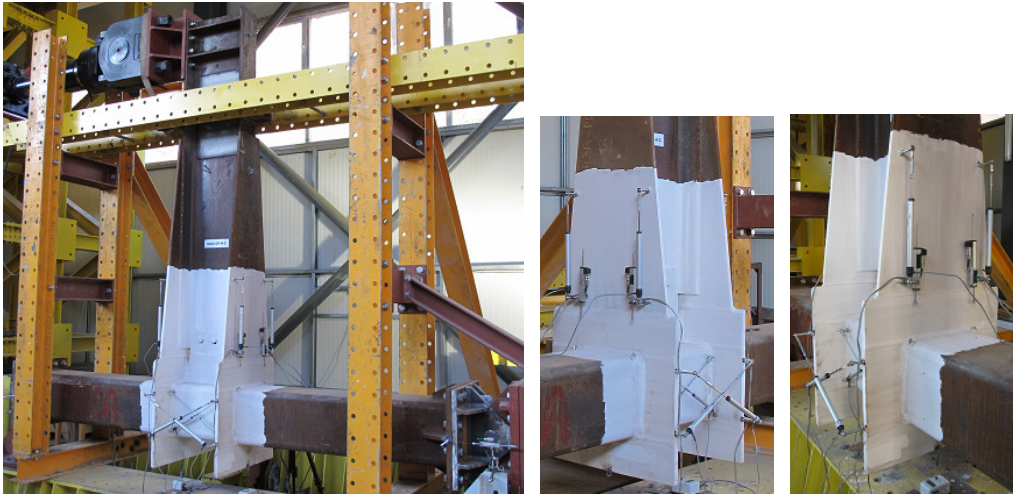


Fig. 5-76. S460-CP-R test assembly and connection zone – before test

S460-CP-R-M

The monotonic response, in terms of moment-rotation curve (computed at column centreline), of the S460-CP-R joint is shown in Fig. 5-77. The yielding sequence of S460-CP-R joint under monotonic loading is illustrated in Annex E. Consequently, the yielding was initiated in the external diaphragm and was followed by local deformations of the cover plate under compression. Fig. 5-77 shows the state of the connection zone corresponding to the end of test.

The measurements performed with the optical 3D system are illustrated in Fig. 5-78. Consequently, the strain " ε_{xy} " in the column panel is shown, corresponding to the points marked on the moment-rotation curve in Fig. 5-77.

S460-CP-R-C

The cyclic response, in terms of moment-rotation curve (computed at column centreline), of the S460-CP-R joint is shown in Fig. 5-79. It can be observed that the hysteretic loops are not symmetrical. This was due to the fact that the hydraulic actuator reached its limit (-650 kN) in the negative direction. The loading was therefore based on the AISC 341 loading protocol in positive direction and in negative direction up to the force limit.

The yielding sequence of S460-CP-R joint under cyclic loading is illustrated in Annex E. Consequently, the yielding was initiated in the external diaphragm and cover plates, and was followed by yielding of the column web panel and fracture of the cover plate under repeated compression-tension cycles. Fig. 5-79 shows the state of the connection zone corresponding to the end of test.

The measurements performed with the optical 3D system are illustrated in Fig. 5-80. Consequently, the strain " ε_{xy} " in the column panel is shown, corresponding to the points marked on the moment-rotation curve in Fig. 5-79. The

horizontal line shape pattern in the middle of the column panel was caused by the internal part of the longitudinal weld (see Fig. 5-2) which was in contact with the concrete core and therefore the local deformations were in some extent reduced by this contact.

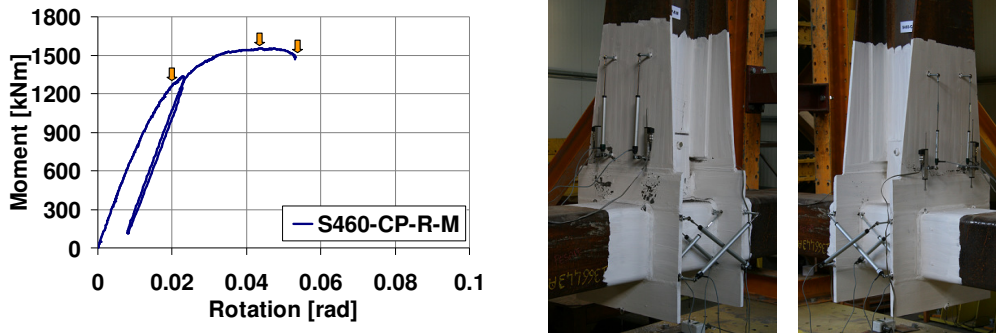


Fig. 5-77. S460-CP-R-M joint: monotonic response and illustration of the failure mode

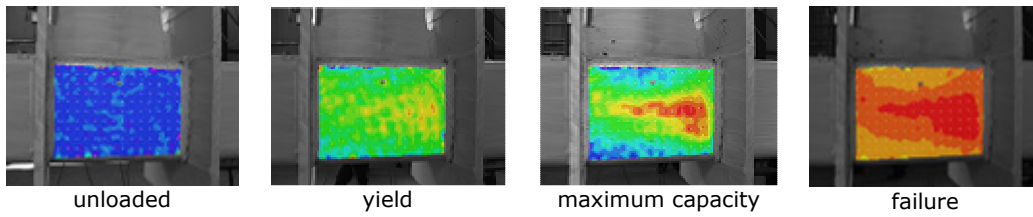


Fig. 5-78. Strain " ϵ_{xy} " in the column panel zone (Vic 3D)

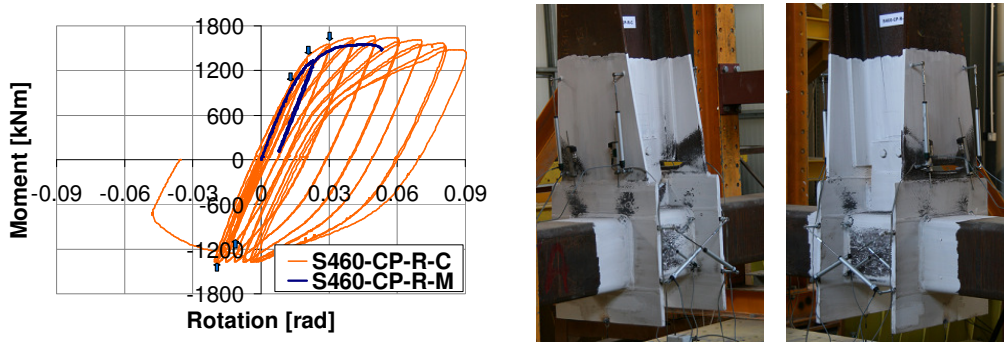


Fig. 5-79. S460-CP-R-C joint: cyclic response and illustration of the failure mode

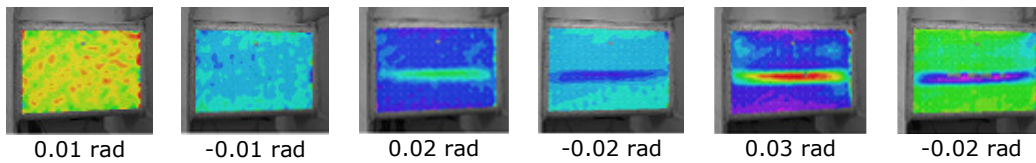


Fig. 5-80. Strain " ϵ_{xy} " in the column panel zone (Vic 3D)

5.6.8. S700-CP-R-M / S700-CP-R-C

The test assembly and the connection zone of the reinforced S700-CP-R joint configuration prior to the testing are illustrated in Fig. 5-81.



Fig. 5-81. S700-CP-R test assembly and connection zone – before test

S700-CP-R-M

The monotonic response, in terms of moment-rotation curve (computed at column centreline), of the S700-CP-R joint is shown in Fig. 5-82. The yielding sequence of S700-CP-R joint under monotonic loading is illustrated in Annex E. Consequently, the yielding was initiated in the compressed cover plate and was followed by failure of the welded connection between plates that composed the external diaphragm. Fig. 5-82 shows the state of the connection zone corresponding to the end of test.

The measurements performed with the optical 3D system are illustrated in Fig. 5-83. Consequently, the strain " ε_{xy} " in the column panel zone is shown, corresponding to the points marked on the moment-rotation curve in Fig. 5-82.

S700-CP-R-C

The cyclic response, in terms of moment-rotation curve (computed at column centreline), of the S700-CP-R joint is shown in Fig. 5-84. The yielding sequence of S700-CP-R joint under cyclic loading is illustrated in Annex E. Consequently, the yielding was initiated in cover plates under compression loads and was followed by failure of the welded connection between plates that composed the external diaphragm. Fig. 5-84 shows the state of the connection zone corresponding to the end of test.

The measurements performed with the optical 3D system are illustrated in Fig. 5-85. Consequently, the strain " ε_{xy} " in the column panel is shown, corresponding to the points marked on the moment-rotation curve in Fig. 5-84. Also in this case, the contact between the concrete core and the longitudinal weld of the tube (see Fig. 5-2) lead to restrained local deformations.

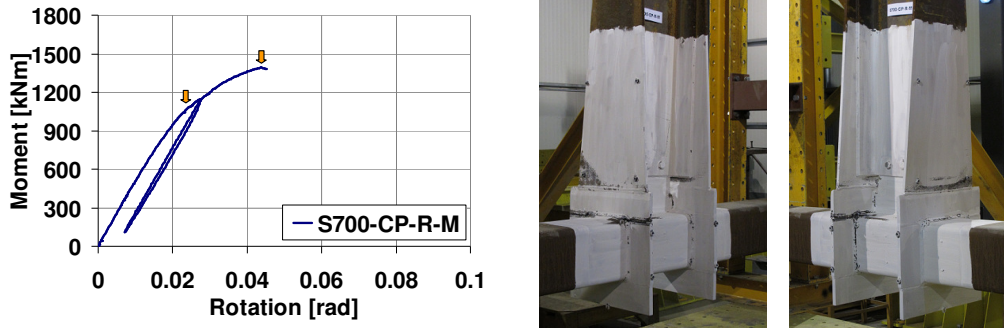


Fig. 5-82. S700-CP-R-M joint: monotonic response and illustration of the failure mode

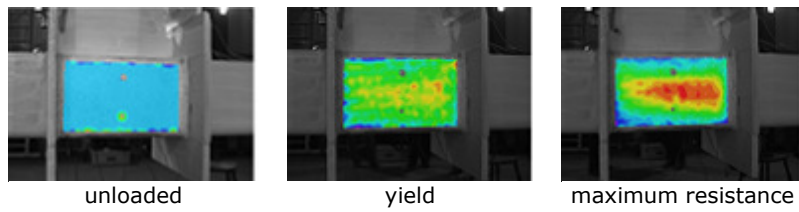


Fig. 5-83. Strain " ϵ_{xy} " in the column panel zone (Vic 3D)

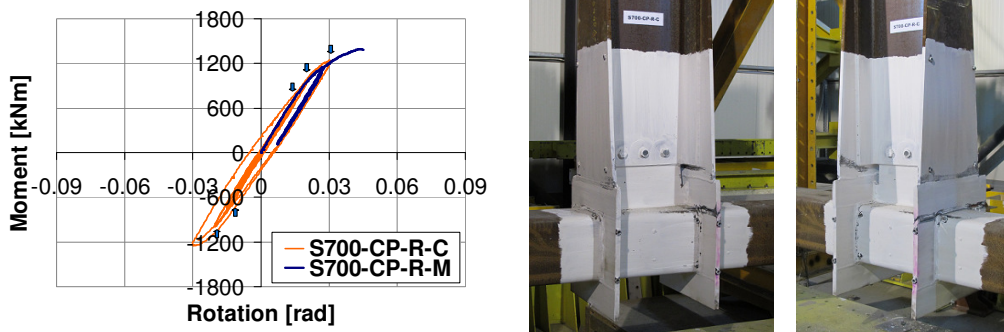


Fig. 5-84. S700-CP-R-C joint: cyclic response and illustration of the failure mode

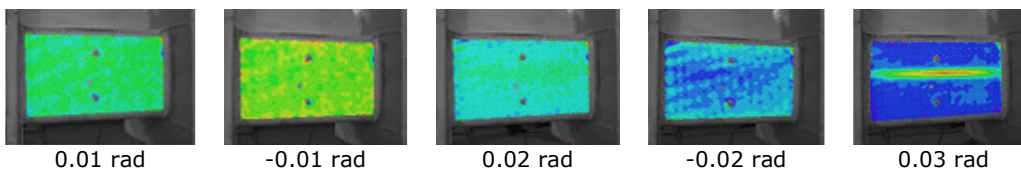


Fig. 5-85. Strain " ϵ_{xy} " in the column panel zone (Vic 3D)

5.6.9. Interpretation of results

In this section an overview is made related to the results obtained on beam-to-column joints. According to this, an evaluation is made considering the following aspects:

- Contribution of components to the joint rotation;
- Overstrength of connection zone;
- Evaluation of energy dissipated by the joints.

Contribution of components to the joint rotation

The contribution of components to the joint rotation, under both monotonic and cyclic loading, is further shown for each joint configuration. The measurements performed during the tests allowed assessing the contribution of the following regions: plastic hinge (dissipative zone), connection (welded connection and external diaphragm), and column web panel.

It can be observed in Fig. 5-86 and Fig. 5-87 for the joints with reduced beam section, and in Fig. 5-88 and Fig. 5-89 for the joints with cover plates, that the main plastic deformations occurred in the dissipative zone of the beam (plastic hinge). The contribution of the connection and column panel to the overall joint rotation was observed to be low. In Fig. 5-86 and Fig. 5-87 the deformations from the connection zone were higher in comparison to the joints with cover plates, due to the fact that the measured region included also the beam flange situated between the reduced beam section and external diaphragm. During the experimental investigations it was observed that low deformations developed also in this area (see the yielding sequence in Annex E).

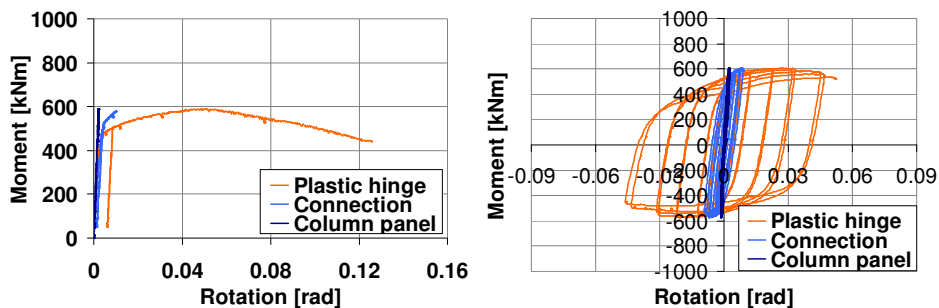


Fig. 5-86. Contribution of components to joint rotation (S460-RBS-M / C)

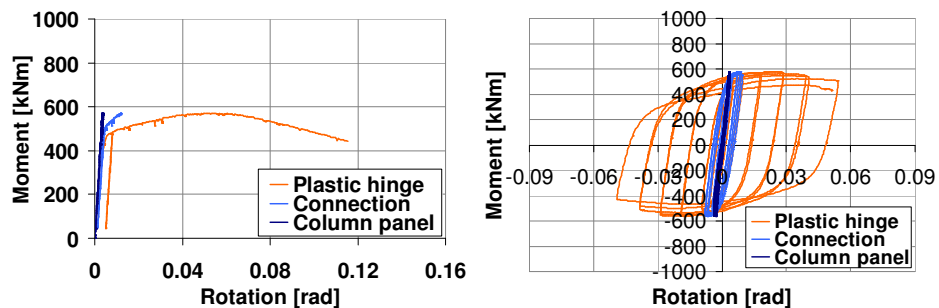


Fig. 5-87. Contribution of components to joint rotation (S700-RBS-M / C)

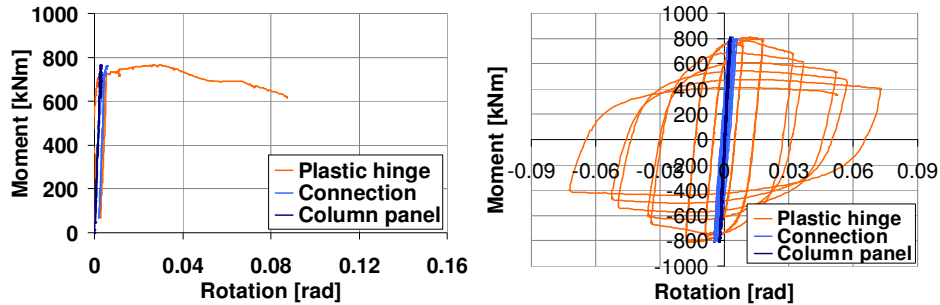


Fig. 5-88. Contribution of components to joint rotation (S460-CP-M / C)

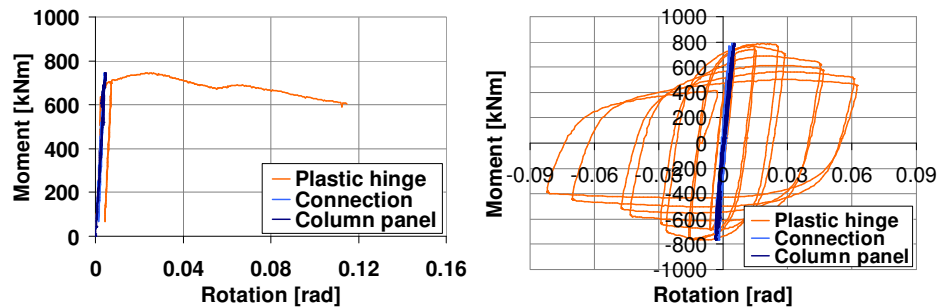


Fig. 5-89. Contribution of components to joint rotation (S700-CP-M / C)

The contribution of components to the joint configurations with strengthened beam is shown in Fig. 5-90, Fig. 5-91, Fig. 5-92 and Fig. 5-93. The deformations within the reinforced beam zone were proved to be low except for the S460-CP-R-C joint where deformations developed in the compressed extended cover plate (reinforced beam zone). The main contribution to the overall joint rotation was given by the connection zone (for strengthened RBS joints), and respectively connection and column panel (for strengthened CP joint). The measurements from the connection zone include the deformations of the external diaphragm.

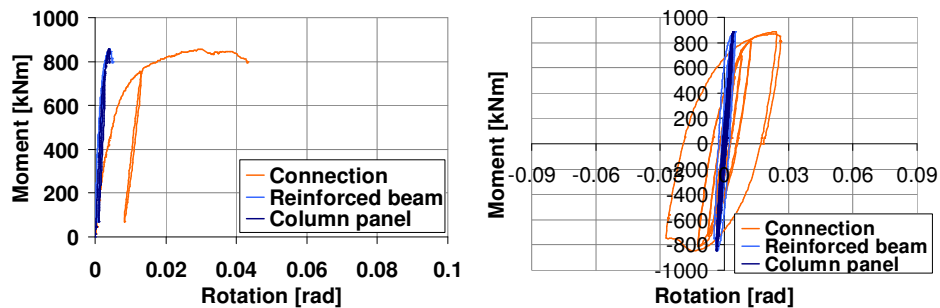


Fig. 5-90. Contribution of components to joint rotation (S460-RBS-R-M / C)

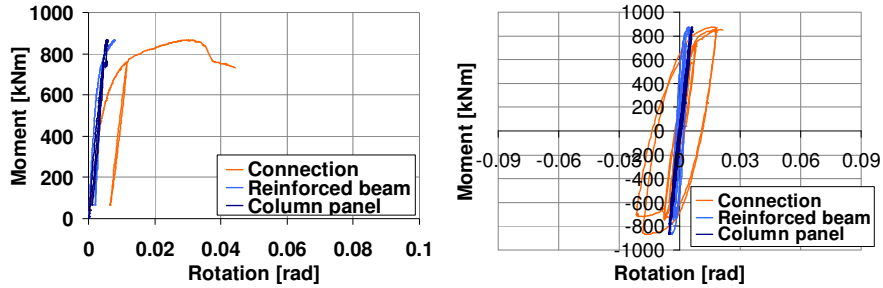


Fig. 5-91. Contribution of components to joint rotation (S700-RBS-R-M / C)

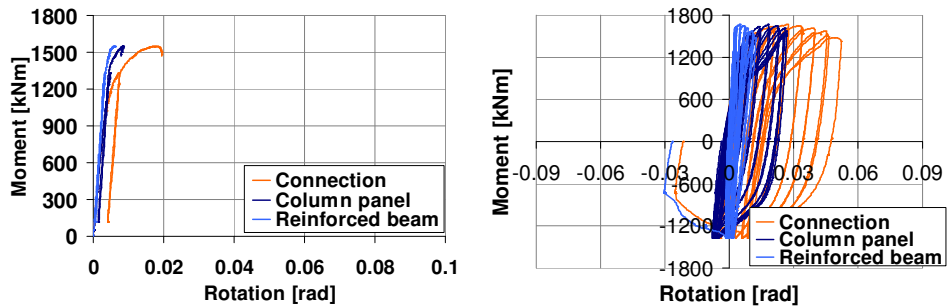


Fig. 5-92. Contribution of components to joint rotation (S460-CP-R-M / C)

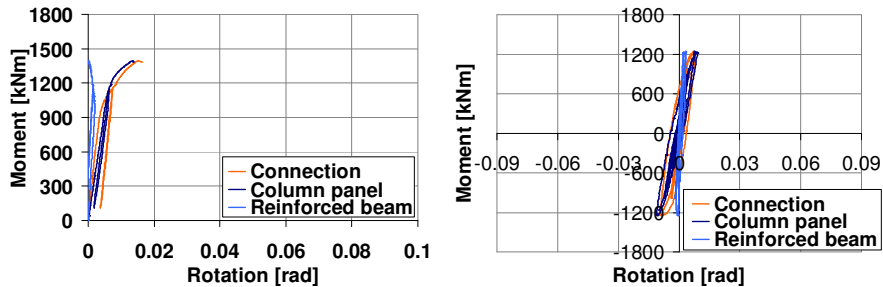


Fig. 5-93. Contribution of components to joint rotation (S700-CP-R-M / C)

Overstrength of connection zone

With the aim to assess the overstrength of the connection zone, a comparison was made between the four designed joints and the corresponding joints with reinforced beam (see Fig. 5-94 and Fig. 5-95). The moment-rotation curves were computed at the connection to the external diaphragm, and the overstrength was evaluated corresponding to the yield point and to maximum capacity. Consequently, the overstrength of the connection zone for the RBS joints (S460 & S700) was evaluated in the amount of 34% and 35% at yield, and respectively 53% and 60% at maximum capacity.

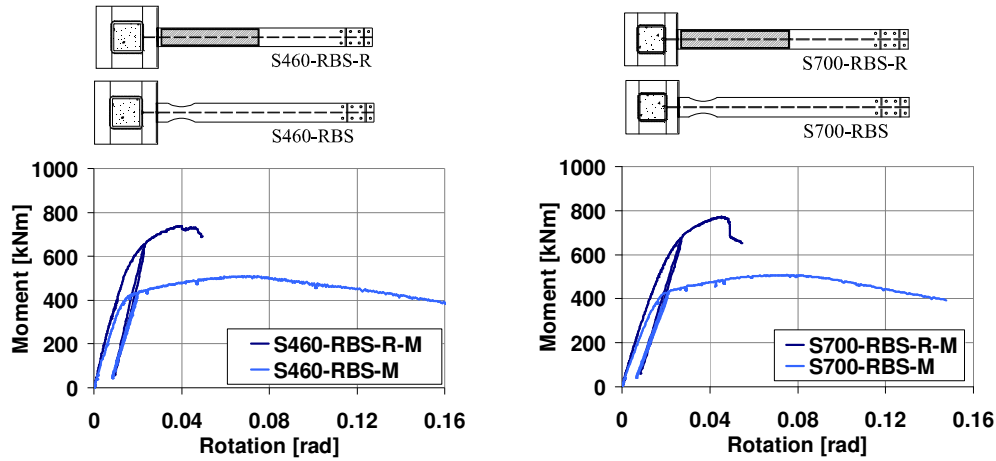


Fig. 5-94. Overstrength of connection zone for RBS joints

The overstrength of the connection zone for the CP joints (S460 & S700) was 55% and 43% at yield, and respectively 101% and 86% at maximum capacity.

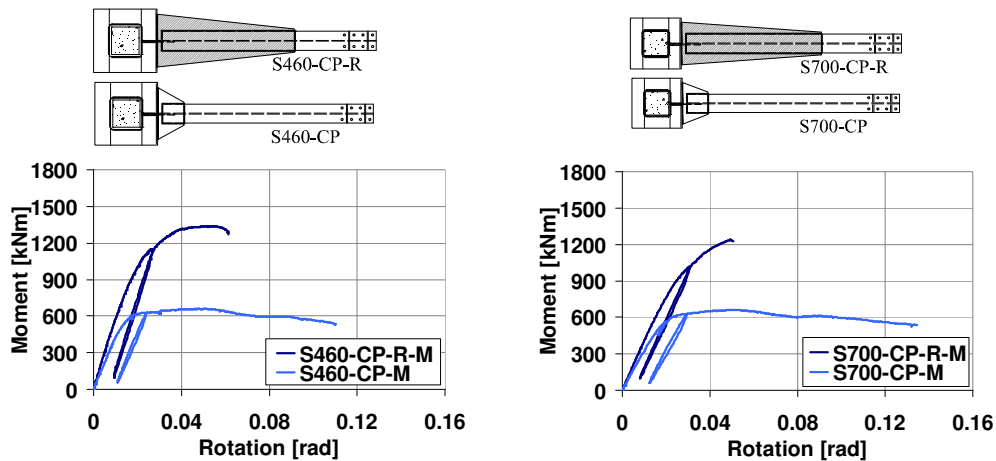


Fig. 5-95. Overstrength of connection zone for CP joints

Evaluation of energy dissipated by the joints

The energy dissipated by the beam-to-column joint assembly was evaluated computing the area enclosed by a hysteresis curve. Consequently, the hysteretic loops and the corresponding dissipated energy are shown in Fig. 5-96 and Fig. 5-97 for joints with reduced beam section, in Fig. 5-98 and Fig. 5-99 for joints with cover plates, in Fig. 5-100 and Fig. 5-101 for strengthened RBS joints, and finally in Fig. 5-102 and Fig. 5-103 for the joints with extended cover plates. A good dissipation capacity can be observed for both RBS and CP joints. The energy absorbed by the heat affected zone (see strengthened RBS joints) was observed to be low. In contrast, the energy absorbed by column web panel, external diaphragm and cover plates (see S460-CP-R-C joint) was significant, but not in the case of S700-CP-R-C joint which evidenced weld failure from the external diaphragm.

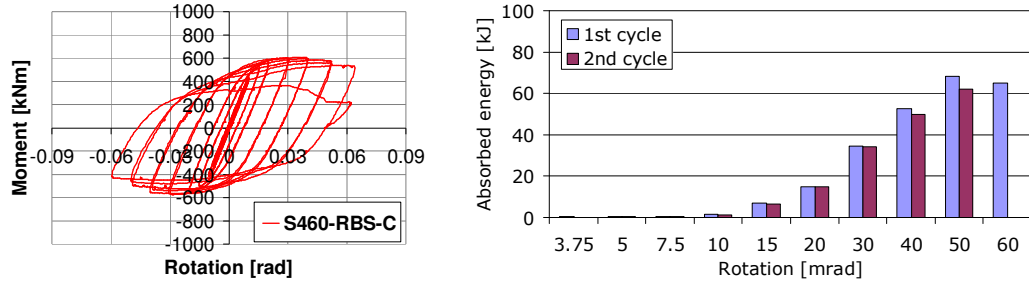


Fig. 5-96. S460-RBS joint: cyclic response and the corresponding dissipated energy

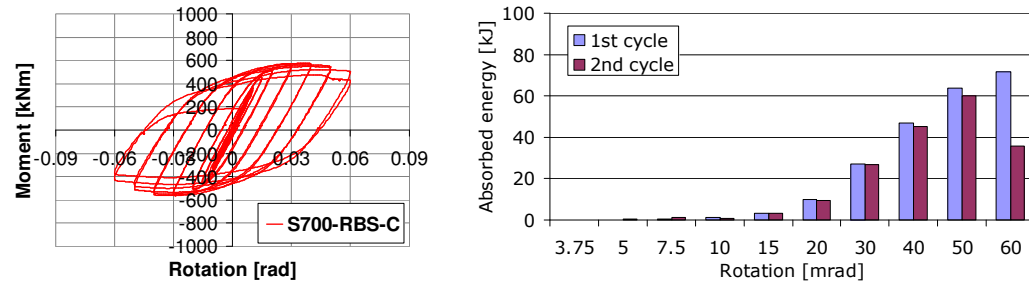


Fig. 5-97. S700-RBS joint: cyclic response and the corresponding dissipated energy

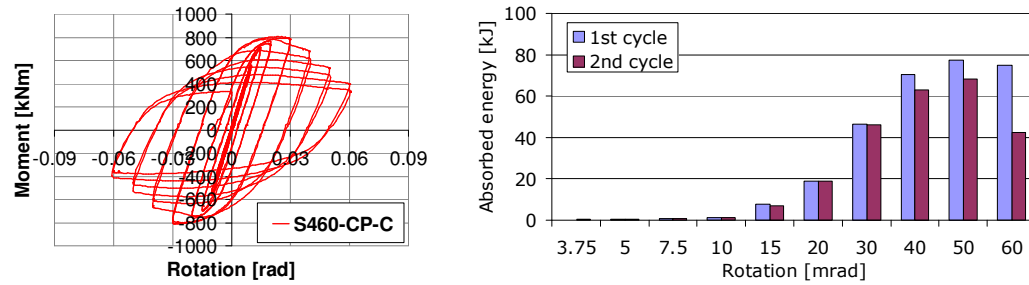


Fig. 5-98. S460-CP joint: cyclic response and the corresponding dissipated energy

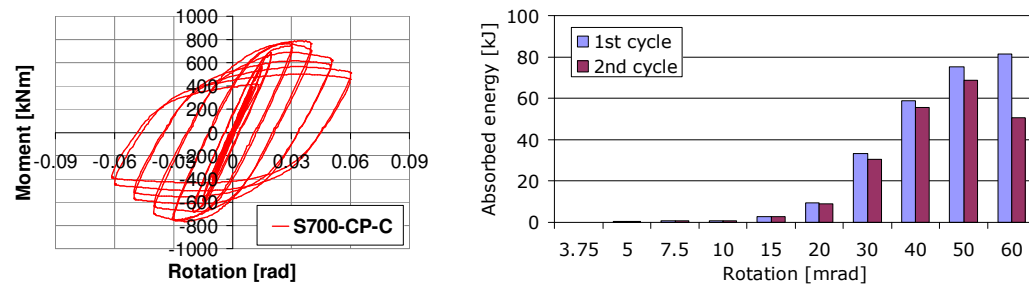


Fig. 5-99. S700-CP joint: cyclic response and the corresponding dissipated energy

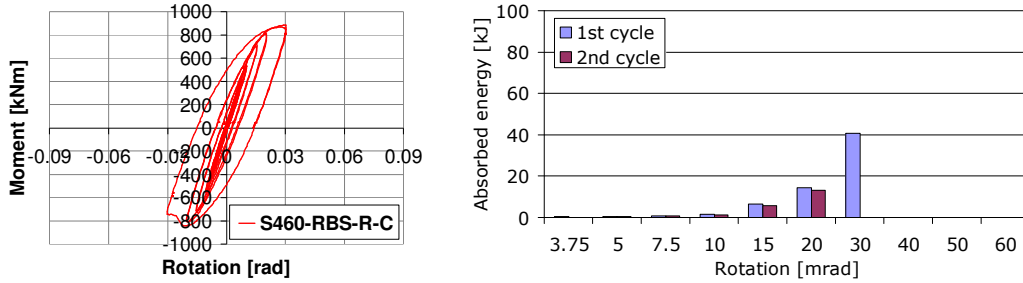


Fig. 5-100. S460-RBS-R joint: cyclic response and the corresponding dissipated energy

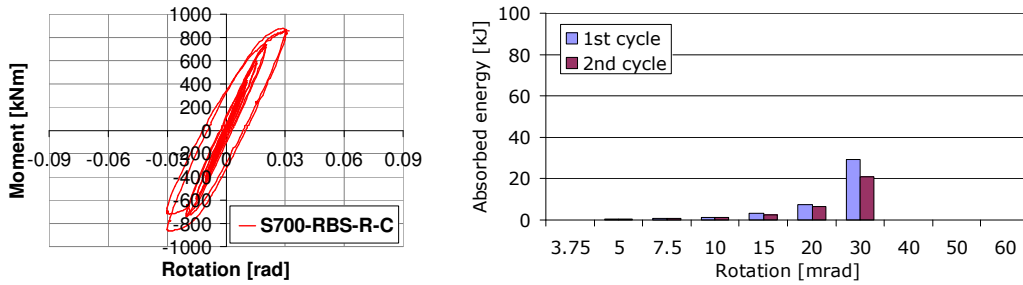


Fig. 5-101. S700-RBS-R joint: cyclic response and the corresponding dissipated energy

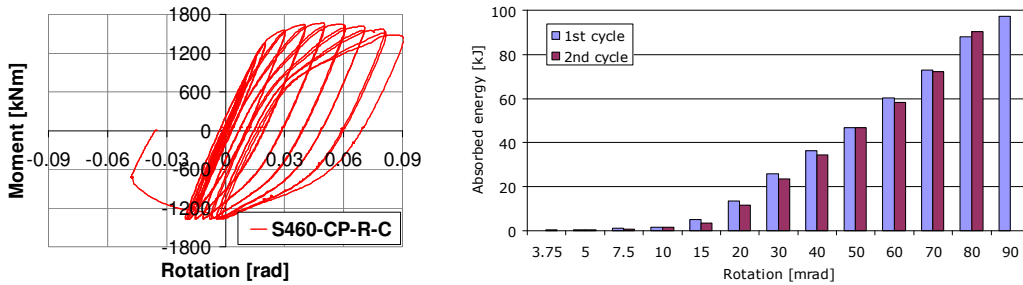


Fig. 5-102. S460-CP-R joint: cyclic response and the corresponding dissipated energy

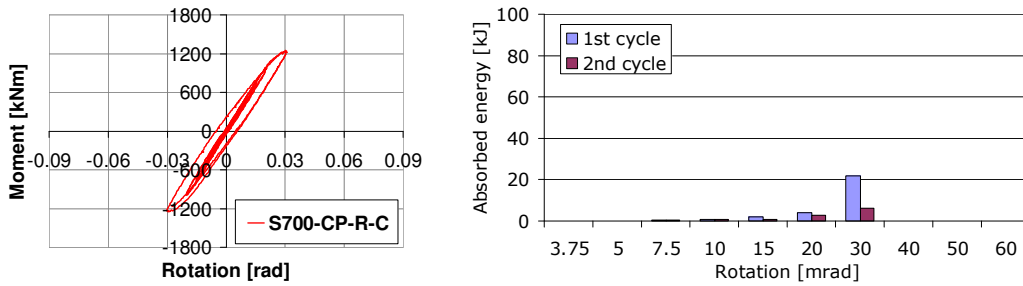


Fig. 5-103. S700-CP-R joint: cyclic response and the corresponding dissipated energy

5.7. NDT quality control of specimens

The first stage of the experimental program consisted of the monotonic investigation of each joint configuration. Due to the unexpected weld failure observed at S700-CP-R-M joint (see Fig. 5-104) an investigation was started with the aim to determine the causes that lead to the failure of the weld.



Fig. 5-104. Weld failure within S700-CP-R-M joint

The investigation [98] consisted in non-destructive testing (NDT) of the welded connections within the reinforced joints (see Fig. 5-105) that were to be tested under cyclic loading conditions. A number of three methods were applied, i.e. liquid penetrant testing (PT), magnetic particle testing (MT), and ultrasonic testing (UT).

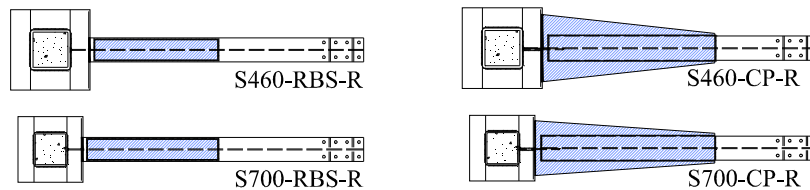


Fig. 5-105. Reinforced beam-to-column joint configurations

5.7.1. Liquid penetrant testing

From the liquid penetrant testing of the welded connections (see Fig. 5-106) no discontinuities have been revealed.



Fig. 5-106. Liquid penetrant testing

5.7.2. Magnetic particle testing

From the magnetic particle testing of the welded connections (see Fig. 5-107) no discontinuities have been revealed.



Fig. 5-107. Magnetic particle testing (S460-RBS-R-C, and S700-CP-R-C)

5.7.3. Ultrasonic testing

For the ultrasonic testing of the welded connections, the measurement device was calibrated using the block A1 considering the 3 mm hole situated at 15 mm from the surface (see Fig. 5-108a). The investigation revealed only local discontinuities (in the allowed range) for the welded connections of the following joints: S460-RBS-R, S700-RBS-R and S460-CP-R. In contrast, for the S700-CP-R joint (see Fig. 5-109), the investigation revealed a full length discontinuity of the welded connection between the plates of the external diaphragm (see Fig. 5-108bc).

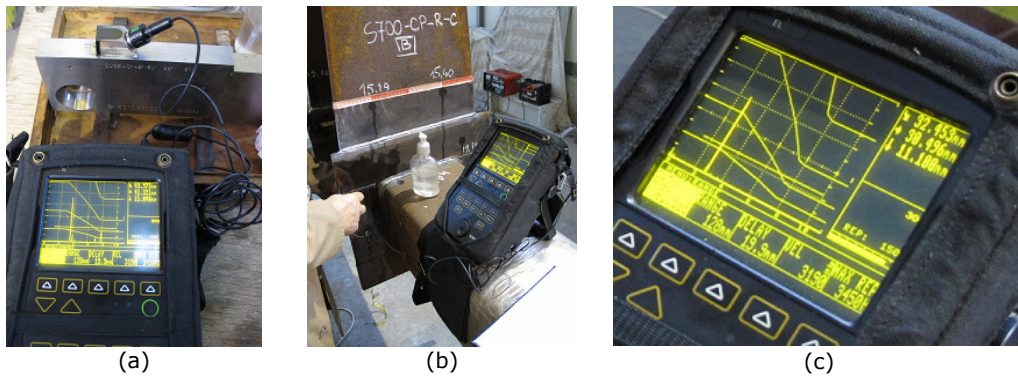


Fig. 5-108. Ultrasonic testing

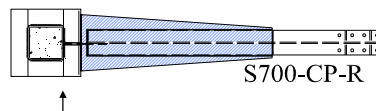


Fig. 5-109. Joint with full length discontinuity of weld between plates of the external diaphragm (un-penetrated weld root)

5.8. Calibration of FE models and simulation of complementary cases

A set of complementary testing cases were considered for the investigation through numerical simulations with the aim to assess the influence of different parameters on the joint behaviour.

In a first step the numerical models that anticipated the behaviour of the joint specimens were calibrated based on the results obtained from the experimental tests performed under monotonic and cyclic loading. Further the experimental program was extended with the numerical study of the following cases:

- Influence of the concrete core – i.e. the response of the joint without concrete core in comparison to the reference joint with CFT column;
- Response of joints with beams welded on two sides and considering the column filled with concrete and without concrete inside of the tube;
- Influence of the axial force – i.e. the response of the joint with axial force in the column ($N=0.5*N_{pl}$) in comparison to the reference model.

5.8.1. Calibration of the numerical models

Beam-to-column joints subjected to monotonic loading

The numerical models of the beam-to-column joints from the pre-test numerical simulations were used for the calibration phase. The material model of each steel component of the joints was already calibrated based on the results from tensile tests (see section 5.5. and Annex D). In addition it was observed that the results from the pre-test numerical simulations were relative close to the results from the experimental investigations. It is to be noted that within the numerical simulations it was not accounted for material fracture or crack propagation, phenomena that were observed at some of the joint specimens (i.e. S460-RBS-R-M, S700-RBS-R-M, and S700-CP-R-M). Because in the numerical models of these joints no fracture developed, the capacity did not suffer as in the experimental tests.

The calibration and refinement of the numerical models was performed considering the measured geometry of the specimens. One of the assumptions from the pre-test investigations was related to the lateral supports of the beam flanges. Consequently, the out of plane deformations were completely restrained in some regions (see the test set-up). However, during the experimental investigations it was observed that the beam was not completely restrained by the out of plane lateral system due to contact tolerances. As a consequence a lateral contact was defined (see Fig. 5-110a) considering a small gap between flanges and the contact elements. In addition, the number of finite elements was reduced using beam elements at the end of the column and beam which were considered as rigid. It was observed that this simplification did not affect the response in comparison to the complete joint model, and allowed reducing the computing time.

From the calibration, a set of numerical models were obtained which were capable to reproduce with a good accuracy the response of the joints in both moment-rotation curve and failure mechanism, i.e. formation of the plastic hinge in the beam (designed joints) and yielding of components (joints with strengthened beam). Consequently, for each beam-to-column joint configuration, a comparison between experimental test and numerical simulation is shown in terms of moment-rotation curve computed at column centreline. The von Mises stress distribution and

the plastic strain is also shown in comparison to the failure mode observed during the test. As a final point, the results from the calibration of the monotonic tests on beam to column joints are shown in Fig. 5-111 and Fig. 5-112 for the joints with reduced beam section, in Fig. 5-113 and Fig. 5-114 for the joints with cover plates, in Fig. 5-115 and Fig. 5-116 for the reinforced RBS joints, and finally in Fig. 5-117 and Fig. 5-118 corresponding to the reinforced CP joints.

Beam-to-column joints subjected to cyclic loading

The numerical models calibrated based on the joints subjected to monotonic loading were further used for the numerical calibration of the cyclic tests. One of the differences was related to the loading procedure. Fig. 5-110b shows a pattern of cyclic loading procedure used in the numerical simulations. As can be seen the first amplitudes correspond to 10 mrad and continue with 15, 20, 30, 40, 50, and 60 mrad considering only one cycle for each amplitude.

Another difference between cyclic and monotonic analyses was related to the material model. A combined isotropic/kinematic hardening model was therefore adopted. The input of the material model contained the yield strength of the modelled steel component and the cyclic hardening parameters as given by Dutta et al. (2010) [99], (i.e. $C_1=42096$, $\gamma_1=594.45$, $Q_\infty=60$, $b=9.71$).

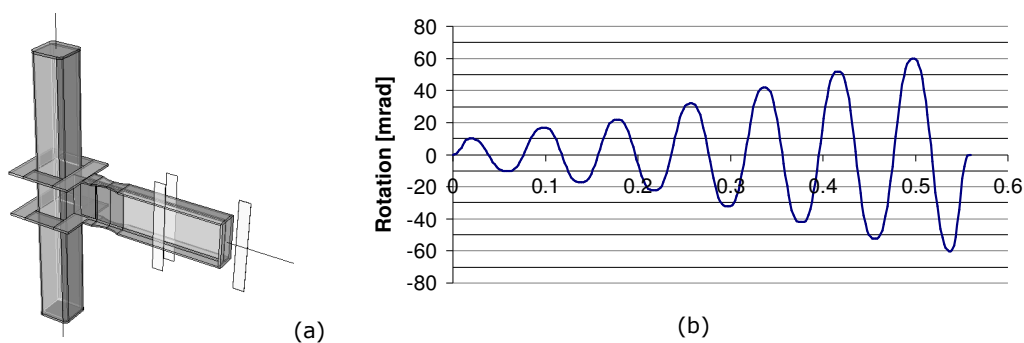


Fig. 5-110. Beam-to-column joint with lateral contact (a), and cyclic loading procedure (b)

The results from the cyclic analysis are shown for each beam-to-column joint configuration in terms moment-rotation curve (computed at column centreline) as well as stress distribution and plastic strain. An illustration of the failure mode, as obtained from the experimental investigations, is shown as well.

The comparison between test and numerical simulation is shown in Fig. 5-119 and Fig. 5-120 for joints with reduced beam section, in Fig. 5-121 and Fig. 5-122 for joints with cover plates, in Fig. 5-123 and Fig. 5-124 for reinforced RBS joints, and finally in Fig. 5-125 and Fig. 5-126 for reinforced CP joints.

The results from the numerical investigations of the cyclic tests show a good correlation with the experimental results considering the moment-rotation hysteretic loops as well as the failure mechanism (plastic hinge – buckling of flanges and web of beam in the dissipative zone, yielding of components – failure in the heat affected zone of the reinforced RBS joints, plastic deformations in the external diaphragm and column panel zone). In case of S460-CP-R-C joint, the capacity corresponding to the negative amplitudes was obtained higher in the numerical simulations compared to the test where the hydraulic actuator was limited to a force of 650 kN.

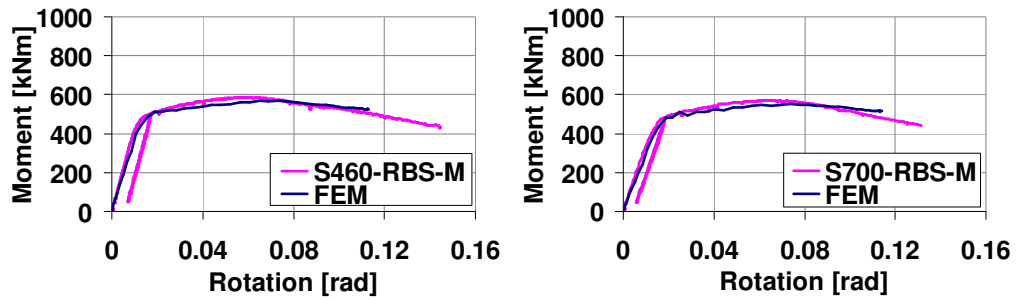


Fig. 5-111. Comparison between test and simulation for RBS joints

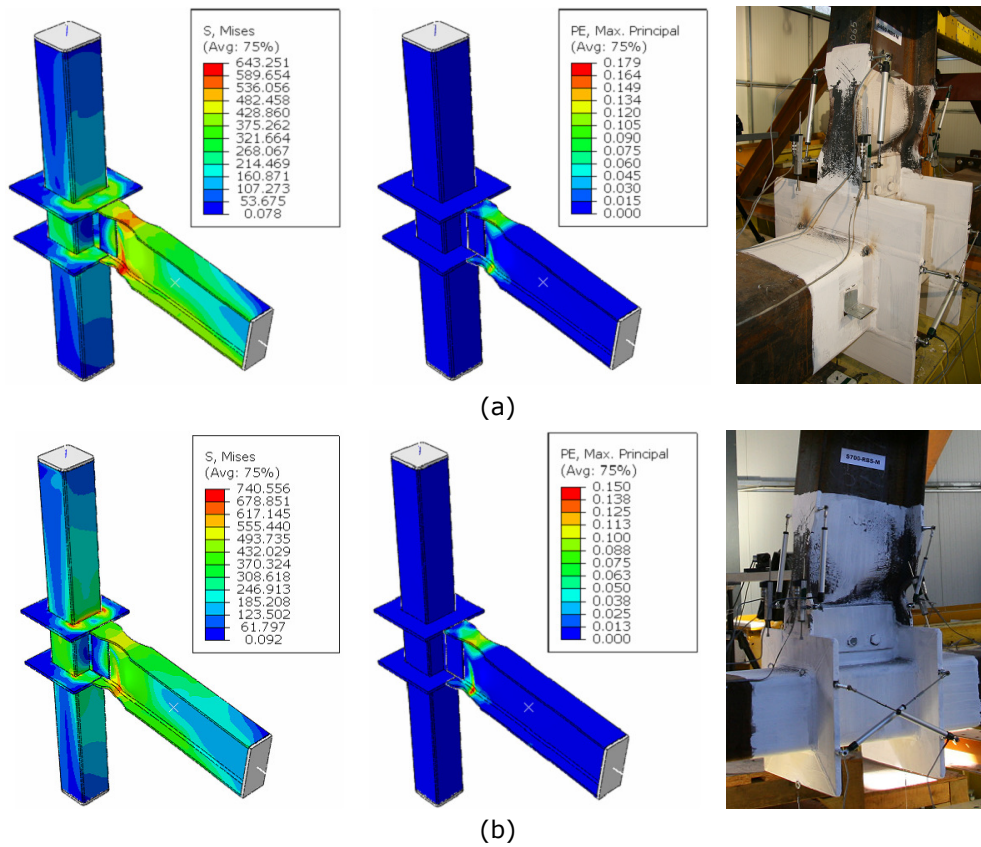


Fig. 5-112. Mises stress, plastic strain, and illustration of failure mode: (a) S460-RBS joint, and (b) S700-RBS joint

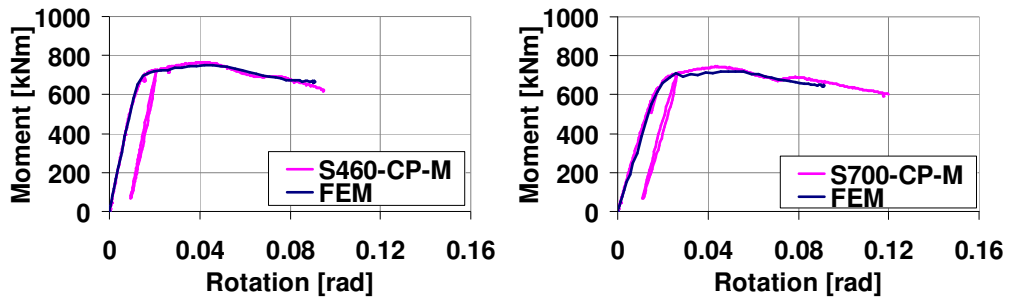


Fig. 5-113. Comparison between test and simulation for CP joints

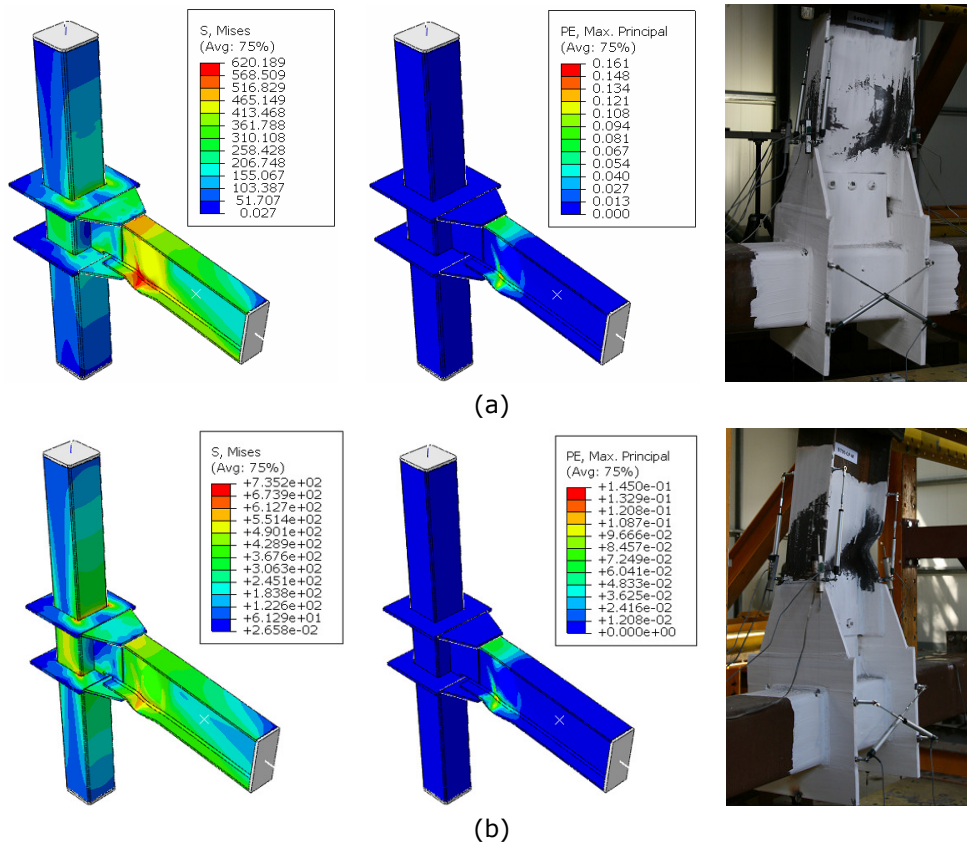


Fig. 5-114. Mises stress, plastic strain, and illustration of failure mode: (a) S460-CP joint, and (b) S700-CP joint

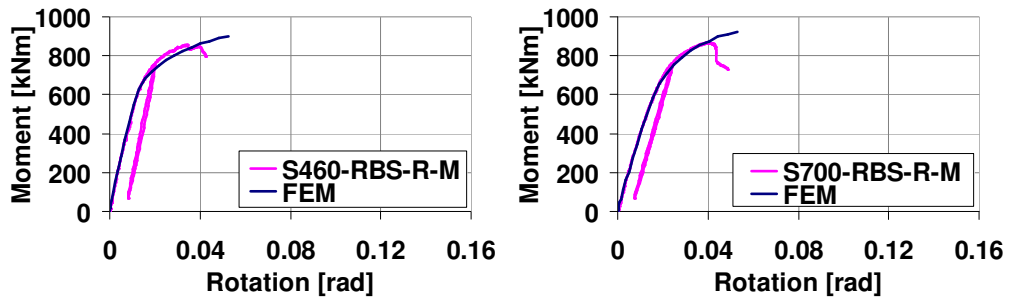


Fig. 5-115. Comparison between test and simulation for reinforced RBS joints

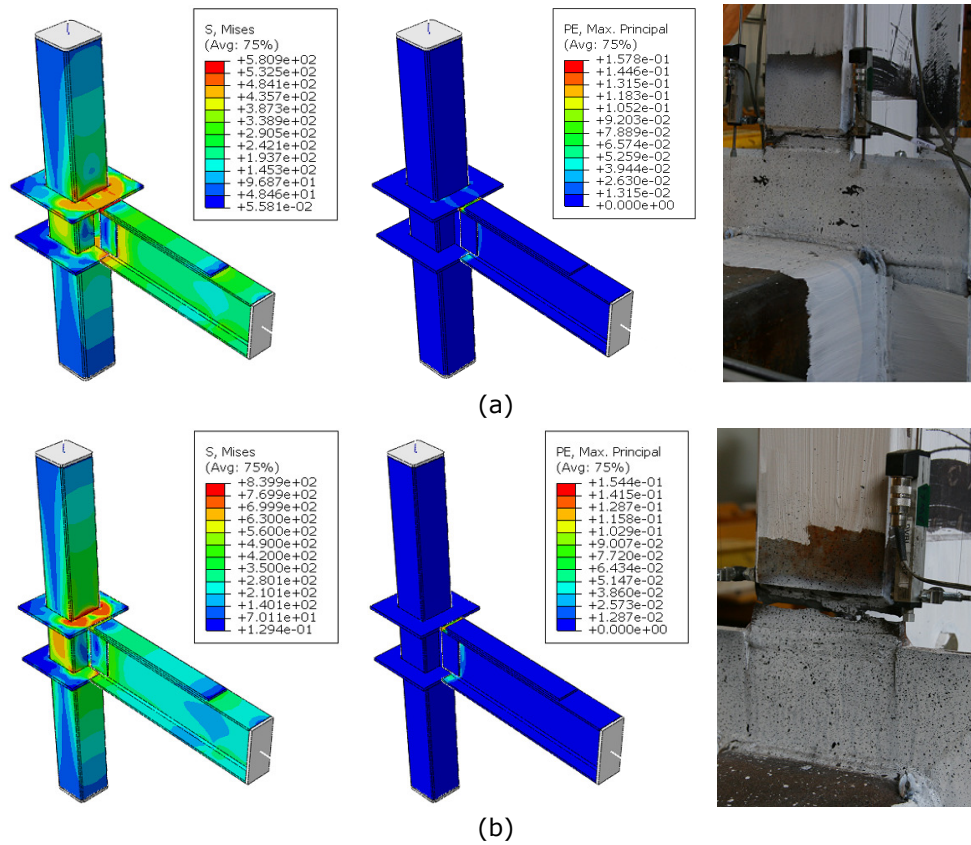


Fig. 5-116. Mises stress, plastic strain, and illustration of failure mode: (a) S460-RBS-R joint, and (b) S700-RBS-R joint

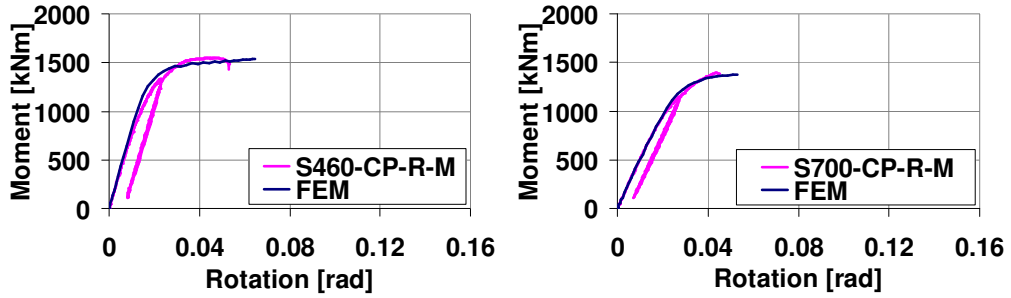


Fig. 5-117. Comparison between test and simulation for reinforced CP joints

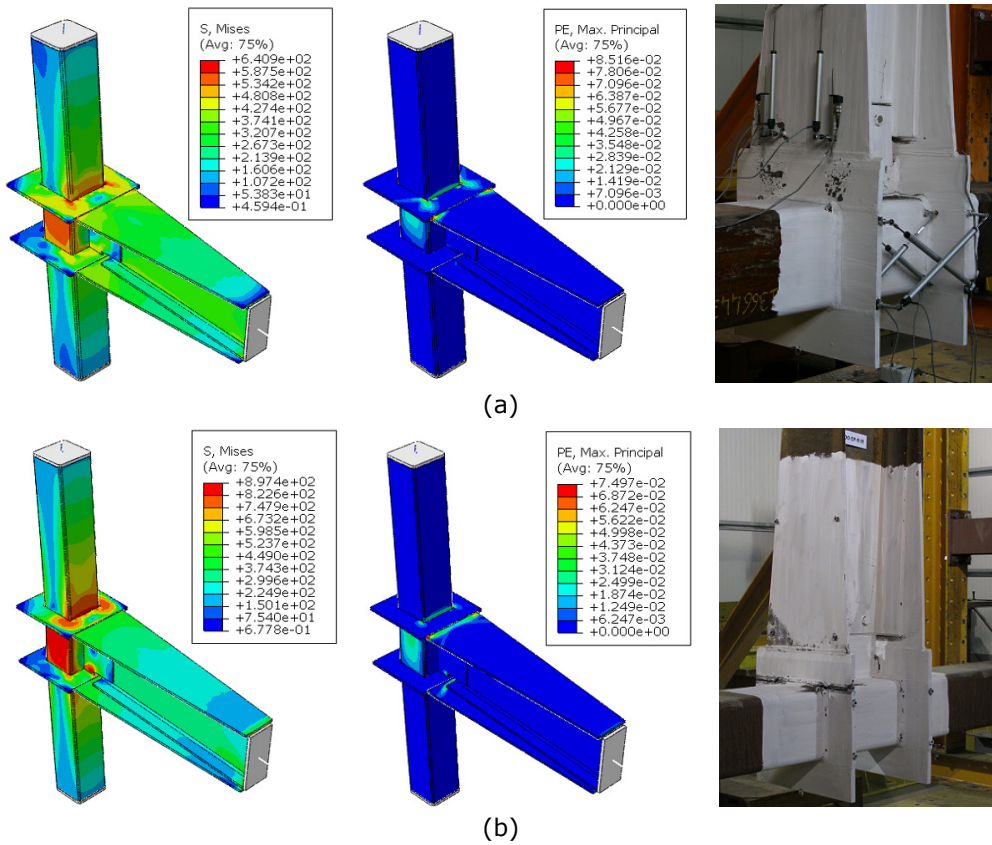


Fig. 5-118. Mises stress, plastic strain, and illustration of failure mode: (a) S460-CP-R joint, and (b) S700-CP-R joint

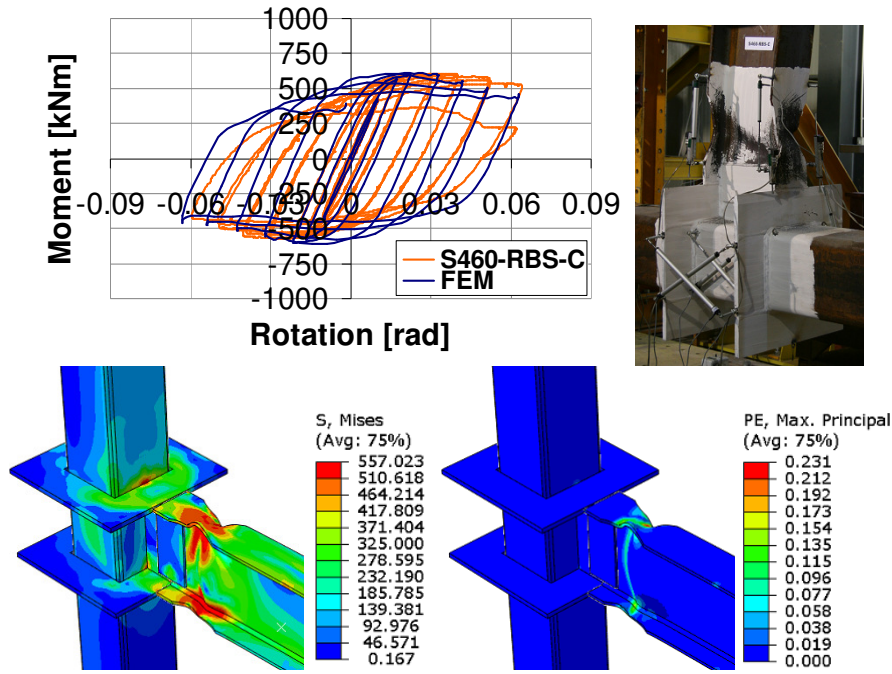


Fig. 5-119. Cyclic response (test and simulation) of S460-RBS joint

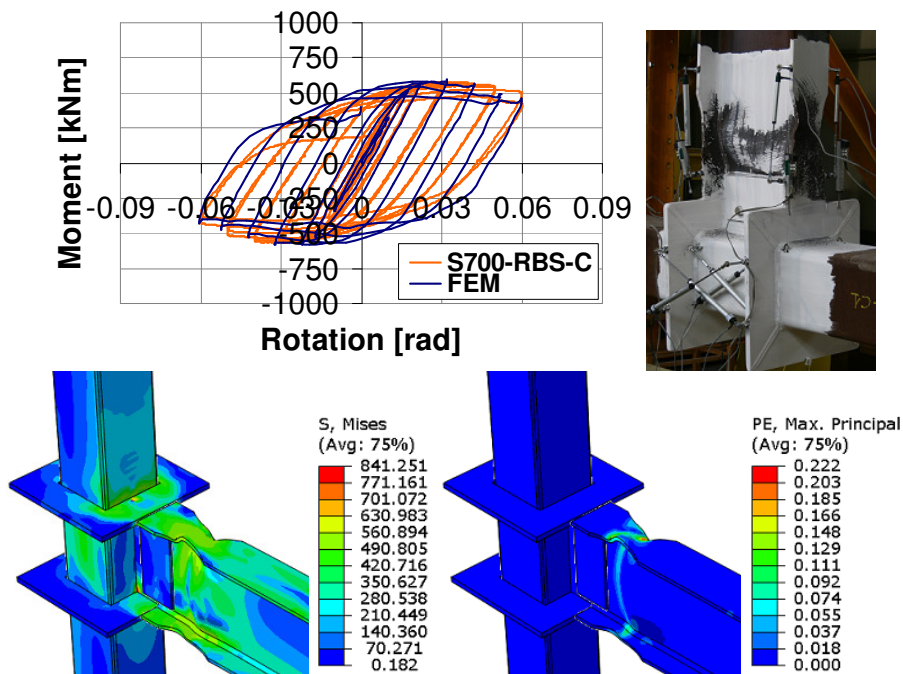


Fig. 5-120. Cyclic response (test and simulation) of S700-RBS joint

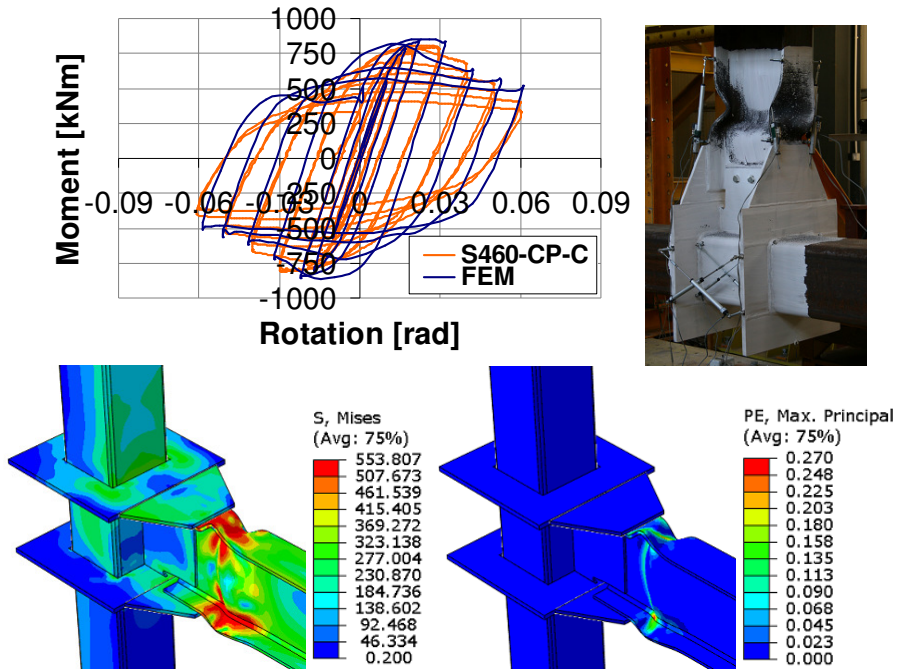


Fig. 5-121. Cyclic response (test and simulation) of S460-CP joint

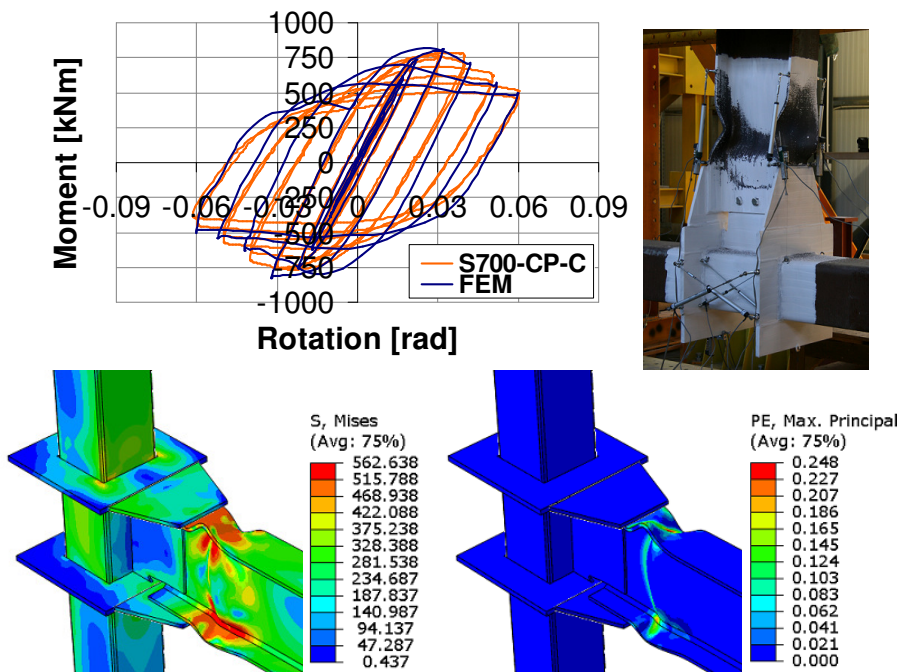


Fig. 5-122. Cyclic response (test and simulation) of S700-CP joint

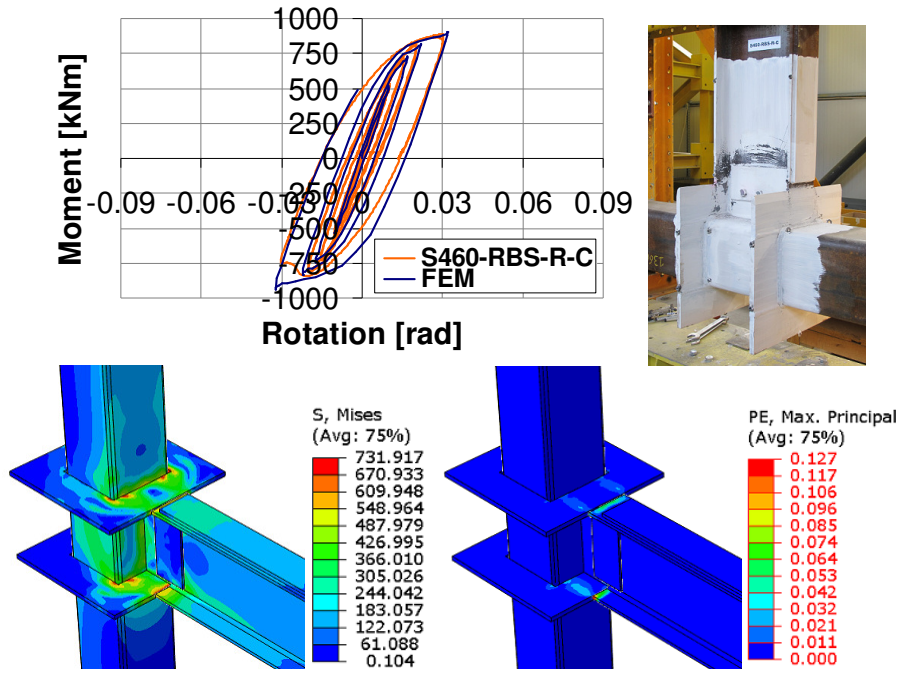


Fig. 5-123. Cyclic response (test and simulation) of S460-RBS-R joint

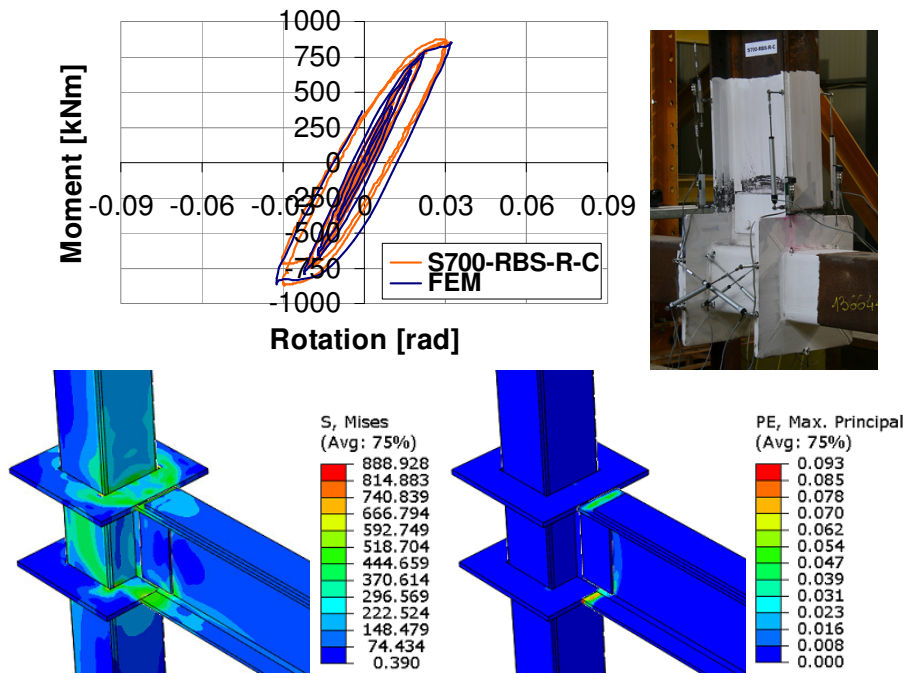


Fig. 5-124. Cyclic response (test and simulation) of S700-RBS-R joint

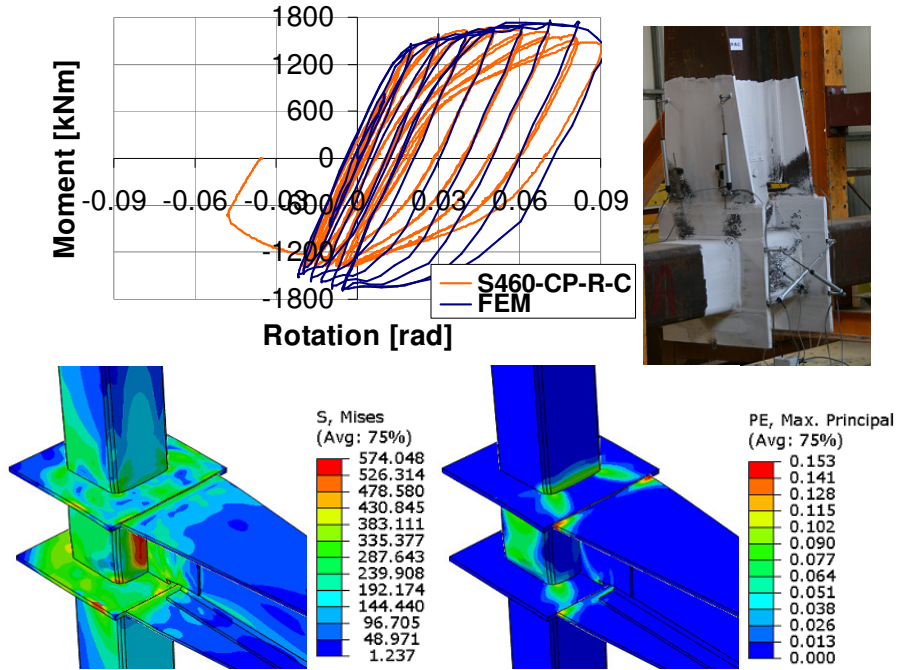


Fig. 5-125. Cyclic response (test and simulation) of S460-CP-R joint

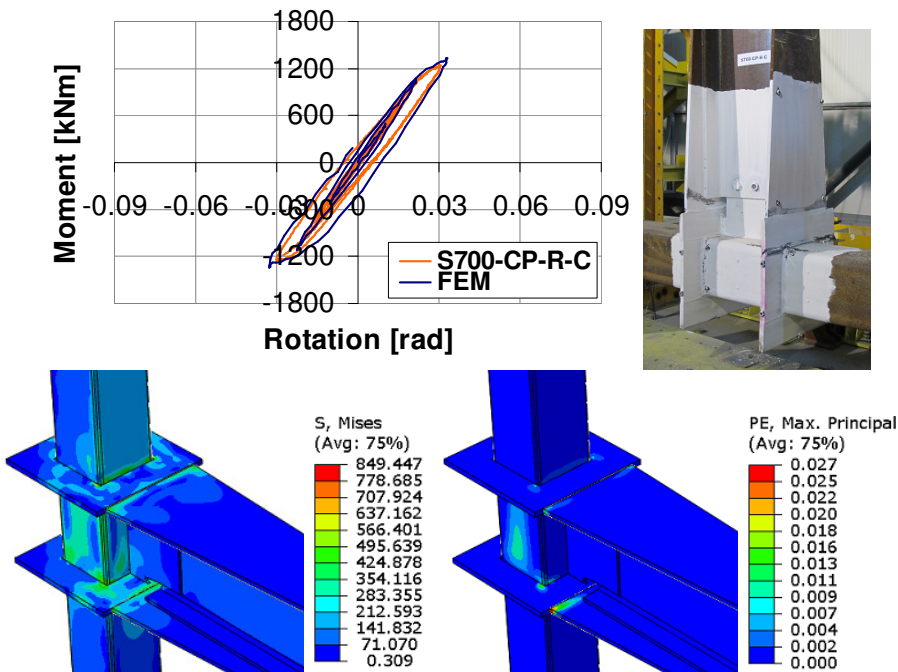


Fig. 5-126. Cyclic response (test and simulation) of S700-CP-R joint

5.8.2. Influence of concrete core

With the aim to evaluate the influence of the concrete core – i.e. the response of the joint without concrete core in comparison to the reference joints with composite column (CF-RHS) – a set of additional numerical simulations were performed on the calibrated numerical models from which the concrete part was eliminated. The results are shown in terms of moment-rotation curve computed at column centreline. It can be observed from Fig. 5-127 for reduced beam section joints and from Fig. 5-128 for cover plate joints, that the absence of concrete core did not affect significantly the response of the four designed joints (only a minor reduction of the capacity was observed). In contrast, for the reinforced joints (extended CP) a significant reduction of capacity can be observed in Fig. 5-129. In these cases, the bending moment and implicitly the shear force in the column web panel were much larger than in the other cases. In other words, the shear force in the column web panel exceeded the capacity of the steel tube in shear, and therefore a higher capacity was corresponding to the joints with concrete core.

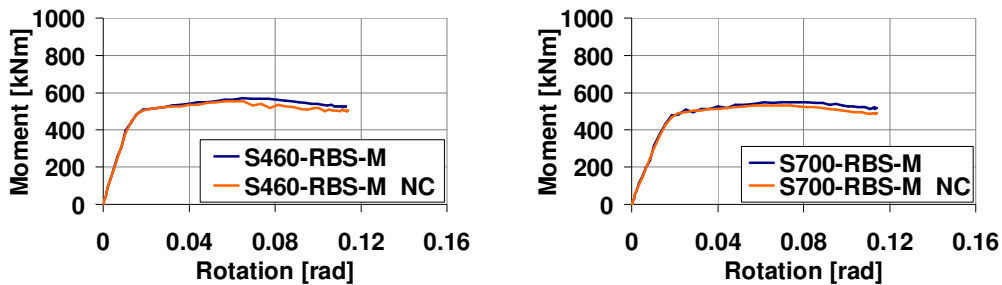


Fig. 5-127. Influence of concrete core – RBS joints

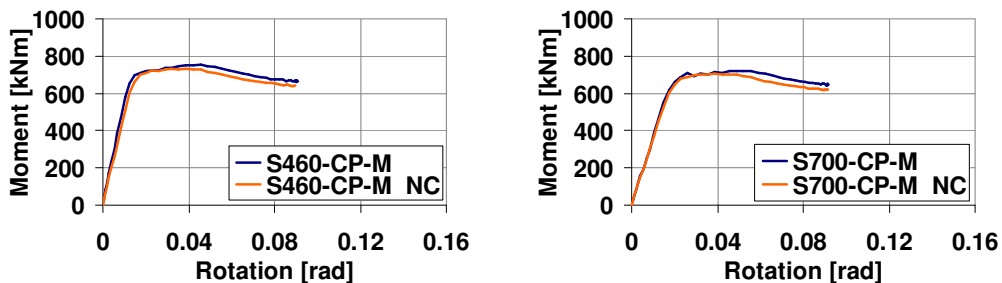


Fig. 5-128. Influence of concrete core – CP joints

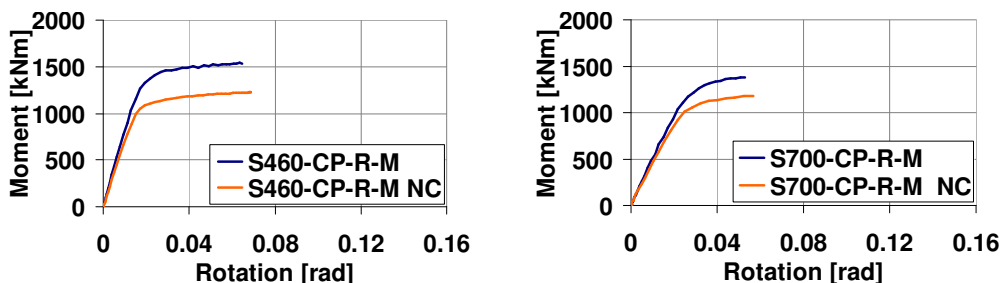


Fig. 5-129. Influence of concrete core – reinforced CP joint

5.8.3. Behaviour of joints with beams welded on two sides

The experimental tests were performed on single sided beam-to-column joints. It was therefore necessary to assess the behaviour of the joints (including column panel) in the situation of loading from two sides which corresponds to a more demanding scenario. Fig. 5-130 and Fig. 5-131 show the stress distribution and plastic strain corresponding to the joints with- and respectively without concrete core. Consequently, for the case with composite column and two beams (FEM 2G), a reduction of the stiffness can be observed in Fig. 5-132a compared to the test curve, but the failure mode was not affected (see in Fig. 5-130 plastic hinges in the beams). The absence of the concrete core (*NC* → *no concrete*) lead to reduction of the capacity (Fig. 5-132b) and yielding of the column web panel (Fig. 5-131) – plastic hinges did not form in the beam as for the joint with concrete core.

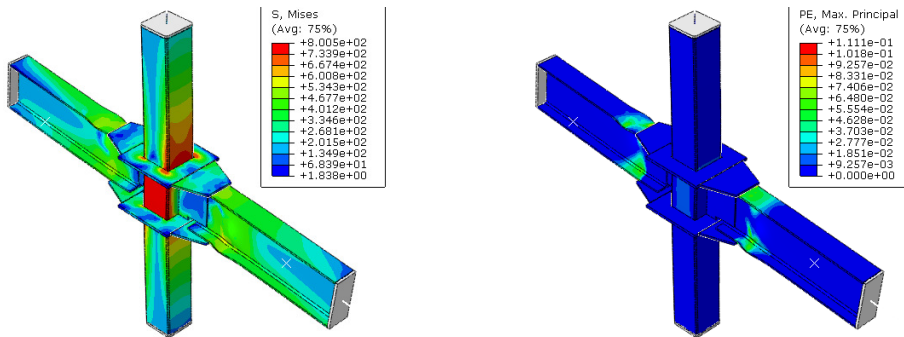


Fig. 5-130. Behaviour of joint with beams welded on two sides (CFT)

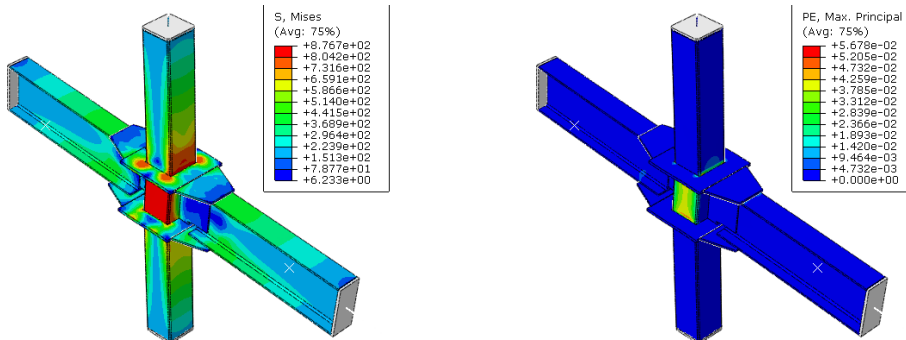


Fig. 5-131. Behaviour of joint with beams welded on two sides (column without concrete core)

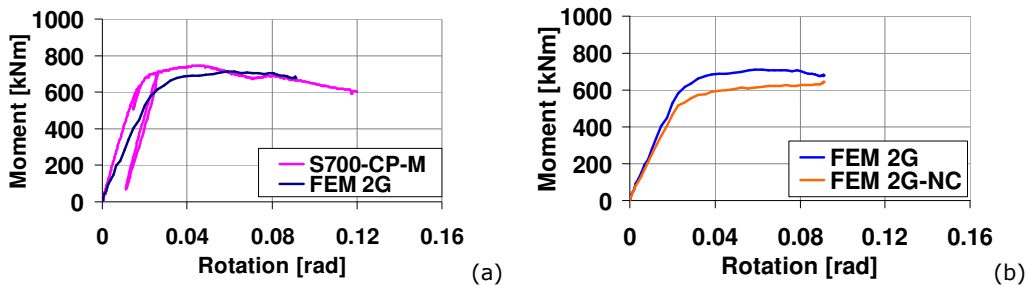


Fig. 5-132. Response of CP joints with beams welded on two sides

A similar investigation was performed also for the joint configuration with reduced beam section. Therefore, Fig. 5-133 and Fig. 5-134 show the stress distribution and plastic strain corresponding to the joints with- and respectively without concrete core. A reduction of the stiffness can be observed also in this case (see Fig. 5-135a) compared to the test curve. The absence of the concrete core did not affect the capacity (see Fig. 5-135b) or the failure mode. Consequently, the plastic hinges developed in the beams (see Fig. 5-134).

The weak-beam/strong-column concept was therefore confirmed for the CP and RBS joints, considering the case with beams welded on two sides, and in addition the study showed the contribution of the concrete core to joint behaviour.

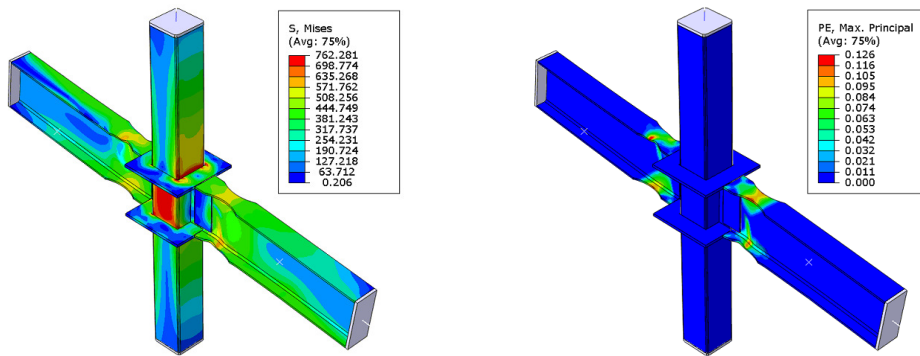


Fig. 5-133. Behaviour of joint with beams welded on two sides (CFT)

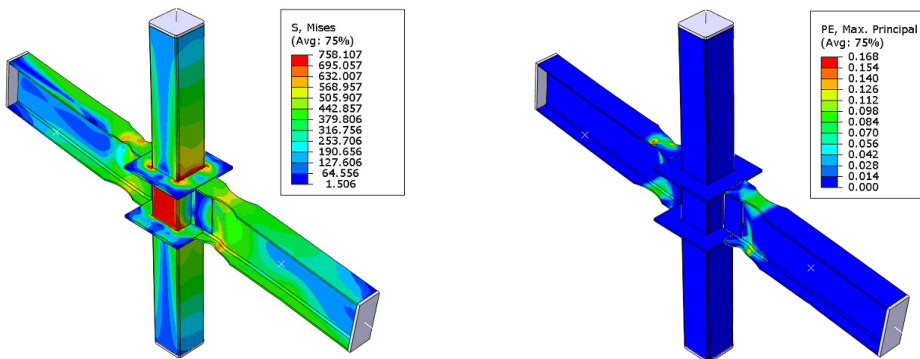


Fig. 5-134. Behaviour of joint with beams welded on two sides (column without concrete core)

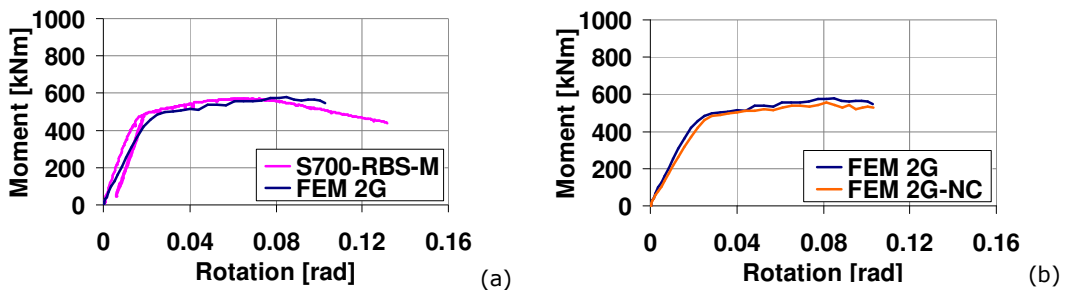


Fig. 5-135. Response of RBS joints with beams welded on two sides

5.8.4. Influence of axial force

With the aim to assess the influence of the axial force in the column with respect to the behaviour of the beam-to-column joint, numerical simulations were performed on one of the joints (S460-CP) considering the following cases:

- Joint with concrete core and an axial force level in the column corresponding to 50% of $N_{pl,Rd,composite}$;
- Joint without concrete core and with an axial force level in the column corresponding to 50% of $N_{pl,Rd,composite}$; it is to be noted that this load level corresponds to 70% of the plastic resistance of the steel tube;
- Joint without concrete core and with an axial force level in the column corresponding to 50% of $N_{pl,Rd,steel}$.

In a first step, the column was axially loaded up to the considered level (see Fig. 5-136a), and in a second step the beam was loaded. The stress distribution and implicitly the failure mechanism of the joints with- and respectively without concrete core are shown in Fig. 5-136b and Fig. 5-136c. The corresponding moment rotation curves are compared in Fig. 5-137. It can be observed that the axial force in the column did not affect the response of the joint with concrete core compared to the reference model, and that the plastic hinge formed in the beam. In contrast, for the joint without concrete core the capacity decreased and column failure occurred.

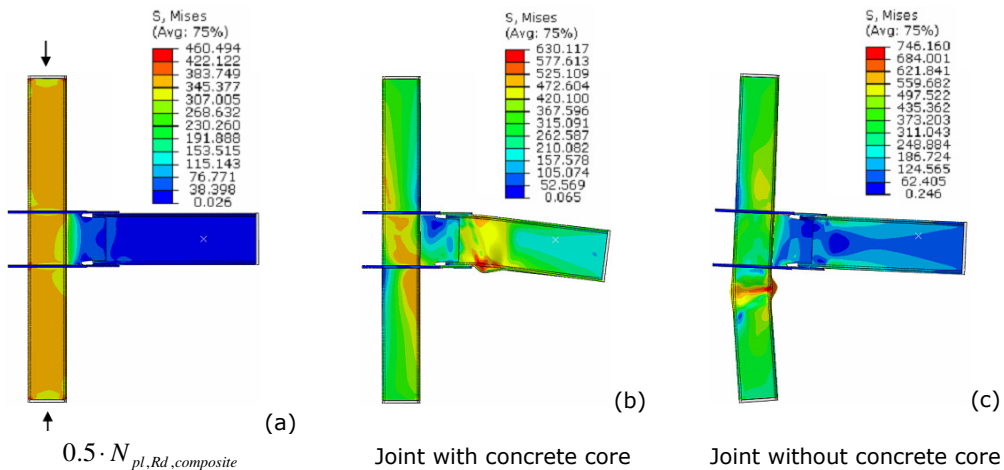


Fig. 5-136. Mises stress - influence of axial force ($0.5 \cdot N_{pl,Rd,composite}$) on S460-CP joints

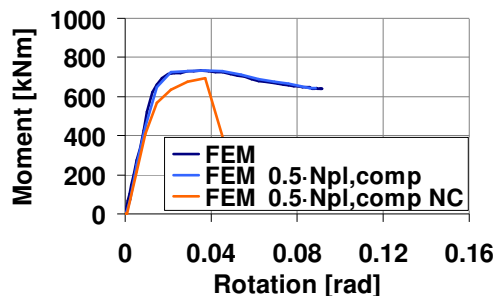


Fig. 5-137. Moment-rotation curves: influence of axial force ($0.5 \cdot N_{pl,Rd,composite}$) on S460-CP joint

The previous case showed the contribution of the concrete core to the robustness of the column. Another case was investigated considering for the joint without concrete core, an axial force acting on the column in amount of 50% of the capable axial force of the steel section ($N_{pl,Rd,steel}$). In a first step, the column was axially loaded up to the considered level (see Fig. 5-138a), and in a second step the beam was loaded. The stress distribution and implicitly the failure mechanism of the joint without concrete core are shown in Fig. 5-138b. The moment-rotation curves are compared in Fig. 5-138c. It can be observed that the axial force in the column ($0.5 \cdot N_{pl,Rd,steel}$) did not affect the response of the joint without concrete core compared to the reference model and that the plastic hinge formed in the beam.

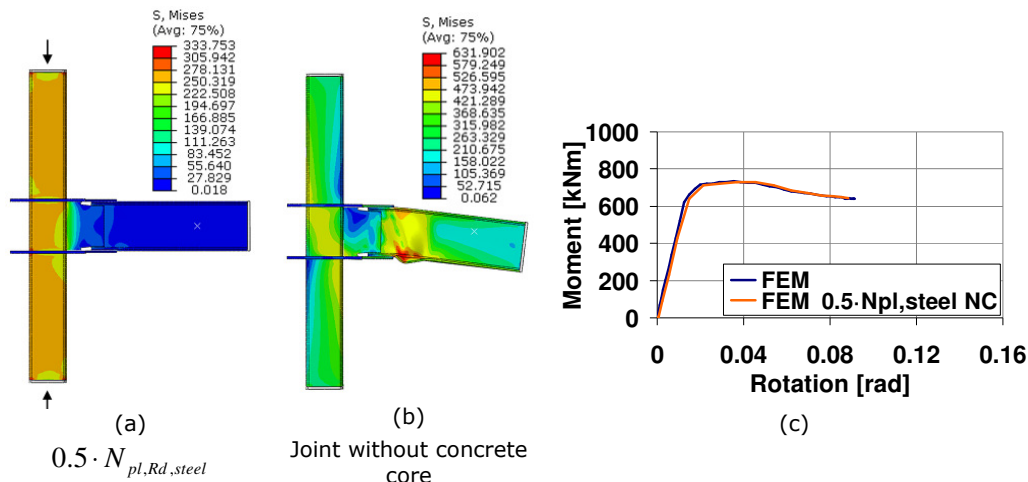


Fig. 5-138. Influence of axial force ($0.5 \cdot N_{pl,Rd,steel}$) on S460-CP joint

The axial force level in the column (from D-CBF) at the 5th floor reported to the plastic design capacity was in amount of 20% at SLS, and 26% at ULS and CPLS. The axial force level in the column at the 1st floor reported to the plastic design capacity was in amount of 36% at SLS, and 40% at ULS and CPLS. Therefore, the axial force levels were lower than 50% as assumed in the numerical investigations, and the response of the joints would not be affected by the axial force in the column.

5.9. Concluding remarks

A detailed presentation was made in relation to the experimental program aimed to evaluate the seismic performance of dual-steel IPE beam-to-CFRHS column welded joints. The experimental program enclosed three phases, i.e. investigation of material samples, investigation of steel-concrete connection, and investigation of beam-to-column joints. For the tests on steel-concrete connection and on joints, a description was made in relation to the specimen configuration, experimental test set-up, instrumentation, and loading protocols. Results from the experimental and numerical investigations were shown, and the main conclusions and observations are further summarised.

Tests on material samples

The tests performed on material covered compression tests on concrete cubes, as well as tensile and Charpy V-notch impact tests on steel samples.

With regard to the tests performed on concrete samples, the average characteristic strength was obtained in amount of 36 N/mm² which is slightly lower than the minimum characteristic strength of 37 N/mm² required for a C30/37 concrete class. With regard to the tests performed on steel samples, it is to be noted that the measurements, for both tensile and Charpy V-notch tests, satisfied the minimum requirements according to each steel grade as specified by the standards EN 10025-2 [6] and EN 10025-6 [8]. Therefore, the steel grade from each component of the beam-to-column joints was confirmed.

Tests on steel-concrete connection

The parameters investigated within the steel-concrete connection tests consisted of loading procedure (monotonic, cyclic), connection (friction, friction+connectors) and steel grade (S460, S700). The aim was to assess the efficiency of shot fired nails in providing the connection between steel tube and concrete core.

The shear strength τ_{Rd} that developed at the interface between steel tube and concrete core was obtained in amount of 0.4 N/mm², which is equal to the value recommended by EN 1994-1 [50] for rectangular hollow sections.

In relation to the specific loading (push-out tests), it was observed that the connectors have a significant contribution to the load transfer from steel tube to the concrete core, in both monotonic and cyclic loading. From the investigation of the behaviour and failure mode, it was observed that under monotonic loading the concrete was crushed in a small amount at the contact with the shot fired nails which bent. Under alternating cycles the nails eventually broke at the interface between concrete core and steel tube. In addition it was observed that from the cyclic loading the capacity of the connectors decreased slightly compared to the monotonic loading.

The shear capacity of the connectors obtained from the experimental tests (37.5 kN) was higher than the computed shear strength (30 kN) using the relation from EN 1994-1 for headed stud connectors. The ultimate strength in amount of 2360 N/mm² (see equation 5.7) was taken according to a report provided by Hilti AG related to shear tests performed on the X-DSH 32 P10 nails [100].

$$P_{Rd} = \frac{0.8 \cdot f_u \cdot \pi \cdot d^2 / 4}{\gamma_v} = \frac{0.8 \cdot 2360 \cdot \pi \cdot 4.5^2 / 4}{1.0} = 30 \text{ kN} \quad (5.7)$$

In conclusion, as observed by Beck [73], the X-DSH 32 P10 shot fired nails proved a significant contribution to the steel-concrete connection considering the monotonic and cyclic loading, as well as HSS tubes (S460 and S700). However, due to the complex behaviour of concrete and shot fired nails, additional investigations (FEM) are necessary to develop a design procedure and recommendations.

Pre-test numerical simulations

The material model for each steel grade was calibrated based on results from tensile tests and used further in the numerical model of the joints. The numerical model used for concrete was obtained based on results from the compression tests and based on a model reported in the literature.

The numerical simulations allowed assessing behaviour (moment-rotation curve, stress distribution and plastic strain) for each joint configuration.

Consequently, the RBS and CP joints evidenced large plastic deformations in the beam which was in agreement with the design assumptions. For the joints with strengthened beam, yielding was initiated in the adjacent area of the welded on-site connection, and respectively in the external diaphragm and column web panel. Therefore, the pre-test numerical simulations proved a good design of the RBS and CP joints, and related to the joints with strengthened beam information was provided concerning the behaviour of the joint components.

Tests on beam-to-column joints

The parameters investigated within the joint tests consisted of loading procedure (monotonic, cyclic), joint type (RBS, CP), steel grade for column (S460, S700), and intended failure mode (beam, connection). The experimental program covered a number of 16 beam-to-column joint specimens. For each case a description was made in relation to the test assembly, observations from test, and the response of the joints subjected to the monotonic and cyclic loading. Interpretation and comparison of results was performed with the aim to assess the participation of components to the joint rotation, the overstrength of the connection zone with respect to the dissipative zone, and the dissipation capacity of the joints.

The experimental investigations performed on beam-to-column joints under both monotonic and cyclic loading evidenced a good conception and design of the joints (RBS and CP) justified by the following observations:

- elastic response of the connection zone;
- formation of the plastic hinge in the beam;
- corresponding to cyclic tests performed according to the AISC 341 [94] loading protocol, the RBS and CP designed joints evidenced rotation capacities of 50 mrad (RBS joints) and respectively 40 mrad (CP joints) for which the degradation of strength and stiffness were not greater than the 20% limit defined in EN 1998-1 [27];
- good response of joint detailing and welded connections with one exception (S700-CP-R-M / C) which evidenced weld failure, however corresponding to a force level higher than the capacity ($F_{v,Rd}$).

Investigations performed on the welded connections lead to the conclusion that in the case of S700-CP-R-M and S700-CP-R-C the weld between plates of the external diaphragm contained a full length discontinuity (along the weld root).

It was observed that the rotation capacity of the designed joints (RBS, CP) was higher (>40 mrad without significant reduction of capacity) in comparison to the seismic rotation demand of the joints from the analysis on frames.

Contribution of components to joint rotation

The contribution to the joint rotation was evaluated for the following regions: dissipative zone (plastic hinge), connection (welded connection and external diaphragm), and column web panel.

For the joints with reduced beam section and with cover plates, the main plastic deformations occurred in the beam (plastic hinge). The contribution of the connection and column panel to the overall joint rotation was observed to be low.

For the joints with reinforced beam, the main contribution to the overall joint rotation was given by the connection zone including external diaphragm (for strengthened RBS joints), and respectively external diaphragm and column panel (for strengthened CP joint).

Overstrength of joints

From the comparison between the four designed joints and the corresponding joints with reinforced beam, the overstrength computed at yield and at maximum capacity, was observed to satisfy the overstrength requirements, from EN 1998-1 [27]. Consequently, the overstrength of the connection zone for the RBS joints (with S460 / S700 RHS) was evaluated at 34% and 35% at yield, and respectively 53% and 60% at maximum capacity. The overstrength of the connection zone for the CP joints (with S460 / S700 RHS) was 55% and 43% at yield, and 101% and 86% at maximum capacity.

Dissipated energy

A good dissipation capacity was observed for the RBS and CP joints. The energy absorbed by the heat affected zone (reinforced RBS joints) was observed to be low. In contrast, the energy absorbed by column web panel, external diaphragm and cover plates corresponding to S460-CP-R-C joint was significant. This observation was not proved in the case of S700-CP-R-C joint specimen, which experienced weld failure within the external diaphragm.

Calibration of numerical models and parametric study

The numerical models that anticipated the behaviour of the joint specimens were calibrated based on results from the experimental tests performed under monotonic and cyclic loading. From the calibration, a set of numerical models were obtained which reproduced with a good accuracy the response of the joints in both moment-rotation curve and failure mechanism, i.e. formation of the plastic hinge in the beam (designed joints) and yielding of components (reinforced joints). This allowed the investigation of complementary testing cases through numerical simulations with the aim to assess the influence of the concrete core, influence of the axial force in the column, and the response of joints with two beams.

Influence of concrete core

It was observed that the absence of the concrete core did not affect significantly the response of the four designed joints (RBS and CP); only a minor reduction of the capacity was observed. In contrast, for the reinforced joints (with extended CP) a significant reduction of capacity was observed. In these cases, the bending moment and implicitly the shear force in the column web panel were much larger than in the other cases. In other words, the shear force in the column web panel exceeded the capacity of the steel tube in shear, and therefore a higher capacity was corresponding to the joints with concrete core. The influence of the concrete core was investigated also for joints with beams welded on two sides and joints with axial force in the column.

Joints with beams welded on two sides

The experimental tests were performed on single sided beam-to-column joints. It was therefore necessary to assess the behaviour of the joint (including column web panel) in the situation of loading from two sides which corresponds to a more demanding scenario. The reference joints for this study were S700-RBS and S700-CP. In comparison to the test curve a reduction of the stiffness was observed, but the capacity was not affected, nor the failure mode (plastic hinges in the beam). The weak-beam/strong-column concept was therefore confirmed for the CP and RBS joints considering the case with beams welded on two sides. In addition the study

showed the contribution of the concrete core to joint behaviour. The absence of the concrete core lead in case of the CP joint to the reduction of the capacity and yielding of the column panel. In contrast, the absence of the concrete core did not affect the capacity or the failure mode for the RBS joint.

Axial force

It was observed that the axial force ($0.5 \cdot N_{pl,Rd,composite}$) in the column did not affect the response of the investigated joint (S460-CP) compared to the reference model and that the plastic hinge formed in the beam. In contrast, for the joint without concrete core the capacity decreased and column failure was observed. It is to be noted that the load level corresponded to 70% of the plastic resistance of the steel tube. Corresponding to a lower axial force level ($0.5 \cdot N_{pl,Rd,steel}$) in the joint without concrete core, the column failure was not evidenced.

The axial force level in the column (from D-CBF) at the 5th floor reported to the plastic design capacity was in amount of 20% at SLS, and 26% at ULS and CPLS. The axial force level in the column at the 1st floor reported to the plastic design capacity was in amount of 36% at SLS, and 40% at ULS and CPLS. Therefore, the axial force levels were lower than 50% as assumed in the numerical investigations, and the response of the joints would not be affected by the axial force in the column.

6. COMPONENT METHOD APPROACH FOR DESIGN OF DUAL STEEL IPE BEAM-TO CFRHS COLUMN WELDED JOINTS

6.1. Introduction

The current chapter is related to the design of beam-to-CFRHS column joints i.e. welded reduced beam section and welded cover plate beam-to-column joints with concrete-filled rectangular hollow-section.

A detailed description is made with regard to the design procedure for each of the two joint typologies. Further, a summary is made for: design relations of the welded connections, design relations for the capacity of the components, and the stiffness coefficients of the components.

In addition, several cases are considered for experimental and numerical validation of the relations for the design capacity of the components. Design flow charts, prepared for each of the two joint typologies, show an overview of the design procedures.

6.2. RBS welded joints

Fig. 6-1 shows the configuration of the joint with reduced beam section. Accordingly, a wide-flange hot rolled beam is connected to a concrete filled tube (CFT) composite column using field welding. In order to alleviate stresses in the beam-to-column connection and to control the location of the plastic hinge, a reduced beam section was used. An external diaphragm has the aim to transfer the forces from beam flanges to the side walls of the column.

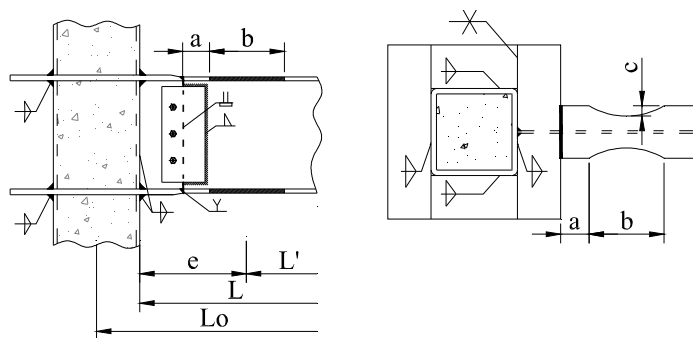


Fig. 6-1. Beam to column joint with reduced beam section

For the design of the joint it was considered:

- Beam: wide-flange hot rolled section realised from S355 steel grade;

- Column: rectangular hollow section (RHS) realised from S460 (respectively S690) steel grade and filled with concrete;
- External diaphragm: plates from S460 (respectively S690) steel grade;
- Vertical column stiffener: plates from S460 (respectively S690) steel grade;
- Geometry of the joint:
 - L - beam span to column face;
 - L' - distance between plastic hinges;
 - e - distance between column face and the centre of RBS;
 - a, b, c - geometry of the reduced beam section.

6.2.1. Plastic hinge (dissipative zone)

Location of the plastic hinge

The position of the plastic hinge is related to the centre of the reduced beam section (RBS). According to AISC 358-05 [87] guidelines, the trial values for the reduced beam section dimensions a, b, c should be chosen as follows:

$$\begin{aligned} 0.5 \cdot b_{beam} &\leq a \leq 0.75 \cdot b_{beam} \\ 0.65 \cdot h_{beam} &\leq b \leq 0.85 \cdot h_{beam} \\ 0.1 \cdot b_{beam} &\leq c \leq 0.25 \cdot b_{beam} \end{aligned} \quad (6.1)$$

Bending moment and shear force in the RBS

The probable maximum moment ($M_{pl,RBS}$) in the plastic hinge is determined by considering that a fully yielded and strain hardened plastic hinge develops in the RBS. The bending moment and shear force ($V_{Ed,RBS}$) at the centre of the RBS are obtained from:

$$M_{pl,RBS} = \frac{\gamma_{sh} \cdot \gamma_{ov} \cdot W_{pl,RBS} \cdot f_y}{\gamma_{M0}} \quad (6.2)$$

$$V_{Ed,RBS} = V_{Ed,G} + V_{Ed,M} \quad (6.3)$$

$$V_{Ed,G} = \frac{[(p + 0.4 \cdot q) \cdot L_0]}{2} \quad (6.4)$$

$$V_{Ed,M} = \frac{2 \cdot M_{pl,RBS}}{L'} \quad (6.5)$$

where:

- γ_{sh} represents the strain hardening ($\gamma_{sh} = 1,10$);
- γ_{ov} is the overstrength factor ($\gamma_{ov} = 1,25$);
- f_y is the nominal yield strength of the beam;
- γ_{M0} is the material safety factor;
- $V_{Ed,G}$ is the shear force from gravity forces in the seismic design situation;
- $V_{Ed,M}$ is the shear force corresponding to the application of the plastic moments;
- p is the permanent load;
- q is the live load;
- $W_{pl,RBS}$ is the plastic section modulus at the centre of the reduced beam and can be determined as:

$$W_{pl,RBS} = W_{pl,beam} - 2 \cdot c \cdot t_f \cdot (h - t_f) \quad (6.6)$$

6.2.2. Welded on-site connection

Evaluation of actions

The probable maximum moment ($M_{Ed,sc}$) and shear force ($V_{Ed,sc}$) at the on-site connection are determined by considering that a fully yielded and strain hardened plastic hinge develops in the RBS:

$$M_{Ed,sc} = M_{pl,RBS} + V_{Ed,RBS} \cdot e' \quad (6.7)$$

$$V_{Ed,sc} = V_{Ed,RBS} \quad (6.8)$$

where e' is the distance from the centre of the RBS to the on site connection.

Evaluation of the capacity

The capacity of the welded on-site connection in terms of bending moment and shear force is:

$$M_{Rd,sc} = \frac{\gamma_{ov} \cdot W_{pl,sc} \cdot f_y}{\gamma_{M0}} \quad (6.9)$$

$$V_{Rd,sc} = \frac{\gamma_{ov} \cdot A_v \cdot f_y}{\sqrt{3} \cdot \gamma_{M0}} \quad (6.10)$$

For the moment and shear resistance of the site-connection, the overstrength factor γ_{ov} is used in order to take into account the fact that the material is the same as in the RBS. The plastic modulus of the gross cross-section of the beam is considered, as no weld access holes are used:

$$W_{pl,sc} = W_{pl,beam} \quad (6.11)$$

Check of the welded connection

The welded connection is checked to bending and shear considering:

$$\frac{M_{Ed,sc}}{M_{Rd,sc}} \leq 1.0 \quad \frac{V_{Ed,sc}}{V_{Rd,sc}} \leq 0.5 \quad (6.12)$$

6.2.3. External diaphragm

Evaluation of actions

The probable maximum moment ($M_{Ed,cf}$) and shear force ($V_{Ed,cf}$) at the column face are determined by considering that a fully yielded and strain hardened plastic hinge develops in the RBS:

$$M_{Ed,cf} = M_{pl,RBS} + V_{Ed,RBS} \cdot e \quad (6.13)$$

$$V_{Ed,cf} = V_{Ed,RBS} \quad (6.14)$$

The force developed in the external diaphragm is determined by considering that the bending moment is carried by diaphragms alone. Therefore, the axial force is obtained dividing the bending moment by the lever arm z :

$$F_{v,Ed} = \frac{M_{Ed,cf}}{z} \quad (6.15)$$

Evaluation of the capacity

The external diaphragm is checked in shear (see Fig. 6-2), neglecting the direct connection to the column wall. Consequently, the design capacity of the external diaphragms in shear is computed with equation (6.16).

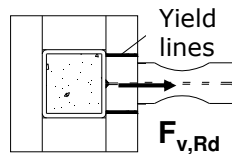


Fig. 6-2. Shear failure of the external diaphragm

$$F_{v,Rd} = \frac{2 \cdot A_v \cdot f_Y}{\sqrt{3} \cdot \gamma_{M0}} \tag{6.16}$$

For the connection between column and vertical stiffener a fillet weld of $0.7 \cdot t_{min}$ is used. The resistance of the welded connection is determined as:

$$F_{w,Rd} = \frac{A_w \cdot f_u}{\sqrt{3} \cdot \beta_w \cdot \gamma_{M2}} \tag{6.17}$$

Check of the external diaphragm and vertical column stiffener

The external diaphragm and welded connection are checked considering:

$$\frac{F_{v,Ed}}{F_{v,Rd}} \leq 1.0 \qquad \frac{V_{Ed,cf}}{F_{w,Rd}} \leq 1.0 \tag{6.18}$$

6.2.6. Column panel zone

Evaluation of actions

Fig. 6-3 illustrates the efforts acting on the column panel zone. In the current case it was assumed that the bending moments in the beam correspond to $\beta=1.0$, i.e. bending moment acting only from one side.

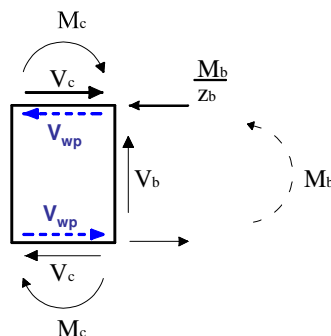


Fig. 6-3. Evaluation of the shear force within the column web panel

The shear force in the column panel zone is determined using the detailed procedure from EN 1993-1-8 (at 5.3(3)) [49]:

$$V_{wp,Ed} = \frac{\sum M_{b,cf}}{z} - V_c \quad (6.19)$$

where $\sum M_{b,cf}$ is the sum of bending moments in the beam at the column face and V_c is the shear force in the column;

$$V_{wp,Ed} = \frac{M_{Ed,cf,red}}{z} - \frac{M_{Ed,cl,red}}{H} \quad (6.20)$$

The bending moments at the column face and column centreline are:

$$M_{Ed,cf,red} = M_{pl,RBS,red} + V_{Ed,RBS,red} \cdot e \quad (6.21)$$

$$M_{Ed,cl,red} = M_{pl,RBS,red} + V_{Ed,RBS,red} \cdot \left(e + \frac{h_c}{2} \right) \quad (6.22)$$

The shear force in the column panel zone corresponds to fully-yielded plastic hinges in the beams framing into the joint. According to EN 1998-1 [27], no overstrength is required ($\gamma_{sh}=1.0$ and $\gamma_{ov}=1.0$).

$$M_{pl,RBS,red} = \frac{W_{pl,RBS} \cdot f_y}{\gamma_{M0}} \quad (6.23)$$

$$V_{Ed,RBS,red} = \frac{M_{pl,RBS,red}}{L'} \quad (6.24)$$

Evaluation of the capacity

Shear strength of the steel tube within the column panel zone is determined according to EN 1993-1-8 [49]:

$$V_{wp,s,Rd} = \frac{0,9 \cdot A_v \cdot f_y}{\sqrt{3} \cdot \gamma_{M0}} \quad (6.25)$$

$$A_v = A \cdot \frac{b_c}{b_c + h_c} \quad (6.26)$$

where A is the cross-section area of the tube, b_c and h_c represent the width and depth of the steel tube, and t_t is the thickness of the tube.

According to EN1994-1 (paragraph 6.7.3.2) [50], in the relationship for the resistance of the concrete for a partially encased wide flange, the coefficient 0.85 may be replaced by 1.0 for concrete filled sections. Therefore, the shear strength from paragraph 8.4.4.1 of EN1994-1 becomes:

$$V_{wp,c,Rd} = 1,0 \cdot v \cdot A_c \cdot f_{cd} \cdot \sin \theta \quad (6.27)$$

where:

$$A_c = 0,8 \cdot (b_c - 2 \cdot t_t) \cdot (h_c - 2 \cdot t_t) \cdot \cos \theta \quad (6.28)$$

$$\theta = \arctg\left(\frac{h_c - 2 \cdot t_t}{z}\right) \quad (6.29)$$

$$v = 0.55 \cdot \left(1 + 2 \cdot \left(\frac{N_{Ed}}{N_{pl,Rd}}\right)\right) \leq 1.1 \quad (6.30)$$

The capacity of the composite section (concrete and steel) of the column web panel, according to EN 1998-1 [27], should be taken as 80% of the two sections together.

$$V_{wp,Rd} = 0,8 \cdot (V_{wp,s,Rd} + V_{wp,c,Rd}) \quad (6.31)$$

Check of the column panel in shear

The check of the column web panel in shear is finally performed using:

$$\frac{V_{wp,Ed}}{V_{wp,Rd}} \leq 1.0 \quad (6.32)$$

6.3. Cover plate welded joints

Fig. 6-4 shows the detailing of the joint with cover plates. Accordingly, a wide-flange hot rolled beam is connected to a concrete filled tube (CFT) composite column using field welding. Cover plates are used in order to reinforce the beam-to-column connection, forcing the plastic hinge to form in the beam. An external diaphragm has the aim to transfer the forces from beam flanges to the side walls of the column.

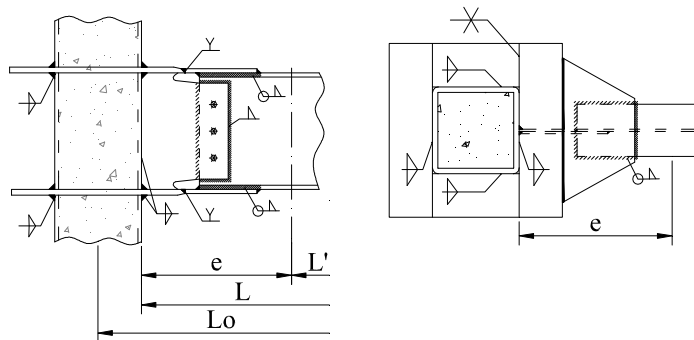


Fig. 6-4. Beam to column joint with cover plates

For the design of the joint it was considered that:

- Beam: wide-flange hot rolled section realised from S355 steel grade;
- Column: rectangular hollow section (RHS) realised from S460 (respectively S690) steel grade and filled with concrete;
- Cover plates: plates from S355 steel grade;
- External diaphragm: plates from S460 (respectively S690) steel grade;

- Vertical column stiffener: plates from S460 (respectively S690) steel grade;
- Geometry of the joint:
 - L - beam span to column face;
 - L' - distance between plastic hinges;
 - e - distance between column face and the centre of plastic hinge.

6.3.1. Plastic hinge (dissipative zone)

Location of the plastic hinge

According to PEER 2000/07 [101], the centre of the plastic hinge is located at a distance equal to $h_{beam}/3$ from the cover plate ending.

Bending moment and shear force in the plastic hinge

The probable maximum moment ($M_{pl,hinge}$) and shear force ($V_{Ed,hinge}$) in the plastic hinge are determined by considering that a fully yielded and strain hardened plastic hinge develops in the beam.

$$M_{pl,hinge} = \frac{\gamma_{sh} \cdot \gamma_{ov} \cdot W_{pl} \cdot f_y}{\gamma_{M0}} \quad (6.33)$$

$$V_{Ed,hinge} = V_{Ed,G} + V_{Ed,M} \quad (6.34)$$

$$V_{Ed,G} = \frac{[(p + 0.4 \cdot q) \cdot L_0]}{2} \quad (6.35)$$

$$V_{Ed,M} = \frac{M_{pl,hinge}}{L'} \quad (6.36)$$

where:

- γ_{sh} represents the strain hardening ($\gamma_{sh} = 1,10$);
- γ_{ov} is the overstrength factor ($\gamma_{ov} = 1,25$);
- f_y is the nominal yield strength of the beam;
- γ_{M0} is the material safety factor;
- W_{pl} is the plastic section modulus of the beam;
- $V_{Ed,G}$ is the shear force from gravity forces in the seismic design situation;
- $V_{Ed,M}$ is the shear force corresponding to the application of the plastic moments;
- p is the permanent load;
- q is the live load;

6.3.2. Welded connection

This section is related to the welded connection between beam flanges and cover plates.

Evaluation of actions

The probable maximum moment ($M_{Ed,sc}$) and shear force ($V_{Ed,sc}$) at the on-site connection are determined by considering that a fully yielded and strain hardened plastic hinge develops in the beam. It is considered that e' is the distance from the centre of the plastic hinge to the on-site connection.

$$M_{Ed,sc} = M_{pl,hinge} + V_{Ed,hinge} \cdot e' \quad (6.37)$$

$$V_{Ed,sc} = V_{Ed,hinge} \quad (6.38)$$

The welded connection between beam flange and cover plate is checked assuming that the flanges carry the moment only, while the web carries the shear force. Consequently, the force in the flange is estimated considering that the lever arm z is equal with the height of the beam h_b :

$$F_{w,Ed} = \frac{M_{Ed,sc}}{z} \quad (6.39)$$

Evaluation of the capacity

The strength of the welded connection is determined as the sum of the resistance of the four fillet welds between cover plate and beam flange (see Fig. 6-5). The symbols a_1, a_2 represent the throat thickness, and l_1, l_2 represent the weld length.

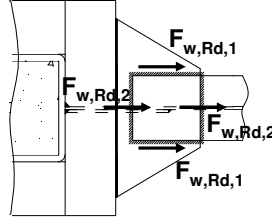


Fig. 6-5. Capable forces of the fillet welds between beam flange and cover plate

$$F_{w,Rd} = 2 \cdot (F_{w,Rd,1} + F_{w,Rd,2}) \quad (6.40)$$

where:

$$F_{w,Rd,1} = a_1 \cdot l_1 \cdot \frac{f_u}{\sqrt{3} \cdot \beta_w \cdot \gamma_{M2}} \quad (6.41)$$

$$F_{w,Rd,2} = a_2 \cdot l_2 \cdot \frac{f_u}{\sqrt{2} \cdot \beta_w \cdot \gamma_{M2}} \quad (6.42)$$

Check of the welded connection

The check of the welded connection is performed as follows:

$$\frac{F_{w,Ed}}{F_{w,Rd}} \leq 1.0 \quad (6.43)$$

6.3.3. Cover plates and on-site connection

Evaluation of the capacity

It is assumed that the cover plates carry moment only, while the web carries the shear force. Therefore, the plastic section modulus is computed as follows:

$$W_{pl,sc} = W_{pl,cp} = 2 \cdot b_{cp} \cdot t_{cp} \cdot \frac{(h_b + t_{cp})}{2} \quad (6.44)$$

$$M_{Rd,sc} = \frac{W_{pl,sc} \cdot f_y}{\gamma_{M0}} \quad (6.45)$$

$$V_{Rd,sc} = \frac{A_v \cdot f_y}{\sqrt{3} \cdot \gamma_{M0}} \quad (6.46)$$

The strength of the fillet weld between vertical stiffener and beam web is determined as:

$$V_{w,Rd} = \frac{A_w \cdot f_u}{\sqrt{3} \cdot \beta_w \cdot \gamma_{M2}} \quad (6.47)$$

Check of the cover plates and on-site connection

The check of the connection is made considering the following relations:

$$\frac{M_{Ed,sc}}{M_{Rd,sc}} \leq 1.0 \quad \frac{V_{Ed,sc}}{V_{Rd,sc}} \leq 0.5 \quad \frac{V_{Ed,sc}}{V_{w,Rd}} \leq 0.5 \quad (6.48)$$

6.3.4. External diaphragm

Evaluation of actions

The probable maximum moment ($M_{Ed,cf}$) and shear force ($V_{Ed,cf}$) at the column face are determined by considering that a fully yielded and strain hardened plastic hinge forms in the beam.

$$M_{Ed,cf} = M_{pl,hinge} + V_{Ed,hinge} \cdot e \quad (6.49)$$

$$V_{Ed,cf} = V_{Ed,hinge} \quad (6.50)$$

The force developed in the external diaphragm is determined by considering that the bending moment is carried by diaphragms alone. Therefore, the axial force is obtained dividing the bending moment by the lever arm z :

$$F_{v,Ed} = \frac{M_{Ed,cf}}{z} \quad (6.51)$$

$$z = h_b + t_{cp} \quad (6.52)$$

Evaluation of the capacity

The diaphragms are checked to fracture along an inclined area A_v (see Fig. 6-6), neglecting the direct connection to the column wall. Consequently, the design capacity of the external diaphragms in shear is computed with equation (6.53).

$$F_{v,Rd} = \frac{2 \cdot A_v \cdot f_y}{\gamma_{M0} \cdot \sqrt{1 + 2 \cdot \cos^2 \alpha}} \quad (6.53)$$

$$A_v = \frac{b_{ed} \cdot t_{ed}}{\cos \alpha} \quad (6.54)$$

where b_{ed} and t_{ed} are the width and the thickness of the external diaphragm;

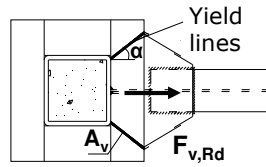


Fig. 6-6. Considered failure mode of the external diaphragm

The stresses acting along the yield surface can be obtained from the following relations:

$$\sigma = \frac{F_{v,Ed} / 2}{A_v} \cdot \sin \alpha \tag{6.55}$$

$$\tau = \frac{F_{v,Ed} / 2}{A_v} \cdot \cos \alpha \tag{6.56}$$

Check of the external diaphragm

The check of the external diaphragm can be made using one of the following relations:

$$\frac{F_{v,Ed}}{F_{v,Rd}} \leq 1,0 \tag{6.57}$$

$$\sigma_{equiv} = \sqrt{\sigma^2 + 3 \cdot \tau^2} \leq \frac{f_y}{\gamma_{M0}} \tag{6.58}$$

6.3.4. Column panel zone

Evaluation of actions

Fig. 6-7 illustrates the efforts acting on the column panel zone. In the current case it was assumed that the bending moments in the beam correspond to $\beta=1.0$, i.e. bending moment acting only from one side.

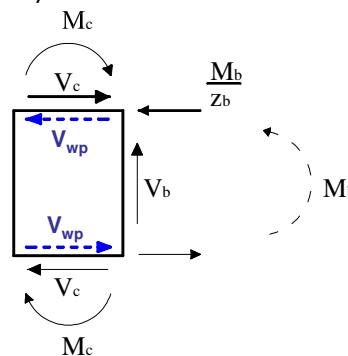


Fig. 6-7. Evaluation of the shear force within the column web panel

The shear force in the column panel zone is determined using the detailed procedure from EN 1993-1-8 (at 5.3(3)) [49].

$$V_{wp,Ed} = \frac{\sum M_{b,cf}}{z} - V_C \quad (6.59)$$

where $\sum M_{b,cf}$ is the sum of bending moments in the beam at the column face and V_C is the shear force in the column;

$$V_{wp,Ed} = \frac{M_{Ed,cf,red}}{z} - \frac{M_{Ed,cl,red}}{H} \quad (6.60)$$

The bending moments at the column face and column centreline are:

$$M_{Ed,cf,red} = M_{pl,hinge,red} + V_{Ed,hinge,red} \cdot e \quad (6.61)$$

$$M_{Ed,cl,red} = M_{pl,hinge,red} + V_{Ed,hinge,red} \cdot \left(e + \frac{h_c}{2} \right) \quad (6.62)$$

The shear force in the column panel zone corresponds to fully-yielded plastic hinges in the beams framing into the joint. According to EN 1998-1 [27], no overstrength is required ($\gamma_{sh}=1.0$ and $\gamma_{ov}=1.0$).

$$M_{pl,hinge,red} = \frac{W_{pl,hinge} \cdot f_y}{\gamma_{M0}} \quad (6.63)$$

$$V_{Ed,M,red} = \frac{M_{pl,hinge,red}}{L'} \quad (6.64)$$

Evaluation of the capacity

Shear strength of the steel tube within the column panel zone is determined according to EN 1993-1-8 [49]:

$$V_{wp,s,Rd} = \frac{0,9 \cdot A_v \cdot f_y}{\sqrt{3} \cdot \gamma_{M0}} \quad (6.65)$$

$$A_v = A \cdot \frac{b_c}{b_c + h_c} \quad (6.66)$$

where A is the cross-section area of the tube, b_c and h_c represent the width and depth of the steel tube, and t_t is the thickness of the tube.

According to EN1994-1 (paragraph 6.7.3.2) [50], in the relationship for the resistance of the concrete for a partially encased wide flange, the coefficient 0.85 may be replaced by 1.0 for concrete filled sections. Therefore, the shear strength from paragraph 8.4.4.1 of EN1994-1 becomes:

$$V_{wp,c,Rd} = 1,0 \cdot v \cdot A_c \cdot f_{cd} \cdot \sin \theta \quad (6.67)$$

where:
$$A_c = 0,8 \cdot (b_c - 2 \cdot t_t) \cdot (h_c - 2 \cdot t_t) \cdot \cos \theta \quad (6.68)$$

$$\theta = \arctg\left(\frac{h_c - 2 \cdot t_t}{z}\right) \quad (6.69)$$

$$v = 0.55 \cdot \left(1 + 2 \cdot \left(\frac{N_{Ed}}{N_{pl,Rd}}\right)\right) \leq 1.1 \quad (6.70)$$

The capacity of the composite section (concrete and steel) of the column web panel, according to EN 1998-1 [27], should be taken as 80% of the two sections together.

$$V_{wp,Rd} = 0,8 \cdot (V_{wp,s,Rd} + V_{wp,c,Rd}) \quad (6.71)$$

Check of the column panel in shear

The check of the column web panel in shear is finally performed using:

$$\frac{V_{wp,Ed}}{V_{wp,Rd}} \leq 1.0 \quad (6.72)$$

6.4. Experimental and numerical validation

The detailed design procedure for the two joint typologies was described in section 6.2 for the RBS joint and in section 6.3 for the CP joint. The design started with the evaluation of efforts from the dissipative zone (see Table 6-1). With these efforts, the joint components and the welded connections were designed so as to possess a higher resistance with the required amount of overstrength. The relations used for the design of the welded connections are shown in Table 6-2. The relations for the design capacity of joint components (cover plate, external diaphragm, and column web panel) are summarised in Table 6-3. For the stiffness evaluation of the joints, Table 6-4 makes an overview of the components and the corresponding stiffness coefficient.

The experimental program allowed assessing the material characteristics of each component, and also the contribution of the components to the response of the joints. The experimental investigation proved a good joint detailing and behaviour of welded connections (i.e. between beam and external diaphragm, between flanges and cover plates, and between cover plates and external diaphragm). The welded connection between plates forming the external diaphragm behaved good as well with exception of S700-CP-R joints, for which the damage was localised in the weld (un-penetrated weld root).

Several cases are further considered for the experimental and numerical validation of the relations for the design capacity of:

- dissipative zone
 - RBS joint / CP joint
- external diaphragm
 - RBS joint / CP joint
- column web panel
 - CF-RHS S460 / CF-RHS S700

Table 6-1 – Dissipative zone (plastic hinge)

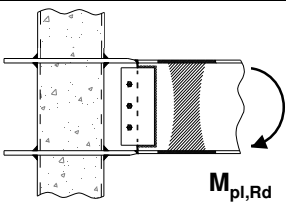
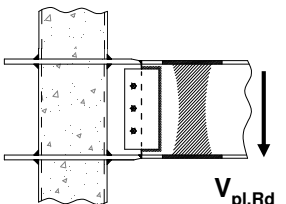
Scheme	Code provisions / Relations used in design
1. Beam in bending	
	Code provision (EN 1993-1-1): $M_{pl,Rd} = \frac{W_{pl} \cdot f_y}{\gamma_{M0}}$
2. Beam web in shear	
	Code provision (EN 1993-1-1): $V_{pl,Rd} = \frac{A_v \cdot f_y}{\sqrt{3} \cdot \gamma_{M0}}$

Table 6-2 – Welded connections

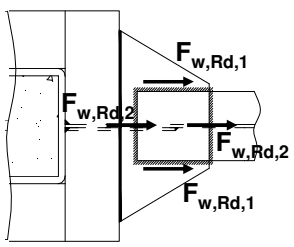
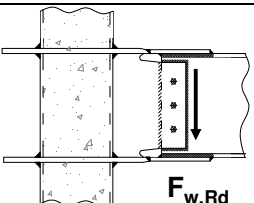
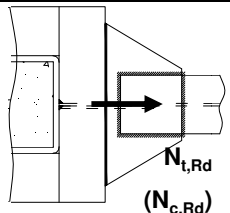
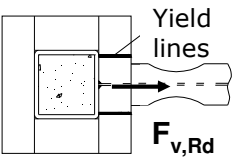
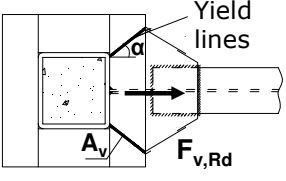
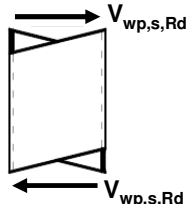
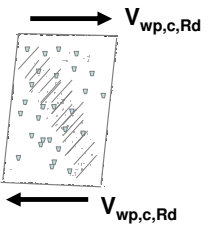
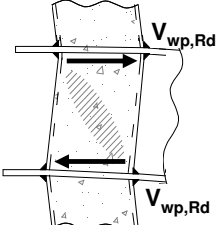
Scheme	Code provisions / Relations used in design
1. Fillet weld all around (beam flange to cover plate)	
	<p>Code provision (EN 1993-1-8): Directional method</p> $\sqrt{\sigma_{\perp}^2 + 3 \cdot (\tau_{\perp}^2 + \tau_{\parallel}^2)} \leq \frac{f_u}{\beta_w \cdot \gamma_{M2}}$ <p>Simplified method for design resistance of a fillet weld</p> $F_{w,Ed} \leq F_{w,Rd}$ $F_{w,Rd} = f_{vw,d} \cdot a$ $f_{vw,d} = \frac{f_u / \sqrt{3}}{\beta_w \cdot \gamma_{M2}}$
	<p>Relations used in design:</p> $F_{w,Rd} = 2 \cdot (F_{w,Rd,1} + F_{w,Rd,2})$ $F_{w,Rd,1} = a_1 \cdot l_1 \cdot \frac{f_u}{\sqrt{3} \cdot \beta_w \cdot \gamma_{M2}}$ $F_{w,Rd,2} = a_2 \cdot l_2 \cdot \frac{f_u}{\sqrt{2} \cdot \beta_w \cdot \gamma_{M2}}$
2. Weld (vertical stiffener to column / beam)	
	<p>Code provision (EN 1993-1-8):</p> $F_{w,Rd} = \frac{A_w \cdot f_u}{\sqrt{3} \cdot \beta_w \cdot \gamma_{M2}}$

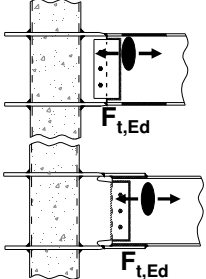
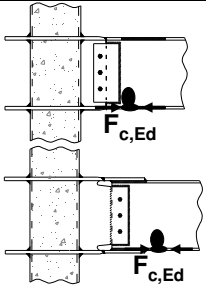
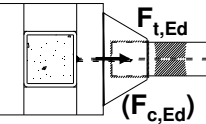
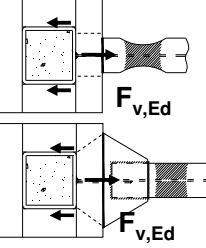
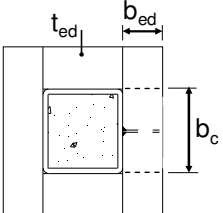
Table 6-3 – Design capacity of components

Scheme	Code provisions / Relations used in design
1. Cover plate in tension/compression	
	<p>Code provision (EN 1993-1-1):</p> $N_{t,Rd} = \frac{A \cdot f_Y}{\gamma_{M0}}$ $N_{c,Rd} = \frac{A \cdot f_Y}{\gamma_{M0}}$

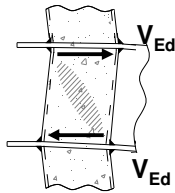
2. External diaphragm in shear	
<p>RBS joint</p> 	<p>Code provision (EN 1993-1-1):</p> $F_{v,Rd} = \frac{(2 \cdot A_v) \cdot f_Y}{\sqrt{3} \cdot \gamma_{M0}}$
<p>CP joint</p> 	<p>Code provisions: - Relations used in design:</p> $\sigma_{eq} = \sqrt{\sigma_{\perp}^2 + 3 \cdot \tau_{\parallel}^2} \leq \frac{f_y}{\gamma_{M0}}$ $F_{v,Rd} = \frac{(2 \cdot A_v) \cdot f_Y}{\gamma_{M0} \cdot \sqrt{1 + 2 \cdot \cos^2 \alpha}}$
3. Column panel in shear	
<p>Steel tube</p> 	<p>Code provisions (EN 1993-1-1):</p> $V_{wp,s,Rd} = \frac{0,9 \cdot A_v \cdot f_y}{\sqrt{3} \cdot \gamma_{M0}}$
<p>Concrete core</p> 	<p>Code provisions (EN 1994-1-1):</p> $V_{wp,c,Rd} = 0,85 \cdot v \cdot A_c \cdot f_{cd} \cdot \sin \theta$ <p>obs: the relation is given for the situation of a partial encased wide flange;</p> <p>Relation used in design:</p> $V_{wp,c,Rd} = 1,0 \cdot v \cdot A_c \cdot f_{cd} \cdot \sin \theta$ <p>obs: the capacity of the concrete core in shear was evaluated using the relation for a partial encased wide flange, but the coefficient 0.85 was replaced with 1.0 considering the column realised as CFT;</p>
<p>Composite section</p> 	<p>Code provisions (EN 1998-1):</p> $V_{wp,Rd} = 0,8 \cdot (V_{wp,s,Rd} + V_{wp,c,Rd})$ <p>obs: According to EN 1998-1, the capacity of the column panel may be assessed considering the contribution of steel component only, or as 80% of the contribution of both steel and concrete; In the design of the joints, it was observed that computing the capacity as 80% of the sum, lead to a lower capacity compared to the steel component alone;</p>

172 COMPONENT METHOD APPROACH FOR DESIGN OF JOINTS 6.

Table 6-4 – Stiffness coefficients for joint components

Scheme	Code provisions
1. Beam web in tension	
	<p>Code provision (EN 1993-1-8):</p> <p><i>For beam web in tension the stiffness coefficient should be taken as equal to infinity. These components need not be taken into account when calculating the rotational stiffness S_j.</i></p> <p>$K_8 = \infty$</p>
2. Beam flange / web in compression	
	<p>Code provision (EN 1993-1-8):</p> <p><i>For beam flange and web in compression the stiffness coefficient should be taken as equal to infinity. These components need not be taken into account when calculating the rotational stiffness S_j.</i></p> <p>$K_7 = \infty$</p>
3. "Cover plate" in tension / compression	
	<p>Code provision (EN 1993-1-8):</p> <p><i>For plates in tension or compression the stiffness coefficient should be taken as equal to infinity. These components need not be taken into account when calculating the rotational stiffness S_j.</i></p> <p>$K_9 = \infty$</p>
4. External diaphragm in shear	
	<p>The stiffness coefficient for the external diaphragm in shear is considered in this study as equal to infinity. It was found that this assumption is valid as long as the relation (as shown below) between the width of the external diaphragm (b_{ed}) and the width of the column (b_c) is satisfied.</p> <div style="display: flex; align-items: center;">  <div style="margin-left: 20px;"> <p>$k_{ed} = \infty$</p> <p>if:</p> <p>$b_{ed} \geq 0.42 \cdot b_c$</p> </div> </div>

5. Column web panel in shear



Code provision (EN 1993-1-8):

The stiffness coefficient corresponding to an unstiffened joint is:

$$k_1 = \frac{0.38 \cdot A_{vc}}{\beta \cdot z}$$

Code provision (EN 1994-1-1):

Where the steel column web is encased in concrete, the stiffness of the panel may be increased to allow for the encasement; the addition $k_{1,c}$ to the stiffness coefficient k_1 may be determined as:

$$k_{1,c} = 0.06 \cdot \frac{E_{cm} \cdot b_c \cdot h_c}{E_a \cdot \beta \cdot z}$$

According to EN 1993-1-8 [49] (§6.3), the rotational stiffness of a joint should be determined from the flexibilities of its basic components (see equation (6.73)), each represented by an elastic stiffness coefficient k_i . Fig. 6-8 shows the component model for the RBS and CP joints. Based on each model, the rotational stiffness for the RBS and CP joints is provided by the two equations i.e. (6.74) and (6.75). The two equations were written for one side of the joint only.

$$S_j = \frac{E \cdot z^2}{\mu \cdot \sum_i \frac{1}{k_i}} \tag{6.73}$$

$$S_{j,RBS} = \frac{E \cdot z^2}{\mu \cdot \left(\frac{1}{k_1 + k_{1,c}} + \frac{1}{k_{ed}} + \frac{1}{k_8} + \frac{1}{k_7} + \frac{1}{k_{ed}} \right)} \tag{6.74}$$

$$S_{j,CP} = \frac{E \cdot z^2}{\mu \cdot \left(\frac{1}{k_1 + k_{1,c}} + \frac{1}{k_{ed}} + \frac{1}{k_9} + \frac{1}{k_8} + \frac{1}{k_7} + \frac{1}{k_9} + \frac{1}{k_{ed}} \right)} \tag{6.75}$$

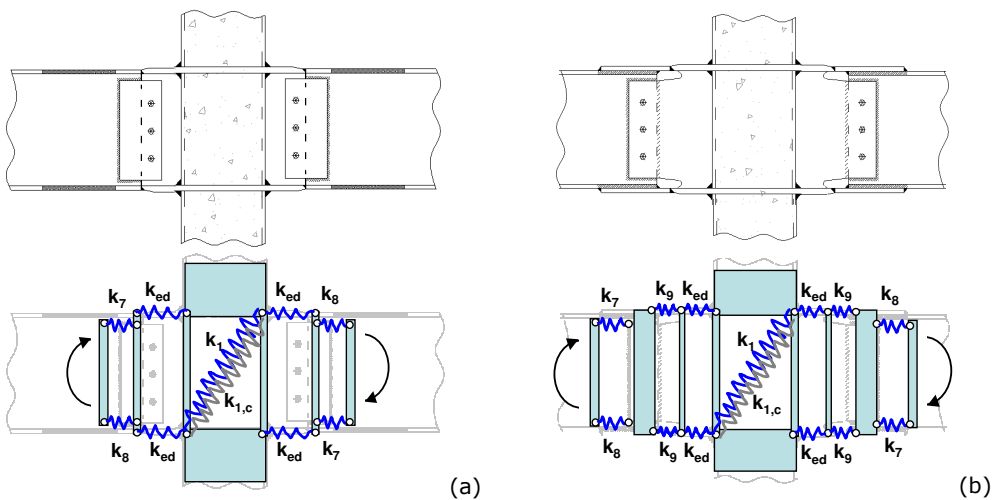


Fig. 6-8. Component model for RBS joint (a), and for CP joint (b)

6.4.1. Dissipative zone (plastic hinge)

A comparison between test and simulation, in terms of moment-rotation curve computed at plastic hinge location, is shown in Table 6-5 for RBS joint and in Table 6-6 for the CP joint. In both cases, the stress distribution and plastic strain (plotted at the end of simulation) confirmed the assumptions used in design i.e. formation of the plastic hinge in the beam, and also were able to reproduce the response of the joints as observed from the tests (see illustrations). The plastic bending moments computed at yield - for the two dissipative zones - are confirmed by both numerical and experimental investigations.

Table 6-5 – Dissipative zone (RBS joint)

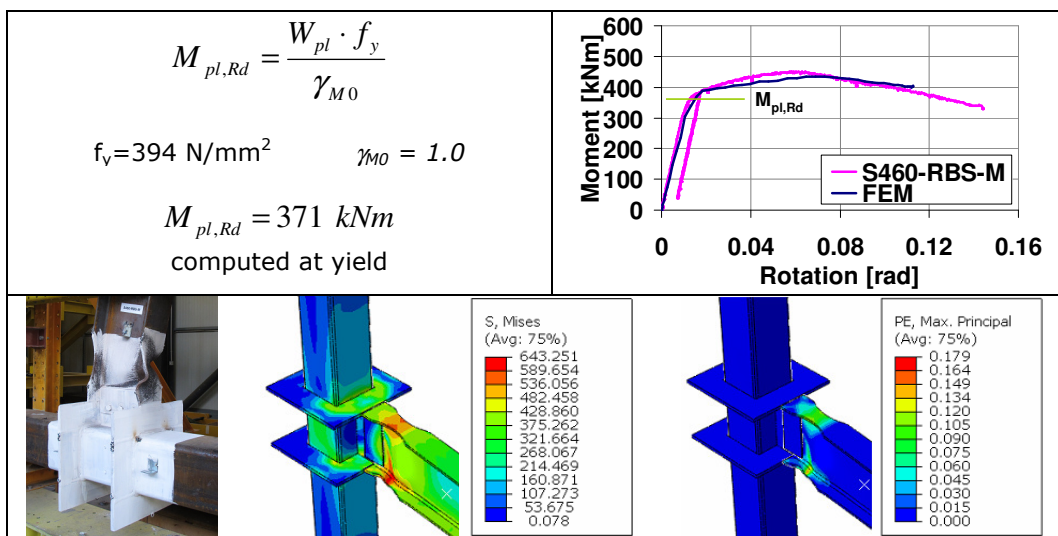
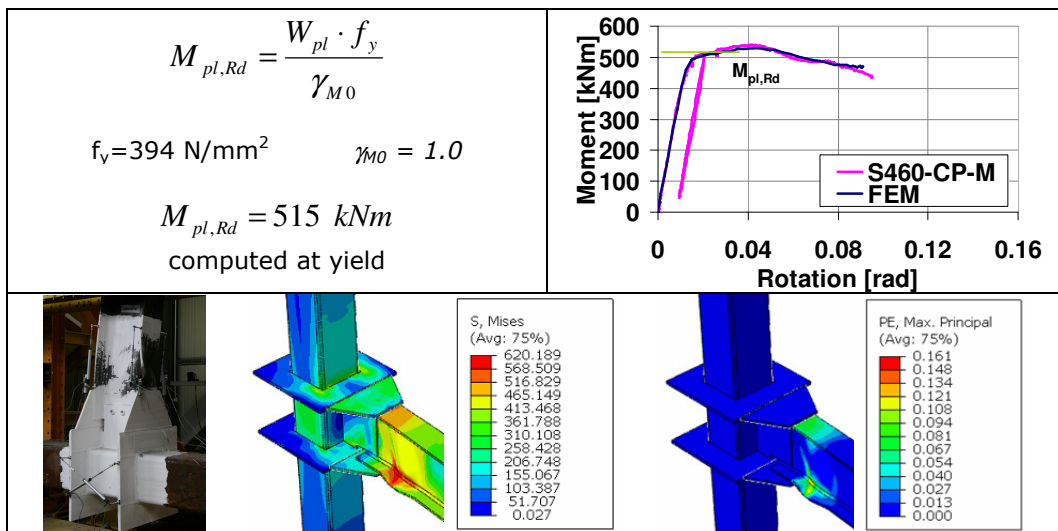


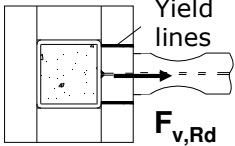
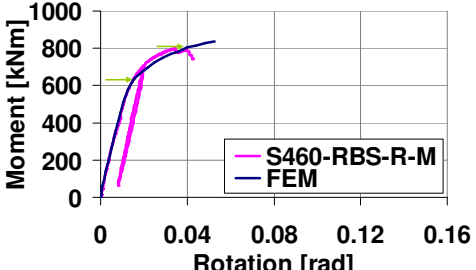

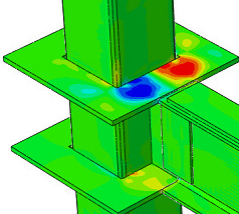
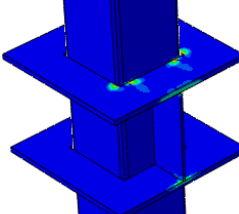

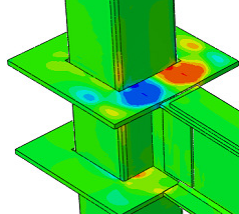
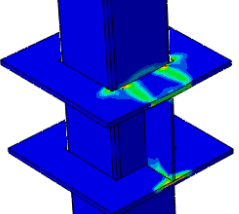
Table 6-6 – Dissipative zone (CP joint)



6.4.2. External diaphragm (S460 steel grade)

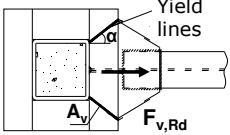
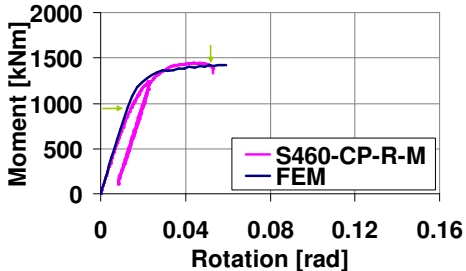

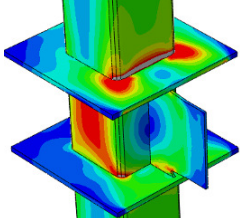
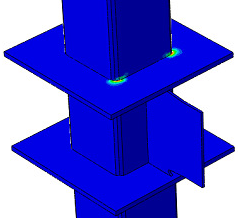

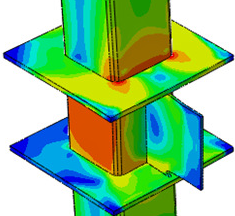
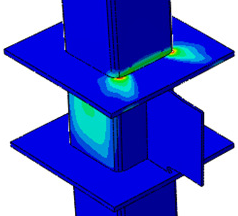
A comparison between test and simulation (M-θ at column face), is shown in Table 6-7 for the S460-RBS-R joint. The capacity of the external diaphragm was computed in the amount of 1604 kN. A comparison between the analytical model, experimental test and numerical simulation is made corresponding to yield and to peak load. A good correlation, in terms of shear stresses, can be observed between the analytical model and the numerical simulation for both – yield point and peak load. Low plastic strains from the FEA confirm the capacity of the diaphragm (1604 kN), and the yield lines confirm the failure mode considered in the analytical model.

Table 6-7 – External diaphragm (S460-RBS-R joint)

 <p>Yield lines</p> <p>$F_{v,Rd}$</p> <p>$f_v = 463 \text{ N/mm}^2$</p> $F_{v,Rd} = \frac{2 \cdot A_v \cdot f_y}{\sqrt{3} \cdot \gamma_{M0}} = 1604 \text{ kN}$	 <p>Moment [kNm]</p> <p>Rotation [rad]</p> <p>— S460-RBS-R-M</p> <p>— FEM</p>
<p>External diaphragm at yield load</p> $F_{v,Ed} = \frac{M_{Ed,cf}}{z} = \frac{630}{0.393} = 1603 \text{ kN}$ $\tau = \frac{F_{v,Ed}}{2 \cdot A_v} = 267 \frac{\text{N}}{\text{mm}^2}$	
 <p>S, S13 (Avg: 75%)</p> <ul style="list-style-type: none"> +2.576e+02 +2.147e+02 +1.718e+02 +1.289e+02 +8.595e+01 +4.303e+01 +1.020e+01 -4.282e+01 -8.575e+01 -1.297e+02 -1.716e+02 -2.145e+02 -2.574e+02 	 <p>PE, Max. Principal (Avg: 75%)</p> <ul style="list-style-type: none"> +1.347e-02 +1.235e-02 +1.123e-02 +1.010e-02 +8.982e-03 +7.859e-03 +6.737e-03 +5.614e-03 +4.491e-03 +3.368e-03 +2.246e-03 +1.123e-03 +0.000e+00
<p>External diaphragm at peak load</p> $F_{v,Ed} = \frac{M_{Ed,cf}}{z} = \frac{800}{0.393} = 2035 \text{ kN}$ $\tau = \frac{F_{v,Ed}}{2 \cdot A_v} = 339 \frac{\text{N}}{\text{mm}^2}$	
 <p>S, S13 (Avg: 75%)</p> <ul style="list-style-type: none"> +3.247e+02 +2.707e+02 +2.166e+02 +1.625e+02 +1.084e+02 +5.434e+01 +2.561e-01 -5.393e+01 -1.079e+02 -1.620e+02 -2.161e+02 -2.702e+02 -3.242e+02 	 <p>PE, Max. Principal (Avg: 75%)</p> <ul style="list-style-type: none"> +4.327e-02 +3.966e-02 +3.606e-02 +3.245e-02 +2.885e-02 +2.524e-02 +2.164e-02 +1.803e-02 +1.442e-02 +1.082e-02 +7.212e-03 +3.606e-03 +0.000e+00

A comparison between test and simulation (M-θ at column face), is shown in Table 6-8 for the S460-CP-R joint. The capacity of the external diaphragm was computed in the amount of 2162 kN. A comparison between the analytical model, experimental test and numerical simulation is made corresponding to yield and to peak load. A good correlation, in terms of equivalent stress, can be observed between the analytical model and FEM simulation for both – yield point and peak load. Low plastic strains from the FEA confirm the capacity of the diaphragm (2162 kN), and the yield lines confirm the failure mode considered in the analytical model.

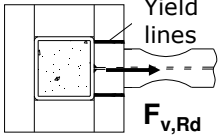
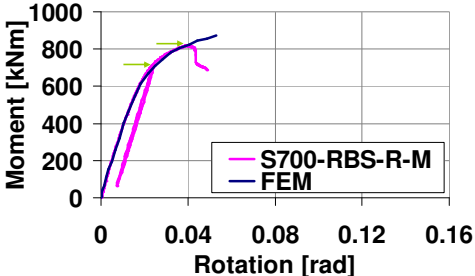

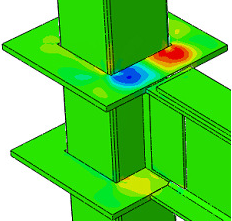
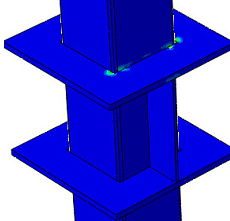

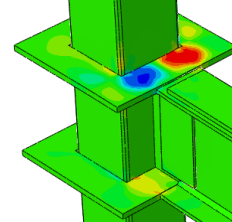
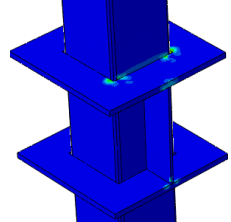
Table 6-8 – External diaphragm (S460-CP-R joint)

 $f_v = 463 \text{ N/mm}^2$ $F_{v,Rd} = \frac{2 \cdot A_v \cdot f_y}{\gamma_{M0} \cdot \sqrt{1 + 2 \cdot \cos^2 \alpha}} = 2162 \text{ kN}$	
$F_{v,Ed} = \frac{M_{Ed,cf}}{z} = \frac{957}{0.42} = 2278 \text{ kN}$ $\sigma_{\perp} = 162 \frac{\text{N}}{\text{mm}^2} \quad \tau_{\parallel} = 242 \frac{\text{N}}{\text{mm}^2}$ $\sigma_{equiv} = 449 \frac{\text{N}}{\text{mm}^2}$	
 <p>S, Mises (Avg: 75%)</p> <ul style="list-style-type: none"> +4.554e+02 +4.174e+02 +3.795e+02 +3.415e+02 +3.036e+02 +2.657e+02 +2.277e+02 +1.898e+02 +1.518e+02 +1.139e+02 +7.595e+01 +3.801e+01 +7.247e-02 	 <p>PE, Max. Principal (Avg: 75%)</p> <ul style="list-style-type: none"> +8.283e-03 +7.593e-03 +6.903e-03 +6.212e-03 +5.522e-03 +4.832e-03 +4.142e-03 +3.451e-03 +2.761e-03 +2.071e-03 +1.381e-03 +6.903e-04 +0.000e+00
$F_{v,Ed} = \frac{M_{Ed,cf}}{z} = \frac{1411}{0.42} = 3359 \text{ kN}$ $\sigma_{\perp} = 238 \frac{\text{N}}{\text{mm}^2} \quad \tau_{\parallel} = 358 \frac{\text{N}}{\text{mm}^2}$ $\sigma_{equiv} = 664 \frac{\text{N}}{\text{mm}^2}$	
 <p>S, Mises (Avg: 75%)</p> <ul style="list-style-type: none"> +6.295e+02 +5.771e+02 +5.247e+02 +4.722e+02 +4.198e+02 +3.674e+02 +3.150e+02 +2.625e+02 +2.101e+02 +1.577e+02 +1.052e+02 +5.280e+01 +3.684e-01 	 <p>PE, Max. Principal (Avg: 75%)</p> <ul style="list-style-type: none"> +6.204e-02 +5.687e-02 +5.170e-02 +4.653e-02 +4.136e-02 +3.619e-02 +3.102e-02 +2.585e-02 +2.068e-02 +1.551e-02 +1.034e-02 +5.170e-03 +0.000e+00

6.4.3. External diaphragm (S690 steel grade)

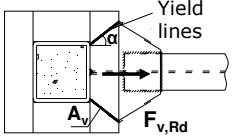
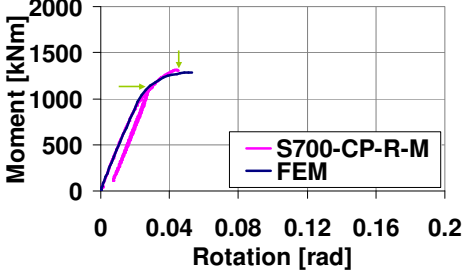

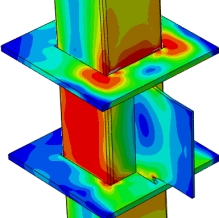
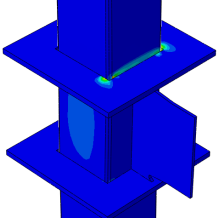

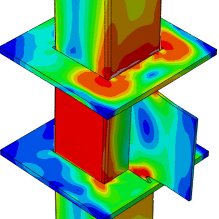
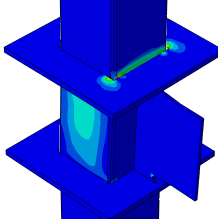
A comparison between test and simulation (M-θ at column face), is shown in Table 6-9 for the S700-RBS-R joint. The capacity of the external diaphragm was computed in the amount of 2009 kN. A comparison between the analytical model, experimental test and numerical simulation is made corresponding to yield and to peak load. A relative good correlation, in terms of shear stresses, can be observed between analytical model and FEM simulation for both – yield point and peak load. Low plastic strains from the FEA corresponding to a load level of 2094 kN confirm the capacity of the diaphragm.

Table 6-9 – External diaphragm (S690-RBS-R joint)

 <p>Yield lines</p> <p>$F_{v,Rd}$</p> <p>$f_v = 725 \text{ N/mm}^2$</p> $F_{v,Rd} = \frac{2 \cdot A_v \cdot f_y}{\sqrt{3} \cdot \gamma_{M0}} = 2009 \text{ kN}$	 <p>Moment [kNm]</p> <p>Rotation [rad]</p> <p>— S700-RBS-R-M</p> <p>— FEM</p>
<p>External diaphragm at yield load</p> $F_{v,Ed} = \frac{M_{Ed,cf}}{z} = \frac{712}{0.393} = 1811 \text{ kN}$ $\tau = \frac{F_{v,Ed}}{2 \cdot A_v} = 377 \frac{\text{N}}{\text{mm}^2}$	
 <p>S, S13 (Avg: 75%)</p> <ul style="list-style-type: none"> +4.117e+02 +3.432e+02 +2.747e+02 +2.062e+02 +1.377e+02 +6.920e+01 +7.012e-01 -6.779e+01 -1.363e+02 -2.048e+02 -2.733e+02 -3.418e+02 -4.103e+02 	 <p>PE, Max. Principal (Avg: 75%)</p> <ul style="list-style-type: none"> +1.858e-02 +1.703e-02 +1.548e-02 +1.394e-02 +1.239e-02 +1.084e-02 +9.291e-03 +7.742e-03 +6.194e-03 +4.645e-03 +3.097e-03 +1.548e-03 +0.000e+00
<p>External diaphragm at peak load</p> $F_{v,Ed} = \frac{M_{Ed,cf}}{z} = \frac{823}{0.393} = 2094 \text{ kN}$ $\tau = \frac{F_{v,Ed}}{2 \cdot A_v} = 436 \frac{\text{N}}{\text{mm}^2}$	
 <p>S, S13 (Avg: 75%)</p> <ul style="list-style-type: none"> +4.237e+02 +3.531e+02 +2.825e+02 +2.119e+02 +1.413e+02 +7.065e+01 +3.340e-02 -7.058e+01 -1.412e+02 -2.118e+02 -2.824e+02 -3.530e+02 -4.236e+02 	 <p>PE, Max. Principal (Avg: 75%)</p> <ul style="list-style-type: none"> +2.082e-02 +1.909e-02 +1.735e-02 +1.562e-02 +1.388e-02 +1.215e-02 +1.041e-02 +8.677e-03 +6.942e-03 +5.206e-03 +3.471e-03 +1.735e-03 +0.000e+00

A comparison between test and simulation (M-θ at column face), is shown in Table 6-10 for the S700-CP-R joint. The capacity of the external diaphragm was computed in the amount of 2708 kN. A comparison between the analytical model, experimental test and numerical simulation is made corresponding to yield and to peak load. A relative good correlation, in terms of equivalent stress, can be observed between analytical model and FEM simulation for both yield point and peak load. Low plastic strains from the FEA confirm the capacity of the diaphragm (2708 kN), and it can be observed that the failure of the weld occurred a corresponding to a load level (3033 kN) above the capacity.

Table 6-10 – External diaphragm (S690-CP-R joint)

 $f_v = 725 \text{ N/mm}^2$ $F_{v,Rd} = \frac{2 \cdot A_v \cdot f_y}{\gamma_{M0} \cdot \sqrt{1 + 2 \cdot \cos^2 \alpha}} = 2708 \text{ kN}$	
$F_{v,Ed} = \frac{M_{Ed,cf}}{z} = \frac{1137}{0.42} = 2707 \text{ kN}$ $\sigma_{\perp} = 260 \frac{\text{N}}{\text{mm}^2} \quad \tau_{\parallel} = 391 \frac{\text{N}}{\text{mm}^2}$ $\sigma_{echiv} = 725 \frac{\text{N}}{\text{mm}^2}$	
 <p>S, Mises (Avg: 75%)</p> <ul style="list-style-type: none"> +8.117e+02 +7.441e+02 +6.765e+02 +6.089e+02 +5.413e+02 +4.737e+02 +4.061e+02 +3.385e+02 +2.709e+02 +2.032e+02 +1.356e+02 +6.804e+01 +4.345e-01 	 <p>PE, Max. Principal (Avg: 75%)</p> <ul style="list-style-type: none"> +2.478e-02 +2.271e-02 +2.065e-02 +1.858e-02 +1.652e-02 +1.445e-02 +1.239e-02 +1.032e-02 +8.259e-03 +6.194e-03 +4.130e-03 +2.065e-03 +0.000e+00
$F_{v,Ed} = \frac{M_{Ed,cf}}{z} = \frac{1274}{0.42} = 3033 \text{ kN}$ $\sigma_{\perp} = 292 \frac{\text{N}}{\text{mm}^2} \quad \tau_{\parallel} = 438 \frac{\text{N}}{\text{mm}^2}$ $\sigma_{echiv} = 812 \frac{\text{N}}{\text{mm}^2}$	
 <p>S, Mises (Avg: 75%)</p> <ul style="list-style-type: none"> +8.381e+02 +7.683e+02 +6.985e+02 +6.288e+02 +5.590e+02 +4.892e+02 +4.194e+02 +3.496e+02 +2.798e+02 +2.100e+02 +1.402e+02 +7.037e+01 +5.762e-01 	 <p>PE, Max. Principal (Avg: 75%)</p> <ul style="list-style-type: none"> +3.805e-02 +3.488e-02 +3.171e-02 +2.854e-02 +2.536e-02 +2.219e-02 +1.902e-02 +1.585e-02 +1.268e-02 +9.512e-03 +6.341e-03 +3.171e-03 +0.000e+00

6.4.4. Column panel

The evaluation of the shear force within the column web panel was performed based on the specific loading and the boundary conditions of the joint assembly (see Fig. 6-9). The corresponding shear forces and bending moments acting on the members of the joint are shown in Fig. 6-10. The efforts acting on the column web panel are shown in Fig. 6-11. It can be observed that the shear force $V_{wp,Ed}$ can be computed based on the equilibrium of forces.

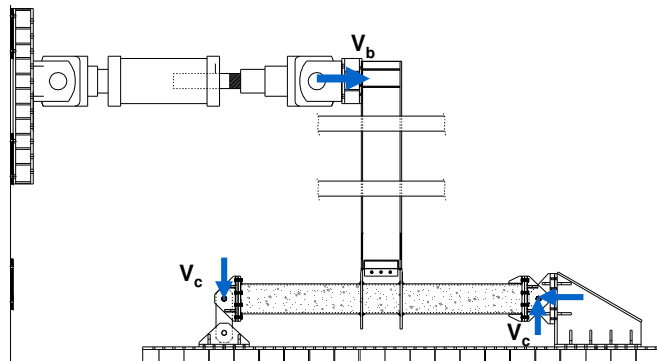


Fig. 6-9. Beam-to-column joint: loading and reactions

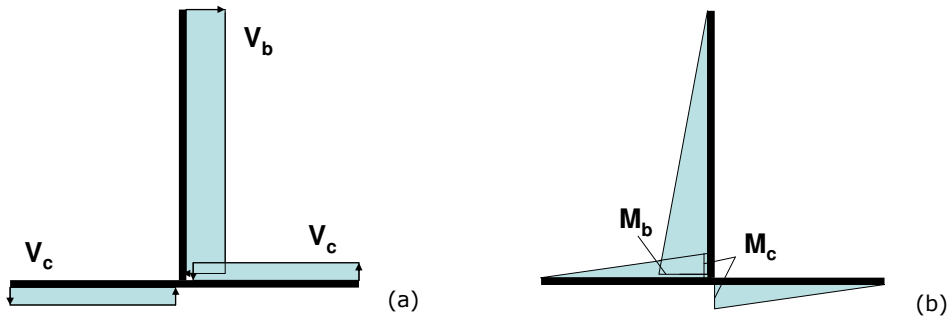


Fig. 6-10. Beam-to-column joint: shear force (a) and bending moment (b)

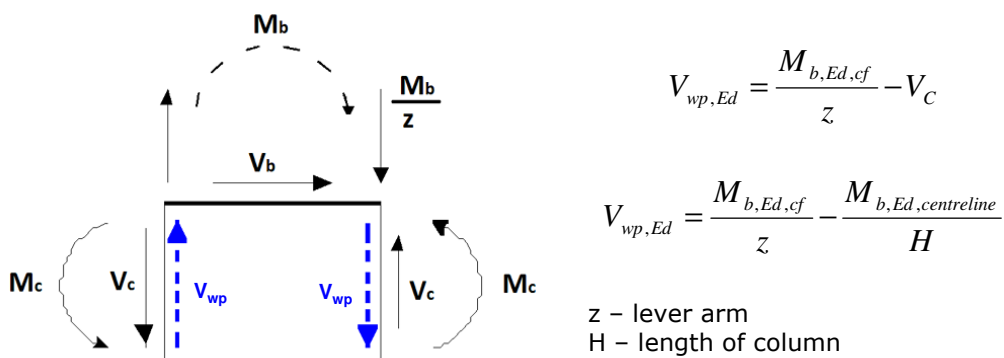


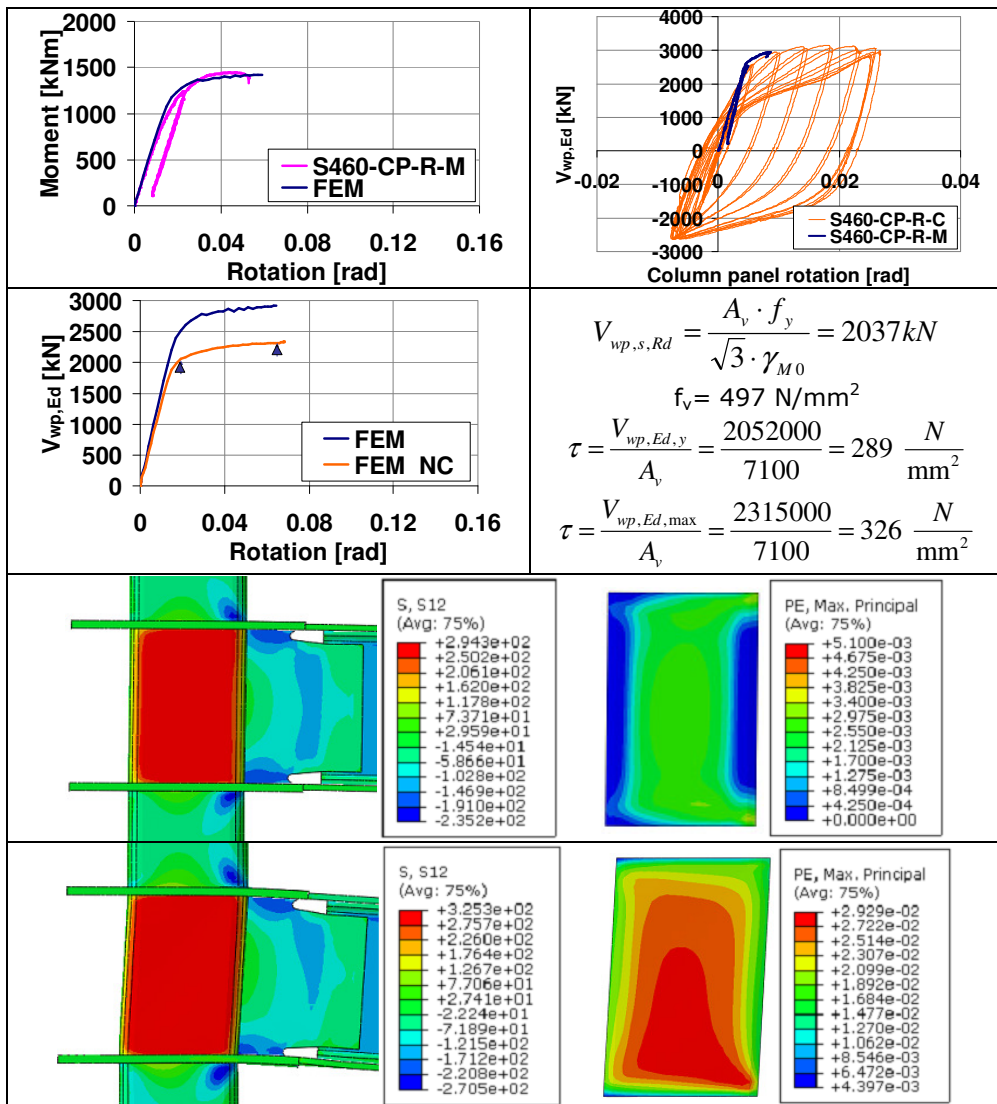
Fig. 6-11. Evaluation of shear force within the column web panel

Column panel (S460 tube)

A comparison between test and simulation (M-θ at column face), is shown in Table 6-11 for the S460-CP-R joint. The capacity of the column panel in shear under both monotonic and cyclic loading is shown as well (V_{wp,Ed} vs. panel rotation).

The capacity of the steel tube in shear was computed in the amount of 2037 kN (the 0.9 coefficient was not taken into account as no axial force acted on the column). A comparison between the analytical model and the numerical simulation of the joint without concrete core is made corresponding to yield and to peak load. Consequently, a good correlation, in terms of shear stress, can be observed between analytical model and FEM simulation for both yield point and peak load. Low plastic strains from the FEA confirm the capacity of the web panel (2037 kN).

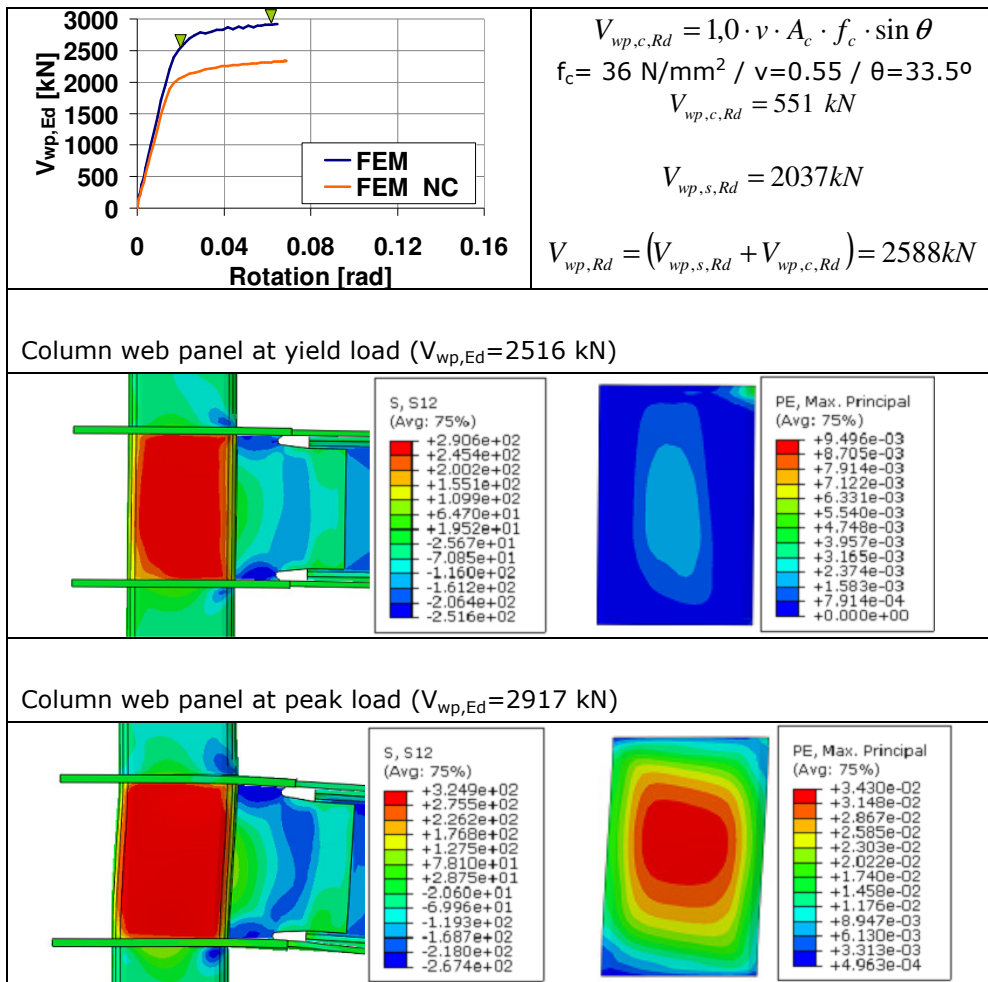
Table 6-11 – Column panel (CF-RHS S460) – validation of steel component



The capacity of the concrete core in shear is computed in Table 6-12 to the amount of 551 kN. Therefore, the capacity of the column web panel in shear, combining the steel and the concrete part, was obtained as 2588 kN. It can be observed that the analytical model is in very good agreement with the experimental results (see $V_{wp,Ed-\gamma}$ from Table 6-11) and with the numerical simulations (see $V_{wp,Ed-\gamma}$ from Table 6-12). The capacities of the steel tube and the concrete core in shear were combined without affecting the total by the 0.8 factor.

The stress distribution and plastic strain within the column panel is shown for the joint with concrete core, corresponding to yield and peak load. It can be observed that the shear stresses from the steel tube are similar in the two cases (without and with concrete core) corresponding to the same rotation.

Table 6-12 – Column panel (CF-RHS S460) – validation of composite section

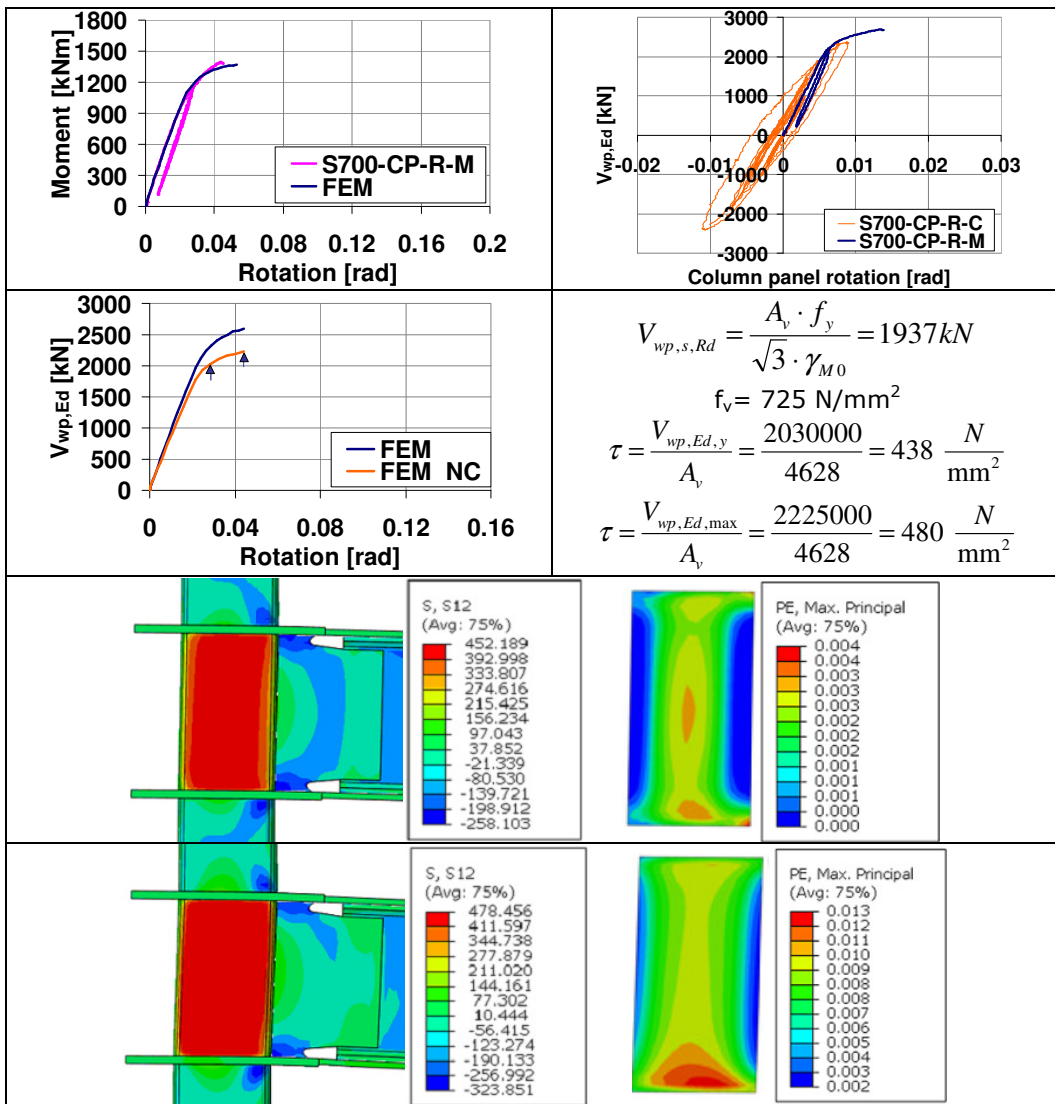


Column panel (S700 tube)

A comparison between test and simulation (M-θ at column face), is shown in Table 6-13 for the S700-CP-R joint. The capacity of the column panel in shear under both monotonic and cyclic loading is shown as well (V_{wp,Ed} vs. panel rotation).

The capacity of the steel tube in shear was computed in the amount of 1937 kN (the 0.9 coefficient was not taken into account as no axial force acted on the column). A comparison between the analytical model and the numerical simulation of the joint without concrete core is made corresponding to yield and to peak load. Consequently, a good correlation, in terms of shear stress, can be observed between analytical model and FEM simulation for both yield point and peak load. Low plastic strains from the FEA confirm the capacity of the web panel (1937 kN).

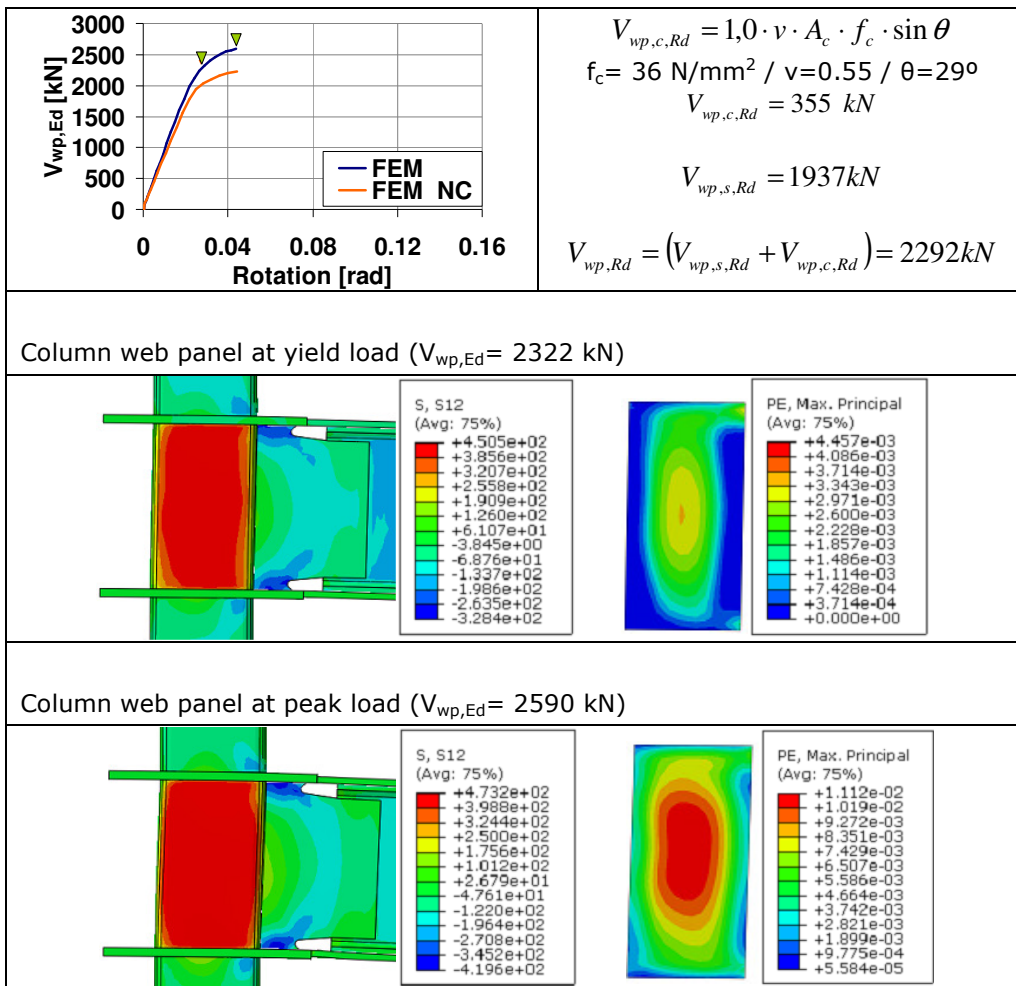
Table 6-13 – Column panel (CF-RHS S700) – validation of steel section



The capacity of the concrete core in shear is computed in Table 6-14 to the amount of 355 kN. Therefore, the capacity of the column web panel in shear, combining the steel and the concrete part, was obtained as 2292 kN. It can be observed that the analytical model is in very good agreement with the experimental results (see $V_{wp,Ed-Y}$ from Table 6-13) and with the numerical simulations (see $V_{wp,Ed-Y}$ from Table 6-14). The capacities of the steel tube and the concrete core in shear were combined without affecting the total by the 0.8 factor.

The stress distribution and plastic strain within the column web panel is shown for the joint with concrete core, corresponding to yield and peak load. It can be observed that the shear stresses from the steel tube are similar in the two cases (without and with concrete core) corresponding to the same rotation.

Table 6-14 – Column panel (CF-RHS S700)



6.5. Design flow chart

The flow chart for the design of a beam-to-column joint with reduced beam section is shown in Fig. 6-12, and the flow chart for the design of a beam-to-column joint with cover plates is shown in Fig. 6-13.

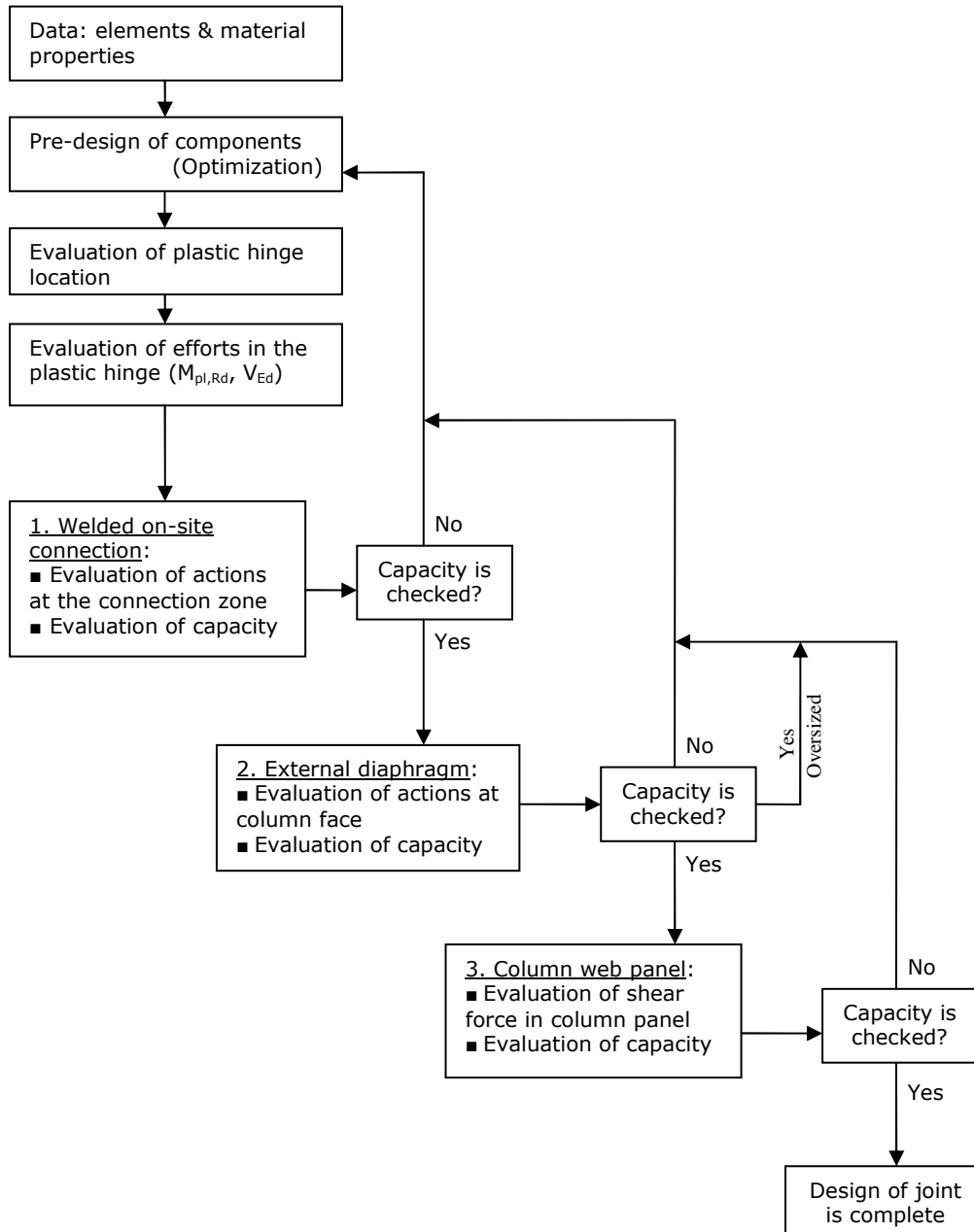


Fig. 6-12. Design flow-chart for reduced beam section joints

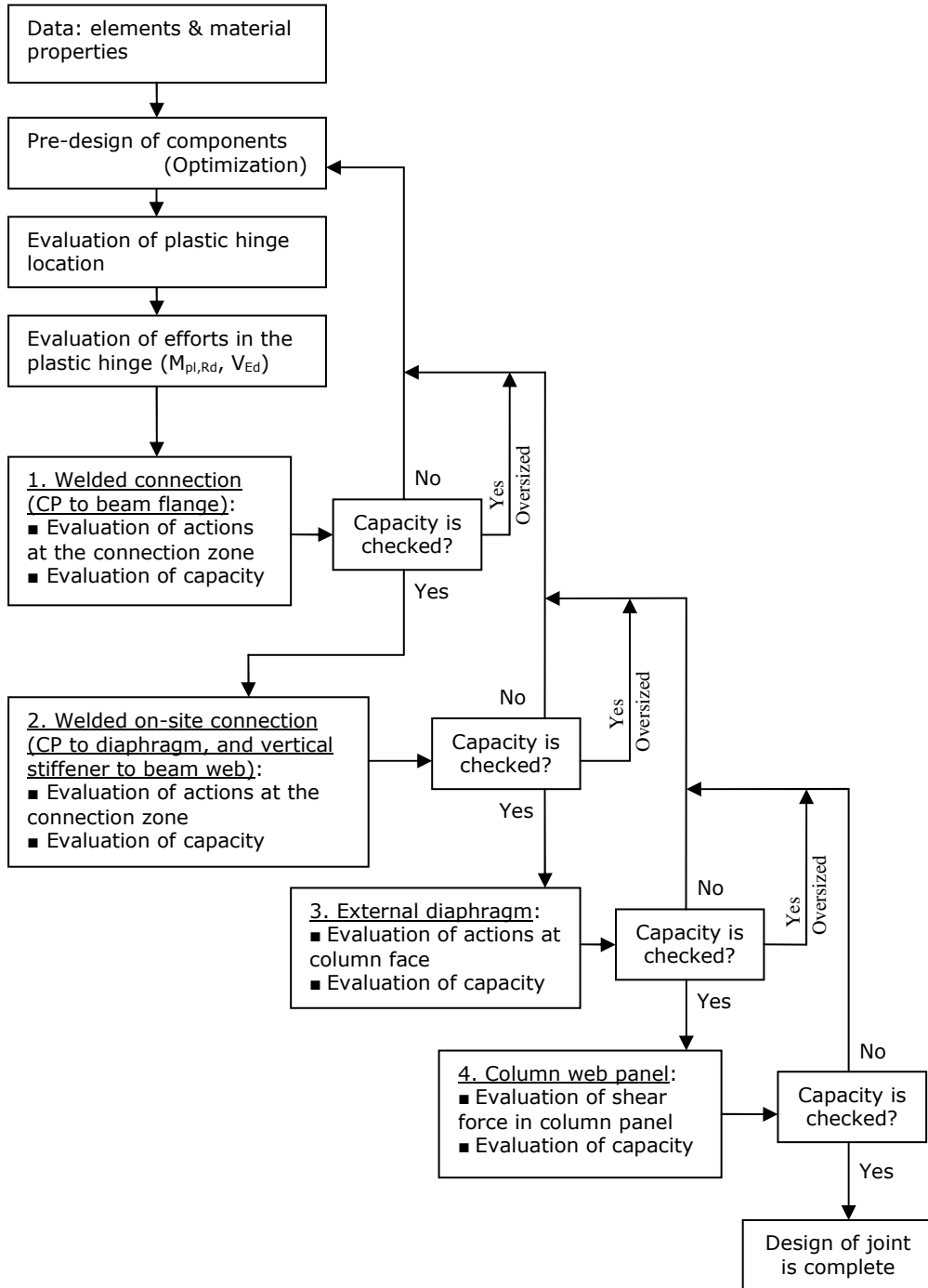


Fig. 6-13. Design flow-chart for cover plate joints

6.6. Concluding remarks

The design procedures for the two joining solutions, i.e. RBS joint and CP joint, were shown. In addition, design flow charts illustrate the design procedure for each of the two joints.

The design of the joints was performed considering plastic hinge formation in the beam. Further with the bending moment and shear force from the plastic hinge, the components of the joint were designed for the required degree of overstrength for non-dissipative connections. The main considered components are the welded on-site connection, the external diaphragm and the column web panel.

A summary was made with regard to:

- relations for the design of the welded connections;
- relations for the capacity of the components;
- stiffness coefficients of the components.

A component model was prepared for RBS and CP joints. Relations for the rotational stiffness of the two joints were obtained based on the equation from EN 1993-1-8 [49] and on the proposed component model. According to EN 1993-1-8 the stiffness coefficients shall be considered as equal to infinite corresponding to the following components: beam web in tension, beam web/flange in compression, and plate in tension. A relation was found between the width of the external diaphragm and the width of the column, based on which the stiffness coefficient of the external diaphragm can be assumed to be infinite.

Therefore, the remaining component with contribution to the rotational stiffness was the column web panel. From the comparison between the rotational stiffness obtained experimentally, and the rotational stiffness computed analytically considering only the contribution of the column web panel, a higher stiffness was observed within the experimental moment-rotation curves. It is to be noted that in the analytical model, the stiffness coefficients of the column web panel were related to an unstiffened joint and to the concrete encasement (partially encased steel section). In contrast, for the case of a concrete filled rectangular hollow section, it is believed that the shear stiffness of the column web panel is influenced in a higher amount by composite effect of the member. Therefore, additional investigations are necessary in order to evaluate the influence on the shear stiffness given by the confining effect of the steel tube, and by the steel-concrete connection and friction.

A set of cases were considered for the experimental and numerical validation of the relations for the design capacity corresponding to:

- dissipative zone
 - RBS joint / CP joint
- external diaphragm
 - RBS joint / CP joint
- column web panel
 - CF-RHS S460 / CF-RHS S700

In relation to the dissipative zone, the formation of the plastic hinge in the beam was confirmed by the numerical and experimental investigations. In addition, the relation for the bending moment was in good agreement with the results.

In relation to the external diaphragms, a comparison was made between the analytical model, experimental test and numerical simulations. The following aspects were observed:

- good correlation between analytical model and FEM, in terms of stresses (shear stresses for RBS-R joints and equivalent stresses for CP-R joints);
- the capacity of the external diaphragm was confirmed (corresponding to a load level equal to the computed design capacity, the plastic strain from FEM evidenced low values);
- yield lines observed from experimental tests and numerical simulations corresponding to external diaphragms from S460 steel grade, confirmed the failure mode considered in the analytical model; for external diaphragms from S690 steel grade, yield lines were not observed, only local concentration of stresses and strain – which is due to the higher capacity of the external diaphragm;
- weld failure in case of S700-CP-R-M joint occurred corresponding to a load level above the computed yield capacity; therefore it was not a premature failure.

In relation to the column web panel, a comparison was made between the analytical model, experimental tests and numerical simulations. The following observations were made:

- good correlation, in terms of shear stress, between analytical model and FEM results;
- the design capacity of the steel tube in shear was confirmed (the 0.9 coefficient was not taken into account in the analytical model as no axial force acted on the column);
- the design capacity of the column web panel in shear computed as the sum of the capacities (steel and concrete) was in very good agreement with the experimental results and with the numerical simulations; in the analytical model the shear capacity of the composite section was not affected by the factor 0.8 as required by EN 1998-1 [27];
- the provisions from EN 1994-1-1 [50] for the shear strength of a column web panel considering a partially encased wide flange section were confirmed also for the case of rectangular hollow sections filled with concrete;

7. CONCLUSIONS OF PHD STUDY. CONTRIBUTIONS OF AUTHOR

7.1. Conclusions of PhD study

Chapter 1: Introduction

An introduction was made to the research topic. The scope and the objectives of the thesis were shown, as well as the research framework.

Chapter 2: High performance steels in construction

A brief introduction was made with regard to steel as a construction material and the significant changes it suffered throughout time – which lead to a group of materials – High Performance Steels (HPS) – defined by good performance in tensile stress, toughness, weldability, cold forming and corrosion, and which are available also for construction industry. Recent studies showed that by using steels with higher resistance/weight ratio material savings can be obtained especially in the case of heavy constructions. The use of high strength steel within seismic resistant structures could be done considering two approaches: (a) dual-steel structures with MCS for dissipative members and HSS for nondissipative members; (b) structures realised with HSS, i.e. S460 steel grade which is characterised by a certain amount of ductility and could be used in structures of medium ductility class (DCM). Tools were developed within current international research projects [30] for choice of material to avoid brittle fracture for monotonic loading and for seismic loading. Examples of application were shown related to the use of high strength in multi-storey buildings from Japan, China, Australia, US, and from Europe.

Chapter 3: Tubular structures for buildings

The third chapter was related to structures of tubular elements for buildings. In introduction general aspects were shown with regard to the geometrical and mechanical properties as well as the manufacturing process of tubular elements. Accordingly, this type of elements are characterised by excellent properties with regard to loading in compression, torsion and bending in all directions. Hollow sections are made of similar steel as used for other steel sections, but can be produced from high strength steel as well. As part of a multi-storey frame, tubular elements are used as braces and/or as columns. Columns realised from steel hollow sections can be filled with concrete with the aim to combine the properties of the two materials, the final element being characterised by higher stiffness, capacity and ductility, as well as enhanced fire resistance in comparison with bare steel configurations. In spite of the advantages of the tubular sections, a special attention needs to be paid to the connections between beams and columns. The framing system with concrete filled columns and joints realised in welded solution has been studied and applied on a large scale in Asia, Australia and America. In contrast, this solution was used at a lower scale in Europe. A description was made concerning the current code provisions in relation to the design of welded beam to CFT column joints, and the shear capacity of the column web panel. Since this solution was used at a lower scale in Europe, a set of limitations were observed.

Therefore, the interest within the current research was related to the assessment of the seismic performance of welded I beam-to-CFRHS column joints for moment resisting frames (MRF) and moment resisting bays of dual frames (MRF+CBF, and MRF+EBF). In relation to the column, the goal was to count on both steel tube and concrete core, and to have a composite action ensured by the use of shot fired nails.

In the design process of the beam-to-column joints it was observed that in order to develop full moment capacity and to assure the required amount of overstrength of the connection, transverse column stiffeners were needed. Consequently, examples of typical joints used in Japan were shown. A summary review of research on welded beam-to-CFT column joints and on the shear connection realised with shot fired nails was made. Finally, application examples were shown in relation to multi-storey buildings with columns realised as concrete filled tubes.

Chapter 4: Performance based seismic design of reference dual steel frames

A brief description was made in relation to the frames (dual-steel frames) that were used as basis for the definition of the experimental program and which were designed within the research project HSS-SERF [86]. The cross-section of the members for the beam-to-column joint specimens was chosen from these frames. For the connection of beams and columns, two joint typologies were proposed considering the welded solution and two joint typologies i.e. with reduced beam section and with cover plates. The configuration and detailing of the two joint (RBS and CP) were shown. Finally, with the aim to assess the seismic demand for the beam-to-column joints, a set of frames were analysed using static and dynamic nonlinear analyses. The position of the plastic hinge and the joint typology (RBS and CP) were taken into account in the analyses of the frames. The results from the investigations were further shown.

For each frame, the target displacement was computed with the N2 method [89] corresponding to three intensity levels $\lambda=0.5$, 1.0, and 1.5. It was observed that MRF's satisfied the immediate occupancy performance level for each of the three intensity levels ($\lambda=0.5$, 1.0, and 1.5). The D-CBF's satisfied the immediate occupancy level $\lambda=0.5$, but at $\lambda=1.0$ and $\lambda=1.5$ the performance levels were not satisfied (braces in compression evidenced failure according to the acceptance criteria from FEMA 356 [91]). The D-EBF's satisfied the immediate occupancy performance level at $\lambda=0.5$, but at $\lambda=1.0$ the plastic rotation demands in links exceeded the rotation capacity and therefore the life safety performance level was not satisfied.

In addition, the results obtained from the dynamic nonlinear analysis lead to the following observations:

- MRF's evidenced a good behaviour: elastic response at $\lambda=0.5$, low plastic deformation in beams at $\lambda=1.0$, and global mechanism corresponding to $\lambda=1.5$; corresponding to the three intensity levels ($\lambda=0.5$, 1.0, and 1.5) MRF's satisfied the immediate occupancy performance level;
- D-CBF's evidenced for both $\lambda=0.5$ and $\lambda=1.0$ brace failure – according to the acceptance criteria provided by FEMA 356 [91]; at $\lambda=1.5$ global structural collapse was observed; therefore the performance levels were not satisfied;
- D-EBF's evidenced yielding of links at $\lambda=0.5$; all links except the last floor were activated at $\lambda=1.0$ – however with low plastic deformations (7.6

mrاد); at $\lambda=1.5$ the plastic deformations in the links increased (14.6 mrad) and plastic hinges developed also in the outer beams; the immediate occupancy performance level was satisfied at both $\lambda=0.5$ and $\lambda=1.0$, and corresponding to $\lambda=1.5$ the collapse prevention performance level was satisfied;

From the comparison between the target displacements obtained with N2 method and the maximum displacement at the top of the building as obtained from the dynamic nonlinear analysis, it was observed that for MRF's and D-CBF's the maximum top displacements were close to the target displacements. In contrast, for D-EBF's the maximum top displacements were significantly lower than the target displacements.

In case of moment resisting frames (MRF), the horizontal forces are mainly resisted by members acting in flexural mode, and therefore the performance of MR joints is crucial. In contrast, the main component of the D-CBF's and D-EBF's in dissipating the seismic energy is represented by braces, and respectively by shear links, while the joints in MRF bays have secondary effect. It was observed that these frames develop plastic hinges mostly in braces (D-CBF) and links (D-EBF), and corresponding to higher intensity levels also in joints. At the three intensity levels the rotation demand for joints within MRF was in amount of 7, 14, and 17 mrad. The rotation demand for joints within D-CBF was obtained in amount of 7 and 14 mrad corresponding to $\lambda=0.5$ and $\lambda=1.0$. In contrast, for D-EBF the rotation demand was lower i.e. 3 mrad ($\lambda=0.5$), 7 mrad ($\lambda=1.0$) and 12 mrad ($\lambda=1.5$). For comparison, the acceptance criteria from FEMA 356 [91] in terms of rotation at SLS, ULS and CPLS for the RBS beam is $0.25\theta_y=2.8$ mrad, $2\theta_y=22.6$ mrad and $3\theta_y=33.9$ mrad; the values for CP beam are $0.25\theta_y=2.7$ mrad, $2\theta_y=21.6$ mrad and $3\theta_y=32.4$ mrad.

Chapter 5: Experimental evaluation of seismic performance of dual steel IPE beam-to CFRHS column welded joints

One of the objectives of the PhD study was to evaluate, through experimental and numerical investigations, the seismic performance of beam-to-column joints, particularly considering:

- Evaluation of the efficiency provided by shot fired nails for the connection between the steel tube and the concrete core;
- Evaluation of structural performance (resistance, rigidity, ductility) of beam-to-column joints according to the proposed solutions;
- Identification of the base components of the joints and connections;
- Calibration, based on joint tests, of a model for advanced investigation with FE;
- Extension of the experimental program through numerical simulations;

A detailed presentation was made in relation to the experimental program that covered extensive experimental investigations which were performed in three phases, i.e. investigation of material samples, investigation of steel-concrete connection, and investigation of full scale beam-to-column joints. A description was made in relation to the specimen configuration, experimental test set-up, instrumentation arrangement, and loading protocols for both tests on steel-concrete connection and tests on joints. Results from the experimental and numerical investigations were then presented, and the main conclusions and observations are further summarised.

Tests on material samples

The tests performed on material covered compression tests on concrete cubes, as well as tensile and Charpy V-notch impact tests on steel samples.

With regard to the tests performed on concrete samples, the average characteristic strength was obtained in amount of 36 N/mm^2 which is slightly lower than the minimum characteristic strength of 37 N/mm^2 required for a C30/37 concrete class. With regard to the tests performed on steel samples, the measurements, for both tensile and Charpy V-notch tests, satisfied the minimum requirements according to each steel grade as specified by the standards EN 10025-2 [6] and EN 10025-6 [8]. Therefore, the steel grade from each component of the beam-to-column joints was confirmed.

Tests on steel-concrete connection

In relation to the steel-concrete connection it was observed that the shear strength that was developed at the interface between steel tube and concrete core was in amount of 0.4 N/mm^2 , which is equal to the value recommended by EN 1994-1 [50] for rectangular hollow sections.

Particular to the specific loading, it was observed that the connectors have a significant contribution to the load transfer from steel tube to the concrete core, in both monotonic and cyclic loading. From the investigation of the behaviour and failure mode, it was observed that under monotonic loading the concrete was crushed in a small amount at the contact with the shot fired nails which bent. Under alternating cycles the nails eventually broke at the interface between concrete core and steel tube. In addition it was observed that from the cyclic loading the capacity of the connectors decreased slightly compared to the monotonic loading. The shear capacity of the connectors obtained from the experimental tests (37.5 kN) was higher than the computed shear strength (30 kN) using the relation from EN 1994-1 for headed stud connectors.

In conclusion, as observed by Beck [73], the X-DSH 32 P10 shot fired nails proved a significant contribution to the steel-concrete connection considering the monotonic and cyclic loading, as well as HSS tubes (S460 and S700). However, due to the complex behaviour of concrete and shot fired nails, additional investigations (including FEM) are necessary to develop a design procedure and recommendations.

Pre-test numerical simulations

Due to the innovative joint configurations, an accurate prediction was needed in order to avoid unacceptable failure during the tests. The material model for each steel grade was calibrated based on results from tensile tests and used further in the numerical model of the joints.

The numerical simulations allowed assessing behaviour of each joint configuration. Consequently, the RBS and CP joints evidenced large plastic deformations in the beam which was in agreement with the design assumptions. For the joints with strengthened beam, yielding was initiated in the adjacent area of the welded on-site connection, respectively in the external diaphragm and column web panel. Therefore, the pre-test numerical simulations proved a good design of the RBS and CP joints, and related to the joints with strengthened beam - information was provided concerning the behaviour of the joint components.

Tests on beam-to-column joints

The parameters investigated within the joint tests consisted of loading procedure (monotonic, cyclic), joint type (RBS, CP), steel grade for column (S460, S700), and intended failure mode (beam, connection). The experimental program covered a number of 16 beam-to-column joint specimens. For each case a description was made in relation to the test assembly, observations from test, and the response of the joints subjected to monotonic and cyclic loading. Interpretation and comparison of results was performed with the aim to assess the participation of components to the joint rotation, the overstrength of the connection zone with respect to the dissipative zone, and the dissipation capacity of the joints.

The experimental investigations performed on beam-to-column joints under both monotonic and cyclic loading evidenced a good conception and design of the joints (RBS and CP) justified by the following observations:

- elastic response of the connection zone;
- formation of the plastic hinge in the beam;
- corresponding to cyclic tests conducted with the AISC 341 [94] loading protocol, the RBS and CP designed joints evidenced rotation capacities of 50 mrad (RBS joints) and respectively 40 mrad (CP joints) for which the degradation of strength and stiffness were not greater than the 20% limit defined in EN 1998-1 [27];
- good response of joint detailing and welded connections with one exception (S700-CP-R-M / C) which evidenced weld failure, however corresponding to a force level higher than the design capacity ($F_{v,Rd}$).

Investigations performed on the welded connections lead to the conclusion that in the case of S700-CP-R-M and S700-CP-R-C joint specimens, the weld between plates of the external diaphragm contained a full length discontinuity representing un-penetrated weld root.

It was observed that the rotation capacity of the designed joints (RBS, CP) was higher (>40 mrad without significant reduction of capacity) in comparison to the seismic rotation demand of the joints from the analysis on frames.

Contribution of components to joint rotation

The contribution to the joint rotation was evaluated in the following regions: dissipative zone (plastic hinge), connection (welded connection and external diaphragm), and column web panel.

For the joints with reduced beam section and with cover plates, the main plastic deformations occurred in the beam (plastic hinge). The contribution of the connection and column web panel to the overall joint rotation was observed to be small. For the joints with reinforced beam, the main contribution to the overall joint rotation was given by the connection zone including external diaphragm (for strengthened RBS joints), and respectively by external diaphragm and column web panel (for strengthened CP joints).

Overstrength of joints

From the comparison between the four designed joints and the corresponding joints with reinforced beam, the overstrength computed at yield and at maximum capacity, was observed to satisfy the overstrength requirements, from EN 1998-1 [27], in comparison to the dissipative zone. Consequently, the overstrength of the connection zone for the RBS joints (with S460 / S700 RHS) was evaluated at 34% and 35% at yield, and respectively 53% and 60% at maximum

capacity. The overstrength of the connection zone for the CP joints (with S460 / S700 RHS) was 55% and 43% at yield, and 101% and 86% at maximum capacity.

Dissipated energy

A good dissipation capacity was observed for the RBS and CP joints. The energy absorbed by the heat affected zone (reinforced RBS joints) was observed to be low. In contrast, the energy absorbed by column web panel, external diaphragm and cover plates corresponding to S460-CP-R-C joint was significant. This observation was not proved in the case of S700-CP-R-C joint specimen, which experienced weld failure within the external diaphragm.

Calibration of numerical models and parametric study

The numerical models that anticipated the behaviour of the joint specimens were calibrated based on results from the experimental tests performed under monotonic and cyclic loading. From the calibration, a set of numerical models were obtained which reproduced with a good accuracy the response of the joints in both moment-rotation curve and failure mechanism, i.e. formation of the plastic hinge in the beam (designed joints) and yielding of components (reinforced joints). This allowed the investigation of complementary testing cases through numerical simulations with the aim to assess the influence of the concrete core, influence of the axial force in the column, and the response of joints with beams welded on two sides.

Influence of concrete core

It was observed that the absence of the concrete core did not affect significantly the response of the four designed joints (RBS and CP); only a minor reduction of the capacity was observed. In contrast, for the reinforced joints (with extended CP) a significant reduction of capacity was observed. In these cases, the bending moment and implicitly the shear force in the column web panel were much larger than in the other cases. In other words, the shear force in the column web panel exceeded the capacity of the steel tube in shear, and therefore a higher capacity was corresponding to the joints with concrete core. The influence of the concrete core was investigated also for joints with beams welded on two sides and joints with axial force in the column.

Joints with beams welded on two sides

The experimental tests were performed on single sided beam-to-column joints. It was therefore necessary to assess the behaviour of the joint (including column web panel) in the situation of loading from two sides which corresponds to a more demanding scenario. The reference joints for this study were S700-RBS and S700-CP. In comparison to the test curve a reduction of the stiffness was observed, but the capacity was not affected, nor the failure mode (plastic hinges in the beam). The weak-beam/strong-column concept was therefore confirmed for the CP and RBS joints considering the case with beams welded on two sides. In addition the study showed the contribution of the concrete core to joint behaviour. The absence of the concrete core lead in case of the CP joint to the reduction of the capacity and yielding of the column web panel, plastic hinges did not develop in the beams. In contrast, the absence of the concrete core did not affect the capacity or the failure mode for the RBS joint.

Axial force

It was observed that the axial force ($0.5 \cdot N_{pl,Rd,composite}$) in the column did not affect the response of the investigated joint (S460-CP) compared to the reference model and that the plastic hinge formed in the beam. In contrast, for the joint without concrete core the capacity decreased and eventually lead to column failure. It is to be noted that the load level corresponded to 70% of the plastic resistance of the steel tube. Corresponding to a lower axial force level ($0.5 \cdot N_{pl,Rd,steel}$) in the joint without concrete core, the column failure was not evidenced.

The axial force level in the column (from D-CBF) at the 5th floor reported to the plastic design capacity was in amount of 20% at SLS, and 26% at both ULS and CPLS. The axial force level in the column at the 1st floor reported to the plastic design capacity was in amount of 36% at SLS, and 40% at both ULS and CPLS. Therefore, the axial force levels were lower than 50% as assumed in the numerical investigations, and the response of the joints would not be affected by the axial force in the column.

Chapter 6: Component method approach for design of dual steel IPE beam-to CFRHS column welded joints

The design procedures for the two joining solutions, i.e. RBS joint and CP joint, were shown. An overview was shown by the design flow charts. Accordingly, the design of the joints was performed considering plastic hinge formation in the beam. Further with the bending moment and shear force from the plastic hinge, the components of the joint were designed for the required degree of overstrength. The main considered components were the welded on-site connection, the external diaphragm and the column web panel.

A summary was made with regard to:

- relations for the design of the welded connections;
- relations for the capacity of the components;
- stiffness coefficients of the components;

In addition, a component model was prepared for RBS and CP joints. The stiffness coefficients were considered according to EN 1993-1-8 [49] as equal to infinite for the following components: beam web in tension, beam web/flange in compression, and plate in tension. A relation was found based on which the stiffness coefficient of the external diaphragm can be assumed to be infinite. Therefore, the remaining component with contribution to the rotational stiffness was the column web panel. The rotational stiffness from the experimental tests was observed to be slightly higher compared to the rotational stiffness computed analytically in which only the contribution of the column web panel was considered. It is to be noted that in the analytical model, the stiffness coefficients of the column web panel were related to an unstiffened joint and to the concrete encasement (partially encased steel section). In contrast, for the case of a concrete filled rectangular hollow section, it is believed that the shear stiffness of the column web panel is influenced in a higher amount by composite effect of the member. Therefore, additional investigations are necessary in order to evaluate the influence on the shear stiffness given by the confining effect of the steel tube, and by the steel-concrete connection and friction.

The experimental and numerical validation of the relations for the design capacity of the main components was performed as well.

In relation to the dissipative zone, the formation of the plastic hinge in the beam was confirmed by the numerical and experimental investigations. In addition, the relation for the bending moment was in good agreement with the results.

In relation to the external diaphragms, a comparison was made between the analytical model, experimental test and numerical simulations. The following aspects were observed:

- good correlation between analytical model and FEM, in terms of stresses (shear stresses for RBS-R joints and equivalent stresses for CP-R joints);
- the design capacity of the external diaphragm was confirmed;
- yield lines observed from experimental tests and numerical simulations confirmed the failure mode considered in the analytical model;
- weld failure in case of S700-CP-R-M joint occurred corresponding to a load level above the computed yield capacity; therefore it was not a premature failure.

In relation to the column web panel, a comparison was made between the analytical model, experimental test and numerical simulations. The following observations were made:

- good correlation, in terms of shear stress, between analytical model and FEM results;
- the design capacity of the steel tube in shear was confirmed (the 0.9 coefficient was not taken into account in the analytical model as no axial force acted on the column);
- the design capacity of the column web panel in shear computed as the sum of the capacities (steel and concrete) was in very good agreement with the experimental results and with the numerical simulations; in the analytical model the shear capacity of the composite section was not affected by the factor 0.8 as required by EN 1998-1 [27];

Therefore the provisions from EN 1994-1-1 [50] for the shear strength of a column web panel considering a partially encased wide flange section were confirmed also for the case of rectangular hollow sections filled with concrete.

7.2. Contributions of the author

The main contribution of the author is represented by the design and execution of a coherent experimental program with the aim to evaluate the seismic performance of multi-storey frames realised considering the dual-steel solution, concrete filled rectangular hollow section columns and welded beam-to-column joints. The experimental program covered extensive experimental investigations carried on material samples (compression tests on concrete samples, as well as Charpy V-notch and tensile tests on steel samples), on steel-concrete connection needed for the composite action of CFT columns, as well as on full scale beam-to-column joints. A record of the main contributions of the author is further shown:

- The proposal of two innovative joining solutions for IPE beam-to-CFRHS column welded joints (novel research in the field in Europe);
- The design of the experiment test set-up for the investigations on steel-concrete connection and on beam-to-column joints;
- The experimental investigations performed on material samples;
- The experimental investigations performed on steel-concrete connection and on beam-to-column joints, both being characterised by a high original character;
- Performance evaluation of a set of dual-steel frames (it is to be noted that the basis of the investigated frames was represented by a set of frames

designed within HSS-SERF research project [1] – see Annex A; the members for the MRF were kept the same, for D-CBF and D-EBF some changes were undertaken in relation to the braces, dissipative links, and beams from the moment resisting bays; in addition the position of the dissipative zone and the joint typology were considered in the analysis);

- Advanced finite element modeling:
 - Calibration of the material models;
 - Pre-test numerical simulation with the aim to anticipate the behaviour of the joints (due to the innovative nature of the joint configurations, an accurate prediction was needed in order to avoid unacceptable failure during the tests);
 - Calibration of the numerical models based on results from the monotonic and cyclic tests;
 - Parametric studies for the investigation of the influence of the concrete core, the behaviour of joint assemblies with beams welded on two sides, and influence of the axial force in the column;
 - Validation of the design capacity of the joint components;
- Elaboration of a design procedure for the studied joints based on the component model approach;

7.3. Dissemination of results

The dissemination of results was performed in the first place in the research project HSS-SERF within several scientific and technical reports. It is to be noted that a set of guidelines will be developed within the project, covering design and detailing rules for connections and joints, design methodology and criteria for moment-resisting frames, design methodology and criteria for concentrically braced frames, and design methodology and criteria for eccentrically braced frames. Therefore, the design procedure of the joints with reduced beam section and with cover plates will be included in the guidelines.

The main results and conclusions of the research have been presented and published in several conferences and national or international journals. A list of the most important papers is presented below.

- **C. Vulcu**, A. Stratan, D. Dubina, "Seismic performance of EB frames of composite CFHS high strength steel columns", Proceedings of the 10th International Conference on Advances in Steel Concrete Composite and Hybrid Structures, ASCCS 2012, Singapore, ISBN-13: 978981-07-2615-7, ISBN-10: 981-07-2615-5, pp 953-960, 2 – 4 July 2012. (doi: 10.3850/978-981-07-2615-7_211).
- **C. Vulcu**, A. Stratan, D. Dubina, S. Bordea, "Seismic performance of dual frames with composite CF-RHS high strength steel columns", 15th World Conference on Earthquake Engineering, 24-28 September 2012, Lisbon, Portugal.
- **C. Vulcu**, A. Stratan, D. Dubina, "Seismic resistant welded connections for MRF of CFT columns and I beams", 7th International Workshop on Connections in Steel Structures, Timisoara, Romania, 30.05-2.06.2012.
- **C. Vulcu**, A. Stratan, D. Dubina, "Evaluation of welded beam-to-CFT column joints", 6th European Conference on Steel and Composite Structures,

EUROSTEEL 2011, Budapest, Hungary, 31 August – 2 September, pp 489-494, 2011.

- **C. Vulcu**, A. Stratan, D. Dubina, "Numerical simulation of the cyclic loading for welded beam-to-CFT column joints of dual-steel frames", Pollack Periodica, ISSN 1788-1994, Akadémiai Kiadó Zrt., Budapest, Hungary, Vol. 7, Nr. 2, pp. 35-46, 2012.
- **C. Vulcu**, A. Stratan, A. Ciutia, D. Dubina, "Beam-to-column joints for seismic resistant dual-steel structures", Pollack Periodica, ISSN 1788-1994, Akadémiai Kiadó Zrt., Budapest, Hungary, Vol. 6, Nr. 2, pp. 49-60, 2011.

In addition, the author was involved in research activities from which the results were published within the following papers:

- **C. Vulcu**, Th. Gernay, R. Zaharia, J.M. Franssen, "Numerical modelling of membrane action of composite slabs in fire situation", Proceedings of the Sixth International Conference on Structures in Fire, Michigan State University, East Lansing, USA, ISBN 978-1-60595-027-3, pp. 474 – 483, 2010.
- R. Zaharia, **C. Vulcu**, O. Vassart, T. Gernay and J. M. Franssen, "Numerical analysis of partially fire protected composite slabs", Steel and Composite Structures, ISSN 1229-9367, e-ISSN 1598-6233, (2013).
- F. Dinu, D. Dubina, C. Neagu, **C. Vulcu**, I. Both, "Experimental and numerical evaluation of a RS coupling beam for moment steel frames in seismic areas", Steel Construction 6 (2013), No. 1, DOI: 10.1002/stco.201310005.
- F. Dinu, D. Dubina, C. Neagu, **C. Vulcu**, D. Marcu, "Experimental calibration of numerical models for short coupling beams of a multi-story frame structure", 15th World Conference on Earthquake Engineering, 24-28 September 2012, Lisbon, Portugal.
- R. Gabor, **C. Vulcu**, A. Stratan, D. Dubina, F. Voica, D. Marcu, D. Alexandrescu, "Experimental and numerical validation of the technical solution of a brace with pinned connections for seismic-resistant multi-story structures", 15th World Conference on Earthquake Engineering, 24-28 September 2012, Lisbon, Portugal.
- A. Stratan, D. Dubina, R. Gabor, **C. Vulcu**, I. Marginean, "Experimental validation of a pinned connection for centric braced frames", 7th International Workshop on Connections in Steel Structures, Timisoara, Romania, 30.05-2.06.2012.

7.4. Acknowledgements

Besides the research activity carried out within the framework of the European Research Project HSS-SERF: "High Strength Steel in Seismic Resistant Building Frames" Grant NO RFSR-CT-2009-00024, the scholarship during the PhD stage of the author was covered from the strategic grant POSDRU/88/1.5/S/50783, Project ID50783 (2009), co-financed by the European Social Fund - Investing in People, within the Sectoral Operational Programme Human Resources Development 2007-2013.

REFERENCES

- [1] Silva L.S., Rebelo C., Serra M., Tenchini A. from (GIPAC); Landolfo R., D'Aniello M., Portioli F. from UNINA; Fülöp L. from VTT, "Selection and pre-design of frames for parametrical study", Mid Term Report HSS-SERF Project: "High Strength Steel in Seismic Resistant Building Frames", Grant N0 RFSR-CT-2009-00024, 2011.
- [2] Kuhlmann U., Kleiner A. from (USTUTT), "Qualification of welding for ductility and strength demands", Mid Term Report HSS-SERF Project: "High Strength Steel in Seismic Resistant Building Frames", Grant N0 RFSR-CT-2009-00024, 2011.
- [3] Jaspart J.-P., Comeliau L., Demonceau J.-F. from (ULG), "Prequalification tests on bolted beam-to-column joints in moment-resisting dual-steel frames", Mid Term Report HSS-SERF Project: "High Strength Steel in Seismic Resistant Building Frames", Grant N0 RFSR-CT-2009-00024, 2011.
- [4] Beg D., Cermelj B., Može P., Lopatic J. from (UL); Dubina D., Vulcu C., Stratan A., Ciutina A. from UPT, "Prequalification tests on welded beam-to-column joints in moment-resisting dual-steel frames", Mid Term Report HSS-SERF Project: "High Strength Steel in Seismic Resistant Building Frames", Grant N0 RFSR-CT-2009-00024, 2011.
- [5] Bjorhovde R., "Development and use of high performance steel", Journal of Constructional Steel Research, 60, 3-5: 393-400. 2004
- [6] EN 10025-2: 2004, Hot rolled products of non-alloy structural steels, Technical delivery conditions for non-alloy structural steels.
- [7] Samuelsson A., Schröter F., "High performance steels in Europe - Production processes, mechanical and chemical properties, fabrication properties" IABSE-Structural Engineering Document No. 8 - Use and application of high performance steels (HPS) for steel structures, 2005.
- [8] EN 10025-6: 2004, Hot rolled products of non-alloy structural steels, Technical delivery conditions for flat products of high yield strength structural steels in the quenched and tempered condition.
- [9] Sedlacek G., Müller C., "The use of very high strength steels in metallic construction"
- [10] Dillinger Hütte GTS, "DILLIMAX", Technical Information No. III/2007.
- [11] ArcelorMittal, "HISTAR-Innovative high strength steels for economical steel structures", www.arcelormittal.com/sections
- [12] Weber L., "Histar High Performance Hot-Rolled Beams", Proceedings Advanced Materials for Construction of Bridges, Buildings, and Other Structures III, Art. 4, 2005.

-
- [13] Hoffmann J., Donnay B., "TMCP applications in sections, bars and rails", PROFILARBED Research – Luxembourg, TMCP TMP-2004.
- [14] Takanashi K., Aburakawa M., Hamaguchi H., "Utilization of high performance steels in urban structures". Advances in Steel Structures ICASS'05, Vol. 2, 1827-1835, Elsevier, London, 2005.
- [15] Chan W.T., Badu S.K., "Use of high-strength structural steel in Hong-Kong". Proc. of the 4th Int. Conf. of Advances in Steel Structures, Shanghai, June 13-15, Late Papers Volume: 25-36, 2005.
- [16] JFE Steel Corporation, "High performance steel with earthquake resistance for building structures" (<http://www.jfe-steel.co.jp/en/products/plate/pop/pop11.html>).
- [17] Japanese Society of Steel Construction and the Japan Iron and Steel Federation: "Seismic response characteristics of steel frames with hysteresis-type dampers and aseismic design method", September 1998.
- [18] The Japan Iron and Steel Federation, and Japan Steel Structure Journal: "New steel products for building structures", 1998.
- [19] Steel Construction – Today and Tomorrow, "Low yield point steel for steel dampers", No. 7, June 2004.
- [20] Steel Construction – Today and Tomorrow, "New weathering steel for unpainted bridges", No. 2, March 2003.
- [21] Steel Construction – Today and Tomorrow, "Weathering steel", No. 2, March 2003.
- [22] Songa G., Maa N., Lib H.-N., "Applications of shape memory alloys in civil structures", Engineering Structures 28, pp. 1266-1274, 2006. (doi:10.1016/j.engstruct.2005.12.010)
- [23] Steel Construction – Today and Tomorrow, "Fire-resistant steel – Excellent Properties at elevated temperatures", No. 3, June 2003.
- [24] Steel Construction – Today and Tomorrow, "Fire-resistant steel – Properties of structural members and joining materials", No. 4, September 2003.
- [25] Johansson B., Collin P., "High-strength steel - the construction material of the future". ECCS TC10 report WG5-129, 1999.
- [26] Fukumoto Y., "New constructional steels and structural stability". Engineering Structures, Vol. 18, No. 10, pp. 786-791, 1996.
- [27] EN1998-1-1, Eurocode 8, Design of structures for earthquake resistance - Part 1, General rules, seismic actions and rules for buildings, CEN, European Committee for Standardization, 2004.
- [28] EN 1993-1-1, Eurocode 3: Design of steel structures - Part 1-1: General rules and rules for buildings, CEN, European Committee for Standardization, 2005.
- [29] EN 1993-1-10, Eurocode 3: Design of steel structures - Part 1-10: Material toughness and through-thickness properties, CEN, European Committee for Standardization, 2005.

200 REFERENCES

- [30] Feldmann M., Eicher B., Schäfer D., Hoffmeister B., Kuck J., Vayas I., Karlos V., Sedlacek G., "Choice of steel material for the plastic design of steel frames including seismic resistant structures", JRC Scientific and Technical Reports, Rev 02-07.06.2011.
- [31] EriksonKirk M., EriksonKirk M., "An upper-shelf fracture toughness master curve for ferritic steels", International Journal of Pressure Vessels and Piping, Vol. 83, No. 8, pp. 571-583, 2006.
- [32] Association française pour la construction, Office technique pour l'utilisation de l'acier, "Les aciers thermomécaniques: une nouvelle génération d'aciers à hautes performances", Paris la defense: OTUA, 1997.
- [33] Helzel M., Green P., "Stainless steel facades", Euro Inox, Second Edition 2002, Building series, Vol. 2, ISBN 2-87997-002-4, 2002.
- [34] Cropped version of "Kio Towers, Plaza de Castilla, Madrid" © Manuel González Olaechea y Franco, (<http://en.wikipedia.org/wiki/File:TorresKio.JPG>), used under a Creative Commons Attribution-Share Alike license: <http://creativecommons.org/licenses/by-sa/3.0/>.
- [35] "Pleiade Towers in Brussels", image by Vulcu C., 2009.
- [36] "Building of Europarlament in Brussels", Author: Karel Jakubec, (http://commons.wikimedia.org/wiki/File:EU_Parlament_3.jpg).
- [37] "The north-east side of Grosvenor Place building in Sydney, Australia", Author: Camw, (http://en.wikipedia.org/wiki/File:Grosvenor_Place.jpg), used under the Creative Commons Attribution-Share Alike 3.0 Unported license: <http://creativecommons.org/licenses/by-sa/3.0/deed.en>.
- [38] "Central Park Perth", Author: Cygnis insignis, (http://en.wikipedia.org/wiki/File:Central_Park_Perth.jpg).
- [39] "The Latitude (Ernst & Young) Bldg. in Sydney", Author: Randwicked, (http://en.wikipedia.org/wiki/File:Latitude_Sydney.jpg), used under the Creative Commons Attribution-Share Alike 2.5 Generic license: <http://creativecommons.org/licenses/by-sa/2.5/deed.en>.
- [40] "Shanghai World Financial Center Far", Author: Ferox Seneca, (http://http://en.wikipedia.org/wiki/File:Shanghai_World_Financial_Center_Far.jpg), used under the Creative Commons Attribution-Share Alike 3.0 Unported license: <http://creativecommons.org/licenses/by-sa/3.0/deed.en>.
- [41] "Yokohama-Landmark-Tower-02", Author: Rs1421, (<http://en.wikipedia.org/wiki/File:Yokohama-Landmark-Tower-02.jpg>), used under the Creative Commons Attribution-Share Alike 3.0 Unported license: <http://creativecommons.org/licenses/by-sa/3.0/deed.en>.
- [42] "The main office of East Japan Railway Company Shinjuku, Tokyo", Author: Ons, (http://commons.wikimedia.org/wiki/File:JR_East_main_office.jpg), used under the Creative Commons Attribution-Share Alike 3.0 Unported license: <http://creativecommons.org/licenses/by-sa/3.0/deed.en>.
- [43] "Mori Tower in Roppongi Hills during the day as seen from Tokyo Tower", Author: Chris 73, (http://commons.wikimedia.org/wiki/File:Roppongi_Hills_Mori_Tower_from_Tokyo_Tower_Day.jpg), used under the Creative

- Commons Attribution-Share Alike 3.0 Unported license: <http://creativecommons.org/licenses/by-sa/3.0/deed.en>.
- [44] "One World Trade Center - 24 Nov", Author: photokohli, ([http://en.wikipedia.org/wiki/File:One World Trade Center - 24 Nov. 2012.jpg](http://en.wikipedia.org/wiki/File:One_World_Trade_Center_-_24_Nov._2012.jpg)), used under the Creative Commons Attribution 2.0 Generic license: <http://creativecommons.org/licenses/by/2.0/deed.en>.
- [45] Wardenier J., "Hollow sections in Structural applications", CIDECT, 2000.
- [46] JFE Steel Corporation, "JFE Column", Cat. No. E1E-004-00.
- [47] TATA Steel, "Hollow sections for structural and mechanical applications".
- [48] Corus Tubes, "Design guide for SHS concrete filled columns", CT26/3:PDF:UK:03/2003
- [49] EN 1993-1-8 (2005), Eurocode 3: Design of steel structures - Part 1-8: Design of joints, CEN, European Committee for Standardization.
- [50] EN 1994-1-1 (2004), Eurocode 4, Design of composite steel and concrete structures - Part 1, General rules and rules for buildings, CEN, European Committee for Standardization.
- [51] Kurobane Y., Packer J.A., Wardenier J., Yeomans N., "Design guide for structural hollow section column connections", CIDECT Series "Construction with hollow steel sections" No. 9, TÜV-Verlag, Köln, Germany, ISBN 3-8249-0802-6, 2004.
- [52] AIJ, "Standard for Structural Calculation of Steel Reinforced Concrete Structures", Architectural Institute of Japan, Tokyo, Japan, 2001.
- [53] Kanatani H., Fujiwara K., Tabuchi M. and Kamba T., "Bending tests on T-connections of RHS chord and RHS or H-shape branch", CIDECT Report 5AF-80/15, 1980.
- [54] Wardenier J., "Hollow section connections", Delft University Press, Delft, The Netherlands, 1982.
- [55] Davies G., Packer J.A., "Predicting the strength of branch-plate RHS connections for punching shear", Canadian Journal of Civil Engineering, Vol. 9, No. 3, pp. 458-467, 1982.
- [56] Lu L.H., "The static strength of I-beam to rectangular hollow section column connections", Ph.D. Thesis, Delft University of Technology, Delft, The Netherlands, 1997.
- [57] Winkel G.D., "The static strength of I-beam to circular hollow section column connections", Ph.D. Thesis, Delft University of Technology, Delft, The Netherlands, 1998.
- [58] Morino S., Tsuda K., "Design and Construction of Concrete-Filled Steel Tube Column System in Japan", Earthquake Engineering and Engineering Seismology, Vol. 4, No. 1, pp. 51-73, 2003.
- [59] Cheng C.T., Chung L.L., "Seismic performance of steel beams to concrete-filled steel tubular column connections", Journal of Constructional Steel Research 59, pp. 405-426. (doi:10.1016/S0143-974X(02)00033-0), 2003.

202 REFERENCES

- [60] Chen C.C., Lin N.J., "Experimental investigation of flange plate connections between concrete-filled tube column and steel beam", 13th World Conference on Earthquake Engineering, Vancouver, B.C., Canada, August 1-6, 2004, Paper No. 476, 2004.
- [61] Shin K.J., Kim I.J., Oh Y.S., Moon T.S., "Behaviour of welded CFT column to H-beam connections with external stiffeners", *Engineering Structures* 26 (2004) pp. 1877–1887, (doi:10.1016/j.engstruct.2004.06.016), 2004.
- [62] Fukumoto T., Morita K., "Elastoplastic Behavior of Panel Zone in Steel Beam-to-Concrete Filled Steel Tube Column Moment Connections", *Journal of Structural Engineering*, Vol. 131, No. 12, December 2005, ASCE, ISSN 0733-9445/2005/12 pp. 1841–1853, 2005.
- [63] Park J.W., Kang S.M., Yang S.C., "Experimental studies of wide flange beam to square concrete-filled tube column joints with stiffening plates around the column", *Journal of Structural Engineering*, Vol. 131, No. 12, December 2005, ASCE, ISSN 0733-9445 / 2005/12 pp. 1866–1876, (DOI:10.1061/(ASCE)0733-9445(2005)131:12(1866)), 2005.
- [64] Chou C.C., Wu C.C., Jao C.K., Wang Y.Y., "Weakened and strengthened steel moment connections", 4th International Conference on Earthquake Engineering Taipei, Taiwan October 12-13, Paper No. 152, 2006.
- [65] Cheng C.T., Chan C.F., Chung L.L., "Seismic behavior of steel beams and CFT column moment-resisting connections with floor slabs", *Journal of Constructional Steel Research* 63, p.p. 1479–1493. (doi:10.1016/j.jcsr.2007.01.014), 2007.
- [66] Ghobadi M.S., Mazroi A., Ghassemieh M., "Cyclic response characteristics of retrofitted moment resisting connections", *Journal of Constructional Steel Research* 65, pp. 586–598. (doi:10.1016/j.jcsr.2008.02.008), 2008.
- [67] Bursi O.S., Ferrario F., Pucinotti R., Zandonini R., "Analysis of steel-concrete composite beam-to-column joints: bolted solutions", *Engineering Conferences International, Composite Construction VI, Copper Mountain, Colorado (USA) July 20-25*.
- [68] Bursi O.S., Cajot L.G, Ferrario F., Garcia J., Plumier A., Pucinotti R., Salvatore W., "Seismic performance of welded steel-concrete composite beam-to-column joints with concrete filled tubes", *The 14th World Conference on Earthquake Engineering, October 12-17 Beijing, China, 2008*.
- [69] Wang W., Chen Y., Li W., Leon R.T., "Bidirectional seismic performance of steel beam to circular tubular column connections with outer diaphragm", *Earthquake Engineering and Structural Dynamics* (2010), (DOI: 10.1002/eqe.1070), 2010.
- [70] Beck H., Reuter M., "Powder actuated fasteners in steel construction", *Steel Construction Calendar 2005 - Stahlbau Kalender 2005* (<http://www.us.hilti.com/fstore/holus/LinkFiles/Stahlbaukalender.pdf>)
- [71] Fink A., "Das Momentenrotationsverhalten von Verbundknoten mit Verbundstützen aus Rechteckhohlprofilen", *Diploma-work, Institute for Steel and Timber Structures, University of Innsbruck, 1997*.

- [72] Larcher T.Z., "Versuche zur Krafteinleitung der Trägerauflagerkräfte bei Hohlprofilverbundstützen mit Setznägeln", Diploma-work, Institute for Steel and Timber Structures, University of Innsbruck, 1997.
- [73] Beck H., "Nailed shear connection in composite tube columns", Second European Conference on Steel Structures, Prague, 26-29 May 1999, pp. 565–568.
- [74] Huber G., "Semi-continuous beam-to-column joints at the Millennium Tower in Vienna, Austria", Steel and Composite Structures, Vol. 1, No. 2, pp. 159-170, 2001.
- [75] Hanswille G., Beck H., Neubauer T., "Design concept of nailed shear connections in composite tube columns", Proceedings of the International Symposium on Connections between Steel and Concrete, RILEM Publications SARL, Print-ISBN: 2-912143-25-X, e-ISBN: 2351580346, Stuttgart, Germany, September 10-12, pp. 1056-1065, 2001.
- [76] "Frankfurt Am Main-Commerzbank Tower-Ansicht vom Eisernen Steg", Author: Mylius, (http://en.wikipedia.org/wiki/File:Frankfurt_Am_Main-Commerzbank_Tower-Ansicht_vom_Eisernen_Steg.jpg), used under the Creative Commons Attribution-Share Alike 3.0 Unported license: <http://creativecommons.org/licenses/by-sa/3.0/deed.en>.
- [77] Bauen mit Stahl, "Stahlgeschossbau - Grundlagen", Dokumentation 612, (<http://www.bauforumstahl.de/upload/documents/publikationen/D612.pdf>) 2007.
- [78] Huber G., "Non-linear calculations of composite sections and semi-continuous joints", Ph.D Thesis, Ernst & Sohn, Berlin, ISBN 3-433-01250-4, 1999.
- [79] Empelmann M., Teutsch M., Steven G., "Expanding the application range of RC-columns by the use of UHPC", Tailor Made Concrete Structures – Walraven & Stoelhorst, Taylor & Francis Group, London, ISBN 978-0-415-47535-8, pp. 461-468, 2008.
- [80] "Posttower Bonn 001", Author: Thomas Robbin, (http://en.wikipedia.org/wiki/File:Posttower_Bonn_001.jpg), used under the Creative Commons Attribution-Share Alike 3.0 Unported license: <http://creativecommons.org/licenses/by-sa/3.0/deed.en>.
- [81] Stahl-Information-Zentrum, "Deutsche Post AG Verwaltungshochhaus Bonn", (<http://www.stahl-info.de/schriftenverzeichnis/pdfs/SF043.pdf>), 2003.
- [82] Best Practice in Steel Construction - Commercial Buildings, "HighLight Towers, Munich", EURO-BUILD in Steel.
- [83] "Highlight Towers Muenchen A9-1", Author: Rufus46, (http://en.wikipedia.org/wiki/File:Highlight_Towers_Muenchen_A9-1.jpg), used under the Creative Commons Attribution-Share Alike 3.0 Unported license: <http://creativecommons.org/licenses/by-sa/3.0/deed.en>.

204 REFERENCES

- [84] Stahl-Information-Zentrum, "Highlight Munich Business Towers", (http://www.stahl-info.de/schriftenverzeichnis/pdfs/SF045_HighLight_Munich_Business_Towers.pdf), 2005.
- [85] EN 1992-1-1 (2004), Eurocode 2: Design of concrete structures - Part 1-1: General rules and rules for buildings, CEN, European Committee for Standardization.
- [86] Silva L.S., Rebelo C., Serra M., Tenchini A. from (GIPAC), "Selection of structural typologies and design of optimized dual-steel multi-storey frames", Mid Term Report HSS-SERF Project: "High Strength Steel in Seismic Resistant Building Frames", Grant N0 RFSR-CT-2009-00024, 2011.
- [87] ANSI/AISC 358-05 (2005), "Prequalified Connections for Special and Intermediate Steel Moment Frames for Seismic Applications", American Institute of Steel Construction.
- [88] FEMA 350, "Recommended Seismic design criteria for new steel moment-frame buildings", Federal Emergency Management Agency, June 2000.
- [89] Fajfar P., "A nonlinear analysis method for performance-based seismic design", Earthquake Spectra, 16(3):573-92, 2000.
- [90] CSI Berkley, SAP2000 v14.2.2, FAQ (2010).
- [91] FEMA 356, "Prestandard and commentary for the seismic rehabilitation of buildings", Federal Emergency Management Agency and American Society of Civil Engineers, Washington DC, USA, 2000.
- [92] Beck H., "Nailed shear connection in composite tube column with Hilti X-DSH 32 P10 - Installation instructions for test samples at University of Timisoara", Hilti AG., 22.11.2010.
- [93] European Convention for Constructional Steelwork, Technical Committee 1 TWG 1.3 - Seismic Design, No. 45, 1986, "Recommended testing procedures for assessing the behaviour of structural elements under cyclic loads".
- [94] ANSI/AISC 341-10 (2010), Seismic Provisions for Structural Steel Buildings, American Institute of Steel Construction.
- [95] Abaqus (2007) Analysis User's Manual I-V. Version 6.7. USA: ABAQUS, Inc., Dassault Systèmes.
- [96] Ali A.M., Farid B.J., and Al-Janabi A.I.M., "Stress-strain relationship for concrete in compression made of local materials", JAU: Eng. Sci., Vol. 2, pp 183-194, 1990.
- [97] Korotkov V., Poprygin D., Ilin K., Ryzhov S., "Determination of dynamic reaction in concrete floors of civil structures of nuclear power plant in accidental drops of heavy objects", ABAQUS Users' Conference, Boston 25-27 May, 2004, pp. 399-408.
- [98] Nastase E., "Technical Report: Non-destructive testing of welded connections (S460-RBS-R-C, S700-RBS-R-C, S460-CP-R-C, S700-CP-R-C)", ARTIMEX Impex, Timisoara 23-25.10.2012.

-
- [99] Dutta A., Dhar S., Acharyya S.K., "Material characterization of SS 316 in low-cycle fatigue loading", *Journal of Materials Science*, Vol. 45, Issue 7, pp. 1782-1789, 2010.
- [100] Hilti AG, Prüfbericht nr. 172268, Prüfobjekt: Hilti Nägel X-DSH 32 P10 Special, Auftragsnummer 555236, 25-27.05.1998.
- [101] Kim T., Whittaker A.S., Gilani A.S.J., Bertero V.V., Takhirov S.M., PEER 2000/07 (2000), "Cover-Plate and Flange-Plate Reinforced Steel Moment-Resisting Connections", Pacific Earthquake Engineering Research Center, University of California, Berkeley, 2000.
- [102] EN 1993-1-5 (2006), Eurocode 3: Design of steel structures - Part 1-5: Plated structural elements, CEN, European Committee for Standardization.

ANNEX A

The cross sections of the members obtained from the design of the frames (see Fig. A-1) performed by GIPAC, UNINA and VTT [1] are shown in Table A-1 for MRF, Table A-2 and Table A-3 for D-CBF, and in Table A-4 and Table A-5 for D-EBF.

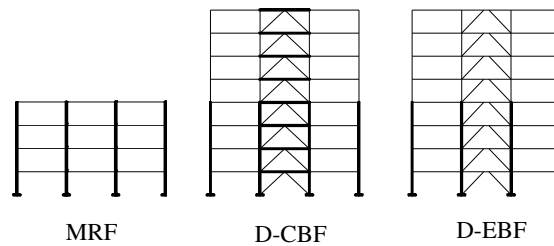


Fig. A-1. Frame typologies

Table A-1 – MRF (S460) – cross section of members [1]

Columns	Beams	
Storeys: 1-4	1-2	3-4
CF-RHS 400x20 S460 / C30/37	IPE 400 S355	IPE 360 S355

Table A-2 – D-CBF (S460) - cross section of members [1]

Storey	Columns	Beams		Braces
		Inner S460	Outer S355	CHS S355
1	CF-RHS 400x16 S460 / C30/37	HEB 450	IPE 500	219.1x10
2				219.1x10
3				193.7x10
4				193.7x8
5	CF-RHS 300x10 S355 / C30/37	HEA 450	IPE 450	168.3x10
6				168.3x8
7				168.3x6
8				139.7x5

Table A-3 – D-CBF (S690) - cross section of members [1]

Storey	Columns	Beams		Braces
		Inner S460	Outer S355	CHS S355
1	CF-BOX 340x16 S690 / C30/37	PRS 405x300x12x21	IPE 500	219.1x10
2				219.1x10
3				193.7x10
4				193.7x8
5	CF-RHS 300x10 S355 / C30/37	315x300x10x18	IPE 450	168.3x10
6				168.3x8
7				168.3x6
8				139.7x5

Table A-4 – D-EBF (S460) - cross section of members [1]

Storey	Columns	Beams		Braces
		Inner (link)	Outer	CHS S355
1	CF-RHS 400x16 S460 / C30/37	HEB 450	HEA 400	273x12
2		HEB 400		244.5x12.5
3		HEB 360		244.5x12
4		HEB 320		219.1x12
5	CF-RHS 300x8 S355 / C30/37	HEB 320	HEA 300	219.1x12
6		HEB 300		193.7x12.5
7		HEB 240		193.7x10
8		HEB 180		HEA 300

Table A-5 – D-EBF (S690) - cross sections of members [1]

Storey	Columns	Beams		Braces
		Inner (link)	Outer	CHS S355
1	CF-BOX 350x12 S690 / C30/37	HEB 450	HEA 400	273x12
2		HEB 400		244.5x12.5
3		HEB 360		244.5x12
4		HEB 320		219.1x12
5	CF-RHS 300x8 S355 / C30/37	HEB 320	HEA 300	219.1x12
6		HEB 300		193.7x12.5
7		HEB 240		193.7x10
8		HEB 180		HEA 300

ANNEX B

Fig. B-1 shows the four designed beam-to-column joints as well as the corresponding joint configurations with reinforced beam. Fig. B-2, Fig. B-3, Fig. B-4 and Fig. B-5 show the geometry of the four designed joints (see Fig. B-1a).

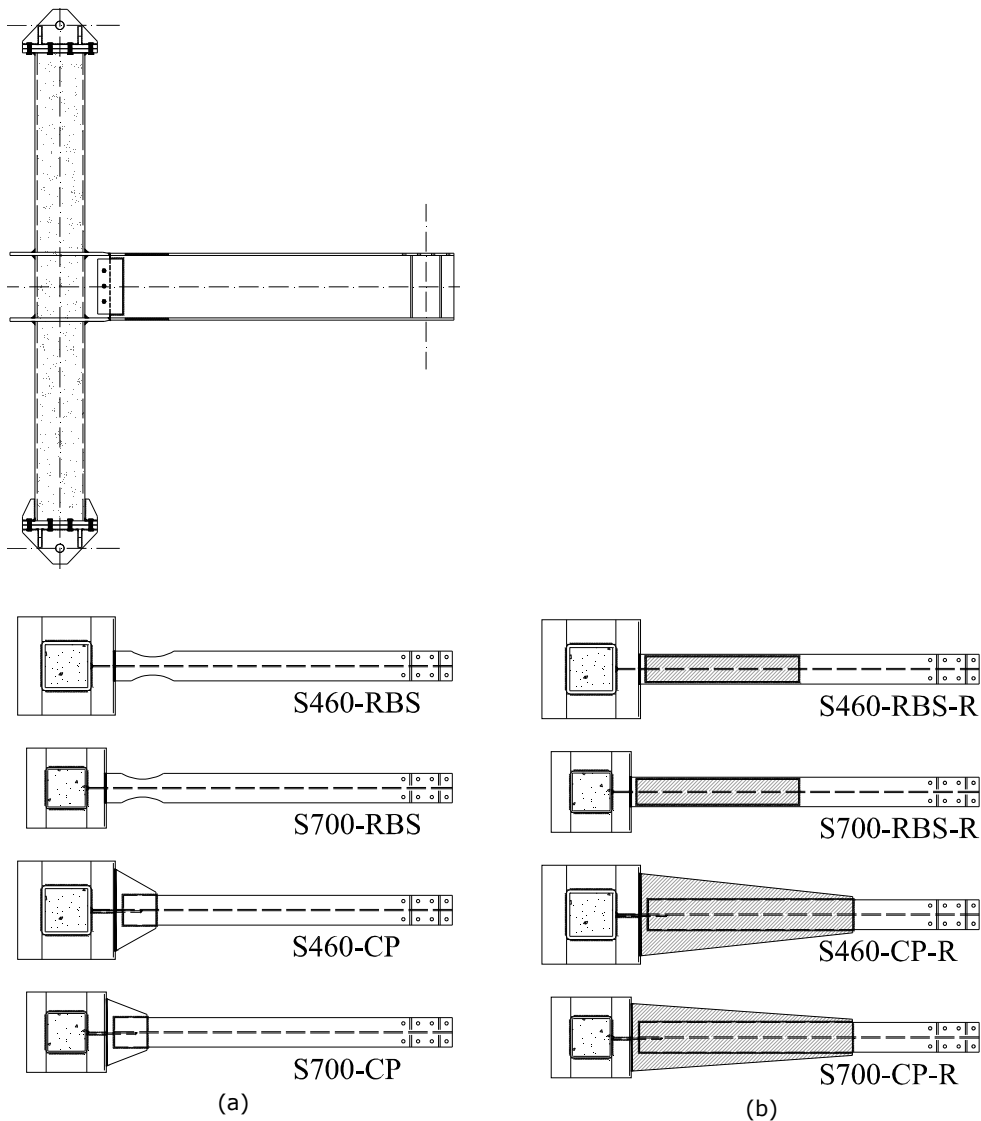


Fig. B-1. Designed beam-to-column joints (a), and corresponding reinforced joints (b)

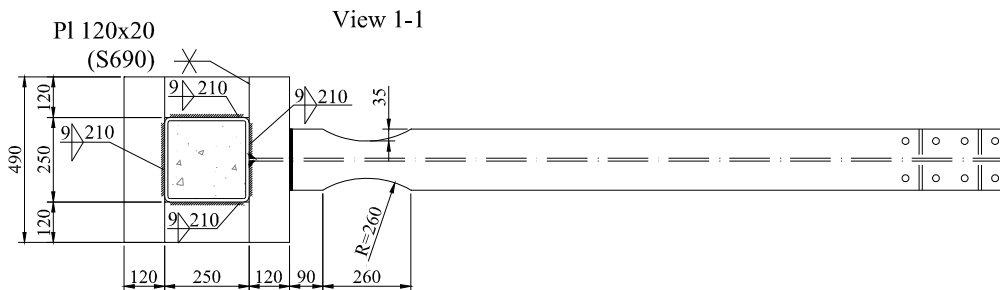
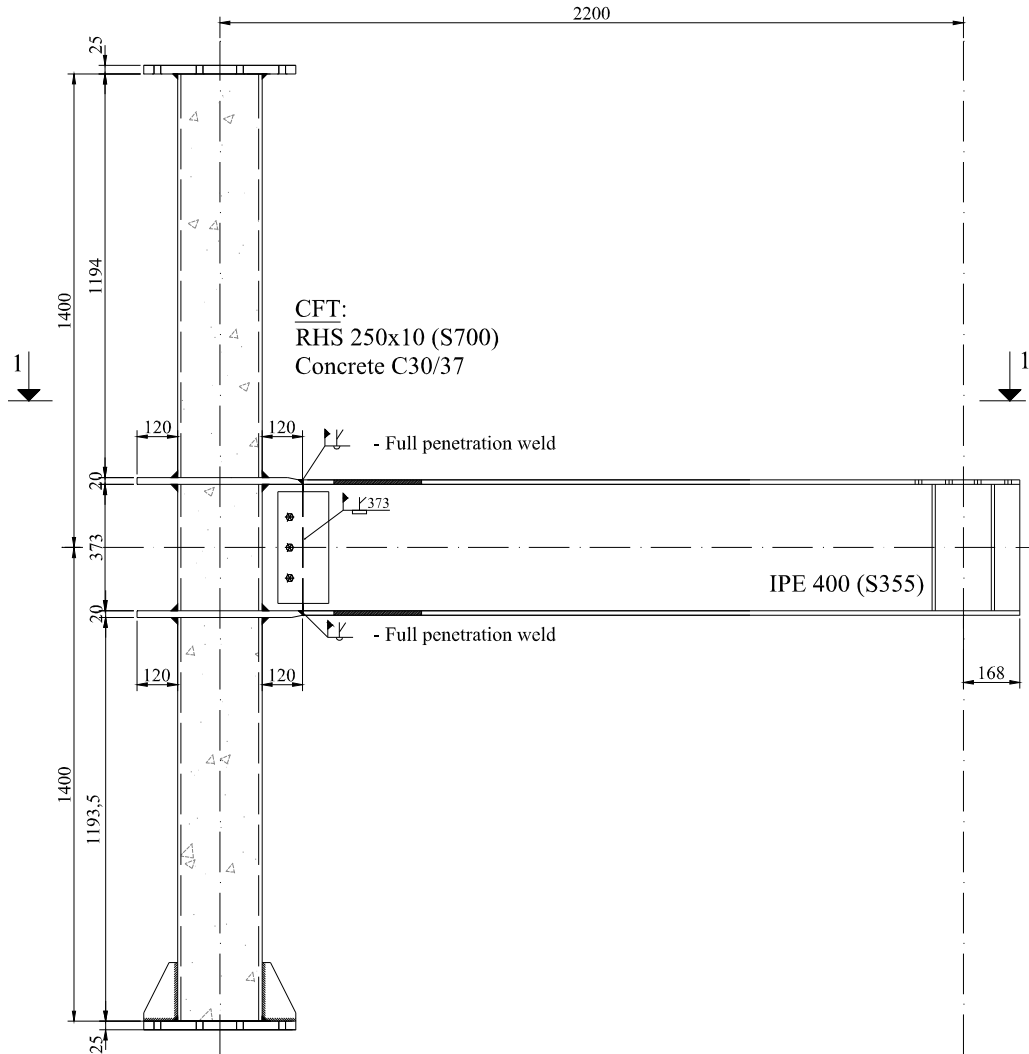


Fig. B-3. Geometry of S700-RBS joint

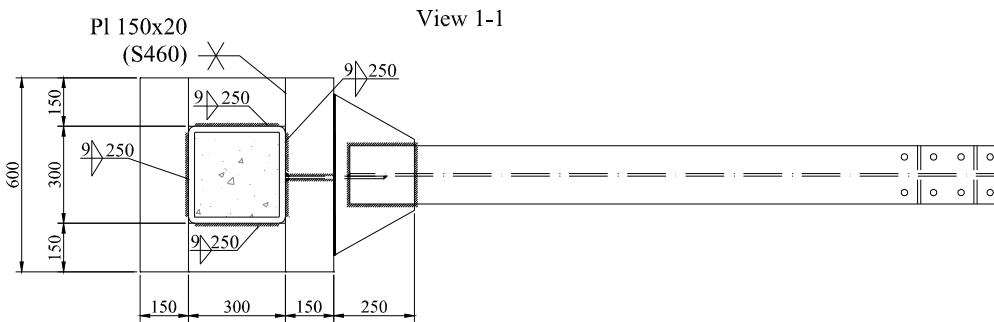
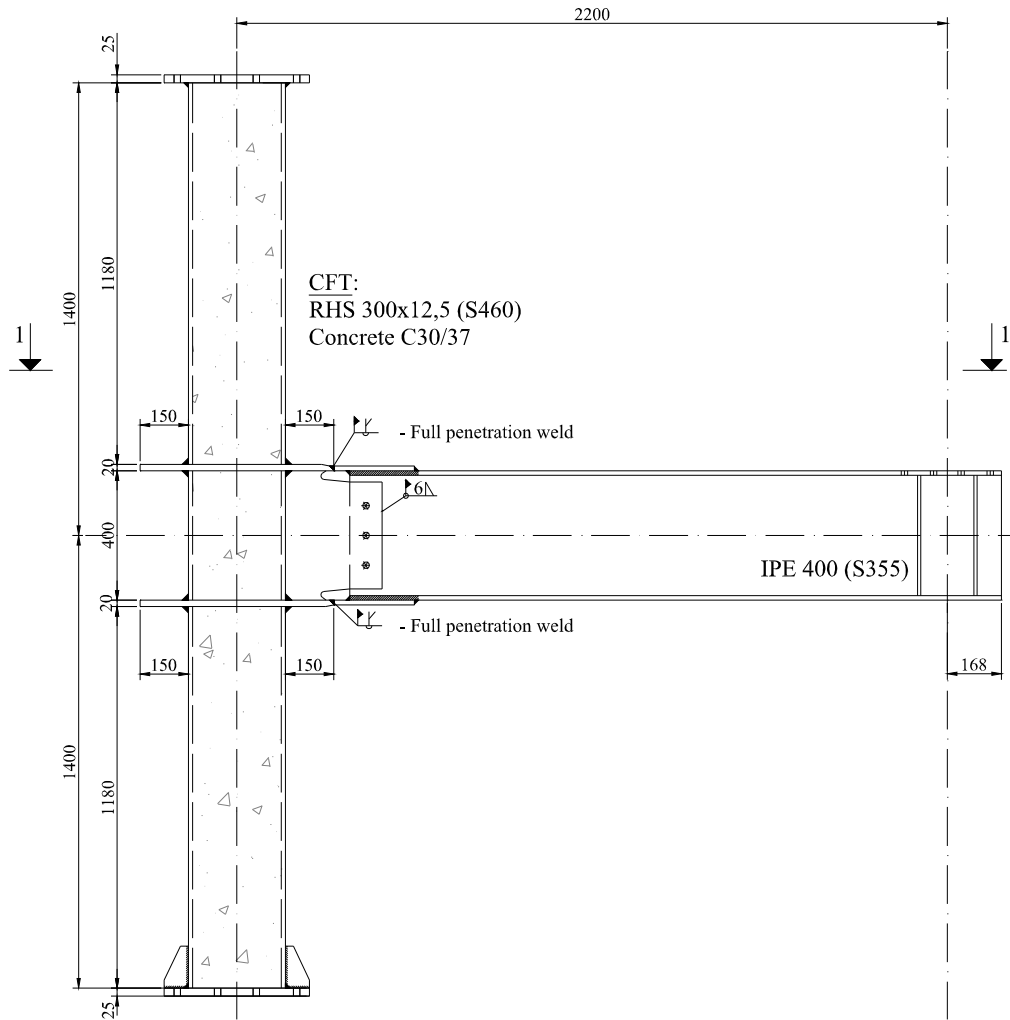


Fig. B-4. Geometry of S460-CP joint

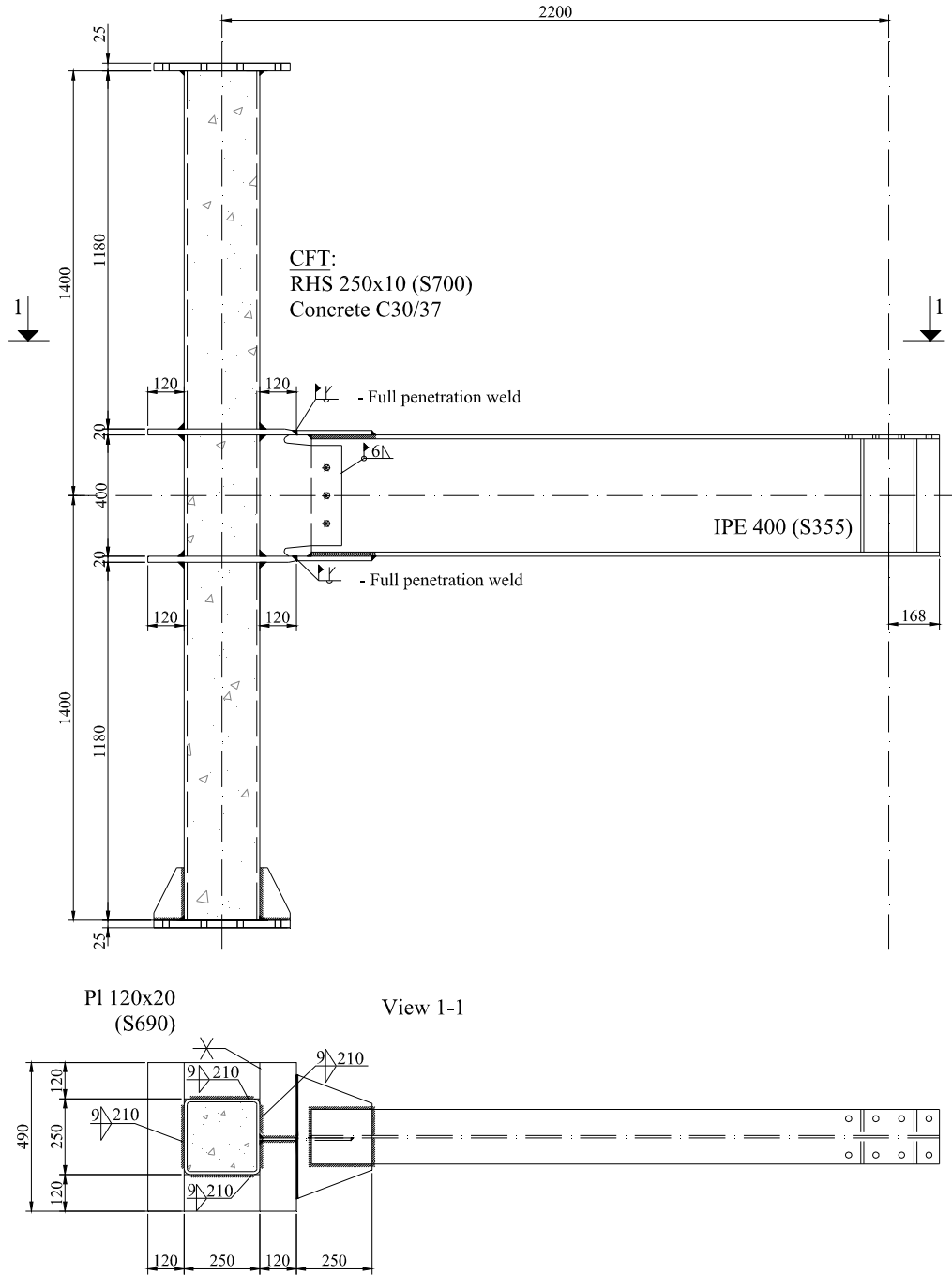


Fig. B-5. Geometry of S700-CP joint

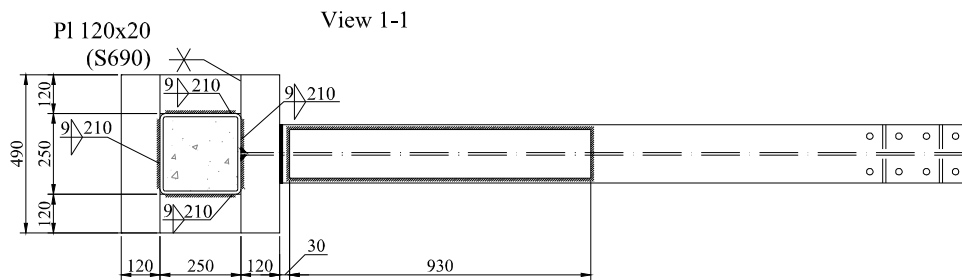
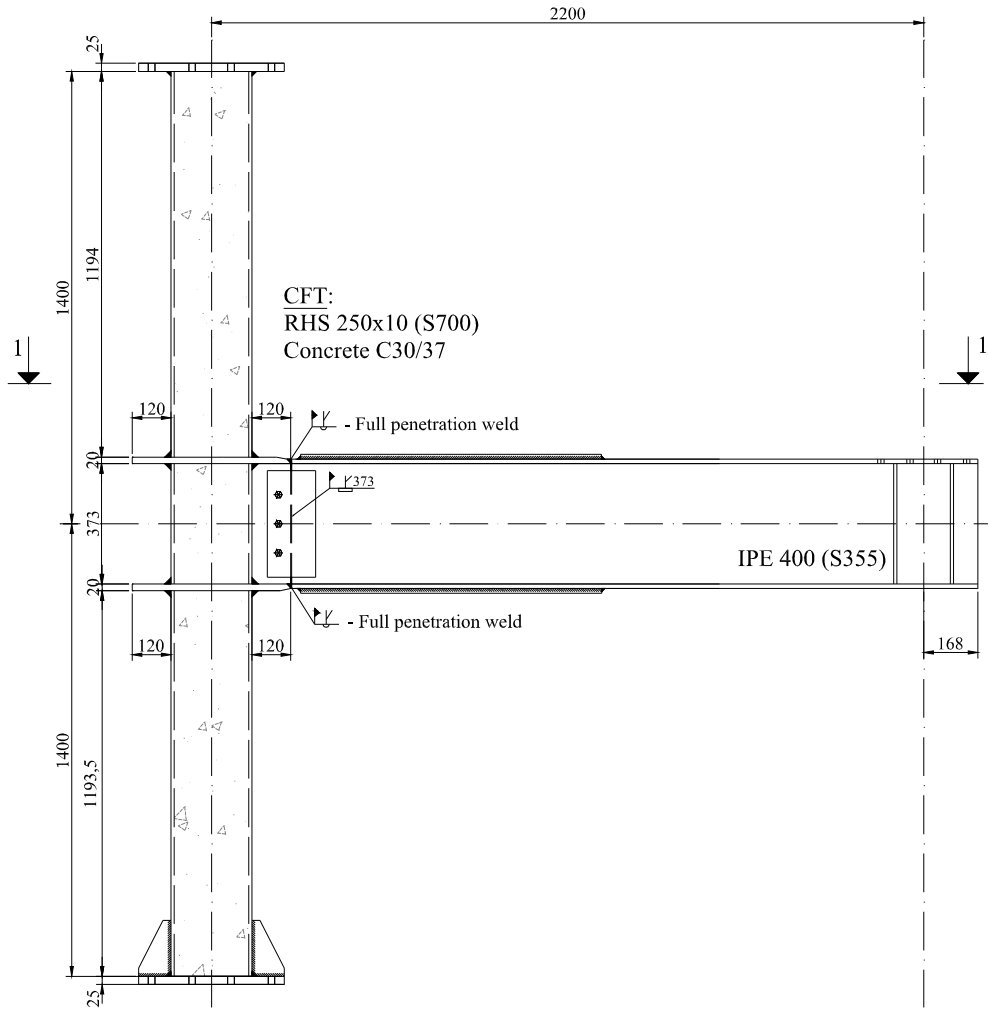


Fig. B-7. Geometry of S700-RBS-R joint

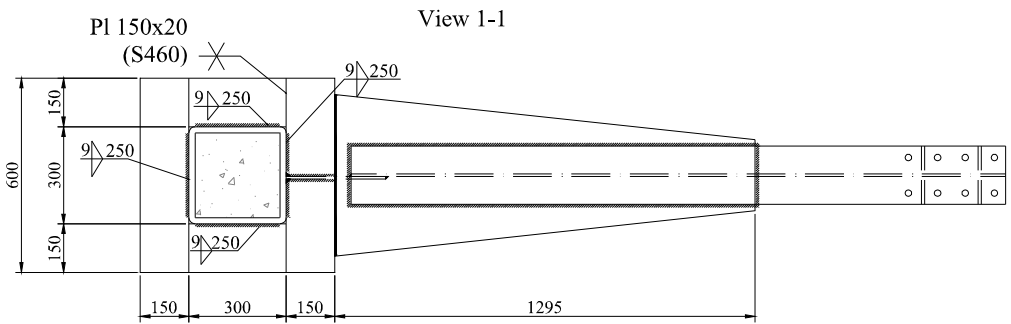
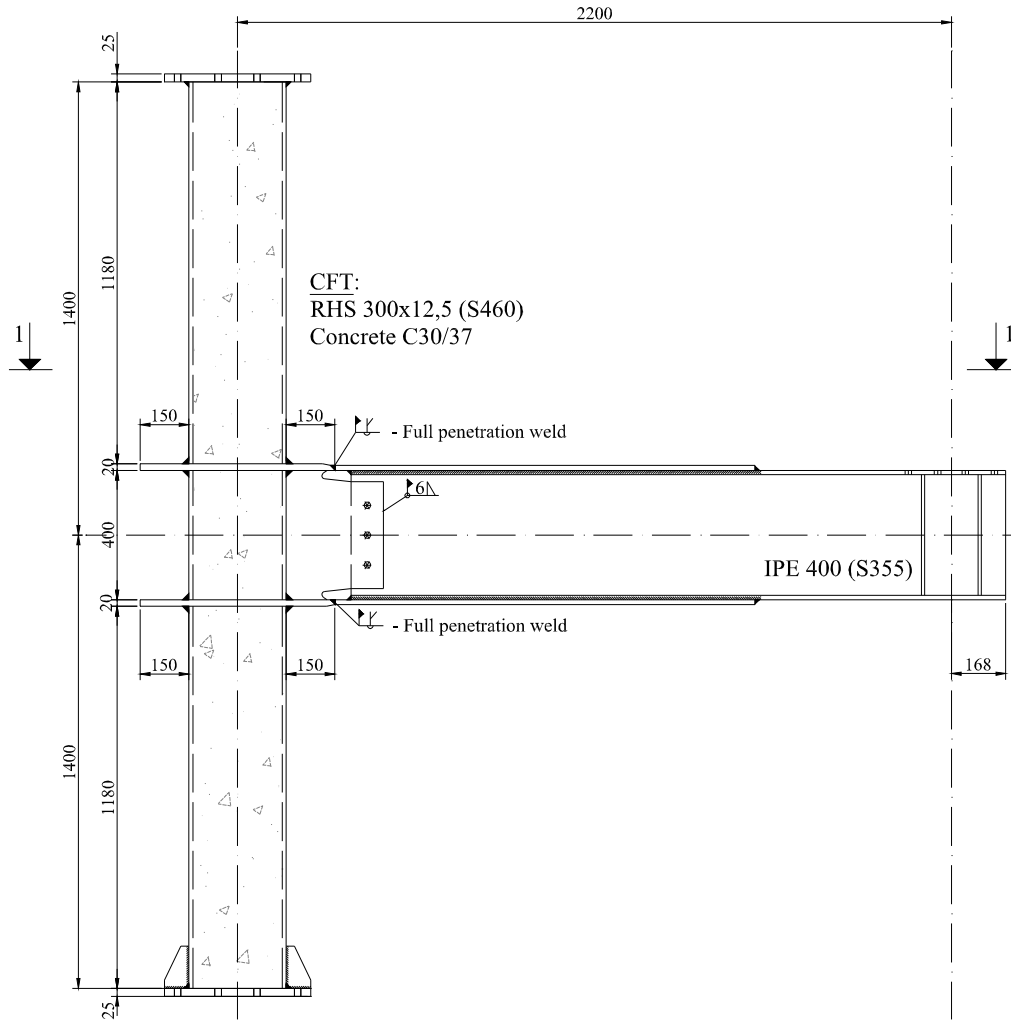


Fig. B-8. Geometry of S460-CP-R joint

ANNEX C

The results obtained from tensile tests on the other steel components (cover plates, splice plate, external diaphragms, and vertical column stiffeners) are presented in Annex C. The tensile tests on steel samples were performed using a universal testing machine (see Fig. C-1). The strain was measured using a video extensometer (see Fig. C-2).

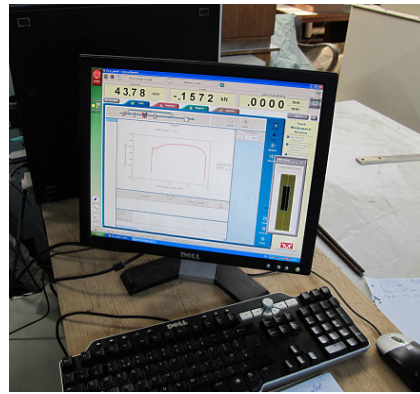
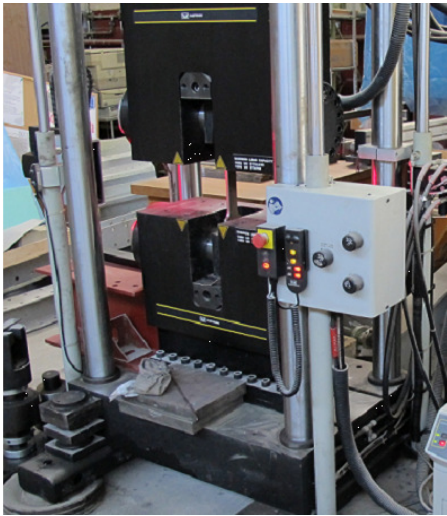


Fig. C-1. Tensile test on steel sample – universal testing machine

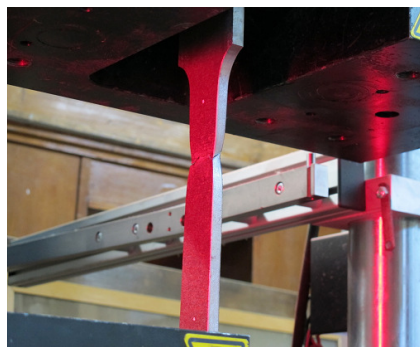
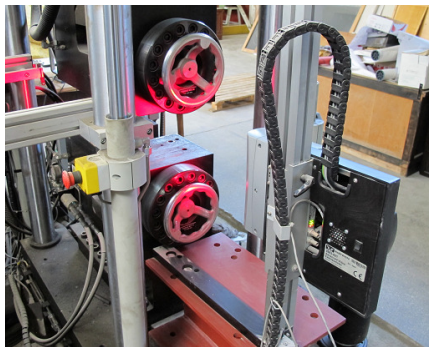


Fig. C-2. Tensile test on steel sample – video extensometer and tested sample

Cover plates – S355 J0

The stress-strain curves and the tested samples are displayed in Fig. C-3. An overview of the measured yield stress, maximum resistance, elongation at fracture and elongation at maximum force, is made in Table C-1. It can be observed that the measured values satisfy the minimum requirements from EN 10025-2:2004* [6].

Table C-1 – Stress and elongation results for cover plates – S355 J0

Sample	R_{eH} [N/mm ²]	R_m [N/mm ²]	A [%]	A_g [%]
S1	432.15	489.39	30.78	16.22
S2	432.24	490.21	31.2	16.11
S3	433.7	409.88	30.53	16.17
Average	432.7	489.14	30.84	16.17
Standard*	355	470 to 630	22	

$$R_m / R_{eH} = 1.13 \tag{C.1}$$

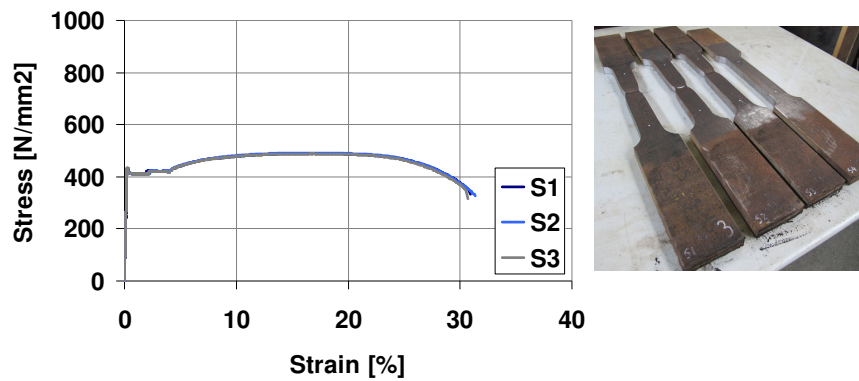


Fig. C-3. Stress-strain curves and tested steel samples

Table C-2 makes an overview of sample geometry, minimum energy at 0°C temperature and measured impact energy. It can be observed that the measured values are significantly higher, and therefore the requirements are satisfied.

Table C-2 – Impact test results for cover plates – S355 J0

		kV _{min} =27J at 0°C		10x10x55	
Sample		S1	S2	S3	S4
kV [J]		298	298	204	-

Splice plate – S355 J2

The stress-strain curves and the tested samples are displayed in Fig. C-4. An overview of the measured yield stress, maximum resistance, elongation at fracture and elongation at maximum force, is made in Table C-3. It can be observed that the measured values satisfy the minimum requirements from EN 10025-2:2004* [6].

Table C-3 – Stress and elongation results for splice plate – S355 J2

Sample	R_{eH} [N/mm ²]	R_m [N/mm ²]	A [%]	A_g [%]
S1	415.45	500.76	26.39	15.26
S2	416.04	502.08	26.67	15.08
S4	414.46	506.2	27.61	15.31
Average	415.31	503.01	26.89	15.22
Standard*	355	470 to 630	22	

$$R_m / R_{eH} = 1.21$$

(C.2)

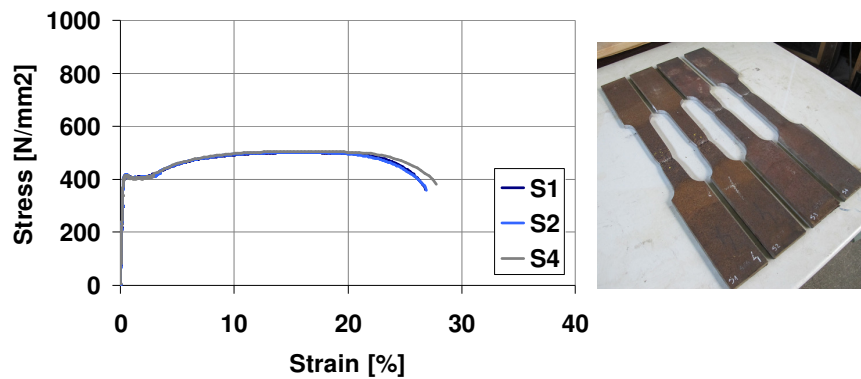


Fig. C-4. Stress-strain curves and tested steel samples

Table C-4 makes an overview of sample geometry, minimum energy at -20°C temperature and measured impact energy. It can be observed that the measured values are significantly higher, and therefore the requirements are satisfied.

Table C-4 – Impact test results for splice plate – S355 J2

Sample	$kV_{min}=27J$ at -20°C			
	10x10x55			
kV [J]	S1	S2	S3	S4
	218	210	236	-

External diaphragm – S460 NL

The stress-strain curves and the tested samples are displayed in Fig. C-5. An overview of the measured yield stress, maximum resistance, elongation at fracture and elongation at maximum force, is made in Table C-5. It can be observed that the measured values satisfy the minimum requirements from EN 10025-6:2004* [8].

Table C-5 – Stress and elongation results for external diaphragm – S460 NL

Sample	R_{eH} [N/mm ²]	R_m [N/mm ²]	A [%]	A_g [%]
S1	466.1	617.79	23.53	13.58
S2	451.26	618.7	23.84	13.58
S3	472.73	620.17	25.16	13.65
Average	463.36	618.88	24.18	13.60
Standard*	460	550 to 720	17	

$$R_m / R_{eH} = 1.33 \tag{C.3}$$

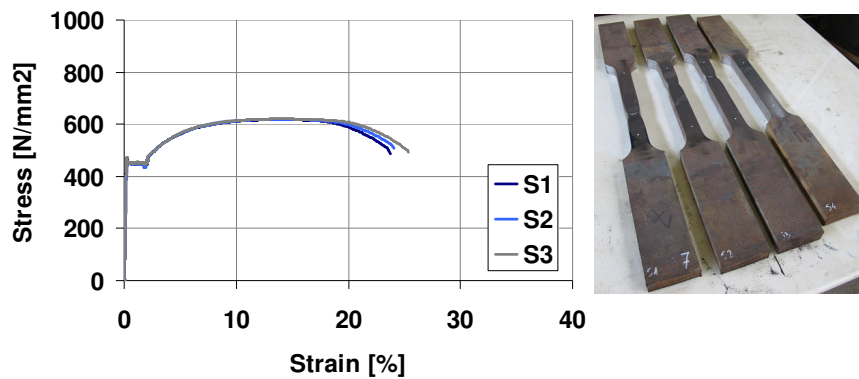
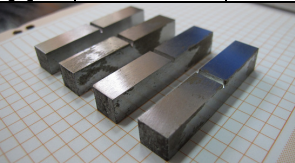
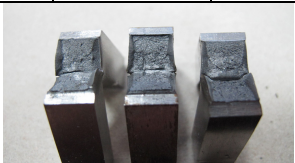


Fig. C-5. Stress-strain curves and tested steel samples

Table C-6 makes an overview of sample geometry, equivalent minimum energy at -30°C temperature and measured impact energy. It can be observed that the measured values are higher, and therefore the requirements are satisfied.

Table C-6 – Impact test results for external diaphragm – S460 NL

		kV _{min} =40J at -30°C		10x10x55	
Sample		S1	S2	S3	S4
kV [J]		56	50	70	-
					

External diaphragm – S690 QL

The stress-strain curves and the tested samples are displayed in Fig. C-6. An overview of the measured yield stress, maximum resistance, elongation at fracture and elongation at maximum force, is made in Table C-7. It can be observed that the measured values satisfy the minimum requirements from EN 10025-6:2004* [8].

Table C-7 – Stress and elongation results for external diaphragm – S690 QL

Sample	R_{p02} [N/mm ²]	R_m [N/mm ²]	A [%]	A_g [%]
S1	727.53	804.62	16.79	5.65
S2	718.62	806.1	15.89	5.42
S3	731.31	810.68	16.13	5.44
Average	725.82	807.13	16.27	5.51
Standard*	690	770 to 940	14	

$$R_m / R_{p02} = 1.11 \quad (C.4)$$

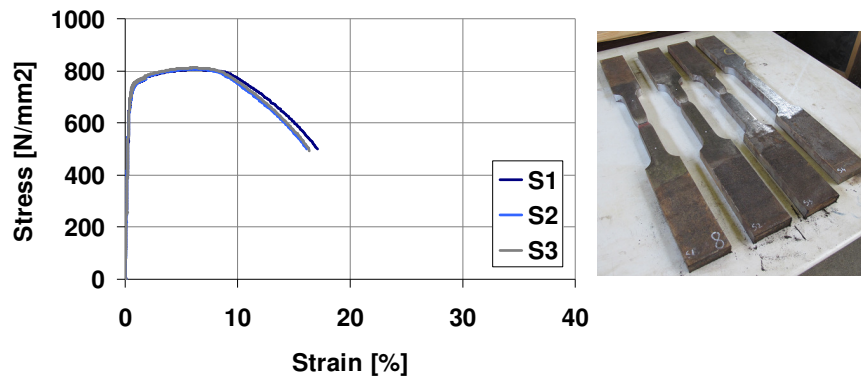




Fig. C-6. Stress-strain curves and tested steel samples

Table C-8 makes an overview of sample geometry, minimum energy at -20°C temperature and measured impact energy. It can be observed that the measured values are significantly higher, and therefore the requirements are satisfied.

Table C-8 – Impact test results for external diaphragm – S690 QL

		kV _{min} =40J at -20°C		10x10x55	
Sample		S1	S2	S3	S4
kV [J]		238	232	230	-

Vertical stiffener – S460 NL

The stress-strain curves and the tested samples are displayed in Fig. C-7. An overview of the measured yield stress, maximum resistance, elongation at fracture and elongation at maximum force, is made in Table C-9. It can be observed that the measured values satisfy the minimum requirements from EN 10025-6:2004* [8].

Table C-9 – Stress and elongation results for vertical stiffener – S460 NL

Sample	R_{eH} [N/mm ²]	R_m [N/mm ²]	A [%]	A_g [%]
S1	493.04	622.12	-	-
S2	496.05	623.38	25.93	13.61
S3	495.14	621.9	-	-
S4	495.92	622.15	-	-
Average	495.04	622.38	25.93	13.61
Standard*	460	550 to 720	17	

$$R_m / R_{eH} = 1.25 \tag{C.5}$$

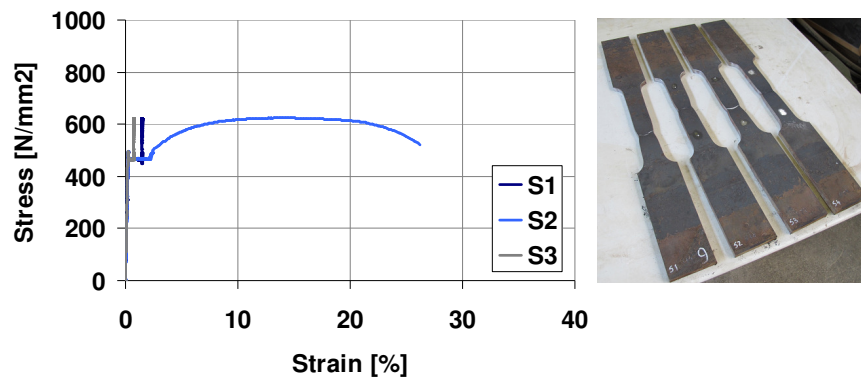


Fig. C-7. Stress-strain curves and tested steel samples

Table C-10 makes an overview of sample geometry, equivalent minimum energy at -30°C temperature and measured impact energy. It can be observed that the measured values are significantly higher, and therefore the requirements are satisfied.

Table C-10 – Impact test results for vertical stiffener – S460 NL

Sample	$kV_{min}=40J$ at $-30^{\circ}C$			
	S1	S2	S3	S4
kV [J]	172	129	156	-

Vertical stiffener – S690 QL

The stress-strain curves and the tested samples are displayed in Fig. C-8. An overview of the measured yield stress, maximum resistance, elongation at fracture and elongation at maximum force, is made in Table C-11. It can be observed that the measured values satisfy the minimum requirements from EN 10025-6:2004* [8].

Table C-11 – Stress and elongation results for vertical stiffener – S690 QL

Sample	R_{p02} [N/mm ²]	R_m [N/mm ²]	A [%]	A_g [%]
S1	812.01	858.04	14.74	5.83
S2	810.4	859.65	14.34	5.85
S3	798.54	846.3	13.49	5.57
Average	806.98	854.66	14.19	5.75
Standard*	690	770 to 940	14	

$$R_m / R_{p02} = 1.06 \quad (C.6)$$

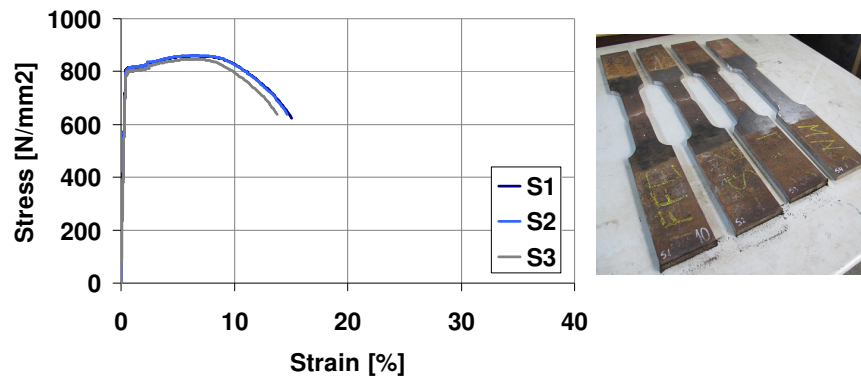


Fig. C-8. Stress-strain curves and tested steel samples

Table C-12 makes an overview of sample geometry, minimum energy at -20°C temperature and measured impact energy. It can be observed that the measured values are significantly higher even though the samples were thinner (7.5 mm), and therefore the requirements are satisfied.

Table C-12 – Impact test results for vertical stiffener – S690 QL

kV _{min} =40J at -20°C				
7.5x10x55				
Sample	S1	S2	S3	S4
kV [J]	146	153	153	-

ANNEX D

Results are shown from the calibration of the material model for: cover plates, splice plate, external diaphragms, and vertical column stiffeners. Table D-1 shows the input for the plastic behaviour. Fig. D-1, Fig. D-2, Fig. D-3, Fig. D-4, Fig. D-5 and Fig. D-6 show the Mises stresses and the plastic strain at fracture and a comparison between test and simulation in terms of force-displacement curve. For calibration, the engineering stress-strain obtained from the tensile tests was transformed into the true stress-strain using equation D.1 and D.2 from EN 1993-1-5 [102]. The two equations can be used up to the ultimate strength. The true stress-strain curves were therefore extended with additional points (see Table D-1).

$$\sigma_{true} = \sigma \cdot (1 + \epsilon) \quad (D.1)$$

$$\epsilon_{true} = \ln(1 + \epsilon) \quad (D.2)$$

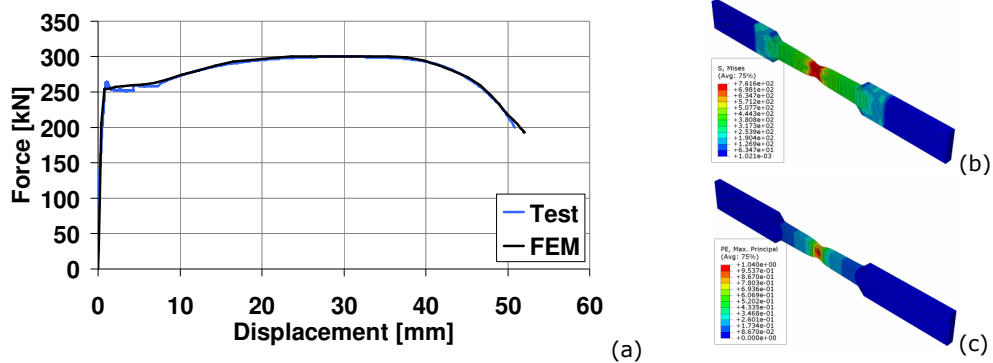


Fig. D-1. Calibration of cover plate (S355) material model: comparison between test and simulation (a); Mises stress (b) and plastic strain (c) at fracture

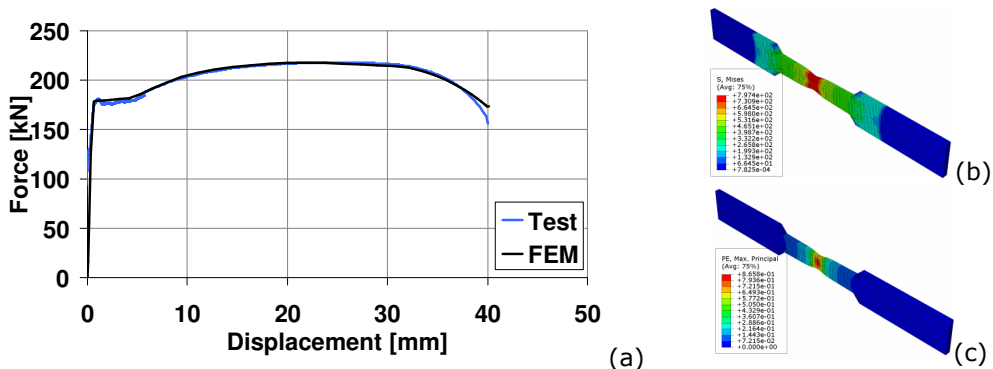


Fig. D-2. Calibration of splice plate (S355) material model: comparison between test and simulation (a); Mises stress (b) and plastic strain (c) at fracture

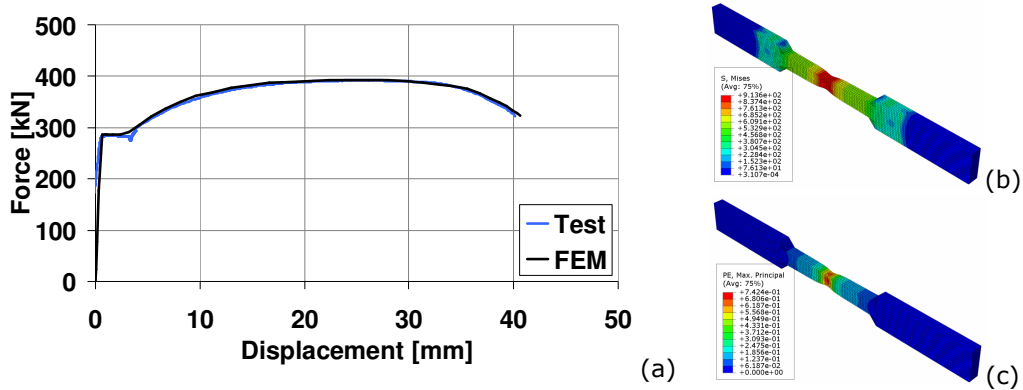


Fig. D-3. Calibration of external diaphragm (S460) material model: comparison between test and simulation (a); Mises stress (b) and plastic strain (c) at fracture

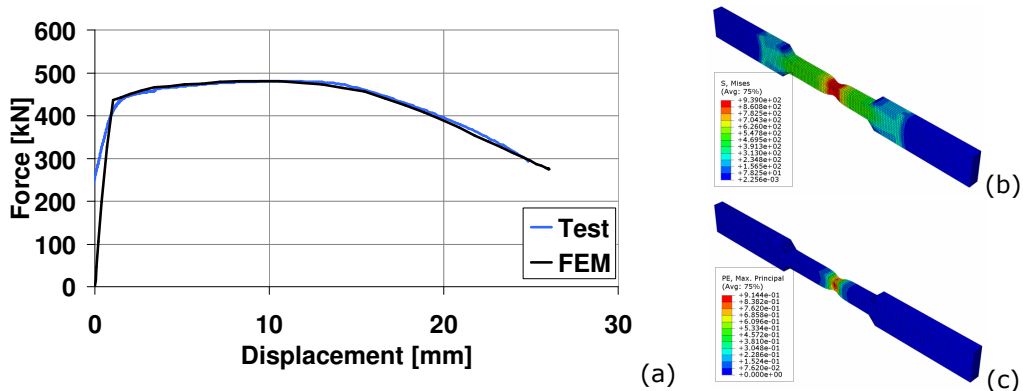


Fig. D-4. Calibration of external diaphragm (S690) material model: comparison between test and simulation (a); Mises stress (b) and plastic strain (c) at fracture

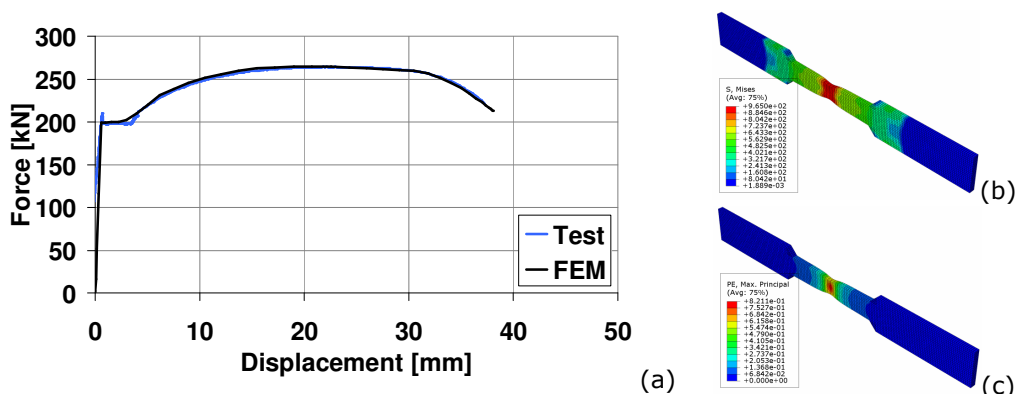


Fig. D-5. Calibration of vertical column stiffener (S460) material model: comparison between test and simulation (a); Mises stress (b) and plastic strain (c) at fracture

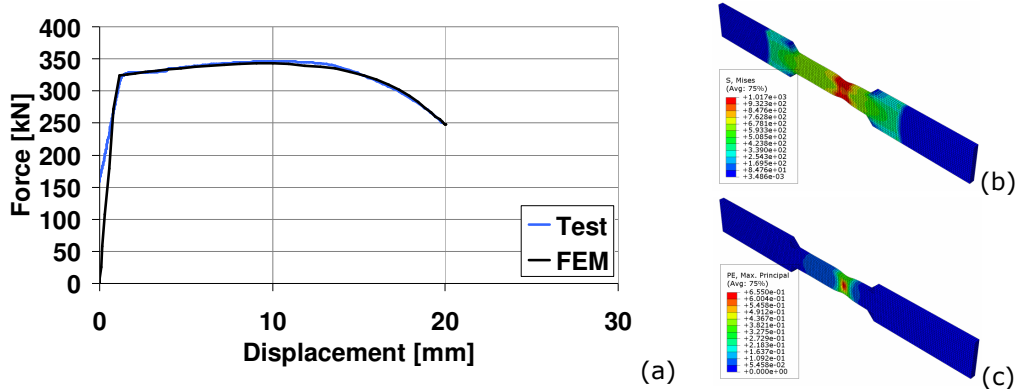


Fig. D-6. Calibration of vertical column stiffener (S690) material model: comparison between test and simulation (a); Mises stress (b) and plastic strain (c) at fracture

Table D-1 – Input for plastic behaviour

Cover plates		Splice plate		Diaphragm S460		Diaphragm S690		Stiffener S460		Stiffener S690	
True stress [N/mm ²]	True plastic strain	True stress [N/mm ²]	True plastic strain	True stress [N/mm ²]	True plastic strain	True stress [N/mm ²]	True plastic strain	True stress [N/mm ²]	True plastic strain	True stress [N/mm ²]	True plastic strain
414.7	0.0000	410.8	0.0000	451.0	0.0000	733.9	0.0000	467.2	0.0000	811.0	0.0000
437.7	0.0393	432.5	0.0297	459.0	0.0154	764.7	0.0058	481.8	0.0197	839.0	0.0170
462.6	0.0481	458.7	0.0370	494.2	0.0210	796.7	0.0144	519.3	0.0237	874.3	0.0316
501.1	0.0688	481.8	0.0476	564.6	0.0377	821.3	0.0275	584.0	0.0410	897.4	0.0451
529.7	0.0944	516.0	0.0691	595.6	0.0480	849.6	0.0451	634.7	0.0621	914.2	0.0592
548.4	0.1164	544.0	0.0942	643.2	0.0705	860.8	0.0556	680.3	0.0939	922.7	0.0712
564.1	0.1390	561.8	0.1148	674.6	0.0940	867.7	0.0677	709.6	0.1272	995.0	0.2000
572.6	0.1532	577.7	0.1390	694.6	0.1148	925.0	0.2000	755.0	0.2000	1020.0	0.4000
665.0	0.3130	715.0	0.4000	706.7	0.1309	938.0	0.4000	890.0	0.4000	800.0	0.8000
775.0	0.6500	790.0	0.6500	716.4	0.1464	939.0	0.8000	940.0	0.6000		
740.0	0.9000	800.0	0.9500	755.0	0.2000			965.0	0.8000		
725.0	1.0000			865.0	0.4000						
				910.0	0.6000						
				915.0	0.8000						

ANNEX E

The yielding sequence observed during the experimental investigations performed on beam-to-column joints is further illustrated for each configuration.

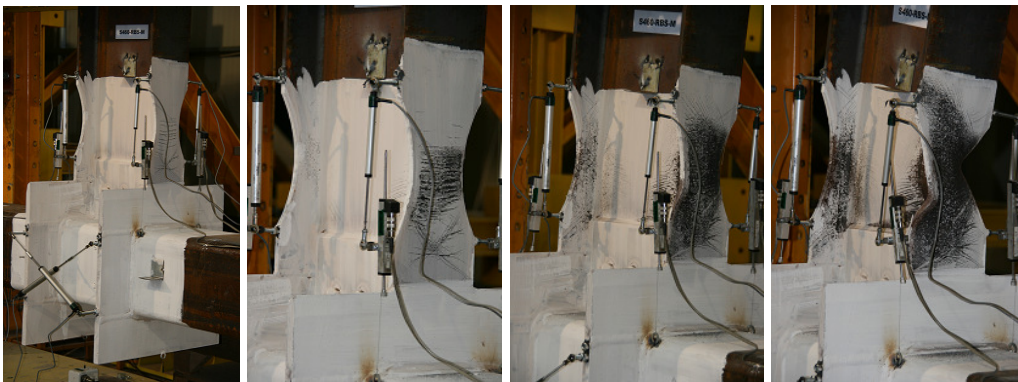


Fig. E-1. Yielding sequence: S460-RBS-M



Fig. E-2. Yielding sequence: S460-RBS-C

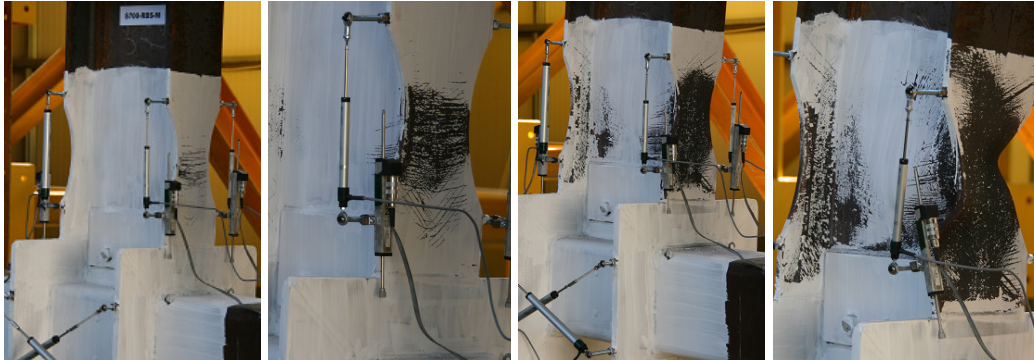


Fig. E-3. Yielding sequence: S700-RBS-M



Fig. E-4. Yielding sequence: S700-RBS-C

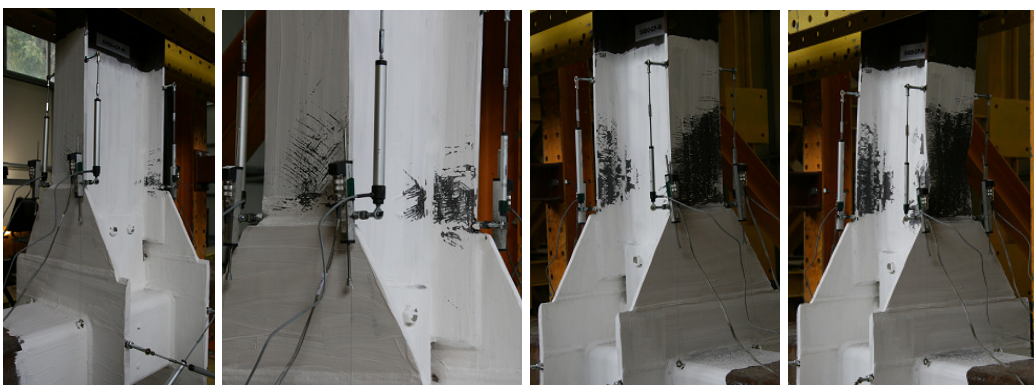


Fig. E-5. Yielding sequence: S460-CP-M

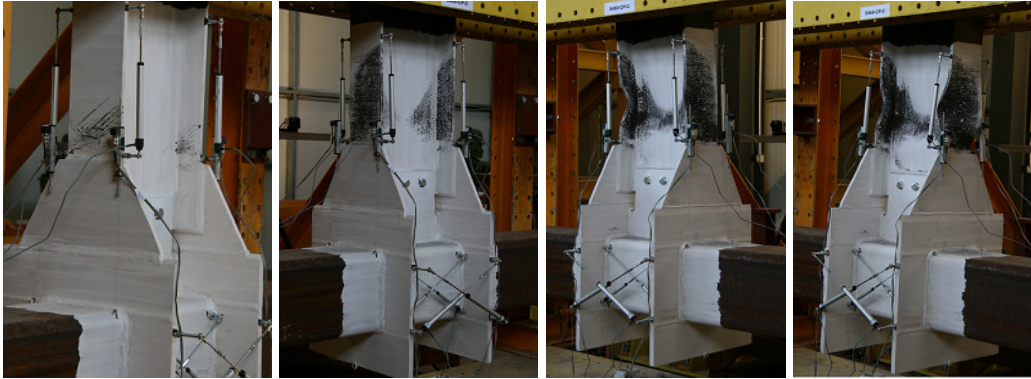


Fig. E-6. Yielding sequence: S460-CP-C

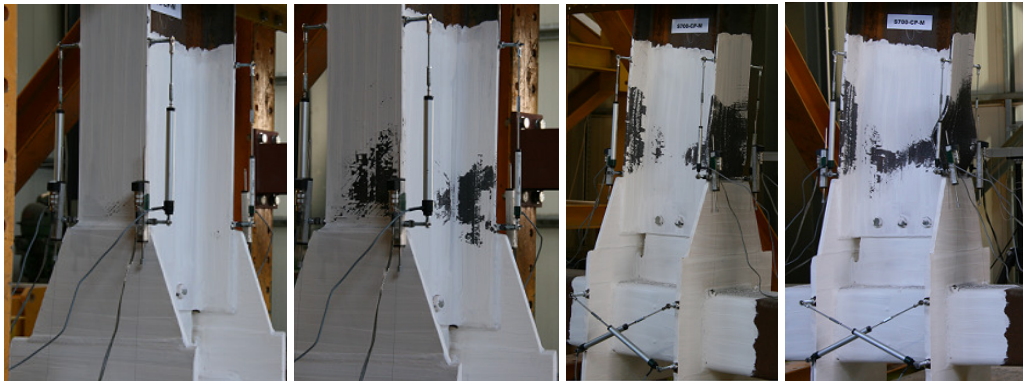


Fig. E-7. Yielding sequence: S700-CP-M

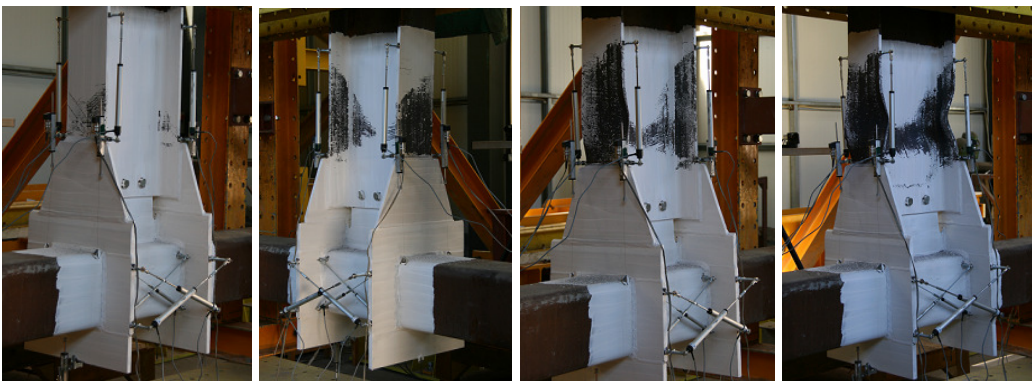


Fig. E-8. Yielding sequence: S700-CP-C

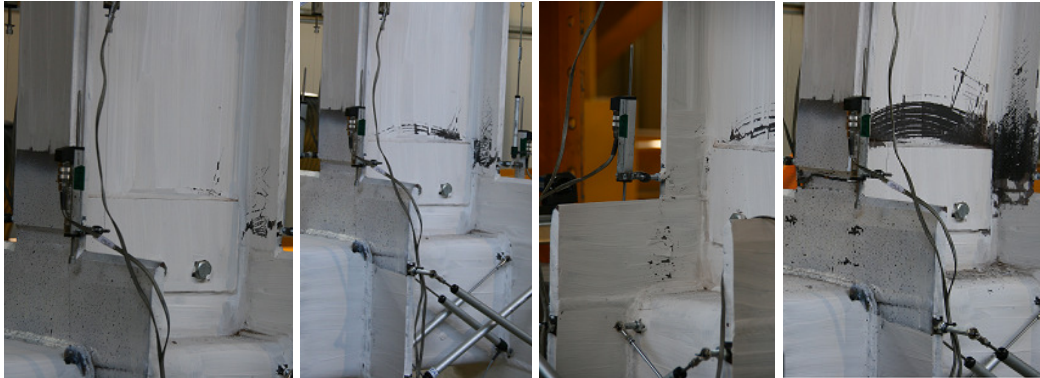


Fig. E-9. Yielding sequence: S460-RBS-R-M



Fig. E-10. Yielding sequence: S460-RBS-R-C

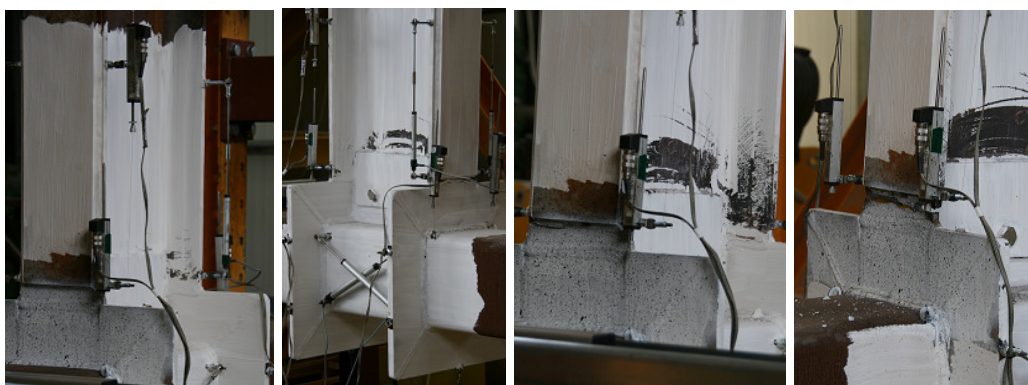


Fig. E-11. Yielding sequence: S700-RBS-R-M

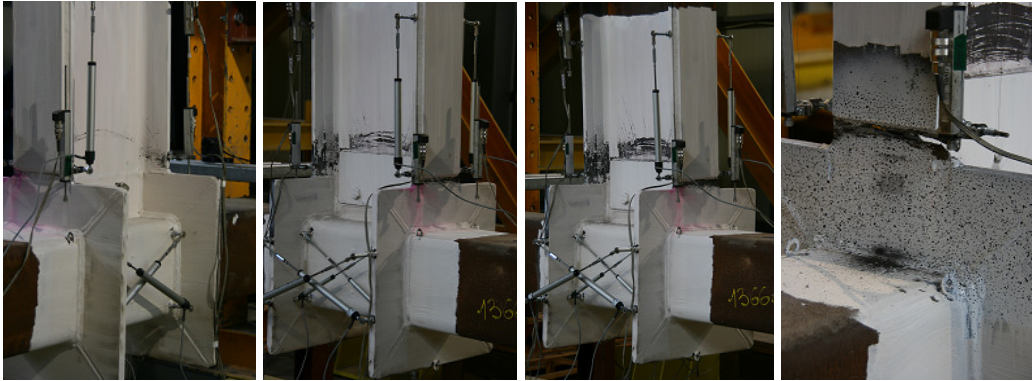


Fig. E-12. Yielding sequence: S700-RBS-R-C



Fig. E-13. Yielding sequence: S460-CP-R-M

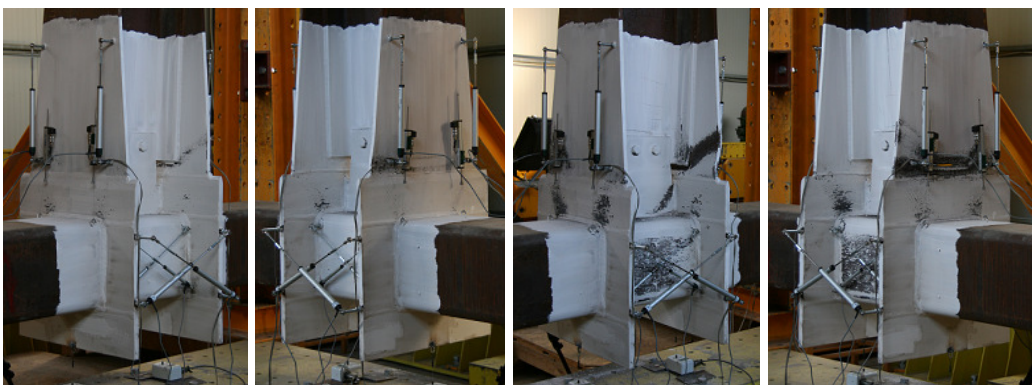


Fig. E-14. Yielding sequence: S460-CP-R-C

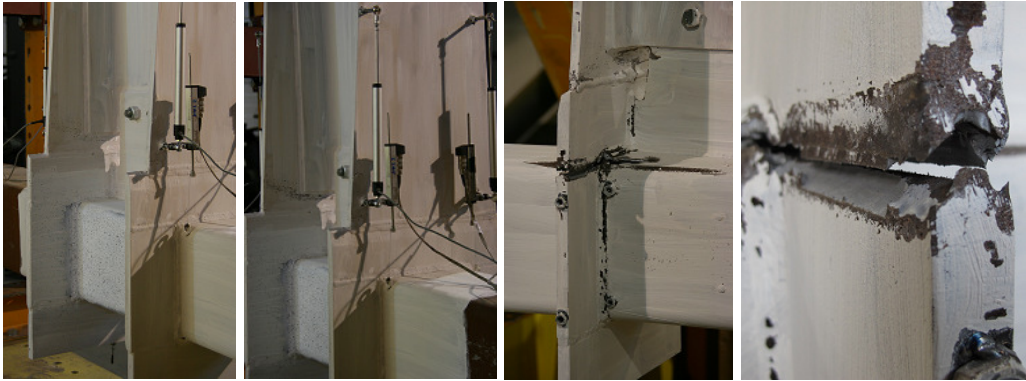


Fig. E-15. Yielding sequence: S700-CP-R-M



Fig. E-16. Yielding sequence: S700-CP-R-C